FOSSIL ENERGY

CONF–810718

1981 ANNUAL HEAVY OIL/EOR CONTRACTOR REPORTS–PROCEEDINGS

For Presentation July 28-30, 1981 in San Francisco

Date Published–July 1981

Fossil Energy Division
San Francisco Operations Office
Department of Energy

National Petroleum Technology Office
U.S. DEPARTMENT OF ENERGY
Tulsa, Oklahoma

CONF-810718
Distribution Category UC-92a

1981 ANNUAL HEAVY OIL/EOR CONTRACTOR REPORTS—PROCEEDINGS

For Presentation at the Sheraton-Palace Hotel
San Francisco, California, July 28-30, 1981

Meeting conducted by
Fossil Energy Division
San Francisco Operations Office
Gordon Dean, *Director*

Alan Leighton
Harold Lechtenberg
Gary Peterson
Eugene Standley

Proceedings presented by
Technology Transfer Section
Bartlesville Energy Technology Center

Date Published—July 1981

U.S. DEPARTMENT OF ENERGY

PREFACE

The 1981 Department of Energy Heavy Oil/EOR Meeting for presentations by contractors will be held at the Sheraton-Palace Hotel in San Francisco, Calif., July 28-30. This is the Fifth Annual Presentation by West Coast Contractors to the Department of Energy. The meeting program will emphasize the recovery of heavy oil and reports will be given on enhanced oil recovery (EOR) by applications of thermal processes, chemical flooding, and miscible flooding. Reports will include field projects, basic research, and environmental studies.

The meeting is sponsored by the Fossil Energy Division of the DOE San Francisco Operations Office. The work is part of the Enhanced Oil Recovery Program of the Department of Energy. The lead laboratory for this work is the Bartlesville Energy Technology Center. Much of the program is carried out by contract, and other contractor meetings are held periodically at other locations.

CONTENTS

ANNUAL HEAVY OIL/EOR CONTRACTOR PROCEEDINGS, 1981

CONTENTS—Continued

IMPROVED OIL RECOVERY BY ALKALINE FLOODING, HUNTINGTON BEACH FIELD

Aminoil USA
Houston, Texas

ABSTRACT

Aminoil is conducting a pilot test of the alkaline flooding process in the Lower Main Zone of the Huntington Beach Field. This area of the field was originally drilled in 1940 and produced by primary techniques until 1969. At that time a pilot waterflood was initiated in Fault Block 22 and 23 using a single, normal 5-spot pattern. Faulting provides partial isolation of these blocks from the rest of the field. Approximately two pore volumes of water have been injected into the 17,000 acre-ft project area which is currently producing at a water oil ratio of 28. The same fault block and pattern where the waterflood was pilot tested is being used for the alkaline flood pilot test program.

Injection of the softened produced water preflush commenced in June 1979 at a 10,000 B/D rate into the four injection wells of the 5-spot pattern. All wells in the project area had either been redrilled or worked over prior to initiation of preflush injection resulting in excellent well performance. Operation of the surface facilities and softening plant has been routine over the period of preflush injection. Alkaline injection commenced on March 10, 1980 at a concentration of 0.2% sodium orthosilicate in 7500 ppm sodium chloride solution at an average injection rate of 8,500 B/D.

Through the end of 1980, the cumulative slug injection was about 7 percent total pore volume. In October the concentration of sodium orthosilicate was raised to 1.0 percent. No response to the alkaline treatment has been observed with the total project oil production rate remaining flat at about 480 B/D.

HISTORY OF PROJECT

Contract DE-AC03-77ET12053 was initiated on July 1, 1977 with anticipated completion of December 31, 1980. The total cost is $2,027,690 of which DOE furnishes $531,374.

ENHANCED RECOVERY WITH MOBILITY AND REACTIVE TENSION AGENTS

Lawrence Berkeley Laboratory
University of California

ABSTRACT

The objectives of the project are: (1) to ascertain the tertiary-mode efficiencies of flooding acidic California crude oils with dilute aqueous bases, and (2) to devise laboratory screening tests which elucidate the governing recovery mechanisms and permit development of an improved mobility-reactive tension agent flooding package. The project involves studies on recovery mechanisms, displacement theory, interfacial tensions and charges, spontaneous emulsification, emulsion stability and emulsion rheology.

During 1980, experiments were conducted in core displacements, chemical transport, and emulsion flow. An initial attempt to model the alkaline displacement process included the chemistry of the acid hydrolysis to produce in situ surfactants. This model revealed a similarity of continuous alkaline flooding to pulsed surfactant flooding, a sensitivity to mobility control, and a chromatographic lag of the alkali at lower pH values for reservoir rocks where sodium-hydrogen base exchange can occur.

For the viscous Wilmington oil, mobility is highly important and a caustic-polymer flood was shown to give increased recovery over a caustic flood. For screening crude oils, properties at equilibrium with the alkaline phase are most pertinent. Orthosilicate and caustic were shown to be equally effective at equivalent pH values. The heavy crude asphaltenes that are not removed by paraffin-isopropanol extraction do not contribute to the reaction with caustic.

The alkali reacts irreversibly with silica to produce silicates. Various forms have different reaction rates-cristobalite, Ottawa sand and kaolinite reacting in that order. A reaction mechanism is under study to provide a means for estimating the lifetime of an alkaline pulse.

A quantitative theory for oil displacement by dilute emulsions was developed. It was found that the process is similar to filtration theory.

HISTORY OF PROJECT

Contract W-7405-ENG-48 was initiated October 1, 1976 and has been extended periodically. Results have been published in a series of Society of Petroleum Engineers reports, SPE 8845, 8995, 8997, as well as in DOE Annual Reports.

ENHANCED OIL RECOVERY BY MICELLAR-POLYMER FLOODING, WILMINGTON FIELD, CALIF.

City of Long Beach
Long Beach, Calif.

ABSTRACT

This project provided for the design and implementation of a micellar-polymer injection project in the HXa Sand, Fault Block VB, Wilmington Field, Calif. The intent was to demonstrate that this process would displace economic quantities of otherwise non-recoverable viscous oil from this reservoir and to determine the suitability of this process to other pools. The project is an application of the Maraflood (TM) Process with technical assistance from Marathon Oil Company.

After 14 months of preflush, the micellar slug was injected starting July 12, 1979 and finishing October 11, 1979. It was immediately followed by the polymer buffer which is injected in steps of decreasing concentration. During the January-March 1981 quarter, the fifth stage with a concentration of 1100 ppm was injected.

Cumulative recovery from the pilot area is approximately 126,000 barrels, of which 74,000 bbls (5 percent of a pore volume) is the incremental recovery. The oil rate declined by 15 percent to 210 b/d during the January-March 1981 quarter and the water-oil ratio increased from the low of 10.1 to over 14.

HISTORY OF PROJECT

The contract between the City of Long Beach and ERDA was signed July 6, 1976. It had an anticipated completion date of December 31, 1980. The total cost was projected at $7,000,000 with the government and the contractor sharing equally.

ALKALINE WATERFLOODING DEMONSTRATION PROJECT
RANGER ZONE, LONG BEACH UNIT, WILMINGTON FIELD CALIFORNIA

by

P.B. Kemp
Department of Oil Properties, City of Long Beach

and

E.H. Mayer
THUMS Long Beach Company

ABSTRACT

No short term solution was found to the floc formed when the concentrated saline brine was added to the soft water-alkali stream. Soft water with alkali but no salt was injected through mid-August, 1980. At that time, alternating weekly injection of soft water-salt and soft water-alkali slugs was begun. This and three well acid jobs restored the injection rate.

Corrosion continued to be a problem. Both the saline and alkaline slugs are to have an inhibitor added. Produced water samples failed to indicate alkaline breakthrough to any of the producers.

Reservoir simulation work indicated that oil rate response and total incremental oil recovery were dependent on the alkaline concentration and alkaline slug size as well as the alkaline flood relative permeability adjustment being postulated. Alkaline consumption was calculated to be very large.

Routine well servicing and surveying continued. Redrilling and major well repair was less than in earlier years.

HISTORY OF PROJECT

The Contract was initiated September 30, 1976 for completion September 30, 1981. The cost was projected at $11,584,572 with the Department of Energy furnishing $4,633,829.

HISTORY OF PILOT

The City of Long Beach - Department of Energy Contract for the pilot was signed September 30, 1976 (The City of Long Beach is Operator of the Long Beach Unit and THUMS Long Beach Company the Field Contractor). The project is an improved waterflood demonstration of alkaline waterflooding in a typical well pattern of the Ranger Zone of the Long Beach Unit portion of the Wilmington Field, California.

The pilot is designed to demonstrate the feasibility of employing alkaline flooding to improve recovery efficiency in a reservoir of the Ranger type, i.e., a stratified heterogeneous, high oil viscosity reservoir where conventional waterflood recovery is relatively poor. The Ranger reservoir is an alternating sand-shale sequence comprising a gross thickness of 850 feet and a net sand thickness of 305 feet. Modeling work has shown that three areas comprise the pilot area that will be affected by the alkaline flooding. These as shown in Figure 1 are:

Prepared for DOE under Contract No. DE-AC03-76ET12407

HISTORY OF PILOT (Cont.)

1. Pattern Area. This is the area in which DOE participates as to costs and incremental oil production. It currently contains 11 producers and the pilot's 8 injectors. It has a surface area of 93 acres.

2. Northern Area. This presently contains 6 producing wells and has an area of 59 acres.

3. Southern Area. It contains 6 producers and has an area of 41 acres.

The background history of the project has been given in the initial proposal to the DOE, four summary papers and four annual reports. (Ref. 1-9.)

From contract inception to January, 1979 laboratory core/fluid testing, facilities design/procurement/installation, reservoir simulation studies and well repair/redrilling occurred. Preflushing with soft water with 1.0% salt began in January, 1979 and continued untill March, 1980. Preflush volume was 10.18 pore volume percent. All of the previous work other than the reservoir stimulation continued in the January, 1979 - March, 1980 period. The alkaline injection facilities were completed and the caustic injection began March 31, 1980. Laboratory testing, well work and facilities maintenance continued. The reservoir modeling work was resumed in April, 1980.

The injection plan calls for the input of 30,000 - 34,000 B/D through the eight injection wells in the following sequence:

1. Alkaline injection. A mixture of 0.4% sodium orthosilicate (sodium hydroxide and sodium silicate) in softened fresh water containing 0.75-1.00% salt will be injected. The alkaline concentration for the later part of the slug may be varied depending on the field results. In any event the total amount of alkali injected will be that in a 60 pore volume percent slug with 0.4% sodium orthosilicate. The slug's injection will extend beyond the DOE cost-incremental revenue sharing period which ends September 30, 1981.

2. Postflushing with soft fresh water with 0.75-1.00% salt.

3. Resumption of normal injection of field produced water.

II. SUMMARY OF PROGRESS 6-1-80 THRU 4-30-81

A. Injection Operations & System Maintenance

Alkaline injection continued and is detailed in Table 1. Because of the divalent ion floc formed when the concentrated salt brine is added to the soft water-alkaline solution, injection of soft water with only alkali was continued thru August 13. Since no viable short-term solution for the floc problem had been found and because the salt was felt essential to the process in the reservoir, alternating weeks of

injection of soft water with alkali and with salt were begun at that point. In order to maintain a composite content of 0.75% salt and 0.4% sodium orthosilicate, during the weeks of injection of each of the different agents, their concentration had to be twice the desired level. To achieve these higher concentrations, it was necessary to change the sodium silicate, sodium hydroxide and sodium chloride concentrate pumps to larger sized equipment. Also, higher pressure drops in the system required sizing up of the centrifugal transfer/charge pumps. The slug injection has been a smooth operation with few operating problems. A spacer of soft water with no chemicals is injected for four hours between the two slugs.

With the temporary removal of the salt, the subsequent weekly schedule for slug injection and three simple injector acid stimulation jobs, total injection rate improved substantially. After August, low injection rates resulted from well work, injection system repairs, water softener problems, oxygen stripping system restrictions and problems with the alkaline concentrate pumps. Two seal replacement jobs on the high pressure injection pump were required.

The alkaline input automation was never fully operational because of a series of problems. Facility work in addition to that noted above included installation of truck delivery area safety spill aprons for the alkaline material. Metering of the total injection stream was a problem; two replacements of the turbine meters were required. Recalibration of the sodium silicate and sodium hydroxide concentrate meters is scheduled.

The water softeners presented a series of problems. High pressure drops across the three units were experienced and various problems with the control valving of the system occurred. Repairs to valves and closer operational control eliminated some of these problems. In an attempt to eliminate hydrocarbon contamination of the water softener resin and reduce the pressure drop across the softeners, each unit was solvent washed. When this failed to decrease the pressure drop, each unit was subsequently entered and serviced. The resin in the primary vessels was found to be in poor condition, being caked and containing oil, siliceous material, bacterial residue and barium. The polisher vessel resin was found to be in reasonably good condition. All the primary vessel resin was replaced in two units and serviced in the third. This temporarily corrected the throughput (pressure) restriction, but resin replacement in the third unit is now planned.

Since the beginning of the preflush injection in 1979, a build-up of non solubles from the salt has occurred in the brine generation tanks. As a consequence, each tank was cleaned out during the year. The shut-off valve on the brine line into the main injection stream appeared to be leaking and causing poor water quality when the alkaline slug was being injected; another ball shut-off valve was installed.

II. A. (cont.)

The small temporary oxygen stripping system compressor on the MWD (fresh) water delivery system was a problem. Water input was restricted at times because of this and oxygen removal was not complete. A new larger permanent compressor was installed in February. This eliminated the inflow water restriction and reduced the oxygen content of the injection water.

B. Laboratory Tests

Figures 2 & 3 summarize the weekly water quality tests of the saline and alkaline injection slugs. For the soft water-salt fluid, the periods of high hardness correspond to the periods of water softener problems. For the alkaline solution the poor filterability (slope) tests are related to water softener problems or higher than background salt contents.

Corrosion rates were high while the small O_2 stripping system compressor was in operation. These decreased substantially when the larger permanent machine was installed. However, subsequent short term (1-week duration) checks indicated corrosion was high with the salt solution and lower when the orthosilicate was being input. Since overall corrosion rates were unacceptably high even with the O_2 stripping system operating properly, a decision was made to begin continuous treatment of both the alkaline and saline injection fluids with a cationic, surfactant type corrosion inhibitor. IFT tests indicated this material, in the low concentrations to be used, has no adverse effect on the crude-alkaline water system.

In an attempt to define and find a solution for the salt-alkali incompatibility, a series of laboratory tests were made. These indicated the soft domestic water being used was unstable bacteriologically over extended time periods; Arizona and Searles Lake salts had lower hardness than the solar dried Ocean Salt being used; sodium orthosilicate solutions were more incompatible with the brine than sodium hydroxide; the soft domestic water contained detrimental agents other than the calcium and magnesium; reducing the salt concentration reduced the plugging (precipitate) problem; and an anti-nucleation agent, NTA, EDTA, STPP or lignosulfonate dispersing agents, were in most cases not totally and economically effective in minimizing the plugging regardless of the salt type being used. Because of the indicated current unavailability of the two low hardness salts, only hardness precipitation-filtration or softening of the concentrated brine appeared feasible. Space and logistic problems mitigate against the precipitation-filtration approach. Two commercially available chelating resins showed considerable promise for softening of the saturated "soft water" brine.

Monthly samples of waters produced from the pilot area producers were obtained and tested for pH, hardness, silica and salinity. No evidence of premature alkaline breakthrough was noted. However, a gradual decline of the mineral content of the water from the producers nearest the injectors and wells B-705, B-706, B-707 and B-837 was evident.

II. B. (cont.)

Samples from observation wells to the east and west of the pilot area and B-631-IA to the south did not indicate communication or incompetence of the bounding faults. The oil gravity of B-710-A after redrilling increased substantially indicating that more of the zone was producing after the work. A new series of oil gravity samples showed a general decrease which is interpreted to indicate less production from the lower Ranger subzones.

Other than one final long term pulse test with tracers, the work at California State University, Long Beach is completed and was detailed in the 4th annual report. (Ref.9)

C. Reservoir Simulation

The core flood test results were critically examined and waterflood and alkaline flood relative permeability curves derived. These are shown in Figure 4. The lab tests also yielded a total alkaline consumption of 2.446 meq alkalinity/100 grams rock. Of this, 1.0 meq was determined to be short term or instantaneous consumption. The balance was the long term-rate dependent consumption. A maximum of 2.000 meq/100 grams for this was set. It was felt, lacking additional lab data, the increase of this consumption either would be initially rapid, with the rate of increase decreasing with time, or it would be constant with time. The two consumption curves resulting (expressed in engineering units) are shown in Figure 5.

The N-Hance model used incorporates three mechanisms of alkaline consumption: (1) Instantaneous rock consumption; (2) long term (rate dependent) consumption; (3) and divalent ion (in formation water) consumption.

With the core derived data, the model was used first to match selected core flood data, adjust the relative permeability curves to fit the grid size and then to simulate behavior in the Fo_1 and Fo_2 sand layer in the southeast of the pattern (Figure 1).

A waterflood prediction and 8 alkaline flood predictions were made. In seven of the alkaline cases, linear adjustment was made between the water and alkaline relative permeability curves depending on the active alkaline concentration in each cell (the two curves in Figure 4 denoted as caustic flood represent those for the maximum concentration being injected* and the waterflood curves are for 0% alkaline concentration). In the other alkaline case, the maximum relative permeability adjustment occurred when an active alkaline concentration of 0.01 weight percent alkali occurred in a cell.

Pertinent reservoir data and results are summarized in Tables 2, 3 and 4 and Figures 6,7 and 8. These indicate the results of the flood are dependent on the relative permeability adjustment mechanism presumed, the rate of alkaline consumption, the concentration of alkali and the total volume of the alkaline slug.

* Except for the variable concentration case where the maximum relative permeability adjustment occurred at a concentration of 0.4%.

II. C. (cont.)

While oil rate response is better for a more concentrated slug, less cumulative incremental oil is recovered (assuming equal amounts of alkali) because of the smaller size of the mobility controlled slug. Total alkaline consumption is dependent on the long term alkaline consumption used, being the same ultimately regardless of the injected alkaline concentration.

Simulation of the full pilot occurred. Because the recent increase in oil price justifies additional development, the area was regridded on a finer mesh and the history match, over a longer period, redone. A new base case waterflood prediction was made including the anticipated infill drilling. Two alkaline flood predictions were made under the same infill program. Both used 0.4% alkali and the accelerated long term consumption function. In one case the relative permeability adjustment was linearly dependent on concentration; in the other, the maximum adjustment was made when a 0.01% alkali concentration was reached.

The results are shown in Tables 5 and 6.

The results are disappointing from the standpoint of the amount of the incremental oil recovery. The increases occur late and their magnitude and location are dependent on the relative permeability adjustment mechanism utilized. Alkaline consumption of the area was very high.

D. Well Work

One observation injector located east of the Temple Avenue Fault (B-829-I) and one northern area producer (B-710) were redrilled. B-710 was redrilled to increase its low productivity and not for mechanical reasons. Wireline survey tools were recovered in one pattern area producer (B-114), a bridge plug to exclude a lower bad liner section was run in westerly observation well (A-303-A) and a full zone inner liner to re-establish sand control was run in northern area well B-106-A. North flank aquifer injector B-833-I was down at the end of the period awaiting major repair work or redrilling.

There was a total of 31 pump change/routine well servicing jobs. Nine of these were in the northern area, 8 in the pattern area, 4 in the southern area, 5 in westerly observation wells and 5 in easterly observation producers. Injectors B-107-I (Tbg. #2), B-119-IA and B-831-IB were acidized to remove the salt-alkali floc blockage. Observation well A-242-I and pattern area injectors B-709-I and B-828-IA were acidized to remove suspected tubing restrictions. B-110-IA had its flow controller for the Fo changed to improve the vertical injection distribution.

A total of 31 static pressure surveys were run -- 5 in the southern, 7 in the pattern, 5 in the northern, 9 in easterly observation wells and 5 in observation wells to the west. Two observation and one southern area producers had operating pressures taken. There were 9 wireline feeler surveys to check for fill. Water entry surveys were completed in 2 northern, 12 pattern, 3 southern and 1 easterly observation wells.

II. D. (cont.)

There was a total of 31 pump change/routine well servicing jobs. Nine of these were in the northern area, 8 in the pattern area, 4 in the southern area, 5 in westerly observation wells and 5 in easterly observation producers. Injectors B-107-I (Tbg. #2), B-119-IA and B-831-IB were acidized to remove the salt-alkali floc blockage. Observation well A-242-I and pattern area injectors B-709-I and B-828-IA were acidized to remove suspected tubing restrictions. B-110-IA had its flow controller for the Fo changed to improve the vertical injection distribution.

A total of 31 static pressure surveys were run -- 5 in the southern, 7 in the pattern, 5 in the northern, 9 in easterly observation wells and 5 in observation wells to the west. Two observation and one southern area producers had operating pressures taken. There were 9 wireline feeler surveys to check for fill. Water entry surveys were completed in 2 northern, 12 pattern, 3 southern and 1 easterly observation wells. Twenty-four spinner surveys were obtained. None of these various surveys showed abnormalities that could be attributed to the alkaline injection.

E. Performance

Figures 9, 10 and 11 illustrate the performance of the northern, southern and pattern areas. For the pattern, the injection rate increased as the salt-alkali plugging was overcome. The June-July, 1980 increase in oil rate and decrease in WOR is a result of well tester recalibration. The gross and net rates dropped starting in January due to well downtime and servicing operations. By April, 1981, the rates were back to essentially normal levels. The WOR trend was gradually increasing throughout the period.

In the northern area, the major increase in gross and net rates and decrease in WOR in late 1980 result from the completion of the high volume, low cut redrill of B-710. The other fluctuations are a result of well downtime and servicing, especially in the row of wells offset to the injection.

For the southern area, the WOR trend was generally increasing. The dip in rates in December, January and February is due to well downtime and servicing with rates being restored in March and April. Since the oil rate came up substantially in April, the WOR showed a sharp drop back to what should be a more typical value.

No change in any of the areas attributable to alkaline injection was noted.

F. Miscellaneous

Pre-purchase of the alkaline chemicals occurred during the year. Total recoupments under the tertiary incentive program for the pattern area during the report period were $10,631,968.75 with D.O.E. being credited with $282,482.49. As a result of the prior major well work in the pattern area, additional oil was produced there. During the 11-month period covered by this report, this amounted to 48,479 bbl. with a total value of $1,235,897.59; D.O.E.'s 40% share of this was $494,359.03.

REFERENCES

1. "Improved Secondary Oil Recovery by Controlled Waterflooding Pilot Demonstration; Wilmington Field, Long Beach Unit, Ranger Zone, Fault Block VIII-Part II, Technical Proposal." Prepared for ERDA by the Department of Oil Properties and THUMS Long Beach Company, E(49-18)-2296, April 23, 1976.

2. Carmichael, J. D., and Alpay, O. A.,: "Caustic Waterflooding Demonstration Project, Ranger Zone, Long Beach Unit, Wilmington Field, California." Transactions of the Third ERDA Symposium on Enlhanced Oil and Gas Recovery & Improved Drilling Methods, Tulsa, Oklahoma, August 30 - September 1, 1977. Pg. B-2/1-18.

3. "Caustic Waterflooding Demonstration Project, Ranger Zone, Long Beach Unit, Wilmington Field, Califonia. Annual Report for the Period October, 1976 - June, 1977." Report SAN/1396-1. Prepared for DOE by the City of Long Beach, Department of Oil Properties and THUMS Long Beach Company under Contract No. EF-77-C-03-1396.

4. Carmichael. J. D., Mayer, E. H., Alpay, O. A., Boyle, P. R.: "Caustic Waterflooding Demonstration Project, Ranger Zone, Long Beach Unit, Wilmington Field, California (Covering Period June, 1977 - April, 1978)." Transactions of the Fourth DOE Symposium on Enhanced Oil and Gas Recovery & Improved Drilling Methods; Tulsa, Oklahoma,August 29 - 31, 1978. Pg. B-9/1-14.

5. "Caustic Waterflooding Demonstration Project, Ranger Zone, Long Beach Unit, Wilmington Field, California. Second Annual Report, July, 1977 - May, 1978." Report SAN/1396-2. Prepared for DOE by City of Long Beach, Department of Oil Properties and THUMS Long Beach Company under Contract No. EF-77-C-03-1396.

6. Carmichael, J. D., Mayer, E. H., Alpay, O. A., Boyle, P. R., "Caustic Waterflooding Demonstration Project, Ranger Zone, Long Beach Unit, Wilmington Field, California (Covering Period May, 1978 - April, 1979)." Transactions of the Fifth Annual DOE Symposium on Enhanced Oil and Gas Recovery & Improved Drilling Technology; Tulsa, Oklahoma, August 23 - 24, 1979. Pg. C-3/1-14.

7. "Caustic Waterflooding Demonstration Project, Ranger Zone, Long Beach Unit, Wilmington Field, California. Third Annual Report, June, 1978 - May, 1979." Report SAN/1396-3. Prepared for DOE by City of Long Beach Department of Oil Properties and THUMS Long Beach Company under Contract No. EF-77-C-03-1396.

8. Carmichael, J. D., Mayer, E. H., "Alkaline Waterflooding Demonstration Project, Ranger Zone, Long Beach Unit, Wilmington Field, California (June, 1979 - May, 1980) Enhanced Oil Recovery - Chemical Flooding - Annual Report Fiscal Year 1980, DOE/BETC/IC 80-3, Vol. 2, F-5/1-8.

9. "Alkaline Waterflooding Demonstration Project, Ranger Zone, Long Beach Unit, Wilmington Field, California. Fourth Annual Report, June 1979 - May, 1980." Report DOE/ET/12047-32 (3 Volumes). Prepared for DOE by City of Long Beach, Department of Oil Properties and THUMS Long Beach Company under Contract DE-AC03-76ET12407.

TABLE 1

RANGER FAULT BLOCK VII PILOT
ALKALINE INJECTION STATISTICS
COMPOSITE COMPOSITION - WEIGHT%

MONTH/YEAR	RATE BBL/CALENDAR DAY	NO. DAYS ALKALINE INPUT	NO. DAYS SALT INPUT	SALT %	SODIUM ORTHOSILICATE %	SODIUM SILICATE %	SODIUM HYDROXIDE %	SiO_2 %	REMARKS
June, 1980	25,214	30	0	---	0.5376	0.2741	0.3467	0.1688	
July, 1980	29,625	31	0	---	0.4253	0.2256	0.2628	0.1389	
Aug. 1-13, 1980	28,956	13	0	---	0.5406	0.3296	0.2776	0.2030	Total fresh-alkali injection 5-13 thru 8-13 2,075,360 bbl.
Aug.14-31, 1980	30,175	7	11	0.8305	0.2609	0.1689	0.1211	0.1040	Start of alternating 1 week slug injection
September, 1980	32,666	14	16	0.6985	0.3506	0.2155	0.1777	0.1327	
October, 1980	32,424	16	15	0.5827	0.2759	0.1494	0.1665	0.0920	
November, 1980	30,995	16	14	0.5436	0.7678	0.4554	0.4110	0.2804	
December, 1980	29,208	11	20	0.8337	0.2937	0.1745	0.1568	0.1074	
January, 1981	28,319	17	14	0.5906	0.5159	0.3232	0.2536	0.1990	
February, 1981	31,555	14	14	0.6700	0.3574	0.1769	0.2375	0.1089	
March, 1981	32,884	17	14	0.6223	0.3760	0.1853	0.2509	0.1141	
April, 1981	30,759	15	15	0.7539	0.4158	0.2178	0.2605	0.1341	

Comparison of actual deliveries and metered chemical injected Volumes for 1980 (March - December) indicate the sodium silicate contents calculated above are high by 31.50% and sodium hydroxide high by 22.45% For 4 months of 1981 (January - April) comparison of deliveries and metered chemical volumes indicate the sodium silicate contents calculated above are high by 17.88% and sodium hydroxide high by 2.24%.

TABLE 2

ALKALINE SLUG OPTIMIZATION STUDIES

BASE DATA FOR STUDY AREA

(Includes B-701, B-711, B-712, B-838, B-831-I, B-836-I)

Reservoir Pore Volume of 4 Producers, 2 Injectors Fo_1+Fo_2 Area (PV)	1,879,000 Res. Bbl.
Initial Oil in Place (TOIP)	1,231,000 ST. Bbl.
Waterflood Oil Recovery:	
To 5-01-79	562,000 ST. Bbl.
% TOIP	45.65
@ PV	29.91
Waterflood Oil Recovery 5-01-79	
To economic limit of 150 WOR (11-1-85)	84,800 ST. Bbl.
Cumulative Waterflood Oil Recovery	646,800 ST. Bbl.
% TOIP	52.54
% PV	34.42
Injection Rate 5-01-79 on to End (7.5 PV%/Yr.±).	4,806 B/D
Start of Alkaline Injection 5-24-80	
Preflush Injection - 1.0% Salt-Soft Water Solution (390 Days)	1,874,340 ST. Bbl.
% PV	99.75

Updated 5-1-81

TABLE 3

ALKALINE SLUG OPTIMIZATION STUDIES

OIL RECOVERY DATA

5-1-79 to Economic Limit

Alkaline Slug Description	Long Term Consumption	Oil Recovery MST Bbl.	Economic Limit (150 WOR) Date	Incremental Oil Recovery Above Water Flood M Bbl.	% TOIP	% PV
Waterflood	-	84.8	11-01-85	-	-	-
Pro-Rated Alkaline Relative Permeability Adjustment						
60 PV % 0.4% Alkali, 1.0% Salt	Accelerated Rate	174.0	7-03-89	89.2	7.25	4.75
32 PV % 0.8% Alkali, 1.0% Salt	Accelerated Rate	137.9	9-01-86	53.1	4.31	2.83
32 PV % 0.8% Alkali, 1% Salt	Constant Rate	143.5	6-05-86	58.7	4.77	3.12
32 PV % 0.8% Alkali, 1% Salt	None	159.8	7-01-86	75.0	6.09	3.99
24 PV % 1.0% Alkali, 1% Salt	Accelerated Rate	122.1	12-06-85	37.3	3.03	1.99
24 PV % 1.0% Alkali, 1% Salt	None	142.3	10-21-85	57.5	4.67	3.06
48.6 PV % Variable Alkali Content* 1 % Salt	Accelerated Rate	162.0	2-16-88	77.5	6.30	4.12
Minimum Threshold Alkaline Relative Permeability Adjustment						
60 PV % 0.4% Alkali 1.0% Salt	Accelerated Rate	226.0	5-28-90	141.2	11.47	7.51

* 0.4% orthosilicate for first 1.5 years, 1.0% for next 1.0 year, 0.8% for 1.0 year, 0.4% for 1.0% year and 0.2% for 2.0% years.

Updated 5-1-81

TABLE 4

ALKALINE SLUG OPTIMIZATION STUDIES

PREFLUSH, CHEMICAL SLUG & POST FLUSH DATA

	Size	End of Injection
Preflush Size	100 PV %	-
Chemical Size		
0.4% Alkali Cases	748 PV %	5-25-88
0.8% Alkali Cases	398 PV %	8-29-84
1.0% Alkali Cases	299 PV %	8-05-83
Variable Concentration Alkali Case	606 PV %	11-20-86
Post Flush (End Alkaline Slug to Economic Limit)		Size
Pro-Rated Alkaline Relative Permeability Adjustment		
0.4% Alkali, Accelerated Long Term Consumption Case		103 PV %
0.8% Alkali, Accelerated Long Term Consumption Case		187 PV %
0.8% Alkali, Constant Long Term Consumption Case		165 PV %
0.8% Alkali, No Long Term Consumption Case		170 PV %
1.0% Alkali, Accelerated Long Term Consumption Case		218 PV %
1.0% Alkali, No Long Term Consumption Case		206 PV %
Variable Alkali Concentration, Accelerated Long Term Consumption Case		116 PV %
Minimum Threshold Alkaline Relative Permeability Adjustment		
0.4% Alkali, Accelerated Long Term Consumption Case		188 PV %

TABLE 5

COMPARISON OF PILOT AREA BASE WATER FLOOD & ALKALINE FLOOD SIMULATION #1
(CONCENTRATION PRORATED ALKALINE RELATIVE PERMEABILITY ADJUSTMENT)
PREDICTIONS AT DECEMBER 31, 1994

Area	Subzone	Alkaline Flood BO/D	Waterflood BO/D	△ BO/D	Alkaline Flood Cum. Oil - M Bbl.	Waterflood Cum. Oil M Bbl.	△ M Bbl.	Alkaline Flood BW/D	Water-flood BW/D	△ BW/D	Alkaline Flood Cum. Water M Bbl.	Waterflood Cum. Water M Bbl.	△ M Bbl.
Entire Pilot Area	All	1,665	1,471	+194	40,622	39,891	+731	36,241	34,888	+1,353	239,503	232,809	+6,694
Pattern Area	Fo_1+Fo_2	87	83	+ 4	4,164	4,059	+105	6,909	7,013	- 104	63,230	62,253	+ 977
Pattern Area	Fo_3	12	10	+ 2	333	331	+ 2	0	0	0	14	13	+ 1
Pattern Area	F	77	45	+ 32	2,990	2,871	+119	3,028	2,644	+ 384	20,549	19,396	+1,153
Pattern Area	H	74	48	+ 26	1,751	1,742	+ 9	1,221	1,225	- 4	8,876	8,808	+ 68
Pattern Area	X	74	70	+ 4	3,580	3,560	+ 20	2,015	1,989	+ 26	15,925	15,659	+ 266
Pattern Area	G	54	55	- 1	1,791	1,787	+ 4	743	715	+ 28	5,250	5,147	+ 103
Pattern Area	G_4	29	27	+ 2	706	699	+ 7	617	624	- 7	2,923	2,891	+ 32
Northern Area	Fo_1+Fo_2	175	145	+ 30	3,740	3,691	+ 49	6,991	6,413	+ 578	35,411	34,515	+ 896
Northern Area	Fo_3	17	16	+ 1	226	223	+ 3	114	107	+ 7	244	240	+ 4
Northern Area	F	330	215	+115	6,102	5,769	+333	5,702	4,802	+ 900	22,157	19,814	+2,343
Northern Area	H	127	129	- 2	1,746	1,759	- 13	761	810	- 49	3,356	3,349	+ 7
Northern Area	X	73	72	+ 1	542	544	- 2	748	790	- 42	3,815	3,823	- 8
Southern Area	$Fo_1+Fo_2+Fo_3$	213	204	+ 9	4,958	4,908	+ 50	4,697	4,754	- 57	38,545	37,884	+ 661
Southern Area	F + H	143	147	- 4	3,780	3,760	+ 20	1,950	2,238	- 288	13,706	13,815	- 109
Southern Area	X → G_4	204	204	0	4,214	4,187	+ 27	743	766	- 23	5,412	5,165	+ 247

TABLE 6

COMPARISON OF PILOT AREA BASE WATER FLOOD & ALKALINE FLOOD SIMULATION #2
(MINIMUM THRESHOLD ALKALINE RELATIVE PERMEABILITY ADJUSTMENT)
PREDICTIONS AT DECEMBER 31, 1994

Area	Subzone	Alkaline Flood BO/D	Waterflood BO/D	△ BO/D	Alkaline Flood Cum. Oil - M Bbl.	Waterflood Cum. Oil M Bbl.	△ M Bbl.	Alkaline Flood BW/D	Water-flood BW/D	△ BW/D	Alkaline Flood Cum. Water M Bbl.	Waterflood Cum. Water M Bbl.	△ M Bbl.
Entire Pilot Area	All	1,711	1,471	+ 240	41,156	39,891	+1,265	35,737	34,888	+ 849	239,588	232,809	6,779
Pattern Area	Fo_1+Fo_2	78	83	- 5	4,425	4,059	+ 266	6,703	7,013	- 310	65,648	62,253	+3,395
Pattern Area	Fo_3	12	10	+ 2	333	331	+ 2	0	0	0	14	13	+ 1
Pattern Area	F	78	45	+ 33	3,048	2,871	+ 177	3,066	2,644	+ 422	20,545	19,396	+1,149
Pattern Area	H	51	48	+ 3	1,762	1,742	+ 20	1,211	1,225	- 14	8,845	8,808	+ 37
Pattern Area	X	78	70	+ 8	3,622	3,560	+ 62	2,054	1,989	+ 65	15,703	15,659	+ 44
Pattern Area	G	54	55	- 1	1,795	1,787	+ 8	727	715	+ 12	5,249	5,147	+ 102
Pattern Area	G_4	29	27	+ 2	715	699	+ 16	613	624	- 11	2,912	2,891	+ 21
Northern Area	Fo_1+Fo_2	175	145	+ 30	3,720	3,691	+ 29	6,528	6,413	+ 115	32,114	34,515	-2,401
Northern Area	Fo_3	17	16	+ 1	226	223	+ 3	110	107	+ 3	245	240	+ 5
Northern Area	F	338	215	+ 123	6,123	5,769	+ 354	5,755	4,802	+ 953	21,979	19,814	+2,165
Northern Area	H	131	129	+ 2	1,752	1,759	- 7	776	810	- 34	3,308	3,349	- 41
Northern Area	X	72	72	0	542	544	- 2	765	790	- 25	3,804	3,823	- 19
Southern Area	$Fo_1+Fo_2+Fo_3$	247	204	+ 43	5,046	4,908	+ 138	4,793	4,754	+ 39	40,155	37,884	+2,271
Southern Area	F + H	146	147	- 7	3,814	3,760	+ 54	1,911	2,238	- 327	13,612	13,815	- 203
Southern Area	X → G_4	204	204	0	4,227	4,187	+ 40	723	766	- 43	5,454	5,165	+ 289

FIG. 1

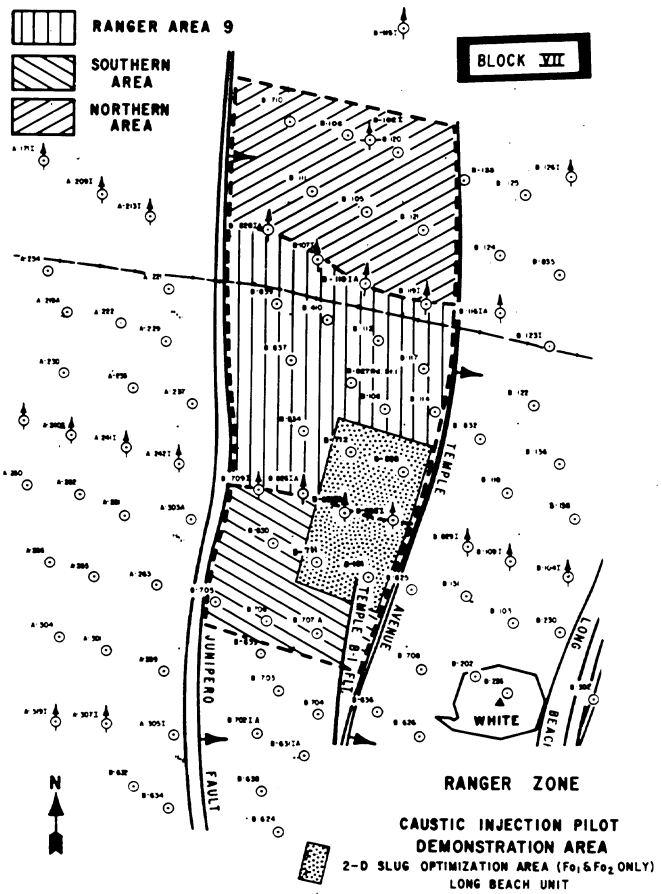

FIG. 2

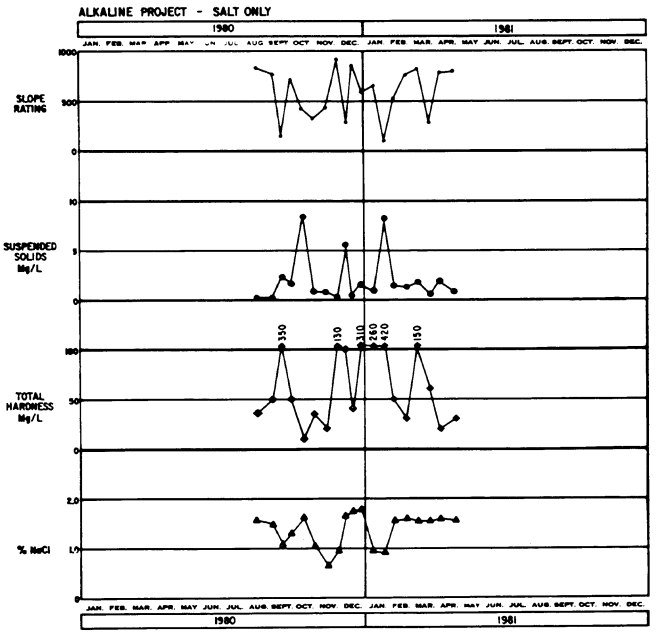

FIG. 3

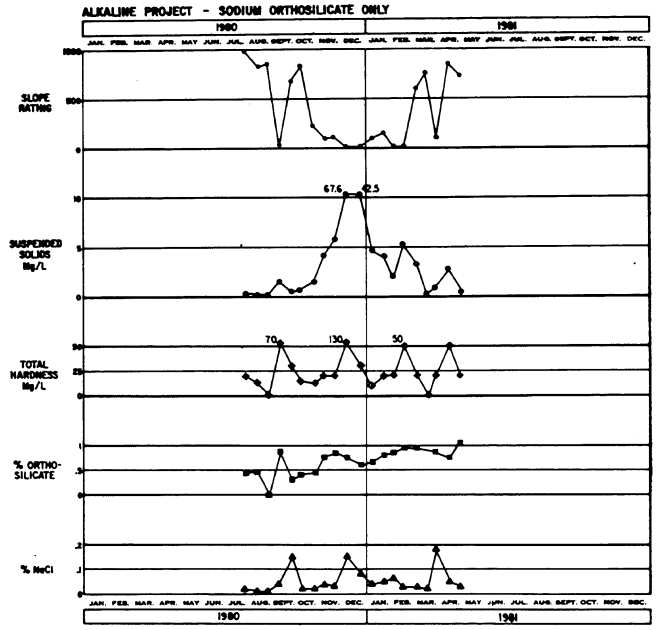

RELATIVE PERMEABILITY CURVES FIG. 4
Slug Size Optimization Study

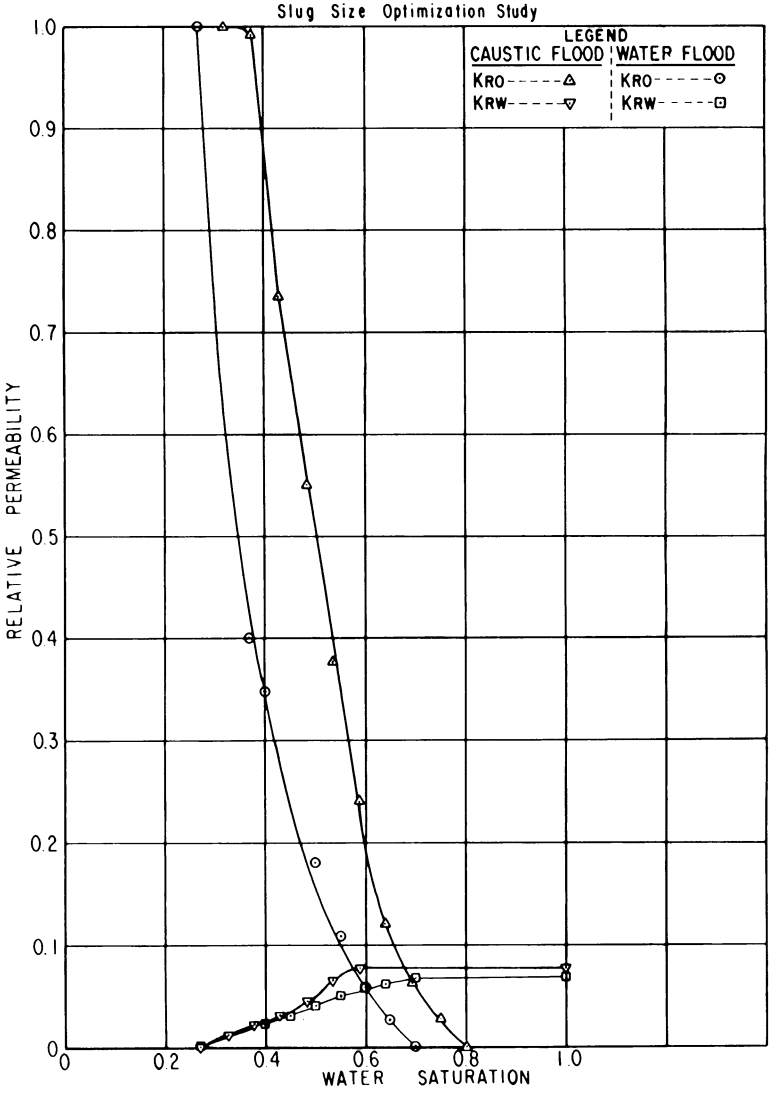

FIG. 5

LONG TERM ALKALINE CONSUMPTION CURVES
Slug Size Optimization Study

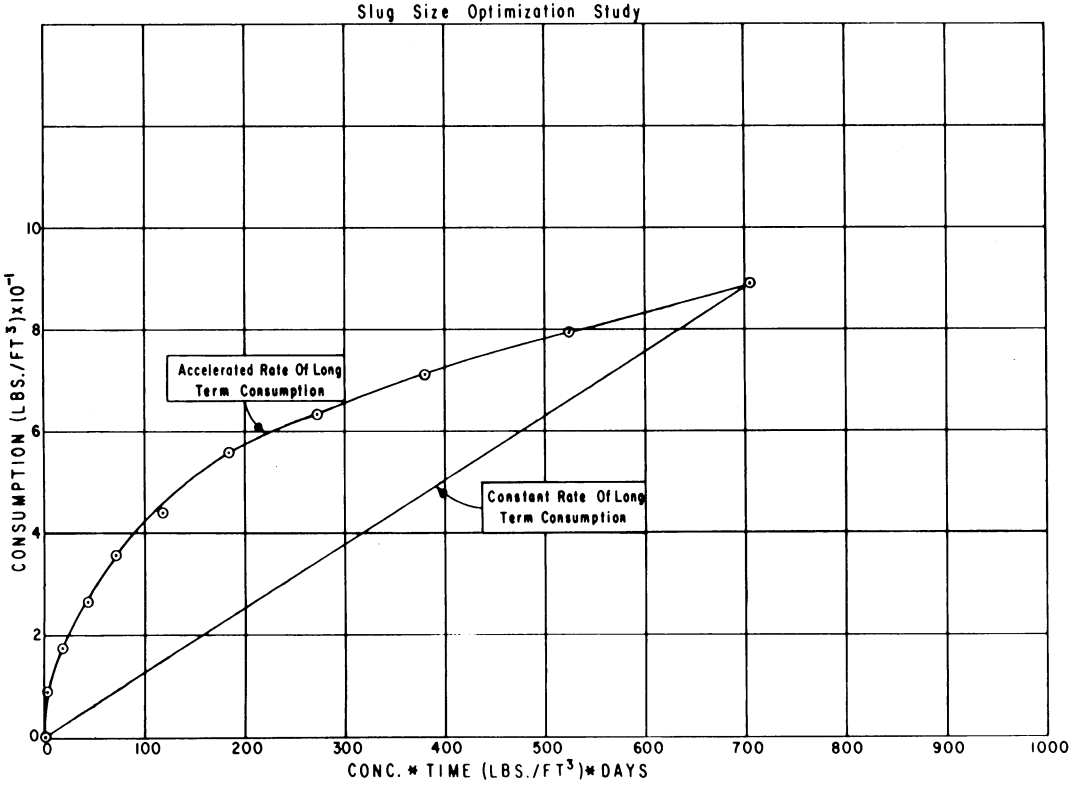

FIG. 6

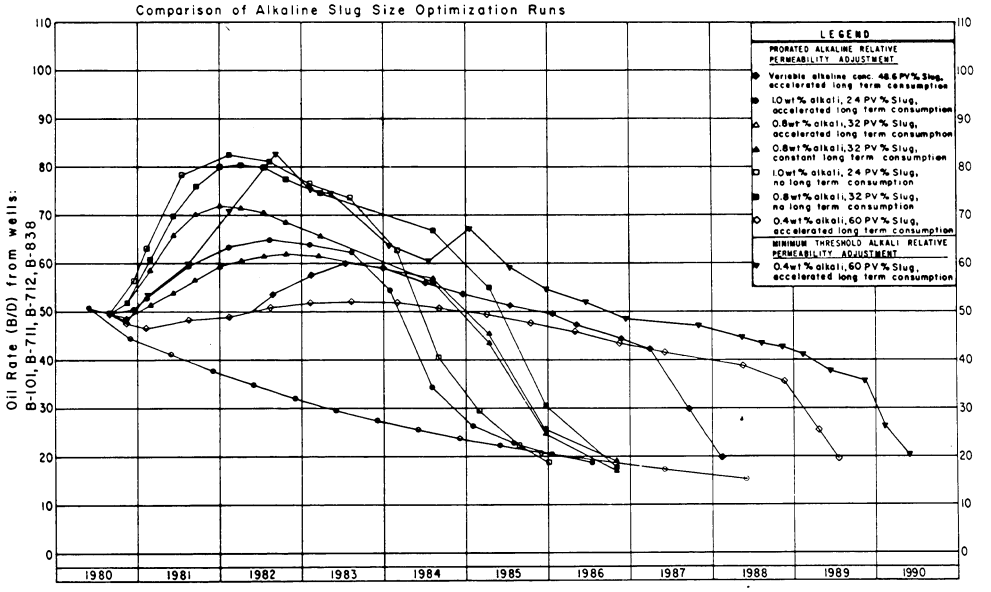

FIG. 7

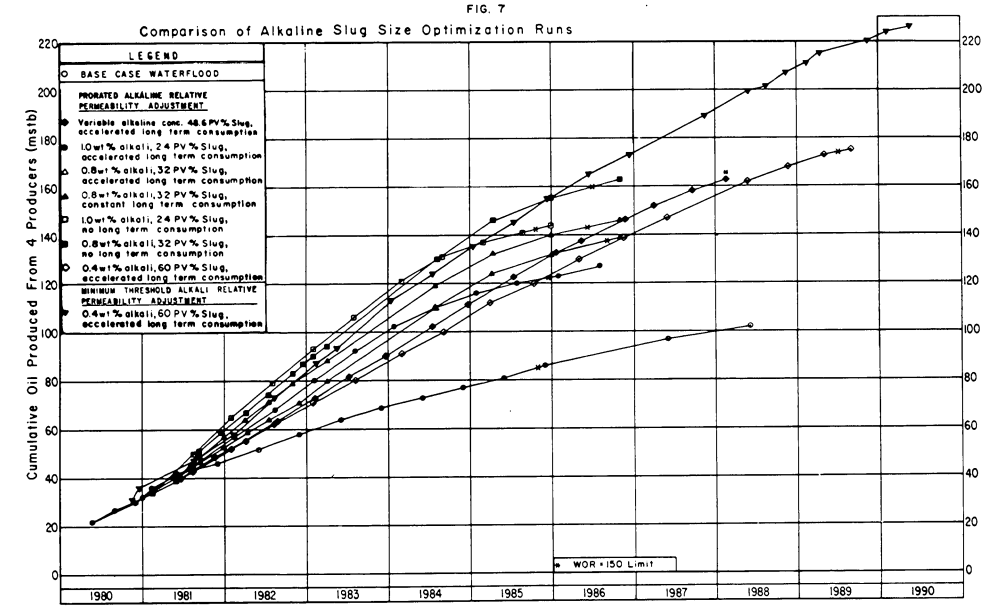

FIG. 8

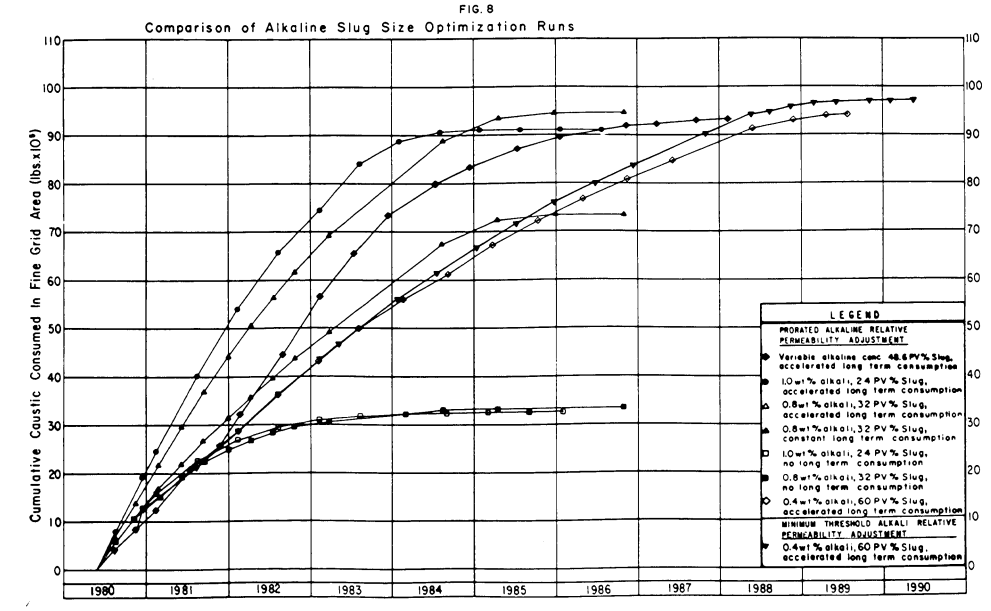

FIG. 9

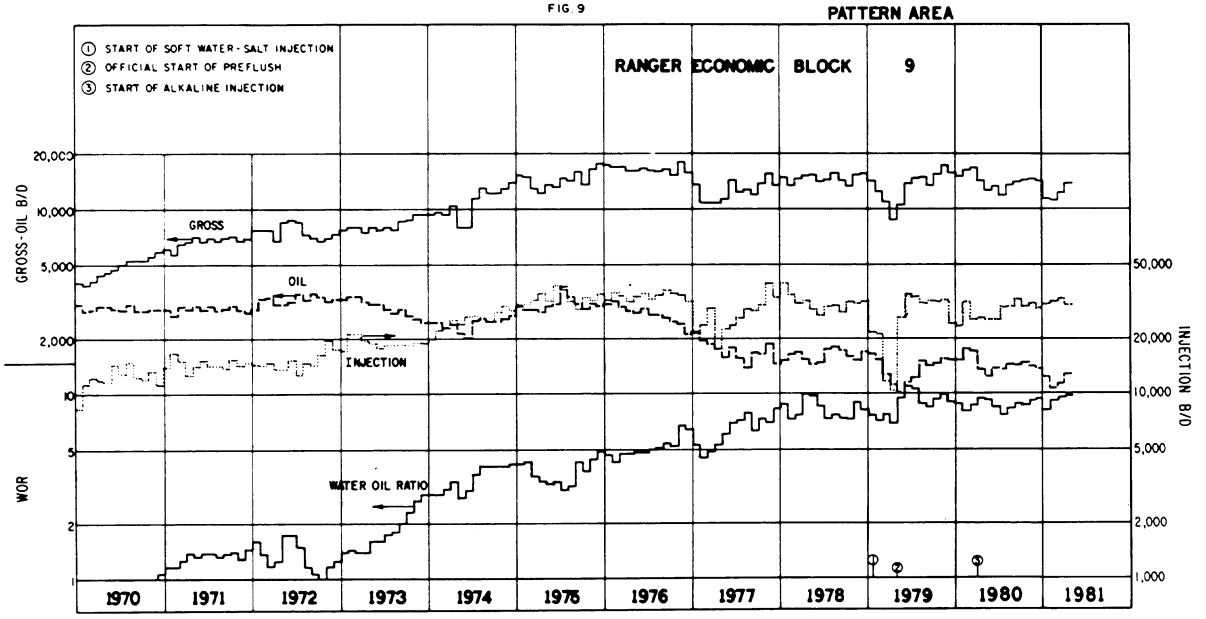

FIG. 10

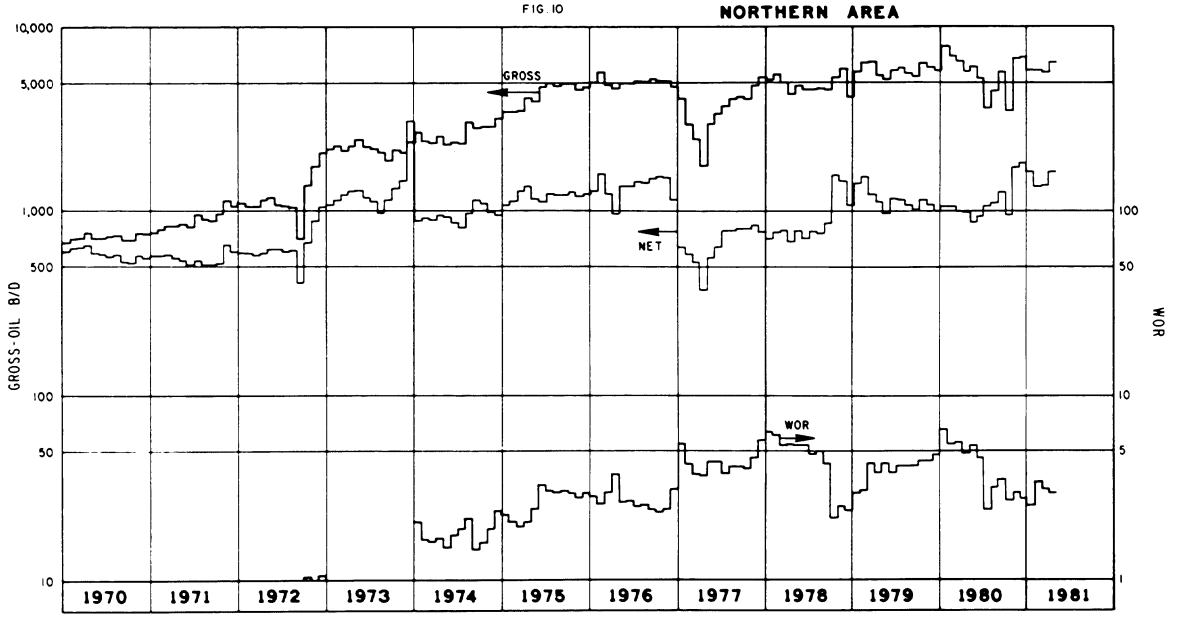

FIG. 11

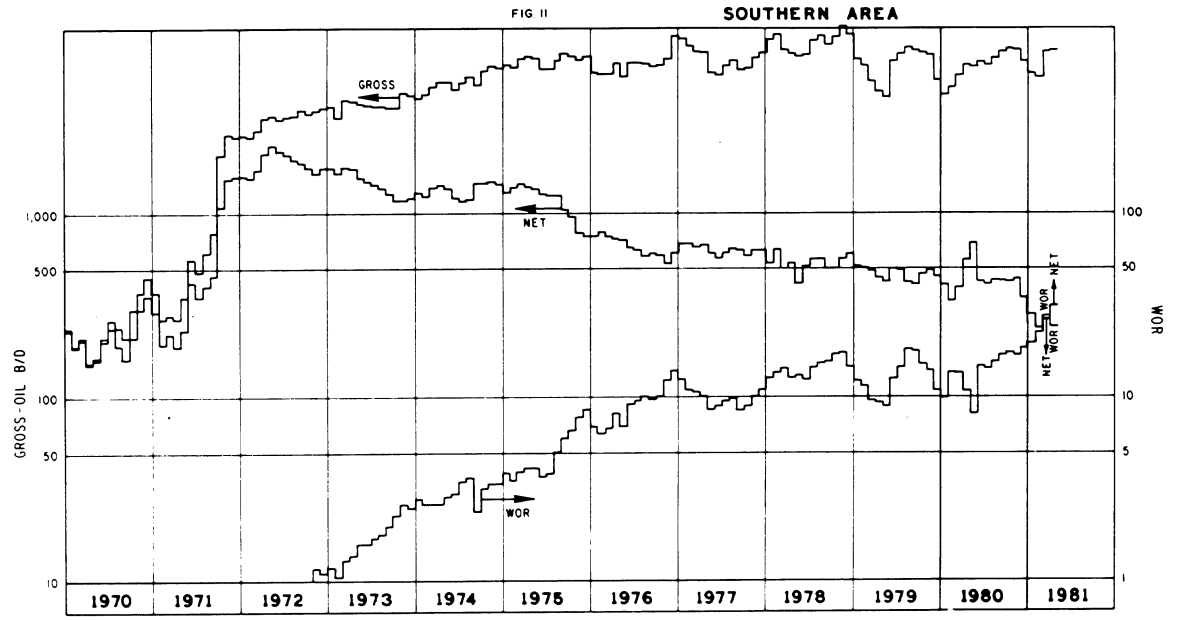

CARBON DIOXIDE FOR THE RECOVERY OF CRUDE OIL

by

T.M. Doscher, R. Oyekan, and S. Gharib
Department of Petroleum Engineering
University of Southern California
Los Angeles, California 90007

ABSTRACT

The study of the use of carbon dioxide for the recovery of residual crude oil has continued into the third year. The most recent studies on displacement of residual oil in the scaled physical models have centered on the use of viscous aqueous solutions to follow slugs of carbon dioxide. The results indicate a positive benefit in the use of these viscous solutions only when less than an optimum slug of carbon dioxide is injected.

Solubility and swelling tests on crude oils of a gravity less than the 45° Appalachian crude, which had already been studied in great detail, have also been undertaken so that eventually these characteristics can be correlated with displacement efficiency. A marked reduction in solubility of the carbon dioxide and swelling of the crude has been observed when working with 20° crudes from south Texas fields.

Following up on previous conclusions that the effect of carbon dioxide in mobilizing and displacing residual crude oil is primarily due to solution and swelling, a search was made for other gases that would have a comparable effect in order to develop further support for the hypothesis. Literature studies indicated that nitrous oxide had many similar molecular and physical properties to those of carbon dioxide; including solubility in organic fluids. Initial studies have now proven that nitrous oxide does displace residual crude oil in the scaled models even somewhat more efficiently than does carbon dioxide. However, it does not appear that nitrous oxide is a cost effective substitute for carbon dioxide.

HISTORY OF PROJECT

Contract EY-76-S-03-0113 was initiated August 28, 1978 to be completed in May 1981 at a cost of $387,890. A report covering work through 1980 was presented at the DOE/SPE Meeting on Enhanced Oil Recovery in Tulsa, April 5-8, 1981.

Prepared for DOE under Contract EY-76-S-03-0113.

II. INTRODUCTION

Earlier work on the use of scaled physical models for the study of the recovery of residual crude oil by the injection of carbon dioxide have led to the following conclusions:

1. The mobilization and displacement of residual crude oil by carbon dioxide occurs as a result of the following sequential phemomena: a) the displacement of the mobile water, b) the solution of the carbon dioxide in the residual crude, c) the swelling of the crude and restoration of mobility to the erstwhile non-mobile phase, and d) the displacement of the solution of carbon dioxide in crude oil by dense carbon dioxide.

2. Calculations based on a perfect, sequential series of such phenomena lead to the conclusion that the minimum quanitity of continuously injected carbon dioxide required to recover a barrel of residual crude oil will be no less than 6000 SCF/B for a high residual saturation of a crude that has a swelling factor of 1.5 or more, but more likely of the order 10,000 SCF/B for crudes at a residual saturation of less than 30 p.v.% and displaying a more modest swelling factor.

3. Experiments have indeed shown that the actual ratios observed in displacing residual crude oil are far in excess of the minimum, "theoretical" values referred to above; 20,000 to 30,000 SCF/B have been shown to be required to displace 20 to 30 p.v.% residuals from low permeability, uniform sandstone prototypical reservoirs. These ratios are in accord with most of the results that have been reported for field pilot operations and demonstrtion projects.

4. Displacement efficiency has been shown to increase steadily with pressure up to that pressure at which the change in density of carbon dioxide with pressure approaches a zero value. The effect of an increasing temperature on decreasing the density and solubility of carbon dioxide in crude oil, and hence in decreaseing the efficiency with which crude oil is recovered, can be compensated for by an appropriate increase in pressure. The so-called "minimum miscibility pressure" is, in the light of these results, seen to be the "(maximum) pressure required to maximize the displacement efficiency" at any given temperature.

5. There is an optimum size of carbon dioxide slug, followed by a chase water flood, that results in a maximum recovery of residual oil when the total fluid injected is limited to, say, one pore volume. The process appears to comprise solution and swelling of the crude such that the saturation of the oil phase exceeds the minimum required for restoration of mobility, and then the displacement of the mobile oil by the water flood. The subsequently reached residual saturation appears to be somewhat less than the original residual saturation, perhaps because of the lower viscosity of the oil phase diluted with carbon dioxide. However, the chief factor leading to the an increased recovery of the crude is the fact that the residual oil phase saturation is now crude

oil diluted with carbon dioxide.

A slug larger than the optimum results in the establishment of a free carbon dioxide saturation in an interval throughout the system which then acts as a thief zone. As a result of the high transmissibility of the injected carbon dioxide through this interval, the efficiency of the parallel displaement of crude is seriously reduced. In a uniform reservoir, the free carbon dioxide saturation is established at the top of the reservoir as a result of gravity segregation.

6. Because of the high mobility of the carbon dioxide it fingers throughout the reservoir very rapidly. This, together with its low molecular weight results in the establishment of a saturation of carbon dioxide which exceeds 0.6 mol fraction. Above this saturation, the oil-carbon dioxide system is comprised of two phases. At low pressures one of the phases is a dilute solution of carbon dioxide in crude and the second phase is low density carbon dioxide. At elevated pressures (say, above 1000 psi) the two phases are a 60 mol percent solution of carbon dioxide in crude oil and a phase which is primarily dense carbon dioxide containing some if not all of the low molecular weight components of the crude oil. However, in either case the weight fraction of the crude or its components dissolved in the rich carbon dioxide phase is very low. Therefore, additional recovery of crude oil after signficant break through of carbon dioxide to the producing well occurs will be a very slow process involving the throughput of very large quantities of carbon dioxide.

Economic recovery of residual crude appears to be that crude oil which mixes with the leading edge of the carbon dioxide fingers. Here, the pressure is high, the mol fraction of carbon dioxide is below 0.6 mol fraction, and the carbon dioxide-crude oil system comprises only a single phase.

7. Because of the high mobility and low density of carbon dioxide in comparison to the mobile water saturating a reservoir following a water flood, high injection rates and close spacing are necessary to secure good results in carbon dioxide flooding.

III. THE EFFECT OF HIGHER VISCOSITY CHASE WATER ON THE EFFICIENCY OF THE CARBON DIOXIDE SLUG.

Figure 1 shows the results of two experiments in which a less than optimum slug of carbon dioxide was used prior to the injection of chase water. It is apparent that a slight increase in the recovery of the residual oil results from the substitution of a viscous chase fluid, 10 cps. water for the ordinary 1 cp. water. Repeated experiments have shown that this small, but significant increment in recovery is real. Figure 2 shows the slight difference in the resulting ratio of injected carbon dioxide to produced crude oil that results from the small difference in total recovery.

Virtually no difference in recovery however results from the use of the viscous chase fluid if an optimum slug of carbon dioxide was injected. At this time there is no apparent explanation for the observed phenomena, nor any concept as to how to extrapolate the observation to a an economically useful improvement in the process. Certainly, the small increse in recovery that is shown is not sufficient to offset the cost of increasing the viscosity of the chase fluid.

It should be reemphasized, however, that as shown by the data plotted in Figure 1, the use of a slug of carbon dioxide followed by water drastically lowers the carbon dioxide requirements to recover a barrel of crude oil in these uniform, low permeability prototype reservoirs. (The description of the prototype and the models is described in detail in previous reports, see for example SPE/DOE 9787, Tulsa, Oklahoma, April 1981.)

IV. COMPARATIVE STUDIES OF SOLUBILITY AND SWELLING OF VARIOUS CRUDES.

Since solution of the carbon dioxide and consequent swelling of the crude oil have been identified in these studies as being the major factors in effecting the recovery of resdiual crude oil, a series of studies has been begun to compare the swelling of various crudes from reservoirs in the United States. It is anticipated that the funds still available to the project will permit the correlation of the observed swelling of the crudes with the efficiency with which they are displaced in the scaled models.

To illustrate the differences in solubility and swelling that do occur between different crudes, Figures 4 and 5 show the observed differences in solution and swelling of a 45° Appalachian crude and a 20.8° south Texas crude oil. It is to be noted that although the solubility of the carbon dioxide in the high gravity crude is almost

twice that in the lower gravity crude, the swelling factor is proportionately higher per dissolved mass of carbon dioxide in the latter. This phenomenon is reflected in a decrease in the density of the solution as compared to that of the low gravity oil whereas the density of the solution of carbon dioxide in the high gravity oil increases in comparison to that of the oil itself.

VI. THE EQUIVALENCE OF NITROUS OXIDE TO CARBON DIOXIDE

A study of the literature on the physico-chemical properties of gases, to be documented later, has indicated the equivalence of nitrous oxide to carbon dioxide; particularly with respect to its solubility in organic liquids. Pursuant to the conclusion that solution and swelling are the chief factors affecting the mobilization and displacement of residual crude oil, it was expected that nitrous oxide would perform comparably to carbon dioxide in displacing residual crude oil. The results of the experiment shown in Figure 6 indicates the hypothesis is confirmed.

Some additional work will be done with nitrous oxide, however preliminary studies of its cost and availability indicate that it is not a cost effective substitute for carbon dioxide.

VII. CONCLUSIONS

Continued studies on the recovery of residual crude oil by carbon dioxide have further confirmed that the controlling mechanism is the solution and subsequent swelling of the crude oil followed by its displacement by free carbon dioxide and/or water. Nitrous oxide, which has similar solution properties to carbon dioxide is equally effective in the recovery of residual crude oil.

The quantity of carbon dioxide required to recover a barrel of residual crude oil, when the gas is injected continuously, is far too high for the process to be considered economic unless the carbon dioxide can be made available at a cost not much above one dollar per thousand cubic feet. Alternate schemes for achieving economic usage of the carbon dioxide will depend on recycling a large fraction of the ultimate amount of carbon dioxide that is injected, or using a near optimum sized slug of carbon dioxide followed by water injection.

At this time it would appear that the lower solubility of carbon dioxide in low gravity and hot crudes, and the consequently lowered swelling of such fluids, will further restrict the economic use of carbon dioxide to high gravity residual oil saturations.

FIGURE 1

COMPARISON OF OIL RECOVERY WITH DIFFERENT VISCOSITIES

OF CHASE WATER CO2 SLUG SIZE = 0.15 P.V.

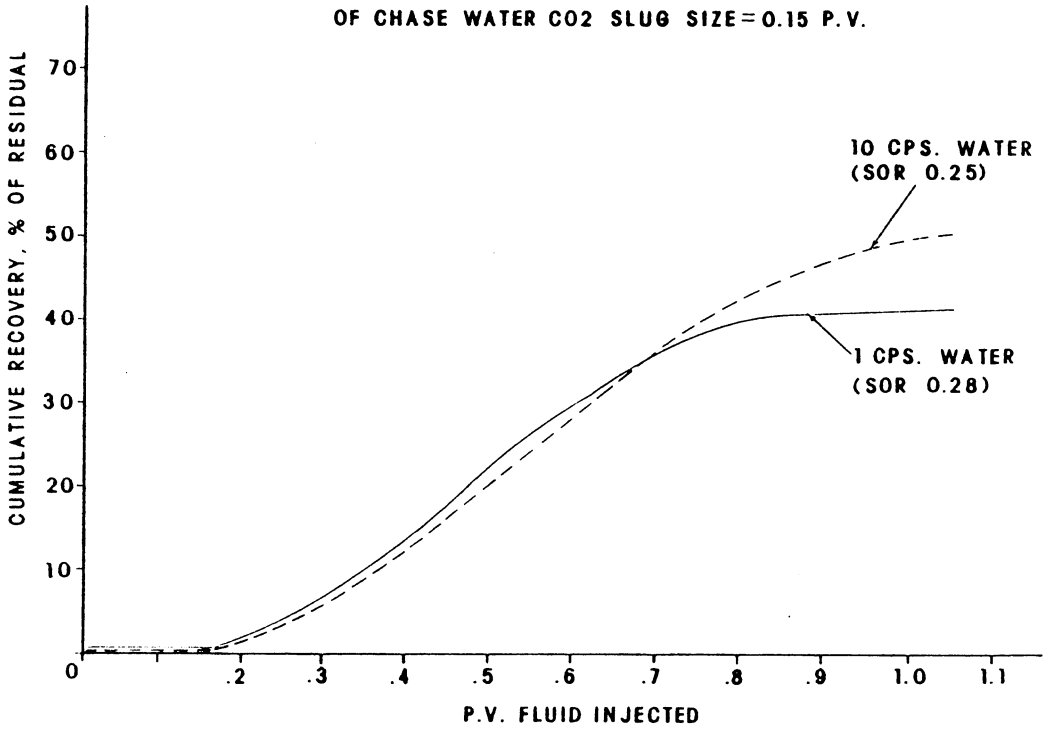

FIGURE 2

DISPLACEMENT EFFICIENCY OF CO2 SLUGS CO2 SLUG SIZE = 0.15 P.V.

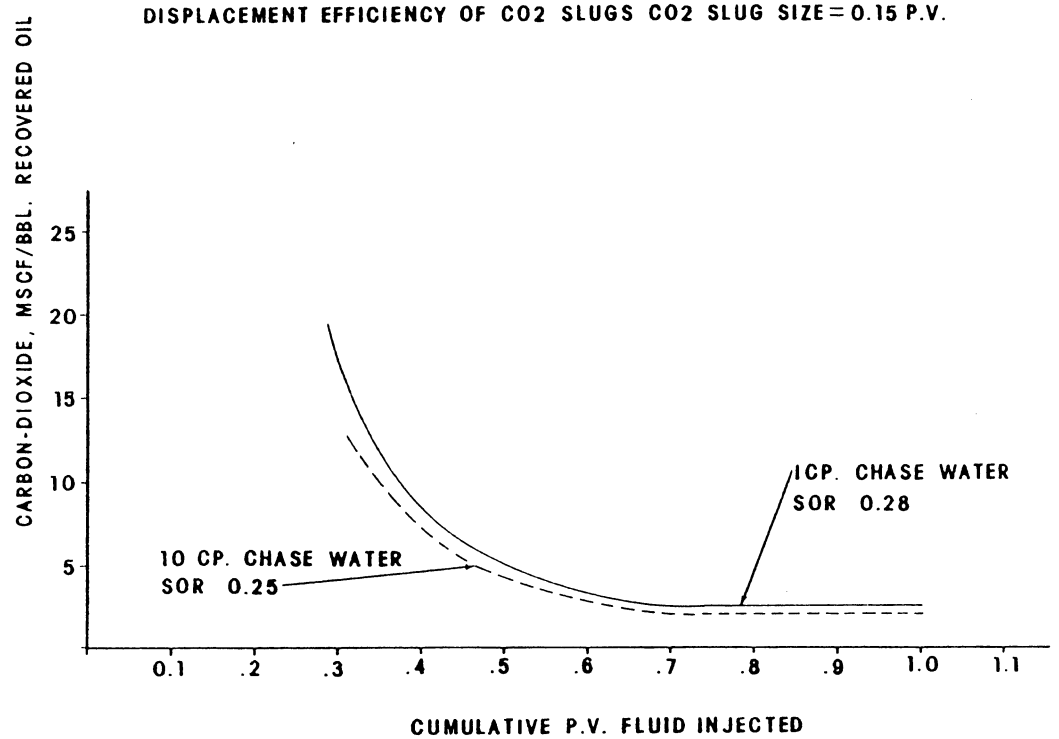

FIGURE 3

COMPARISON OF OIL RECOVERY WITH DIFFERENT VISCOSITIES OF CHASE WATER CO2 SLUG SIZE=0.15 P.V. SOR=0.28

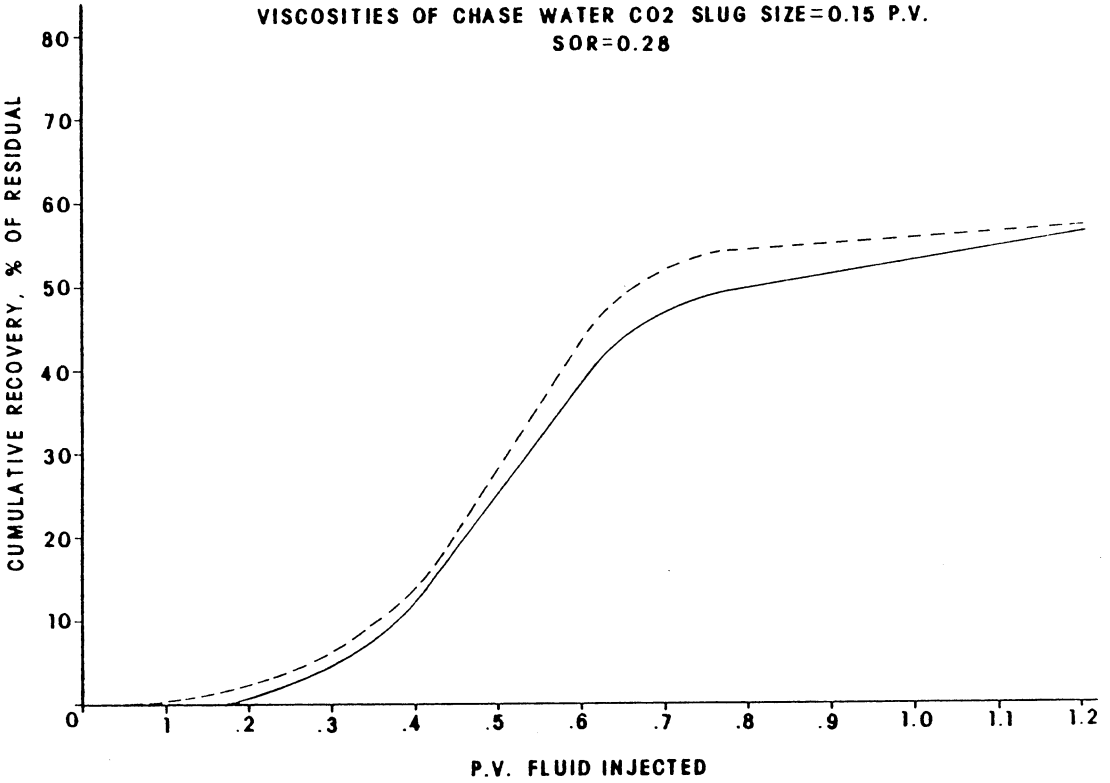

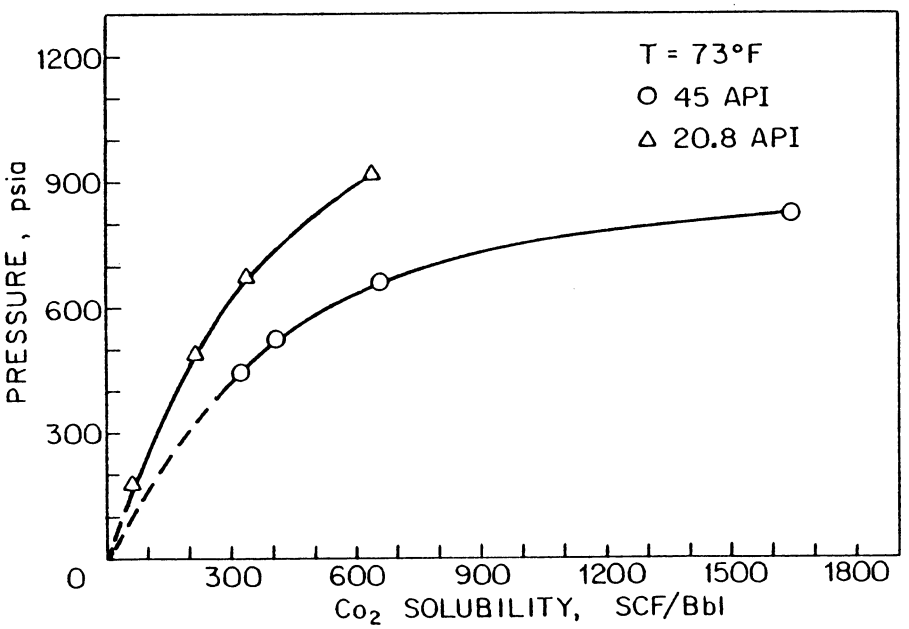

FIGURE 4

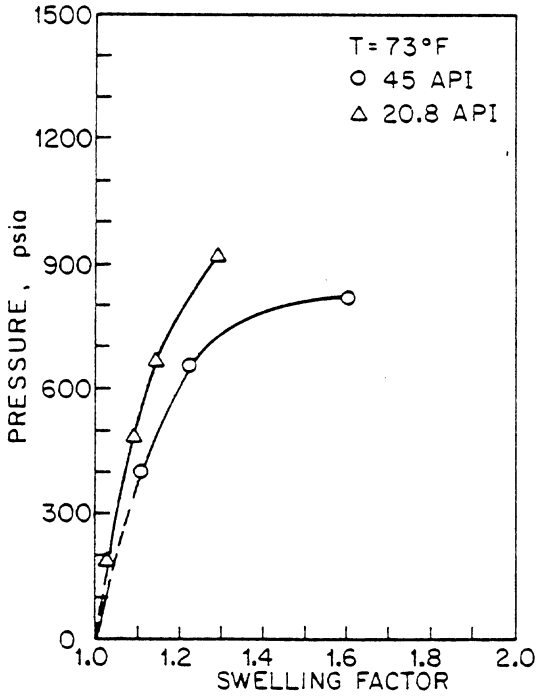

FIGURE 5

FIGURE 6
EFFICIENCY OF NITROUS OXIDE IN RECOVERING RESIDUAL
CRUDE SLUG SIZE=0.15 P.V. · SOR=0.28

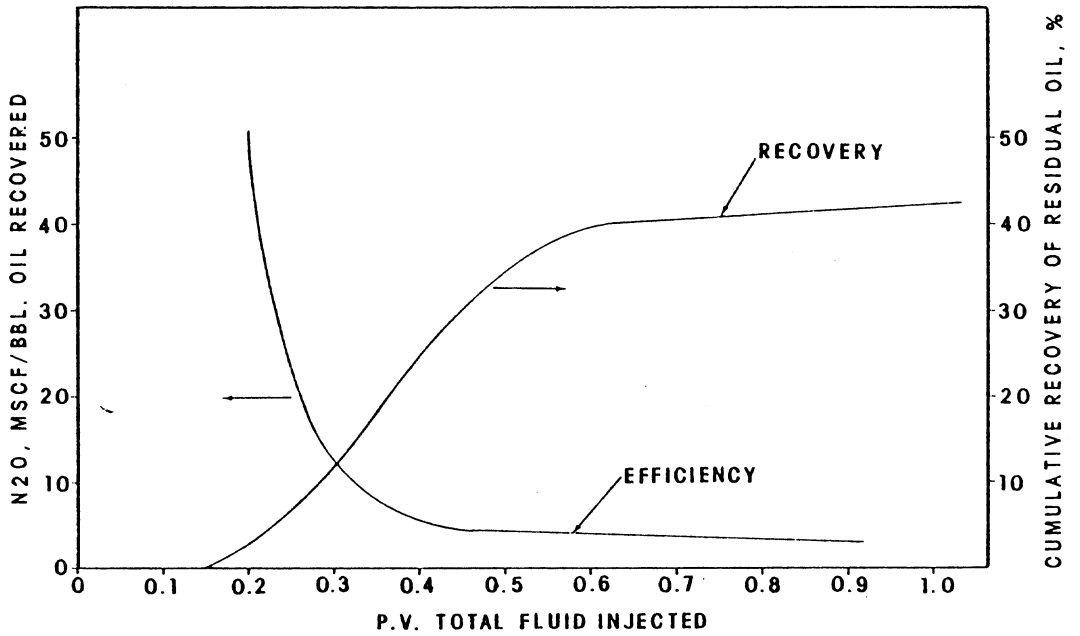

ROLE OF CLAYS IN ENHANCED RECOVERY OF PETROLEUM

by

W. H. Somerton and C. J. Radke
Departments of Mechanical and Chemical Engineering
and Lawrence Berkeley Laboratory
University of California
Berkeley, CA 94720

ABSTRACT

Clays present in oil producing formations may have an important effect on the success or failure of an enhanced recovery operation. The large surface area of clays and the usually high reactivity of these surfaces may lead to loss of injected chemicals by adsorption, exchange or dissolution. Disruption of the equilibrium of the rock and its contained fluids caused by injecting fluids of different chemical composition may result in the release and migration of fines and subsequent deposition in pore necks or other restrictions in the structure of the rock. This may cause serious reduction in flow capacity of the rock.

Reported in this paper are the results of study of a number of cores from California oil producing formations which are possible candidates for enhanced recovery operations. Mineral compositions and structural characteristics of the cores are reported with particular emphasis being given to the clays (less than 2 μm). The relative amount of clays, their surface area, mineral composition and cation exchange capacities are determined with the aim of obtaining correlations with chemical loss and fluid flow characteristics. The relative locations of clays and their distribution in these unconsolidated cores are being studied by new preparation techniques.

Two of the most important findings are: 1) Although most cores showed a serious reduction in permeability upon changing the chemistry of the flowing fluid, no direct correlation with amount of clays or type of minerals contained therein could be established. However, the relative locations of the clays do seem to have a bearing on the change in flow capacity, 2) Chemical dissolution is substantially more pronounced for amorphous silica and finely divided quartz than for other minerals including kaolinite, montmorillonite, and feldspar.

HISTORY OF PROJECT

This project was initiated October 1, 1979 with a government award of $55,000. It is a joint effort of Lawrence Berkeley Laboratory and the University of California.

INTRODUCTION

The greatest deterrent to the successful application of chemical methods of enhanced recovery of petroleum is the loss of chemicals injected into the formation to non-oil recovery processes. These chemical loss processes include adsorption onto mineral surfaces, chemical reactions with rock and fluids in the formation, possibly leading to precipitation and plugging of the formation, and trapping in parts of the rock structure so that the chemicals become unavailable for displacing oil. Chemicals that may be injected include

Prepared for the Department of Energy under Contract Number W-7405-ENG 48

surfactants, polymers, and caustic solutions which react with organic acids in the crude oil to produce surfactants in-situ. These losses are most pronounced in fine-grained reservoir rocks containing substantial amounts of clays.

In light of the above problems, the objectives of this research are to characterize typical reservoir formations as to mineral contents and structural characteristics of the rocks, evaluate their chemical loss characteristics, gain an understanding of the mechanisms and develop techniques for minimizing the deleterious effects. The nature of the reservoir rock, including its mineral and clay content, also affects the application of thermal recovery methods. Studies of the problems of steam condensate-clay reactions in steam injection have been started and the role of clays in fuel deposition in the in-situ combustion technique will be studied in the near future.

Core samples have been procured from several California oil producing formations which are possible candidates for enhanced recovery operations. To date cores studied are from several zones of the Wilmington field, Lower Main zone of the Huntington Beach field, Temblor zone of the Coalinga field and, most recently cores from the Chanac zone of the Kern Front field. Mineralogical and petrological test results for all but the Kern Front cores have been reported earlier [1,2]. Most of the techniques used have also been described [4]. Appendix A shows a typical report for one of the Kern Front cores.

Injection of fluids having different chemistry from fluids in the reservoir, with which the rocks are in equilibrium, may cause the release and migration of and subsequent plugging by fines in the reservoir rock. Fines are held onto larger mineral grains by Van der Waal's forces and electric charges. Any injected fluid which disrupts these forces may cause the release of fines. These fines are carried by drag force of the fluid until they are either recaptured by larger grains or are trapped in pore necks. The result can be a substantial decrease in permeability of the rock. Flow tests have been developed to test the effects of injecting fluids of different chemistry which might be used in an enhanced recovery project. Fluids are flowed at constant reservoir flow rates until stabilized conditions are achieved and changes in flow capacity are noted.

The third important part of this work is determination of rock-fluid interactions. Cation exchange capacities (CEC) have been measured for a number of the cores. Absolute values of CEC were found to be low for Wilmington cores but the values obtained correlated well with the montmorillonite content of the cores [2]. Alkali exchange studies of Wilmington cores showed exchange capacities lower than for calcium-sodium but probably of significant levels for field application [3]. And finally, the dissolution of minerals appears to be an important consumer of injected chemicals. New work in this area will be reported later.

TECHNICAL PROGRESS

Mineral Analyses

Details of mineral analysis of the cores have been presented by Lai [4]. Briefly, the test specimens are carefully selected to avoid contamination by drilling fluid solids. It was noted that in some unconsolidated cores mud

filled fractures were present which had to be carefully avoided. Oil was removed by extraction with toluene and, in most cases, followed by a pyridine wash to remove heavy residual hydrocarbons. The extracted sample was dry- and then wet-sieved through a 325 mesh (43 μm) screen. The < 2 μm material was separated from the fine fraction by settling in water to which a wetting agent (Calgon) was added.

X-ray diffraction was run on three samples of the extracted cores: total sample, < 43 μm fines and < 2 μm clays. The clay fraction was tested for the purpose of more accurate determination of clay minerals. The scanning electron microscope (SEM) with EDAX (energy dispersive analysis of X-rays) was used to confirm the mineral composition and to give some notion as to the structure of the sample.

The BET apparatus was used to determine the surface areas of the < 220 μm and the < 2 μm fractions, the results being reported in terms of the total sample. These results have been correlated with the montmorillonite content of the cores.

Results of mineral analyses for a Kern Front core sample is shown in Appendix A. In addition to the above data, a petrographic description based on a thin-section study is presented.

Changes in the procedure for preparing test specimens for thin-section and SEM studies have been made to obtain a better determination of the natural spatial relationships of mineral grains, i.e., the locations of clay minerals and other fines relative to the larger mineral grains. This, of course, is extremely difficult to do in the case of unconsolidated sands and impossible to accomplish if the sands are first extracted by solvents. It is important to know the location of fines both from the standpoint of their roles in chemical loss and in fines migration. We are now selecting intact chunks of the core, held together by the viscous oil, and are vacuum drying them rather than extracting them. If great care is taken, the residual heavy hydrocarbons will hold the chunk together enough so that SEM studies may be made. For petrographic microscope studies, the chunk is impregnated with red epoxy and thin-sections prepared. We believe these procedures cause minimal disturbances of the spatial relationships of the mineral grains.

Thin-section studies on samples prepared by the above procedures using a petrographic microscope with polarized light indicate that the visible clay minerals in Wilmington core samples exist in clusters rather than being widely dispersed throughout the test specimen. It is possible that finer clay particles, too small to be observed by the petrographic microscope, may well be widely dispersed throughout the sample. The Kern Front core, on the other hand, showed little in the way of clay minerals but did show abundant fragments of feldspar and quartz attached to larger grains. The clay minerals present in the Kern Front cores are present primarily as nodules or streaks within the unconsolidated sands.

SEM photos of a Wilmington core sample prepared by the above technique (see Figs. 1a,b) showed that biotite was the dominant clay-type mineral. Long wrinkled sheets of biotite formed the flow channels in many cases. The presence of other clay minerals could not be confirmed either by morphology or by EDAX analysis. These findings indicate that much more attention needs to be given,

in the case of Wilmington sands, to the base exchange and dissolution characteristics of biotite. SEM photos of the Kern Front core (see Figs. 2a,b,c) again showed little in the way of clay minerals but did show, as in the thin-section, abundant fragments of feldspar and quartz attached to larger grains.

Studies are now in progress on Kern Front core sections which are believed to have been swept by steam in the steam flooding operations applied to this field. Our goal is to determine whether any changes in the mineral character of the cores have occurred due to contact with steam. An effort is being made to distinguish between steamed and unsteamed core sections by differences in the oil saturation and in the salinity of the associated brine.

Fluid Flow Tests

Fluid flow tests are run on the cores to determine changes in flow behavior due to the sequential flow of different fluids which might be used in an enhanced recovery operation. The unextracted, unconsolidated core material is packed into stainless steel tubes to porosities and permeabilities as close to reservoir values at possible. The oil is extracted by passing through several pore volumes of Chevron 410H solvent followed by isopropyl alcohol. In some cases the cores were pyridine treated to remove heavy hydrocarbons left on the mineral grain surfaces by other solvents. After packing and extraction, the sand pack is vacuum saturated with synthetic formation brine. The core is then brought to reservoir temperature and flow of the desired sequence of fluids is commenced. Flow of each fluid continues at 1.5 feet/day (2 PV/day) until the permeability stabilizes. A steady condition is usually attained after flow of 2-4 pore volumes of each fluid. Flow effluent is collected in 5-9 ml increments for further analyses, which may include salinity, pH, and calcium and silica ion determinations.

Results of three recent tests reported by Minner [5] are shown in Figs. 3-5. The first Ranger zone sample, Fig. 3, displayed fairly constant permeabilities to the simulated (synthetic) brine and the more concentrated NaCℓ solution, values being close to nitrogen permeability. Upon introduction of the less concentrated NaCℓ solution, a drastic drop in permeability was observed, stabilizing at about one-tenth of the nitrogen value. Upon introduction of the NaOH solution, flow became quite unstable. After several pore volumes, stable flow was again obtained. Reflooding with synthetic brine showed lowered but stable permeability until the flow direction was reversed. The permeability immediately increased by a factor of four and then, after an unstable period, returned to the lower value.

The pyridine treated Ranger sample displayed very different behavior as shown in Fig. 4. Flow was unstable to the synthetic brine showing quite a sharp drop in permeability down to only six percent of the nitrogen value. The permeability then remained constant for the rest of the test except upon flow reversal late in the test while flowing synthetic brine. Here a four-fold increase again occurred but rapidly returned to the lower stabilized value.

The Lower Main zone sand behaved differently from either of the above samples. The initial permeability to the synthetic brine was less than 20 percent of the nitrogen permeability value, as shown in Fig. 5. Upon introduction of the NaCℓ solution, permeability dropped drastically to less

than five percent of the nitrogen value. Through the remainder of the tests, the permeability dropped gradually without regard to fluid type, to less than two percent of the nitrogen value. Upon reversal of flow of the synthetic brine near the end of the test, no sharp increase in permeability was noted.

Tests on Kern Front cores are still in progress but indications are that these cores are relatively insensitive to changes in the composition of the flowing fluid. This may reflect the lack of clay minerals in the sand portions of the cores.

Although more data are needed to confirm the above test results, there is a strong correlation of flow behavior with type of sand, method of treatment, and types of fluids flowing through the sand pack. Fines migration and plugging seem to be important in permeability reduction in Ranger zone sands but the mechanism of fines release seems to be associated with the pretreatment of the sands. On the other hand, in the case of Lower Main zone sand, clay swelling may also be involved in the permeability reduction.

Fines Release

Since flow tube studies indicate that the release and migration of fines and subsequent plugging are probably the major cause of permeability reduction, a study was initiated to evaluate the effects of changing fluid composition on release of fines. The type and concentration of ions in the fluid affects the charge on solid surfaces with which it is in contact. The forces tending to attract smaller particles to larger grains are also affected. These effects need to be known for model studies of the release, migration and plugging by fines.

The methods used for fines release study have been fully described by Prescott [6]. Briefly, a soils test method is used in which the settling of fines in a fluid is timed to give particle size and a sensitive hydrometer is used to measure concentration of the suspended particles. Well dispersed systems should show a greater proportion of fine particles than would flocculated systems. Thus fines would tend to be released in the dispersed system.

Early results for Ranger zone composite sand indicated that the settling time increased in the order: synthetic brine, 2.86% NaCℓ, 1.00% NaCℓ and 1.0% NaCℓ + 1.0% NaOH. This indicated that the mineral grains became better dispersed in the same order that permeability was reduced in early flow tests. In other words, more fines were released with each change in fluid composition.

Recent settling tests were run on sand samples from the Ranger, Upper Ranger, Lower Tar, and Upper Terminal zones of the Wilmington field. Results were generally less conclusive than the earlier tests, there being only a slight correlation between settling times and fluid composition. An interesting result which did occur is shown in Figs. 6a,b from Prescott's work [6], in which toluene and toluene plus pyridine extracted sands from the Upper Terminal zone are compared. The pyridine treated sands show much better dispersion and thus, much easier release of fines. This is in good agreement with flow tube tests which show greater permeability reduction for pyridine treated sands. One would conclude that heavy hydrocarbons absorbed on mineral grain surfaces tend to minimize release of and plugging by fines. One should also note in Fig. 6a that the toluene extracted sand in the presence of NaOH solution

shows better dispersion than for other fluids, approaching the amount of dispersion for the pyridine treated sand. This cannot be positively correlated with the flow tube results, however. A final note is that the pyridine treated sands showed excellent reproducibility on duplicate tests, the toluene treated sands showing much poorer reproducibility.

Since the above tests did not provide quantitative information needed for model studies, a number of improvements are being made in the test apparatus. The amount of handling upon change of fluids, with possible loss of fines, has been minimized. A higher concentration of solids is being used to improve accuracy of measurements. To test the calibration of the system, a finely ground sample of quartz sand was run in both the present apparatus and in a Microtrack optical particle size analyzer. The results of the two sets of measurements were surprisingly close giving credence to the improved technique.

Chemical Loss

Results of chemical loss studies are presented in the report of the companion project [7]. Alkaline dissolution kinetics of several minerals have been studied in stirred batch tests. Results of dissolution and release of silicon in 0.1 molar sodium hydroxide solution at 70°C show that after 90 hours Cristobalite produced twice as much Si with half the surface area as crushed Ottawa sand. Kaolinite and Montmorillonite produced about 1/10th the amount of Si and had tremendously larger surface areas. We conclude that the form in which the Si exists in the minerals has an overriding effect on dissolution. These findings are important because the loss of caustic is strongly related to the almost unlimited supply of the most common minerals (amorphous and crystalline silica) in sedimentary rocks. Model studies show that the loss of hydroxide by dissolution and ion exchange at residence times which would apply to reservoir operations, could be so severe as to negate any beneficial effects of a caustic slug.

Some work has been started on the flow of polymers in oil field cores. Equipment has been designed and preliminary tests have been successfully completed. We plan to study the effects of the rock on the polymers and the effect of polymers on flow characteristics of the cores.

ACKNOWLEDGEMENTS

This work has been supported by the U.S. Department of Energy on contract number W-7405-ENG48. The authors wish to acknowledge the important contributions made by the following graduate students: Cheng-H. Lai, William Minner and Tom Prescott. The recent mineral analysis work was done by Research Associate, A. Jaouni.

REFERENCES

1. Somerton, W. H. and Radke, C. J., "Role of clays in the enhanced recovery of petroleum," First Joint SPE/DOE Symposium on Enhanced Oil Recovery, Tulsa, Oklahoma (1980), SPE 8845.

2. Somerton, W. H. and Radke, C. J., "Role of clays in enhanced recovery of petroleum," DOE project annual report, July 1, 1980, University of California, Berkeley.

3. Radke, C. J. and Somerton, W. H., "Enhanced recovery with mobility and reactive tension agents," DOE project annual report, July 1, 1980, University of California, Berkeley.

4. Lai, C. H., "Identification of clay minerals in California oil sands," Master of Science Research Report, March, 1981, University of California, Berkeley.

5. Minner, W. A., "Water sensitivity of California oil sands," Master of Science Research Report, October, 1980, University of California, Berkeley.

6. Prescott, T. A., "A study of release of fines in California oil sands," Master of Science Research Report, September, 1980, University of California, Berkeley.

7. Radke, C. J. and Somerton, W. H., "Enhanced recovery with mobility and reactive tension agents," DOE Annual Project Report, July 1981, University of California, Berkeley.

APPENDIX A

Core: Mitchell 67 - 1578 ft.

Petrographic Description:

This core is made up of light gray in color, coarse to medium grained and poorly sorted sand. Small nodules and thin lenses of clay were widely dispersed throughout the sample. The sand was saturated with oil but the clay nodules and lenses were not. The mineral grains are angular. The sand is immature both compositionally and texturally and was derived from plutonic and volcanic provenance. Little, if any, diagenesis has affected the sediment as evidenced by the absence of post-depositional compaction.

From thin section studies, the sand has the following mineral composition:

a. 55-60% monocrystalline quartz, mainly of plutonic origin, showing undulose extinction in thin section;

b. 25-30% feldspars including plagioclose and K-spar in nearly equal amounts;

c. 15-20% lithic fragments containing predominately chert and volcanics;

d. 1-2% of biotite:

e. accessory minerals including epidote, hornblende, sphene and magnitite.

X-Ray Analysis

Size	Mont.	Kaol./Chlor.	Mica	Quartz	Zeolite	Feldspar
< 2μm	30	5	5	15	3	30
<43μm	3	3	-	35	3	50
total	-	-	-	70*	-	25

Grain Size Analysis

Fraction	W% (of total)
< 220μm (60 mesh)	28.0
< 43μm (325 mesh)	6.0
< 43-2μm	5.2
< 2μm	0.8

*Includes quartz contained in lithic fragments reported in thin section analysis.

Surface Area (BET)

< 2μm	12.23 m^2/g	(whole rock basis ≃ 0.10 m^2/g)
< 220μm	0.98 m^2/g	(whole rock basis ≃ 0.27 m^2/g)

SEM - EDAX Analysis

Showed almost entirely quartz and feldspar grains with no clay minerals in evidence. Showed a great many fine mineral particles on the surfaces of larger grains. Conclude that clay is present entirely in form of nodules or thin lenses.

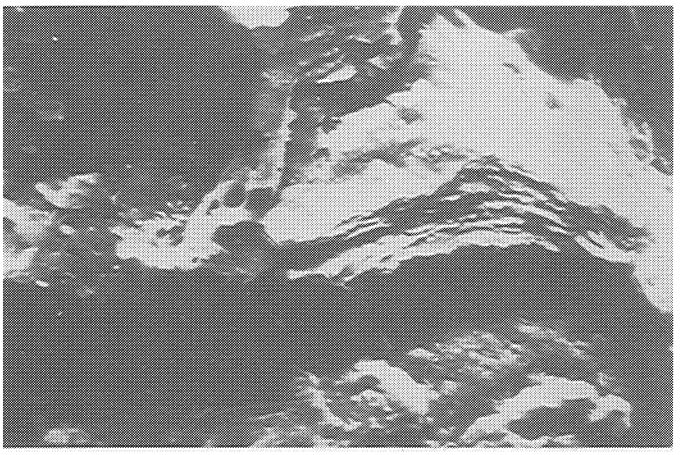

Fig. 1a. SEM photograph of Wilmington Ranger zone oil sand. 20 μm.

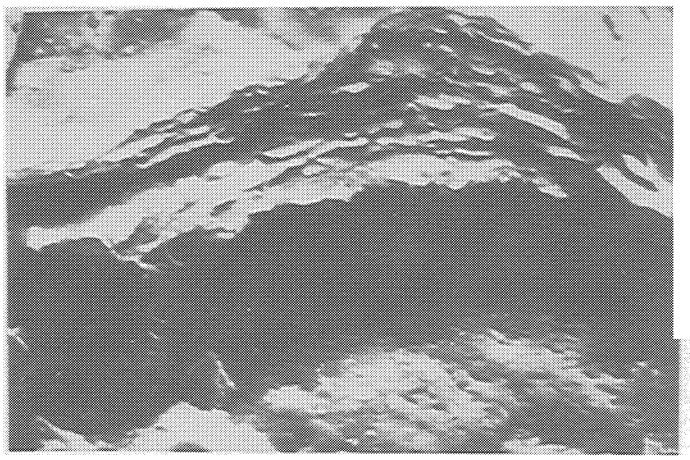

Fig. 1b. SEM photograph of Wilmington Ranger zone oil sand. 10 μm.

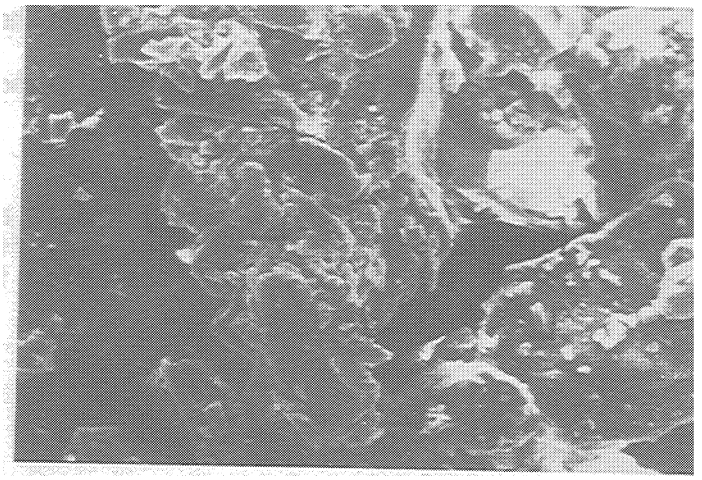

Fig. 2a. SEM photograph of Kern Front oil sand. 40 μm.

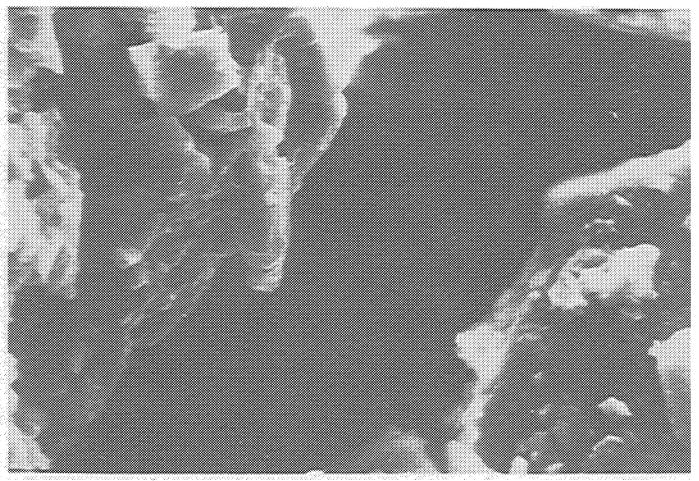

Fig. 2b. SEM photograph of Kern Front oil sand. 10 μm.

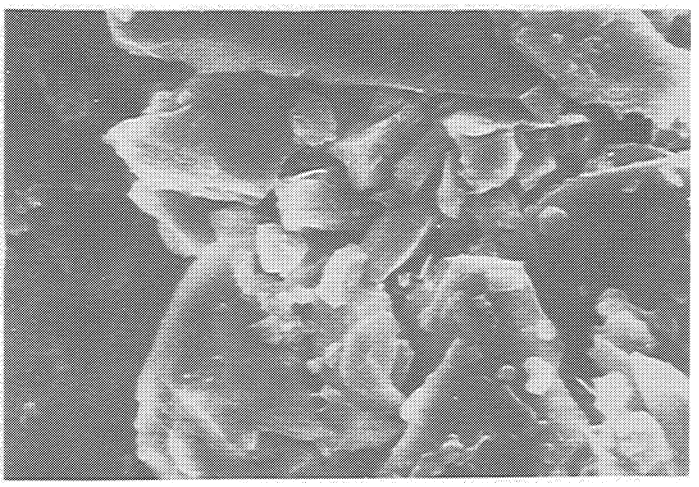

Fig. 2c. SEM photograph of Kern Front oil sand. 10 μm.

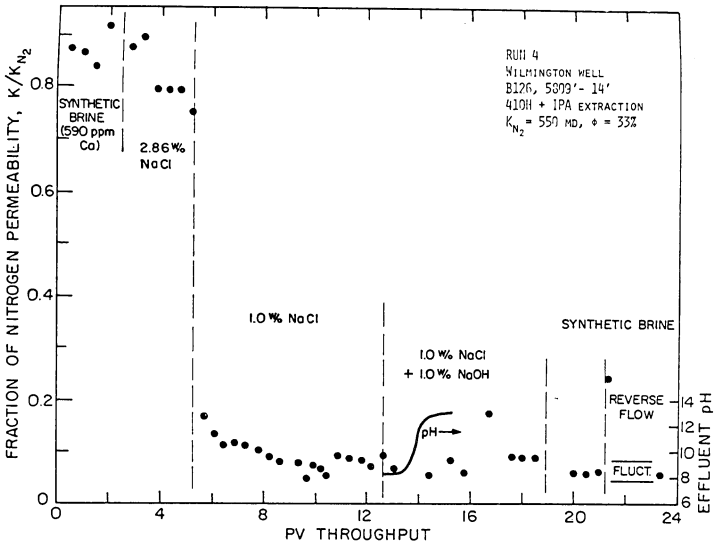

Fig. 3. Effect of fluid cycling on permeability of Wilmington core.

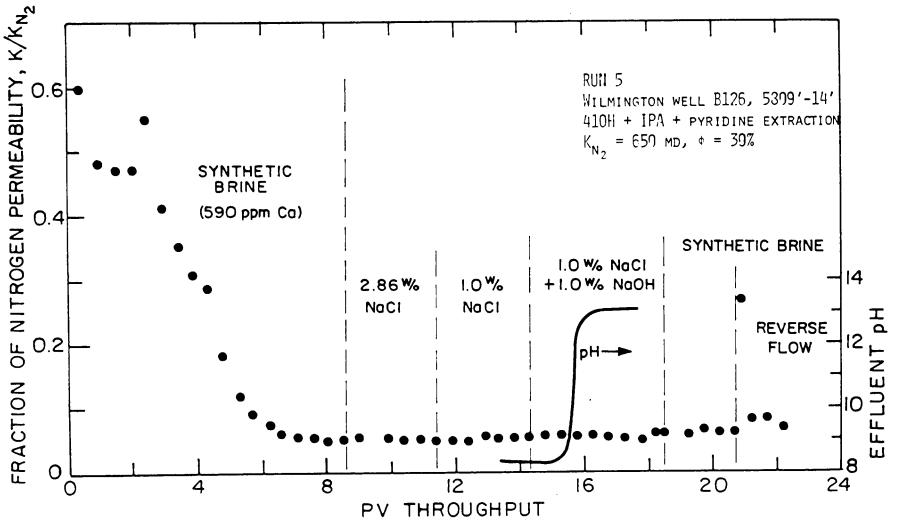

Fig. 4. Effect of fluid cycling on pyridine treated Wilmington core.

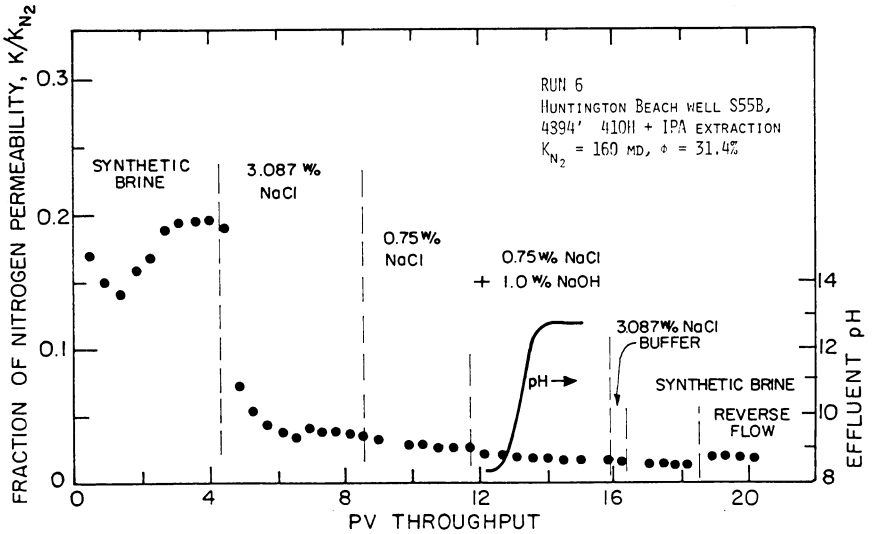

Fig. 5. Effect of fluid cycling on Permeability of Huntington Beach core.

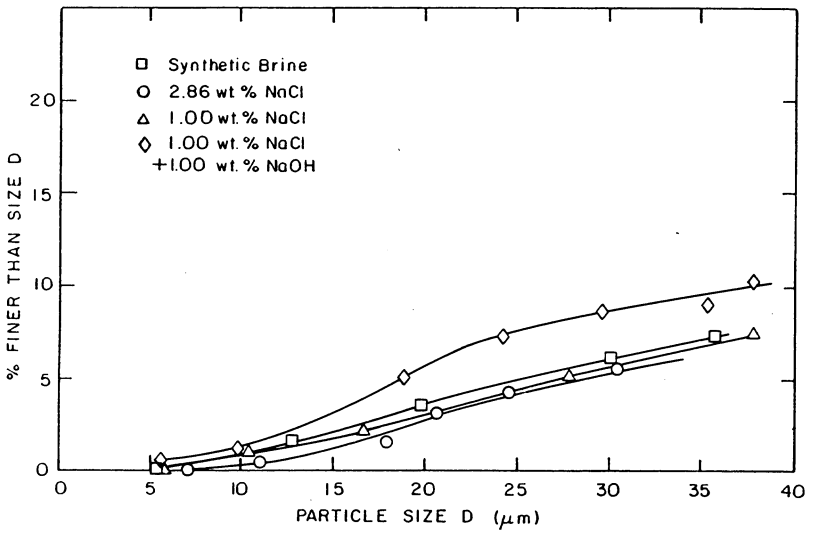

Fig. 6a. Size distribution of Toluene extracted Wilmington core.

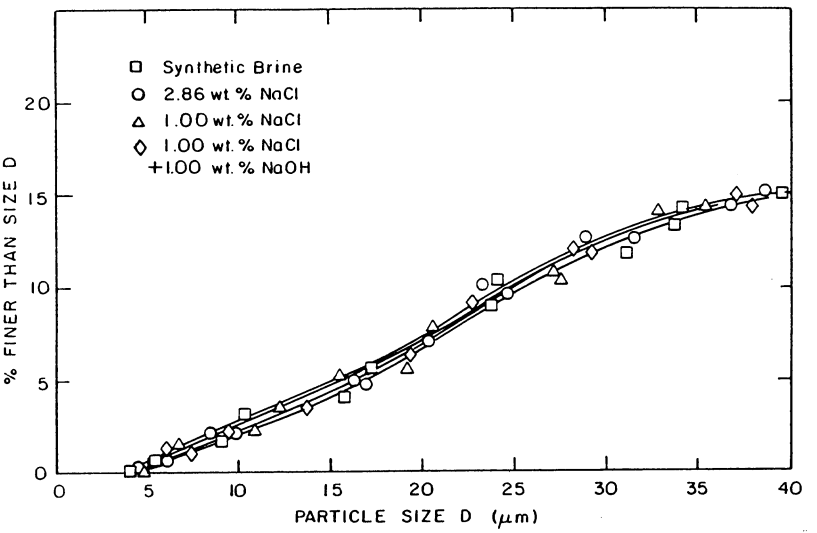

Fig. 6b. Size distribution of pyridine treated Wilmington core.

BODCAU IN SITU COMBUSTION PROJECT
BELLEVUE FIELD, LOUISIANA

by
Conrad Joseph, Project Manager
and
James G. Hardin, Project Engineer

Cities Service Company
P.O. Box 12026
Jackson, MS 39211

ABSTRACT

The Bodcau In Situ Combustion Project (DOE Contract DE-AC03-76ET-12057) is being conducted in the shallow upper cretaceous Nacatoch sand in the Bellevue Field, Bossier Parish, Louisiana. Five elongated patterns encompassing 20 acres were developed for the demonstration of a commercial scale project utilizing forward combustion with simultaneous air and water injection.

The air injection phase of the project was terminated April 10, 1981, with the conversion of the fifth injector to water injection only. During the combustion phase 10 BCF of air and 2.64 MMBW were injected, resulting in the recovery of 626 M barrels of 19°API crude oil. Post burn core holes were drilled in one of the patterns to evaluate the sweep efficiency of the process.

During the combustion phase, operating expenses and taxes have amounted to $6.16 million, an average of $11.25 per net barrel. Total investments for the project have been $1.69 million.

PROJECT HISTORY

The Bodcau In Situ Combustion Project covers five patterns and 20 acres of Cities Service Company's project in the Bellevue Field, which was begun in 1970[1] and now covers 160 acres with 44 patterns having been developed[1]. Figure 1 shows the general location of the field in northwestern Louisiana. Important reservoir and fluid characteristics are shown in Table 1.

Ignition of the five pattern injectors was accomplished in August and September of 1976[2]. Dry forward combustion was maintained until March of 1977 when the injectors were reperforated to allow water injection into the upper section of the Nacatoch sand simultaneously with air injection into the base of the zone. A fossiliferous lime interval provides partial separation of the two injected fluids. The purpose of water injection was to improve vertical sweep efficiency by forcing the combustion to expand farther out in the lower section of the reservoir before rising to the top 15 to 20 feet, thereby heating a larger volume of the reservoir.

Prepared for D.O.E. under Contract Number DE-AC03-76ET12057

Three sets of falloff and pulse tests were conducted to describe changes in directional permeabilities resulting from continued combustion[3]. Five temperature observation wells were drilled to monitor the progress of combustion in the five patterns. Locations of these wells plus the injectors and producers are shown in Figure 2, also showing structure of the Nacatoch sand.

Originally, the five patterns included only the five injectors and 29 producers. Pattern 12 injector was redrilled in 1977 because of a casing failure caused by ignition and nine additional producers were drilled along the south border of the project area in late 1978 and early 1979. The additional producers were drilled to prevent excessive drainage by the offsetting operator who had drilled producers along this lease boundary without supporting injection. It is estimated that a minimum of 30,000 barrels has been lost to these wells over the past three years.

Response to the combustion phase was evident almost immediately. Production increased from 75 BOPD in July 1976 to over 200 BOPD in October, and steadily increased to a maximum of 601 BOPD in March of 1978. Production held relatively stable at rates between 350 and 450 BOPD from April 1978 to December 1979 before experiencing a sharp decline, shown in Figure 3.

During this period of high production rates, effects of combustion were evident at the observation wells and especially at the producers. Observation well 13-7 is the only observation well which exhibited the high formation temperatures which were anticipated. A reading of 1060°F was measured there in March 1978. Other observation wells, less ideally located, measured maximum temperatures of from 240°F to 420°F. Producing wells, however, became difficult to operate by late 1977, requiring remedial cement squeeze jobs to shut off perforations through which high combustion gas rates carrying formation sand eroded the downhole pumping equipment. Remedial work at wells along the north line of the project area became so frequent and difficult that in February 1979 these wells were shut in to allow the combustion front to advance farther to the south and stimulate the producers in that direction. This redistribution proved successful as south line producers rapidly stimulated and more than made up for the reduction in total wells. The north line wells were not returned to producing status until July 1980. The number of remedial cement squeezes annually from 1977 through 1980 was 12, 42, 29 and 37 respectively.

On February 17, 1980, an explosion occurred in the air injection system, destroying the distribution lines and severely damaging the large compressor. Buildup of a lubricant film on the inside walls of the air injection lines is suspected as being the most likely cause of the explosion. The distribution system was repaired and compressors #1 and #2 were on stream within 48 hours. Compressor #3 was repaired and was back in service on April 9, 1980. To prevent future explosions, the injection lines are being flushed at six month intervals with a caustic solution and the high temperature shut downs were reset to 300°F, well below the autoignition temperature of Anderol 500 which is used as the lubricant for all three units.

PAST YEAR DEVELOPMENTS

Termination of air injection was begun on October 1, 1980. Pattern 15 was the first one converted to waterflood as it had the highest ratio of air injected per acre-foot of pay of the five. The termination dates and cumulative air and water injection for each pattern through March 1981 are shown in Table 2. Historical injection of air and water into the project area is shown in Figure 4.

In order to better evaluate the performance of the simultaneous air and water combustion process, four wells were drilled, cored and logged in pattern 15. Results of the program have not been fully analyzed; however, several initial observations may be made:

(1) Structure played a significant role in the process as applied. Air preferentially migrated up structure while water moved down, causing variations in the in situ combustion process ranging from dry to quenched combustion at various positions.

(2) The several hard lime streaks apparently maintained separation of the injected fluids behind the leading edge of the waterflood, but ahead of the water did not impede the migration of air to the very top of the zone.

(3) Residual oil saturation in the burned intervals is zero, indicating a highly efficient process.

(4) Significant reductions in oil saturation in intervals above the hard streak down dip of the injector may indicate quenched combustion or a hot waterflood. Analysis of clay alterations may indicate exactly which process occurred.

(5) The simultaneous air and water injection process with partial vertical separation is not ideally suited to reservoirs with appreciable structure when applied in a pattern type development.

During the combustion phase of the project a total of 626,008 barrels of oil was recovered, approximately 31.5% of the estimated oil in place. Since February 1980, production rates have decreased dramatically, averaging only 252 BOPD from March 1980 through March 1981. Production in March 1981 was only 165 BOPD. Much of this decline has been caused by the lack of continuous injection during the period of air termination. The injectors must be squeeze cemented to shut off the upper perforations and drilled out, reperforated and often acidized to allow for injection of 1000 BWPD into the lower portion of the reservoir. Typically it has taken three weeks per well to reestablish injection at the desired rate. Now that all five patterns have been converted, the production rate should stabilize or slightly increase.

One of the primary reasons for DOE participation in this project is to publish information regarding the economics of such projects. Initial estimated project expenditures were $8.23 million. Through March 1981, actual expenditures have been $8.79 million, with one year of operations remaining in the contract. Additional work beyond the initial scope of work for the project, including the drilling of nine additional producing wells, four post burn core holes and extraordinary repairs to damaged compressors has added $518,137 in unplanned costs. A summary of project cumulative expenditures is shown in Table 3. It should be noted that all of the decontrol tax has been incurred over the past twelve months, causing project expenses to double during this period.

References:

1. Little, T. P., Bodcau In Situ Combustion Project "Pre-Contract Work and Plan for Project Development", Cities Service Company Topical Report, January 1978.

2. Joseph, C., Bodcau In Situ Combustion Project "Ignition", Cities Service Company Topical Report, May 1977

3. Bandyopadhyay, P. and Joseph, C., Bodcau In Situ Combustion Project "Pressure Transient Testing", Cities Service Company Topical Report, January 1978.

TABLE 1

AVERAGE RESERVOIR & PROJECT AREA DATA

Porosity	33.9%	Pattern Area	19 acres
Permeability	700 md	Average Thickness	54' net
Water Saturation	27.4%	Net Pay Volume	1039 acre-feet
Reservoir Temperature	75°F	Oil Saturation	1909 B/AF
Reservoir Pressure	40 psig	Oil in Place	1,984,000 bbls
Crude Gravity	19° API	Estimated Recovery	700,000 barrels
Crude Viscosity @ 75°F	676 CP	Dip Angle	4.5°
Crude Viscosity @ 140°F	51 CP		

TABLE 2

CUMULATIVE INJECTION THROUGH APRIL 1981 SUMMARY

	INJECTION		RATIO	
PATTERN	MCF	BBLS	BBLS/MMCF	DATE AIR TERMINATED
12	2,009,908	632,279	315	April 10, 1981
13	2,180,163	390,234	179	March 2, 1981
14	2,042,579	377,158	185	February 9, 1981
15	1,904,564	452,842	238	October 1, 1980
16	1,861,261	462,250	248	November 3, 1980

TABLE 3

PROJECT CUMULATIVE EXPENDITURES

Category	Expenditure	Cost per barrel*
Lease Operation	787,130.76	1.44
Lease Maintenance	1,488,565.40	2.72
Compression Facility	1,184,678.40	2.16
Severance Tax	1,652,013.97	3.02
Decontrol Tax	1,050,013.00	1.92
Overhead	1,065,121.14	1.94
Depletion & Depreciation**	1,233,707.00	2.25
	8,461,229.67	15.45

* Costs determined on a net barrel basis assuming a net revenue interest of 87.5%, yielding 547,757 net barrels.

** D&D figured on a per barrel basis assuming an ultimate recovery of 612,500 net barrels.

FIGURE 1

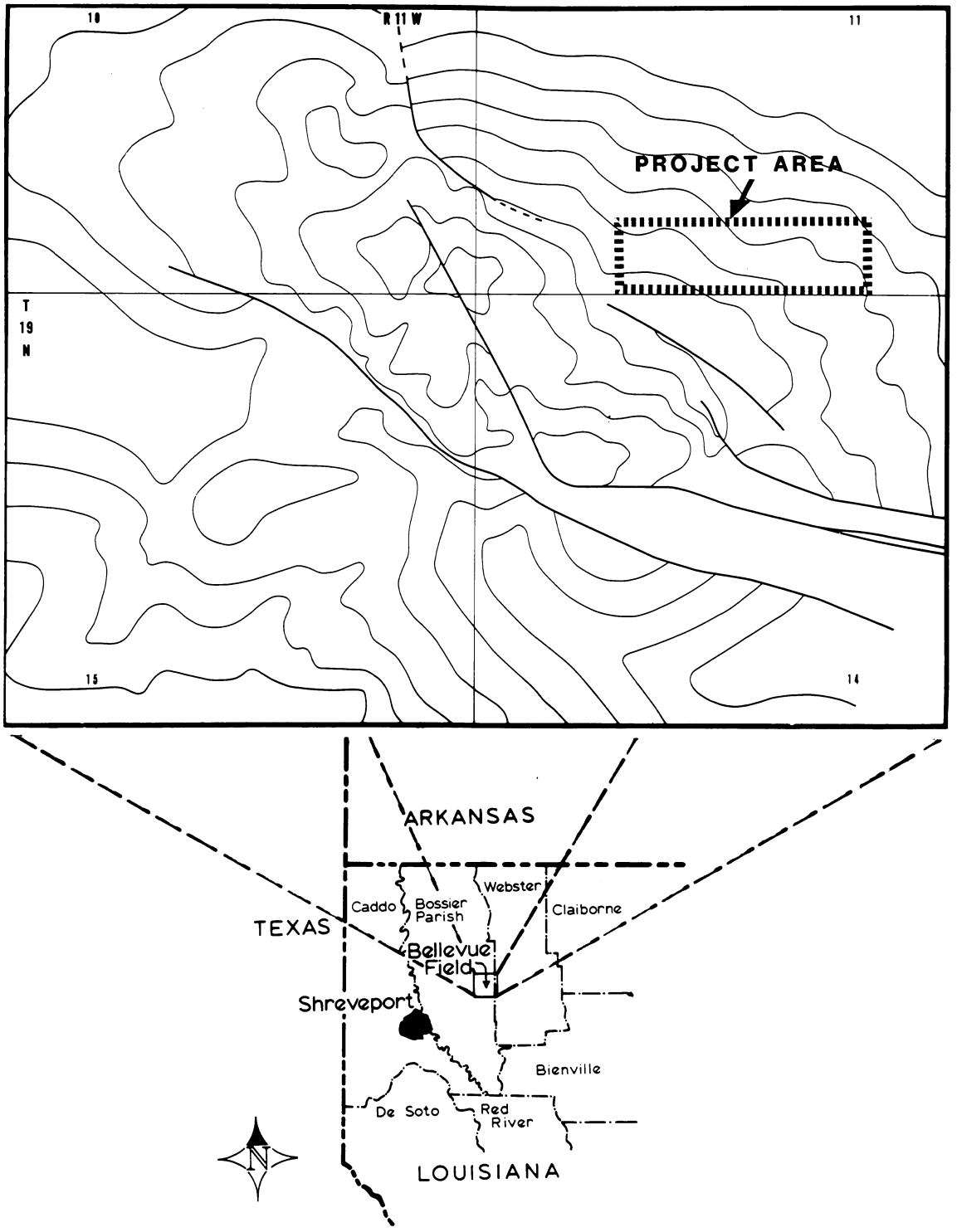

General Location Map

BELLEVUE FIELD

Bossier Parish, Louisiana

FIGURE 2

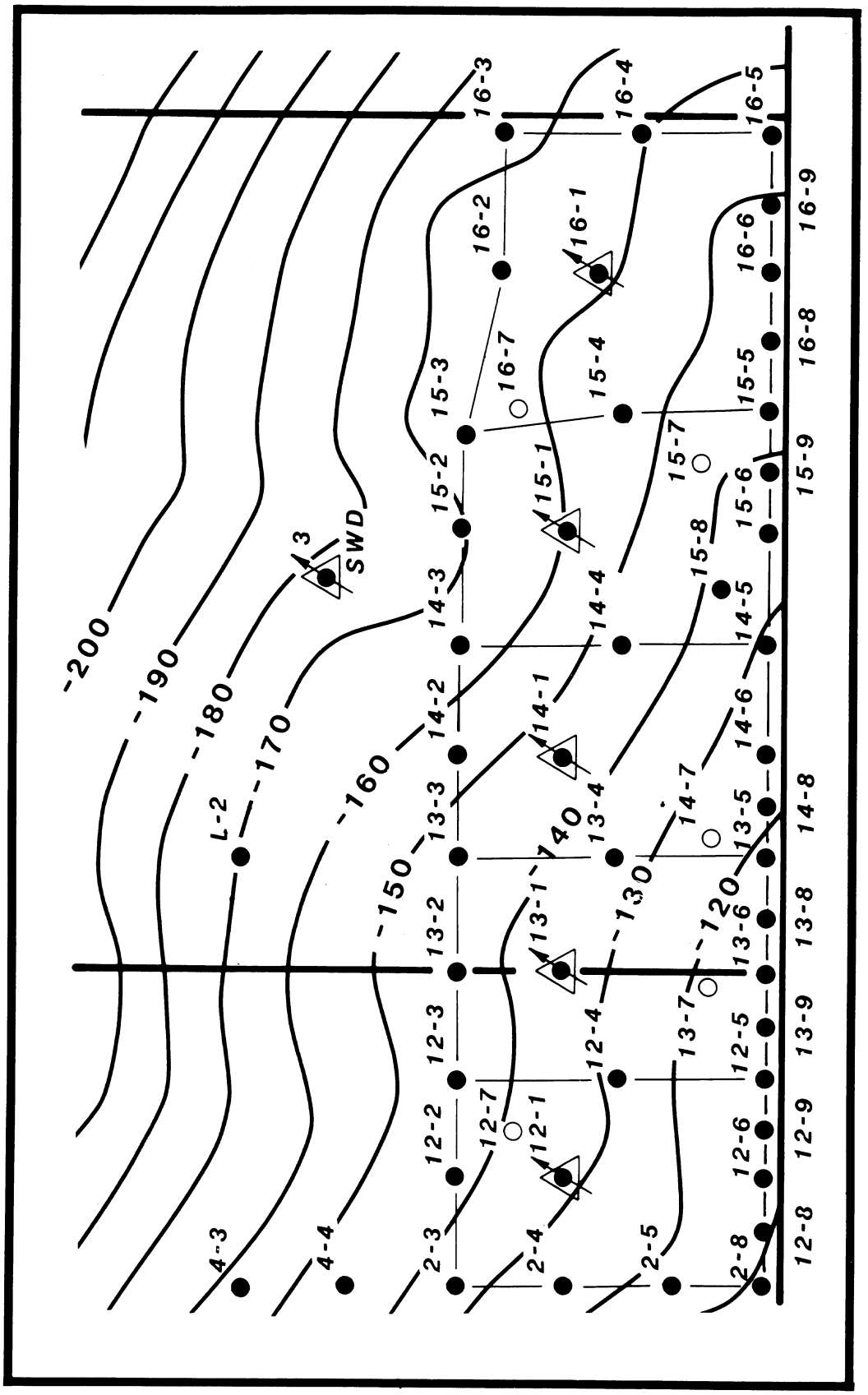

PROJECT AREA STRUCTURE MAP

0 200' 400' 600'

FIGURE 3

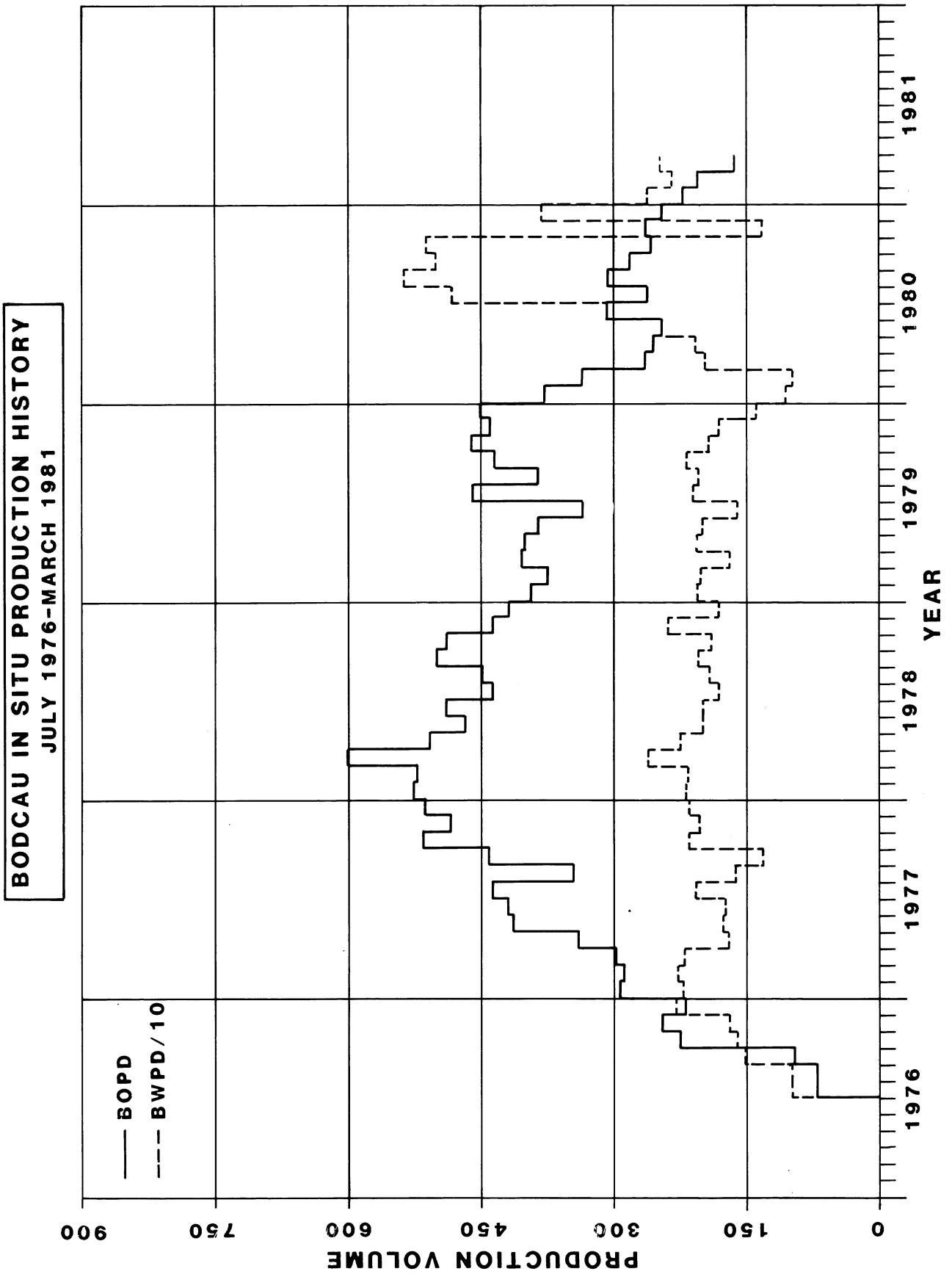
BODCAU IN SITU PRODUCTION HISTORY
JULY 1976-MARCH 1981
BOPD
BWPD/10
PRODUCTION VOLUME
0
150
300
450
600
750
900
YEAR
1976
1977
1978
1979
1980
1981

FIGURE 4

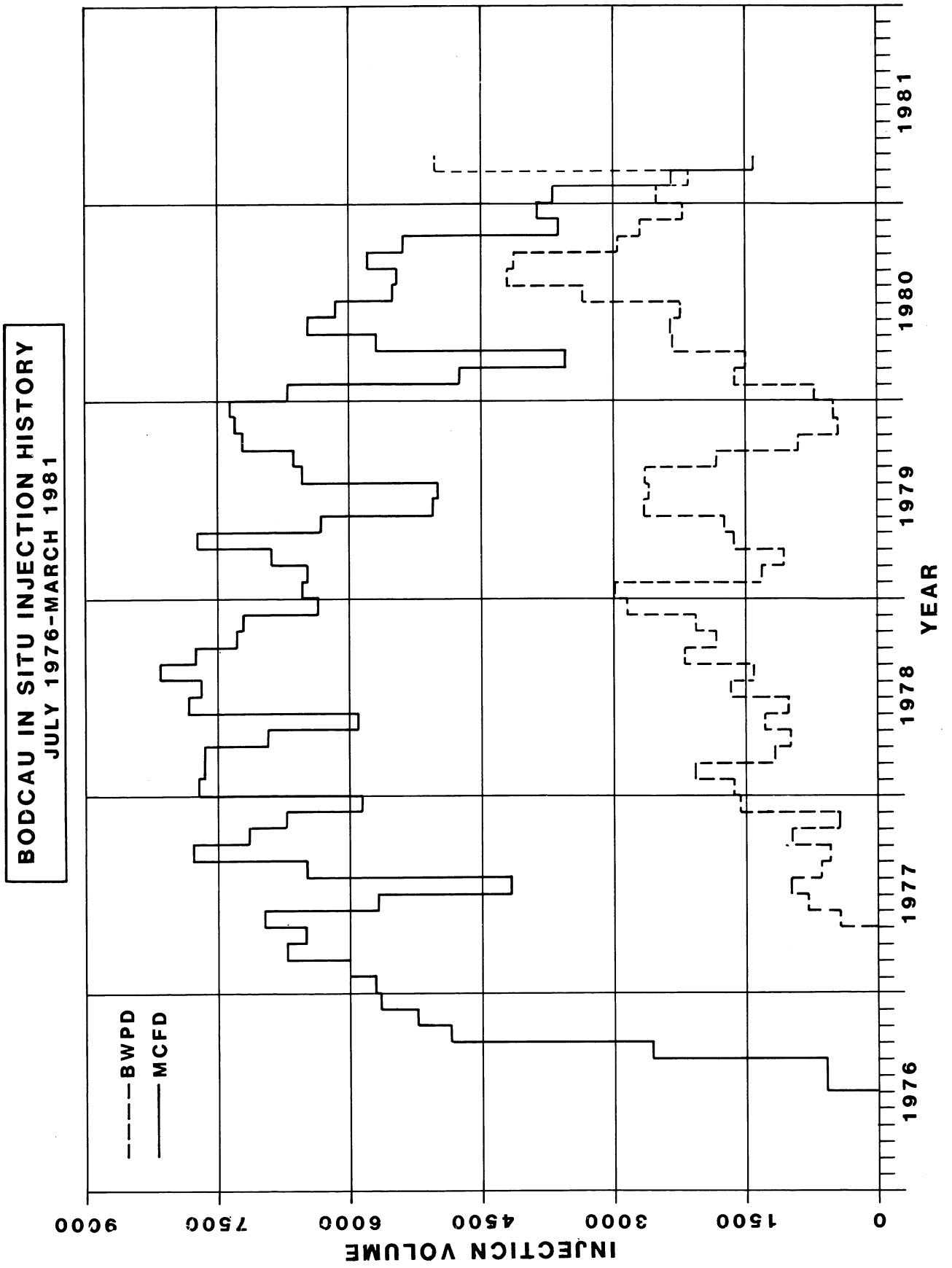
BODCAU IN SITU INJECTION HISTORY
JULY 1976-MARCH 1981
BWPD
MCFD
INJECTION VOLUME
0
1500
3000
4500
6000
7500
9000
YEAR
1976
1977
1978
1979
1980
1981

ANALYSIS OF REACTIONS OCCURRING IN IN-SITU COMBUSTION

by

M. R. Fassihi and W. E. Brigham
Stanford University Petroleum Research Institute
(SUPRI) Stanford, CA

ABSTRACT

Continuous analysis of gases produced from a small packed bed reactor filled with oil sand made it possible to identify and measure three consecutive chemical reactions as the temperature of oxidation increased: a) low-temperature oxidation appears to occur between the gas and liquid phases; b) middle-temperature fuel deposition reactions appear to be homogeneous (gas-gas); and c) high-temperature fuel combustion reactions appear to be heterogeneous (gas-solid). The latter was found to be the rate determining step in clean sands.

Natural cores from the reservoirs were found to have different kinetic performances than the clean sand matrices. This was attributed to the following reasons: a) clay and metallic additives lower the activation energy of the combustion reaction and hence shift the rate-determining step; and b) finer sands adsorb more fuel.

The proposed kinetic model was found to be applicable to the five oils tested and hence maybe generalized for application to any oil

HISTORY

SUPRI's work on in-situ combustion has focused on: a) studying the actual mechanism of this process in laboratory experiments; b) evaluating field projects and their performance; and c) interrelating laboratory and field results.

The laboratory phase of this project commenced with conventional combustion tube runs. Satman and Brigham proposed a mathematical model to simulate the steam plateau phenomena (1). To simulate frontal behavior, it was necessary to understand the oxidation reactions of crude oil in porous media, and hence kinetic runs were conducted.

The experimental equipment used and the preliminary results of this work were described in a previous paper (2). This paper presents the laboratory results and the proposed kinetic models for fuel oxidation in in-situ combustion.

Prepared for the Department of Energy under Contract No. DE AC03 76ET12056.

INTRODUCTION

In-situ combustion oil recovery has been discovered to have field-wide relevance, especially in very viscous oil reservoirs because of its generation of high oxidation heat underground which leads to the mobilization of crude oil. Knowledge of crude oil oxidation reactions is imperative for predicting in-situ combustion performance. However, due to the complex nature of crude oil, its oxidation behavior has been the least understood reaction. Therefore, laboratory and field correlations were developed to estimate important parameters such as fuel availability (3-5). Although valid for one field, these correlations do not depict other field conditions because the nature of the reactions leading to fuel depositions was not considered.

In this paper, a model is proposed to analyze the reactions that occur as a combustion front approaches an oil sand sample. Then, the effects of different oils, matrices, and metallic additives on these reactions are discussed

EXPERIMENTAL EQUIPMENT

The main equipment used in this study included a special reactor, oven, temperature controller, three continuous gas analyzers for carbon dioxide, carbon monoxide, and oxygen, and auxiliary flow and pressure equipment. The details of laboratory setup and the properties of crude oils used were described in an earlier publication (2).

PROCEDURE

The oil sand samples were subjected to a linear temperature rise of 55°C/hr (100°F/hr) to simulate the thermal history of each section of an oil reservoir as it is heated by the combustion front encroachment. The produced gases were analyzed continuously and were recorded. For details, see Ref. 2. Table 1 presents the initial pack conditions for kinetic runs.

RESULTS

An example of gases produced as a sample of Huntington Beach oil sand was heated is shown in Fig. 1. Generally, there are two apparent peaks in the production of carbon oxides at different temperatures (2). At high temperatures (around 700°K), the amount of consumed oxygen is comparable to the amount of produced carbon oxides (i.e., CO_2 plus 1/2 CO). But at low temperatures, the oxygen consumed is greater than the carbon oxides produced. At even lower temperatures, some oxygen is consumed but no carbon oxides are produced.

For the crude oils studied, the molar CO_2/CO ratio (λ) and the apparent H/C ratios (η) at different temperatures were calculated (2). Changes in λ indicate the transition between reactions at different temperatures, and η determines the chemical nature of the consumed fuel for these reactions. An example is shown in Fig. 2 where these two parameters are graphed with respect to reaction temperature for a French oil (27°API). The fact that λ is almost constant at high temperatures

indicates that carbon oxides are produced by the same reactions. Correspondingly, the reactions at low temperatures must be numerous and non-unique because at temperatures below about 600°K (620°F), λ varies with temperature.

At low temperatures, η is high, indicating high oxygen consumption for the amount of carbon oxides produced. However, as the temperature is increased, η drops until it reaches the value of the atomic H/C ratio of crude oil at about 600°K. This may be due to the distillation of crude oil. At even higher temperature, η decreases further until it reaches a minimum of about 0.5. This drop is greater than the one observed in the distillation process (η for the residue of Huntington Beach oil was 1.5). This decrease is attributed to further pyrolysis of the fuel at higher temperatures and is in agreement with the results of Burger and Sahuquet (6). (For a detailed analysis of the effect of distillation and pyrolysis on η and λ please see Ref. 7.)

As a result of the preceding sections, the following conclusions can be drawn:

1) At lower temperatures, the crude oil undergoes an oxidation reaction without generating carbon oxides.

2) As the temperature is raised, distillation coupled with pyrolysis produces hydrogen gas and some light hydrocarbons in the gas phase. A major part of these hydrocarbons are produced without being oxidized. However, oxygen reacts with the remainder of these gases and hence, medium-temperature oxidation occurs.

3) At higher temperatures, this reaction is completed and a heterogeneous reaction begins. Here, the reactants are oxygen in the gas phase and heavy residue of oil deposited on the solid matrix.

Effect of Pressure on λ and Peak Location

The average values of λ calculated at high temperatures in different runs using Huntington Beach Oil are graphed vs partial pressure of oxygen in Fig. 3. It appears that λ increases slightly with higher pressure. The straight line shown is drawn through the data obtained using Huntington Beach oil and has the following equation:

$$\lambda = 0.228 \ln p_{O_2} + 1.404 \quad (1)$$

where

p_{O_2} = Partial Pressure of Oxygen, kPa

The location of the high-temperature peak was also shifted to lower temperatures as pressure increased. An example is shown in Fig. 4 where peak temperature is plotted against the partial pressure of oxygen. The same behavior was observed for the first peak. These two observations

indicate that the higher the partial pressure of oxygen, the higher the carbon dioxide production and the lower the reaction temperature. In other words, fuel oxidation depends directly on the partial pressure of oxygen.

Modeling of the Reactions

In Appendix A, a model is developed based on Weijdema's kinetic equation (8). In this model, the temperature can be increased linearly with time, and by proper graphing of the variables, a semi-log straight line should result. The variable temperature runs were made to test this model. Using the data in Run No. 110 (Fig. 1), the relative reaction rate (Appendix A) was calculated and is graphed in Fig. 5. Note that the high temperature data fall on a straight line as predicted by Weijdema's model but at lower temperatures (increasing values of 1/T) a departure from the straight line is observed. It is clear from these data that Weijdema's single-reaction model does not adequately describe the reaction kinetics observed.

At high temperatures the amount of carbon oxides formed closely matches the amount of oxygen consumed, but at medium temperatures the oxygen consumed is greater than the carbon oxides formed. Finally, at low temperatures, oxygen is consumed with no carbon oxides formation. This pattern is the basis of an analysis of the data for these separate reactions as described in the following paragraphs.

A straight line was drawn through the high temperature data. From the slope of that line an activation energy, E = 135 kJ/mole, is obtained (Fig. 6, curve I). It was assumed that this reaction also occurs at lower temperatures according to an extrapolation of the high temperature data. The method used is described in Refs. 7 and 9.

By subtracting from the original $\Delta\gamma$ curve (Fig. 7), a new curve (Fig. 7, curve II) is obtained which describes the oxidation behavior at medium temperature range, and curve III in the same figure is obtained which describes the production of carbon oxides in the medium-temperature range.

From curve II of Fig. 6, a calculation of the relative reaction rate, $(\Delta\gamma)/\int_t^\infty \Delta\gamma dt'$ as a function of 1/T leads to the curve labelled II in Fig. 6 (the open triangles). The data are not linear. However, a computation of an equivalent term for the carbon oxides formed, $\delta/\int_t^\infty \delta dt'$, where $\delta = CO_2 + 0.5CO$, from curve III, Fig. 7, shows a definite straight line (curve III, Fig. 6). An activation energy of E = 84 kJ/mole is calculated from the slope of this line. In this figure, although the data scatters considerably, it appears reasonable to assume the oxygen consumption curve in the medium-temperature range follows the same slope as the carbon oxides curve. Using this assumption, the oxygen consumption can be calculated and subtracted from curve II of Fig. 7 and the remainder is represented in curve V (Fig. 7).

When the data from curve V, Fig. 7, is evaluated using the Weijdema integral, $\Delta\gamma/\int_t^\infty \Delta\gamma dt'$, and the result is graphed on Fig. 6, a straight line (curve V) is formed which describes the low-temperature oxidation

reaction. The activation energy calculated from the slope of this line is E = 93 kJ/mole.

Using the computer interactively, this same analysis was applied to other experiments. The results always fit straight lines. However, for different crude oils, the order of the reaction with respect to fuel concentration, n, was different.

Repeatability and Accuracy of Experiments

The trapezoidal rule was used to integrate the area under the oxygen consumption curve. This caused some errors when there was a sharp change in gas concentration. It also introduced some errors into the calculations of curve fitting and extrapolation of the reaction rates to lower temperatures. These calculations were especially sensitive to the choice of the point at which the relative reaction rate curve would deviate from the straight line (Appendix A). Thus, in some runs, using the same fuel, but at different partial pressure of oxygen, the calculated activation energies were not the same (Table 2). This in turn led to the evaluation of a wrong intercept. Therefore, to normalize the data, first, the activation energies which were quite different from the average value, were discarded. Then, using the average value of the calculated activation energies, straight lines of the same slope were drawn through the experimental data points on the Arrhenius plot (Fig. 8). This was achieved by selecting an arbitrary data point at the mid-range of the abscissa as the focal point. For a combustion reaction (Fig. 8), this point was $1.5 \times 10^{-3}\ ^{o}K^{-1}$, respectively. The relative reaction rates evaluated at the focal points for the above three reactions are shown in column 5 of Tables 2 through 4. Finally, the true intercept at each pressure was computed (column 6 of Tables 2-4).

Evaluation of Arrhenius Constant

Appendix A shows that by plotting the true intercept (i.e., $A_r p_{O_2}^{m}$) with respect to partial pressure of oxygen (i.e., p_{O_2}), we can evaluate both the Arrhenius constant, A_r, and the reaction order with respect to oxygen partial pressure, m. Figure 11 illustrates this method for combustion reaction. Similar graphs were obtained for two other reactions. The final reaction rate equations are shown on Tables 2 through 4.

Following the same procedure, the reaction kinetic parameters were evaluated for other crude oils used in the experiments. For these crude oils, only two runs were conducted. Figures 12 and 13 show the straight lines obtained for different reactions using Venezuelan oil. The entire suite of kinetic data for these crude oils are given on Tables 5 and 6. The results show the applicability of the proposed model in evaluation of kinetic parameters for oxidation of crude oil in porous medium.

Diffusion Effects

The first step in the reaction mechanism of crude oil oxidation in a porous medium is the diffusion of oxygen from the bulk gas stream to the fuel on the rock. Using correlations for prediction of the diffusion rate, it was found that the chemical reaction step is much slower than the

diffusion step (7). Therefore, the overall rate appears to be kinetically controlled. Later, this notion was substantiated experimentally when a two-fold increase in the air flow rate did not cause any change in reaction constants.

Effect of Lithology on the Reactions

Investigators have reported the effects of clay content, metallic additives, and surface area of the rock on fuel deposition. Some experiments were run using either the original core or a mixture of sand and clay to study these effects quantitatively. The results of these experiments along with those of Bardon and Gadelle (10), who also studied the effect of metallic additives on these reactions, are reported here.

Effect of Matrix

Some experiments were run using the oil in the original core. These cores were obtained from the Jobo field in Venezuela and from Lynch Canyon field in California. The CO_2/CO ratio was higher for these runs than for the runs using the sand mix.

The reaction rates were calculated using the kinetic model previously mentioned. The Arrhenius plot for Run No. 131 is shown in Fig. 14. (The combustion reaction rate for Venezuelan oil was graphed in Fig. 12 for comparison.) Tables 6 and 7 present the calculated kinetic constants for these reactions.

Figure 12 clearly shows that the activation energy for combustion reaction in the original core is much lower than in the sand mix. The sieve analysis for these matrices confirmed that the sand grains were much finer than the sand mix used in the runs. There were even some silts in these cores.

Bardon and Gadelle (10) investigated the effects of matrix on the oxidation reactions of a French oil. (For the properties of this oil along with the matrix and pack conditions, see Ref. 7.) In their first kinetic experiment (Run No. 1), they used a sand mix of varying grain size while a finer sand was used in their second run. They also conducted an experiment using the original core (Run No. 4). Their data were analyzed using the proposed kinetic model and the resulting Arrhenius graphs are presented in Figs. 15-17.

As is shown, the increase in the surface area (finer sand) resulted in a lower Arrhenius constant for both fuel deposition and fuel combustion without any change in activation energy (Table 8). This surface area dependency shows that the heterogeneous combustion reaction is apparently the result of burning a monolayer of fuel deposited on the rock. However, using the original matrix, both the Arrhenius constant and activation energy change. This is attributed to the presence of about 5% kaolinite in the matrix. Therefore, the effect of clay was studied.

Effect of Clay

In Runs No. 114 and 115, 5% clay was added to the sand pack and the normal procedure for a kinetic run was conducted. In both runs, the

low-temperature peak was found to be higher than the corresponding peaks in Runs No. 127 and 129 in which no clay was used. This implies that in the presence of clay, more fuel is available for oxidation reactions. This may be due to adsorption of hydrocarbons on the clay surface and, hence, low distillation and pyrolysis in porous medium.

The Arrhenius plot for the runs in which clay was used showed that the combustion reaction has a lower dependency on fuel concentration (i.e., $n < 1$) and a smaller activation energy than the ones obtained without clay (i.e., a catalytic effect). These results are shown in Table 9 and are in accordance with the ones previously obtained for French oil (Table 8). Bousaid and Ramey (11) also pointed out the catalytic effect of clay on the combustion reaction. They reported that the addition of 20% clay to sand caused a 10% reduction in the energy of activation of the combustion reaction.

Effect of Metallic Additives

As in most heterogeneous reactions, a catalyst can speed up the high-temperature oxidation reaction. In particular, the presence of metallic additives such as Cu, Ni, Va, Fe, etc., create a catalytic effect which lowers the temperature at which the combustion reaction occurs. This is due to a lower activation energy in the presence of additives. The analysis of the data on the oxidation of the French oil showed that an addition of 2000 ppm Cu to the sand mix lowered the activation energy by about 50% (Table 8). Figures 15 and 16 clearly demonstrate this catalytic effect on both fuel combustion and fuel deposition. However, for LTO reactions, a higher Arrhenius constant was obtained without a significant change in the activation energy when copper was added to the sand mix.

Due to this profound dependency of the kinetic parameter on the matrix compounds, the author believes that all combustion studies should be conducted using the parent cores. If this is not possible, the matrix should be analyzed to see whether metallic and clay additives are present. It is also felt that the existence of clay or a very fine matrix may lead to a successful combustion project in a field.

SUMMARY AND CONCLUSIONS

In this section, the results of the experiments are summarized and conclusions are listed.

Summary

Table 10 summarizes the results of kinetic runs for three different kinds of crude oil using Ottawa sand of the same mesh size.

As is shown, although the energies of activation for both LTO and fuel deposition reactions are similar, they are almost twice as high for fuel combustion reaction. This indicates that the fuel combustion reaction is the slowest reaction and, therefore, is the rate-determining step. It should also be noted that the calculated activation energies

are similar to the reported ones (2,7,11-13), and are almost independent of the type of oil used. However, clay and metallic additives act as catalysts and lower both activation energies and the temperature of combustion reaction. This can cause the rate-determining step to be shifted toward fuel deposition.

Although the reaction order with respect to fuel concentration, n, does not change, the reaction order with respect to oxygen partial pressure, m, varies and is always less than one.

The Arrhenius constants, A_r, are different for different oils. In addition, the A_r for combustion reaction is directly related to the available surface area of the matrix. Knowledge of this relationship and of the quality of crude oils may lead to determination of the amount of fuel available for combustion.

Also, for more reactive oil, the A_r for LTO reactions is higher. Thus, A_r is also a good indicator of whether spontaneous ignition will occur in a rock.

Pressure is an important factor of the frontal behavior because of a combination of the effect of partial pressure of oxygen, p_{O_2}, on these reactions and the effect of total pressure on distillation.

Conclusions

1. An apparatus was designed to study the reaction kinetics of oil oxidation in porous media.

2. A kinetic model was developed to evaluate the experimental data.

3. The overall oxidation mechanism of crude oil in porous medium at different temperatures is an overlap of several consecutive reactions from which three can be distinguished:

   a) LTO reactions are heterogeneous (gas-liquid) without any carbon oxides produced. Spontaneous ignition occurs due to LTO reactions.

   b) Middle-temperature reactions are mainly homogeneous (gas phase) and result from the oxidation of the products of distillation and pyrolysis. These in turn, leave a heavy oil residue on the solid matrix.

   c) High-temperature reactions are heterogeneous (gas and solid phase) and are a result of the combustion of the deposited residue.

4. The superimposed reactions can be easily differentiated by using the proposed model in this report.

5. These reactions are kinetically controlled and diffusion effects were found to be minimal.

6. The combustion reaction is slower than fuel deposition in a clean sand matrix.

7. Metallic additives and clays have catalytic effects on the reactions. Clays and fine sands enhance deposition of more fuel due to the adsorption characteristics on a higher surface area. These additives shift the rate-determining step from fuel combustion toward fuel deposition.

8. It is possible to formulate any frontal behavior in the field by using this model in conjunction with the temperature profile ahead of the front.

9. The correlation obtained for the Apparent H/C ratio and the molar carbon dioxide-carbon monoxide ratio can be used along with the model to estimate combustion heat.

10. Omission of any of these reactions in a combustion simulator may lead to erroneous results in the prediction of overall frontal behavior.

NOMENCLATURE

A = Cross-section area, cm^2

A' = Specific rock surface area per unit bulk volume cm^{-1} or per unit weight of sample, cm^2/g

A_r = Arrhenius constant

C_f = Fuel concentration, g fuel/100g sand

E = Activation Energy, J/g mole

L = Length of the pack, cm

m = Reaction order with respect to oxygen, constant

n = Reaction order with respect to carbon, constant

p = Total pressure, Pa

p_{O_2} = Oxygen partial pressure, Pa

q = Gas flow rate, cc/s

R = Universal gas constant

T = Temperature, °C or °K

t = Time, s

ϕ = Porosity

β = Slope of temperature-time curve, 1/s

β' = Intercept of relative reaction rate curve vs 1/T, 1/s

γ = Oxygen concentration, mole %

δ = Oxygen converted to carbon oxides, more %

ν = Nitrogen concentration, mole %

η = Apparent hydrogen-carbon ratio

λ = Molar carbon dioxide-carbon monoxide ratio

μ = Viscosity

ACKNOWLEDGEMENT

Financial support during the course of this work was provided by the Department of Energy through Stanford University Petroleum Research Institute, contract #E (04-3) 1265. Appreciation is also extended to Dr. Subir K. Sanyal, former SUPRI Manager.

REFERENCES

1. Satman, A., Brigham, W. E., and Ramey, H. J., Jr.: "An Investigation of Steam Plateau Phenomena," Paper SPE 7965, presented at the California Regional Meeting of SPE, Ventura, Ca. (April 18-20, 1979).

2. Fasshihi, M. R., and Brigham, W. E.: "Investigation of Reactions Occurring in in-Situ Combustion," Paper presented at 1981 Annual Heavy Oil/EOR Contractor Presentations--Proceedings, San Francisco, Ca. (July 22-24, 1980).

3. Alexander, J. D., Martin, W. L., and Dew, J. N.: "Factors Affecting Fuel Availability and Composition During In-Situ Combustion," J. of Pet. Tech. (October, 1962), pp. 1154-1164.

4. Martin, W. L., Alexander, J. D., and Dew, J. N.: "Process Variables of In-Situ Combustion," Trans. AIME (1958), Vol. 213, pp. 28-35.

5. Showalter, W. E.: "Combustion-Drive Tests," Soc. Pet. Eng. J. (March, 1963), pp. 53-58.

6. Burger, J. G., and Sahuquet, B. C.: "Les Methods Thermiques De Production Des Hydrocarbures--Combustion In-Situ, Principles Et Etudes De Laboratoire," Revue de L'Institute Francais du Petrole (March-April, 1977), No. 2, pp. 141-188.

7. Fassihi, M. R.: "Analysis of Fuel Oxidation on In-Situ Combustion Oil Recovery," Ph.D. dissertation submitted to the Department of Petroleum Engineering, Stanford University, Stanford, Ca. (April, 1981). Submitted to DOE for publication.

8. Weijdema, J.: "Determination of the Oxidation Kinetics of the In-Situ Combustion Process," Report from Koninklijke/Shell, Exploratie En Produktic Laboratorium, Rijswijk, The Netherlands (1968).

9. Fassihi, M. R., Birgham, W. E., and Ramey, H. J., Jr.: "The Reaction Kinetics of In-Situ Combustion," Paper SPE 9454, presented at the Annual Fall Meeting of SPE, Dallas, Tx. (September 21-24, 1980).

10. Bardon, C., and Gadelle, C.: "Essai de Laboratoire Pour L'Etude de la Combustion In-Situ," Institute Francais du Petrole, Paris (May, 1977).

11. Bousaid, I. S., and Ramey, H. J., Jr.: "Oxidation of Crude Oil in Porous Media," Soc. Pet. Eng. J. (June, 1968), pp. 137-148; Trans. AIME, Vol. 243.

12. Dabbous, M. K., and Fulton, P. F.: "Low-Temperature Oxidation Reaction Kinetics and Effects on the In-Situ Combustion Process," Soc. Pet. Eng. J. (June, 1974), pp. 253-262.

APPENDIX A

DERIVATION OF EQUATIONS FOR NON-ISOTHERMAL OXIDATION

The change in oxygen concentration ($\Delta\gamma$) during the kinetic experiments can be calculated from:

$$\Delta\gamma = \gamma_i - \frac{\nu_i \gamma_o}{1 - CO_2 - CO - \gamma_o} = \frac{\gamma_i(1 - CO_2 - CO) - \gamma_o}{1 - CO_2 - CO - \gamma_o} \qquad (A\text{-}1)$$

The rate of oxygen consumption per unit volume is:

$$\frac{q\Delta\gamma}{AL} = A_r p_{O_2}{}^m C_f{}^n \exp(-E/RT) \qquad (A\text{-}2)$$

This is also equal to the rate of decrease of oil saturation:

$$\frac{q\Delta\gamma}{AL} = -\alpha \frac{dC_f}{dt} \qquad (A\text{-}3)$$

in which α is the proportionality factor, equal to the amount of oxygen in moles that reacts with one gram of the oil.

The rate of oxygen consumption at any time can be obtained by combining Eqs. A-2 and A-3:

$$\frac{q\Delta\gamma}{AL} = A_r p_{O_2}{}^m \exp(-E/RT)\, C_f{}^n = -\alpha \frac{dC_f}{dt} \qquad (A\text{-}4)$$

Integration between $t = t$ and $t = \infty$ yields:

$$\alpha C_f(t) = \int_t^\infty \frac{q\Delta\gamma}{AL}\, dt' \qquad (A\text{-}5)$$

Where $C_f = 0$ at $t = \infty$. From Eq. A-4:

$$C_f^n(t) = \frac{q\Delta\gamma}{AL} \frac{1}{A_r P_{O_2}^m \exp(-E/RT)} \quad \text{(A-6)}$$

If we substitute Eq. A-6 in Eq. A-5, we obtain:

$$\frac{\Delta\gamma}{\left[\int_t^\infty \Delta\gamma dt'\right]^n} = \beta' \exp(-E/RT) \quad \text{(A-7)}$$

where:

$$\beta' = \left(\frac{q}{AL}\right)^{n-1} \frac{A_r P_{O_2}^m}{\alpha^n} \quad \text{(A-8)}$$

Values for the left hand side of Eq. A-7 can be found by graphical integration of the curve $\Delta\gamma = f(t)$. Then the left hand side of Eq. A-7 can be graphed vs 1/T to obtain (-E/R) as the slope, and β' as the intercept. In this paper, the left hand side of Eq. A-7 is called relative reaction rate.

Table 1

INITIAL CONDITIONS FOR KINETICS RUNS

RUN NO.	OIL USED	FLOW RATE scc/s	AVG.PRESSURE kPa	INJ.OXYGEN Mole%	CONDITION	BURNED FUEL g	FUEL/SAND RATIO wt.%	BED THICKNESS cm
101	SAN ARDO	16.7	690	21	ISOTHERMAL	2.402	2.69	9
102	SAN ARDO	16.7	690	21	NON-ISOTHERMAL	0.401	1.72	2
103	SAMPLE NO. 8 (79-4)	8.3	690	21	NON-ISOTHERMAL	0.924	4.57	2
104	HUNTINGTON BEACH	8.3	690	21	NON-ISOTHERMAL	0.866	3.64	2
105	SAMPLE NO. 5 (79-3)	16.7	690	21	NON-ISOTHERMAL	0.577	9.07	1
106	SAMPLE NO. 13 (7903)	16.7	550	21	NON-ISOTHERMAL	3.701	7.76	2.3
107	SAN ARDO	16.7	550	21	ISOTHERMAL	0.604	2.81	2.1
108	VENEZUELA	8.3	550	21	NON-ISOTHERMAL	0.514	4.48	1.2
109	SAMPLE NO. 68 (80-1)	16.7	550	8.3	NON-ISOTHERMAL	1.458	3.89	4.2
110	HUNTINGTON BEACH	7.5	550	8.3	NON-ISOTHERMAL	1.777	3.99	4.3
111	VENEZUELA	8.3	415	8.3	ISOTHERMAL	1.894	3.56	5.5
112	VENEZUELA	8.3	415	8.3	NON-ISOTHERMAL	1.234	3.75	3.5
113	SAMPLE NO. 68 (80-1)	8.3	275	8.3	NON-ISOTHERMAL	0.725	3.72	2.5
114	SAN ARDO (clay added)	8.3	550	21	NON-ISOTHERMAL	0.775	3.45	2.5
115	SAN ARDO (clay added)	8.5	275	8.3	NON-ISOTHERMAL	0.677	3.39	2
116	HUNTINGTON BEACH	10.0	550	21	ISOTHERMAL	1.88	3.80	4.5
117	HUNTINGTON BEACH	10.0	1035	21	NON-ISOTHERMAL	1.260	3.16	4
118	HUNTINGTON BEACH	10.0	138	21	NON-ISOTHERMAL	0.730	3.41	2.2
119	HUNTINGTON BEACH	10.0	552	21	NON-ISOTHERMAL	1.035	3.52	3
120	HUNTINGTON BEACH	10.0	1104	21	NON-ISOTHERMAL	0.984	3.63	2.5
121	HUNTINGTON BEACH	10.0	690	21	NON-ISOTHERMAL	0.757	3.41	2.2
122	HUNTINGTON BEACH	10.0	138	8.3	NON-ISOTHERMAL	1.103	3.44	3
123	HUNTINGTON BEACH	10.0	17	21	NON-ISOTHERMAL	1.177	3.75	3
124	HUNTINGTON BEACH	10.0	235	21	NON-ISOTHERMAL	1.441	3.32	4
125	VENEZUELA	10.0	828	21	NON-ISOTHERMAL	0.784	3.22	2.5
126	VENEZUELA (original core)	10	690	21	NON-ISOTHERMAL	10.242*	----	4
127	SAN ARDO	10	690	21	NON-ISOTHERMAL	0.916	2.54	3
128	HUNTINGTON BEACH	10	41	21	NON-ISOTHERMAL	0.931	3.2	2.7
129	SAN ARDO	10	138	21	NON-ISOTHERMAL	0.814	2.55	3.1
130	LYNCH CANYON (original core)	10	690	21	NON-ISOTHERMAL	-----	----	3.3
131	LYNCH CANYON (original core)	10	690	21	NON-ISOTHERMAL	3.321*	----	1.6

*Total weight reduction of oil sand including water loss.

Table 2: FUEL COMBUSTION REACTION RATE*
(Huntington Beach Crude Oil)

Run No.	$A_r P_{O_2}^m$ 1/s x 10^{-6}	E/R ^oK x 10^{-4}	P_{O_2} kPa	RRR(1.5×10^{-3}) 1/s x 10^{+4}	True Intercept 1/s x 10^{-6}
110	13.30	1.628	54.2	3.45	12.336
117	23.88	1.616	238.7	7.00	25.030
118	7.912	1.611	50.3	2.5	8.940
119	21.07	1.643	137.0	4.1	14.660
120	25.97	1.627	253.0	6.4	22.884
121	18.29	1.628	166.2	4.5	16.090
122	4.03	1.619	19.9	1.15	4.112
124	7.585	1.602	70.5	2.72	9.726
128	4.858	1.608	30.0	1.60	5.721
Average:		1.620			

* $-R_c = 6 \times 10^5 \exp(-135{,}000/RT) P_{O_2}^{0.66} C_f$

Table 3: FUEL DEPOSITION REACTION RATE*
(Huntington Beach Crude Oil)

Run No.	$A_r P_{O_2}^m$ 1/s x 10^{-3}	E/R ^oK x 10^{-3}	P_{O_2} kPa	RRR(1.8×10^{-3}) 1/s x 10^{+4}	True Intercept 1/s x 10^{-3}
110	31.480	10.120	54.2	3.62	10.593**
117	11.630	9.430	238.7	5.00	14.631
118	5.664	9.372	50.3	2.60	7.608
119	21.8	9.857	137	4.3	12.582
120	2.981	8.743	253	4.4	12.87
121	5.63	9.128	166.2	4.2	12.29
122	5.928	9.746	19.9	1.42	4.155
123	6.79	9.675	24.6	1.88	5.501
124	18.040	9.901	70.5	3.2	9.364
128	5.05	9.535	30	1.78	5.208
Average:		9.551			

* $R_f = 1.2 \times 10^3 \exp(-80{,}000/RT) P_{O_2}^{0.46} C_f$

** This was not included in the curve fit

Table 4: LOW-TEMPERATURE OXIDATION RATE*
(Huntington Beach Crude Oil)

Run No.	$A_r P_{O_2}^m$ 1/s x 10^{-3}	E/R ^oK x 10^{-3}	P_{O_2} kPa	RRR(1.95×10^{-3}) 1/s x 10^{+4}	True Intercept 1/s x 10^{-3}
110	1896.	11.15	54.2**	--	--
117	5.915	8.176	238.7	7.	4.678
118	3.851	8.403	50.3	1.85	1.236
119	22.62	8.945	137.**	--	--
120	117.3	9.716	253.**	--	--
121	4.385	8.198	166.2	5.	3.342
122	1.170	7.948	19.9	2.2	1.470
123	1.978	8.135	24.6	1.55	1.036
124	3.445	8.172	70.5	4.1	2.740
128	0.31	7.38	30.0	1.73	1.156
Average:		8.059			

* $R = 1.9 \times 10^2 \exp(-67{,}000/RT) P_{O_2}^{0.57} C_f$

** This was not included in the curve fit

Table 5: KINETIC DATA FOR SAN ARDO CRUDE OIL

1. Fuel Combustion Rate*

Run No.	$A_r P_{O_2}^m$ 1/s x 10^{-5}	E/R °K x 10^{-4}	P_{O_2} kPa	RRR(1.5×10^{-3}) 1/s x 10^4	True Intercept 1/s x 10^{-5}
127	6.705	1.416	166.2	4	7.675
129	4.495	1.433	50.3	2	3.838
Average:		1.425			

* $-R_c = 4 \times 10^4 \exp(-120{,}000/RT)\ P_{O_2}^{0.58}\ C_f$

2. Fuel Deposition Rate**

Run No.	$A_r P_{O_2}^m$ 1/s x 10^{-3}	E/R °K x 10^{-3}	P_{O_2} kPa	RRR(1.8×10^{-3}) 1/s x 10^4	True Intercept 1/s x 10^{-3}
127	3.965	8.884	166.2	4.5	3.564
129	1.975	8.766	50.3	2.75	2.178
Average:		8.825			

** $R_f = 4.5 \times 10^2 \exp(-74{,}000/RT)\ P_{O_2}^{0.4} C_f$

3. Low-Temperature Oxidation Rate***

Run No.	$A_r P_{O_2}^m$ 1/s x 10^{-3}	E/R °K x 10^{-3}	P_{O_2} kPa	RRR(1.95×10^{-3}) 1/s x 10^{+4}	True Intercept 1/s x 10^{-2}
127	1.964	7.847	166.2	4.4	13.19
129	0.563	7.450	50.3	2.8	8.39
Average:		7.648			

*** $R = 1.9 \times 10^2 \exp(-64{,}000/RT)\ P_{O_2}^{0.4} C_f$

Table 6: KINETIC DATA FOR VENEZUELAN OIL

1. Fuel Combustion Rate*

Run No.	$A_r P_{O_2}^m$ 1/s x 10^{-6}	E/R °K x 10^{-4}	P_{O_2} kPa
112*	4.72	1.597	43
125*	6.674	1.597	195
126	7.326×10^{-6}	0.687	166

* - $R_c = 2 \times 10^6 \exp(-133{,}000/RT)\ P_{O_2}^{0.23} C_f$

2. Fuel Deposition Rate**

Run No.	$A_r P_{O_2}^m$ 1/s x 10^{-1}	E/R °K x 10^{-3}	P_{O_2} kPa	RRR(1.8×10^{-3}) 1/s x 10^{+4}	True Intercept 1/s x 10^{-1}
112**	2.102	6.288	43	2.52	1.69
125**	1.747	6.060	195	3.28	2.20
126+	$2.848 \times 10^{+5}$	9.73	166	--	--
Average:		6.174			

** $R_f = 8.8 \exp(-51{,}000/RT)\ P_{O_2}^{0.18} C_f$

3. Low Temperature Oxidation Rate***

Run No.	1/s x 10^{-3}	E/R °K x 10^{-3}	kPa	RRR(1.95×10^{-3}) 1/s x 10^{+4}	True Intercept 1/s x 10^{-3}
112	5.942	8.594	43	3.12	5.034
125	8.343	8.429	195	5.9	9.519
126+	1.929×10^3	1.067×10^1	166	--	--
Average:		8.511			

*** $R = 1. \times 10^3 \exp(-70{,}000/RT)\ P_{O_2}^{0.42} C_f$

+ This was not included in the curve fit

Table 7

KINETIC DATA FOR LYNCH CANYON OIL (Run No. 131)

	FUEL COMBUSTION	FUEL DEPOSITION	LTO REACTION
Intercept, 1/s	7.785×10^6	1.984×10^3	6.808×10^8
E, J/gmole	1.209×10^5	6.645×10^4	1.153×10^5

Table 8 : ANALYSIS OF DATA OF BARDON AND GADELLE

1. Combustion Reaction*

Bed	Intercept, 1/s	$\frac{E/R}{^{o}K \times 10^{-4}}$	n
Sand Mix*	6.25×10^{3}	1.264	1.2
Silica*	1.241×10^{4}	1.277	1.2
Original Matrix	2.287×10^{1}	0.844	1.2
Sand Mix + 2000 PPm Cu	2.8481×10^{-1}	0.486	1.2

* $-R_c = ArP_{O_2}^{m} \exp(-105{,}000/RT)\, C_f^{1.2}$

2. Fuel Deposition Reaction**

Bed	Intercept, 1/s	$\frac{E/R}{^{o}K \times 10^{-3}}$	n
Sand Mix**	3.56×10^{1}	7.546	1.2
Silica**	8.896×10^{1}	7.712	1.2
Original Matrix	1.811×10^{4}	10.361	1.2
Sand Mix + 2000 PPm Cu	7.46×10^{6}	11.485	0.7

** $R_f = ArP_{O_2}^{m} \exp(-63{,}500/RT)\, C_f^{1.2}$

3. Low-Temperature oxidation Reaction***

Bed	Intercept	$\frac{E/R}{^{o}K \times 10^{-4}}$	n
Sand Mix***	5.610×10^{6}	1.415	1.4
Silica	--	--	--
Original Matrix	1.027×10^{9}	1.444	1
Sand Mix + 2000PPm Cu	1.209×10^{8}	1.320	1

*** $R = ArP_{O_2}^{m} \exp(120{,}000/RT)\, C_f^{1.4}$

Table 9

KINETIC DATA FOR COMBUSTION OF SAN ARDO OIL*
(sand with clay)

RUN NO.	P_{O_2}, kPa	Intercept, 1/s	E/R, $^{o}K^{-1}$	m	n	A_r, $(kPa)^{-m}/s$
114	137.2	3.92×10^{3}	7.514×10^{3}	0.55	0.4	260
115	31.3	1.75×10^{3}	7.34×10^{3}	0.55	0.4	260

* $-R_c = 260 \exp(-61{,}000/RT) P_{O_2}^{0.55} C_f^{0.4}$

Table 10

SUMMARY OF KINETIC DATA

$R = A_r \exp(-E/RT) P_{O_2}^{m} C_f^{n}$

CRUDE TYPE	LTO REACTION				FUEL DEPOSITION				FUEL COMBUSTION			
	A_r	E	m	n	A_r	E	m	n	A_r	E	m	n
Huntington Beach	1.9×10^{2}	6.7×10^{4}	0.57	1	1.2×10^{3}	8.0×10^{4}	0.46	1	6×10^{5}	1.35×10^{5}	0.66	1
San Ardo	1.9×10^{2}	6.4×10^{4}	0.4	1	4.5×10^{2}	7.4×10^{4}	0.4	1	4×10^{4}	1.20×10^{5}	0.58	1
Venezuela	1.0×10^{3}	7.0×10^{4}	0.42	1	8.8	5.1×10^{4}	0.18	1	2×10^{6}	1.33×10^{5}	0.23	1

NOTE: The data was obtained using Ottawa Sand.

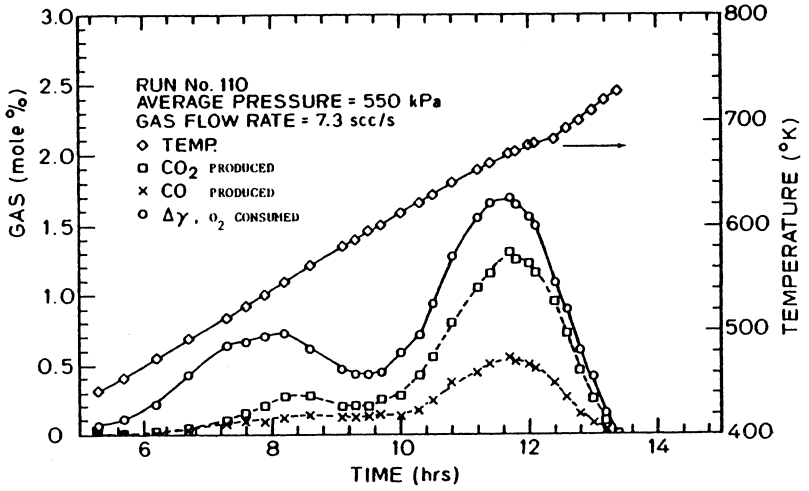

Fig. 1: GAS COMPOSITION AND TEMPERATURE VS TIME FOR HUNTINGTON BEACH OIL

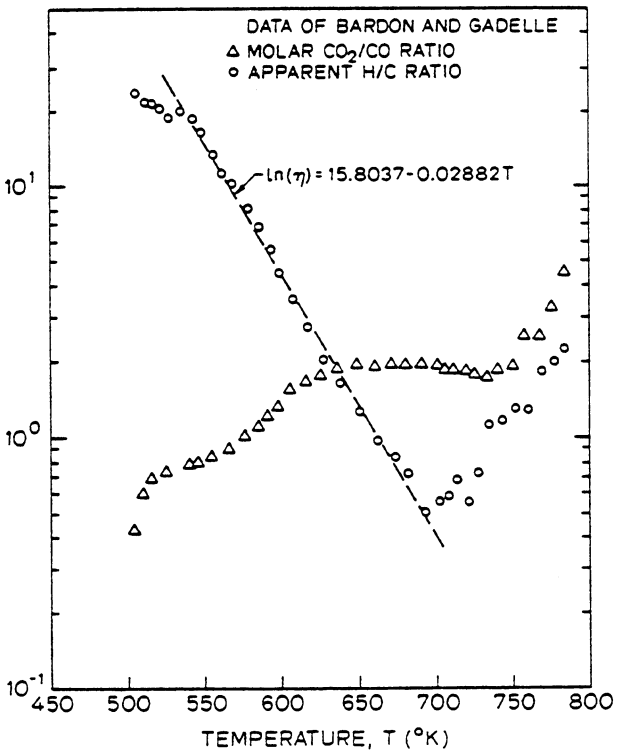

Fig. 2: MOLAR CO_2/CO RATIO AND APPARENT H/C RATIO FOR FRENCH OIL

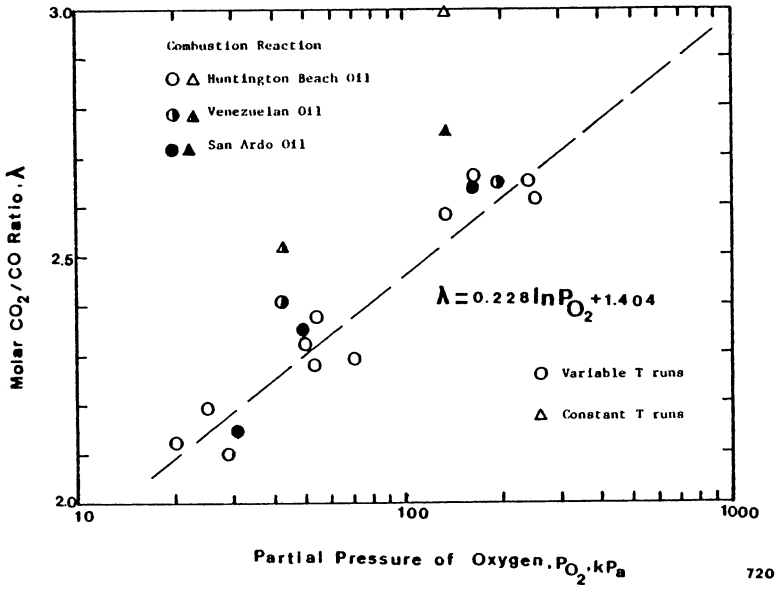

Fig. 3: MOLAR CO_2/CO RATIO VS PRESSURE

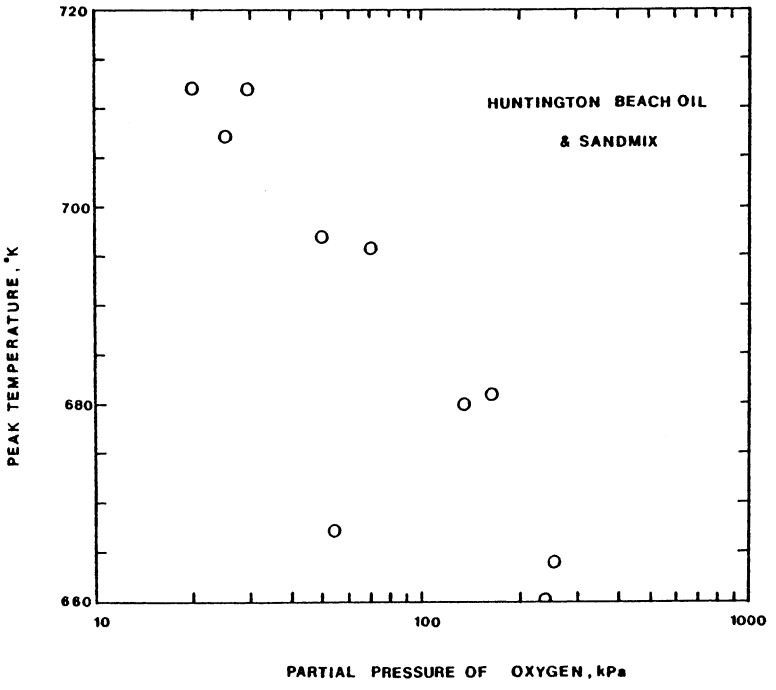

Fig. 4: EFFECT OF PARTIAL PRESSURE OF OXYGEN ON THE LOCATION OF THE SECOND PEAK

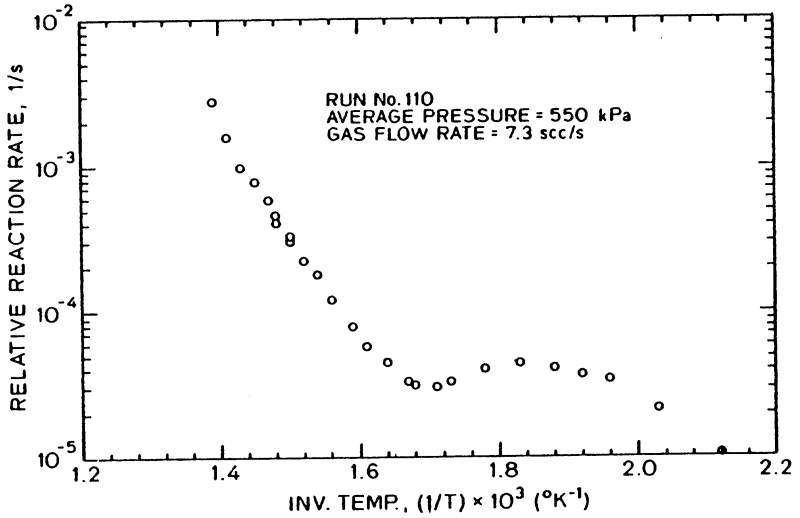

Fig. 5: RELATIVE REACTION RATE VS INVERSE TEMPERATURE FOR RUN NO. 110

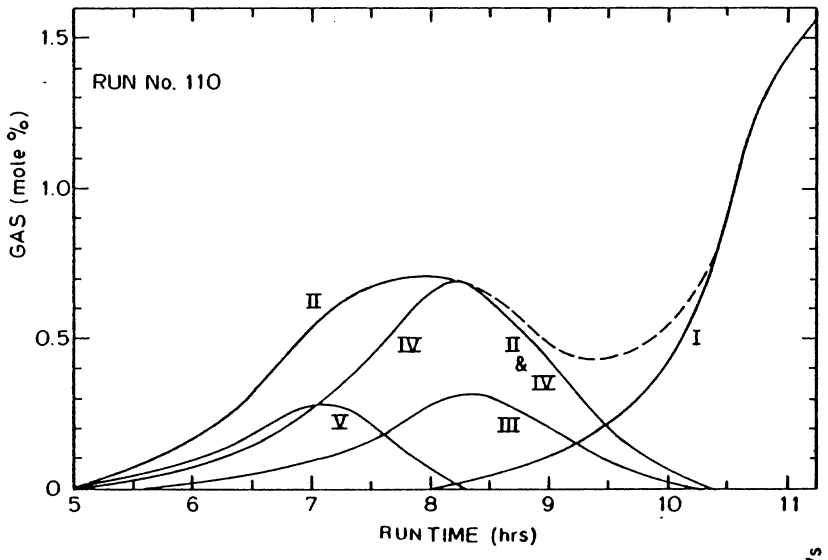

Fig. 7: DECOMPOSITION OF THE CONSUMED OXYGEN IN DIFFERENT REACTIONS

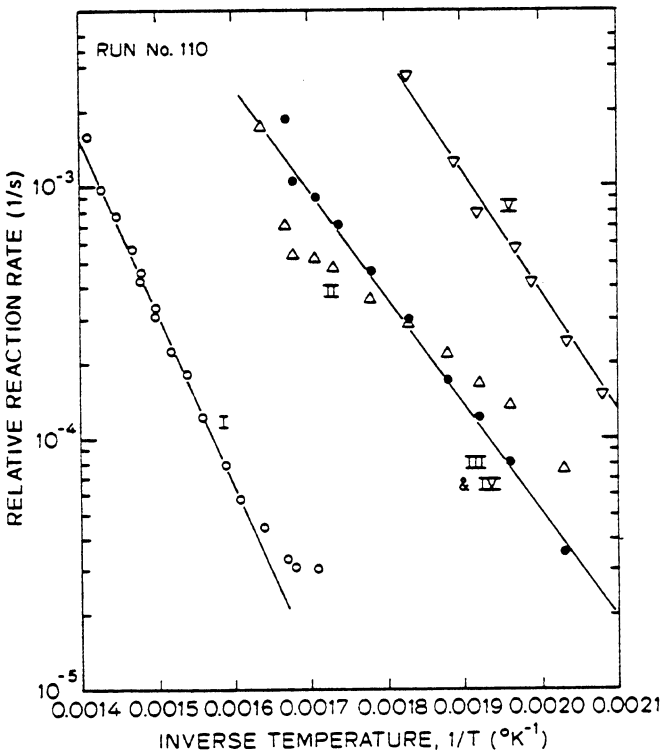

Fig. 6: ARRHENIUS PLOT FOR RUN NO. 110

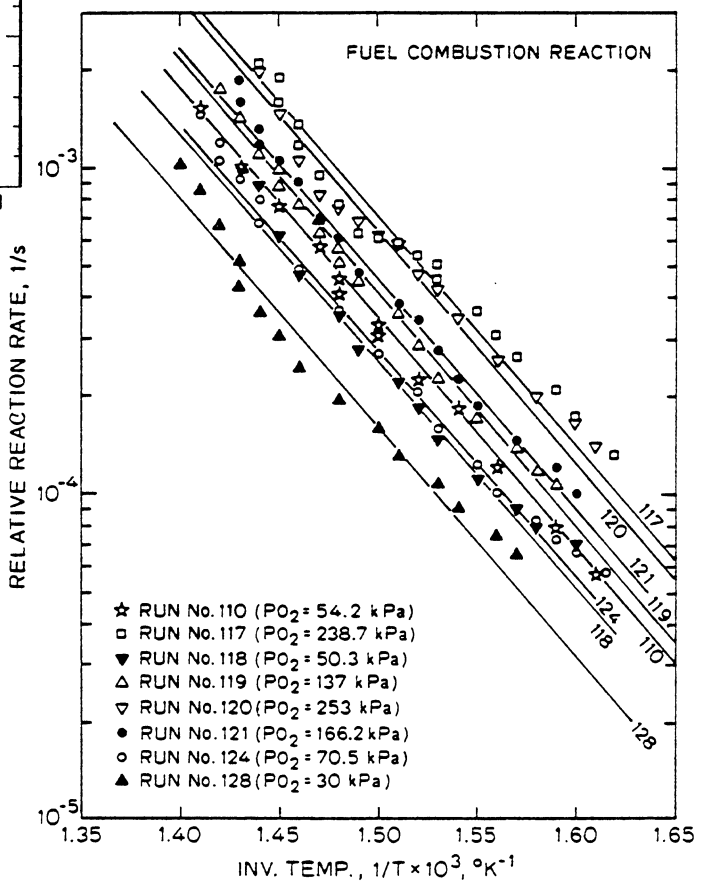

Fig. 8: ARRHENIUS PLOT FOR FUEL COMBUSTION REACTION (HUNTINGTON BEACH OIL)

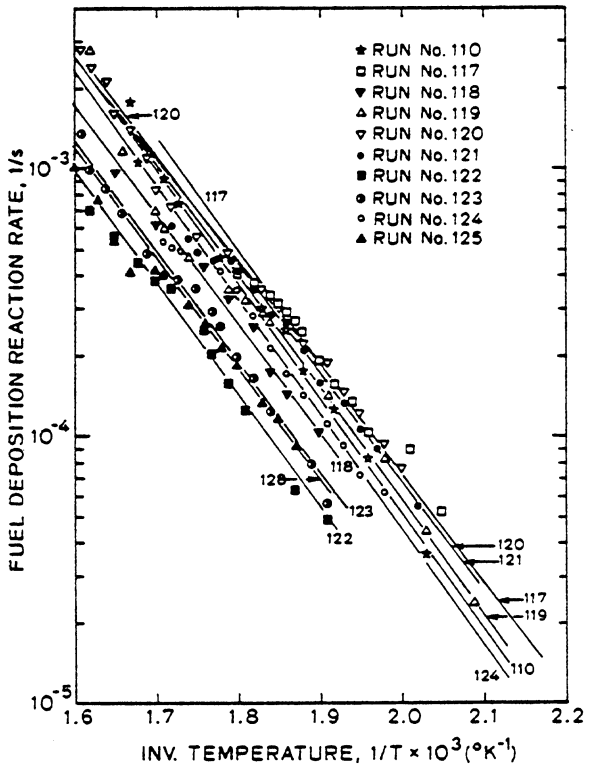

Fig. 9: ARRHENIUS PLOT FOR FUEL DEPOSITION REACTION (HUNTINGTON BEACH OIL)

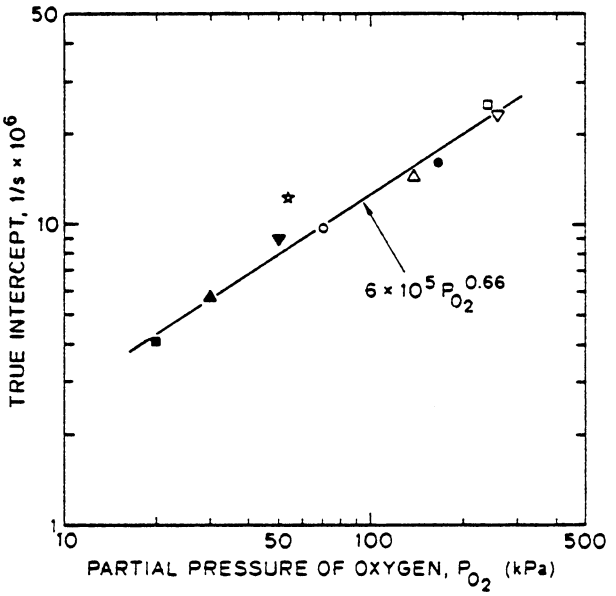

Fig. 11: PLOT OF INTERCEPT VS PRESSURE FOR COMBUSTION REACTION (HUNTINGTON BEACH OIL)

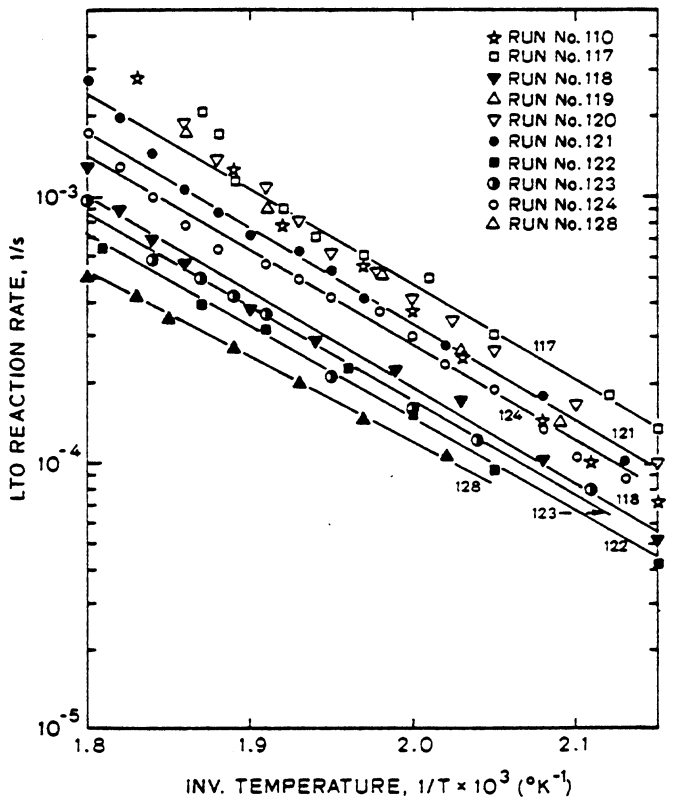

Fig. 10: ARRHENIUS PLOT FOR LTO REACTION (HUNTINGTON BEACH OIL)

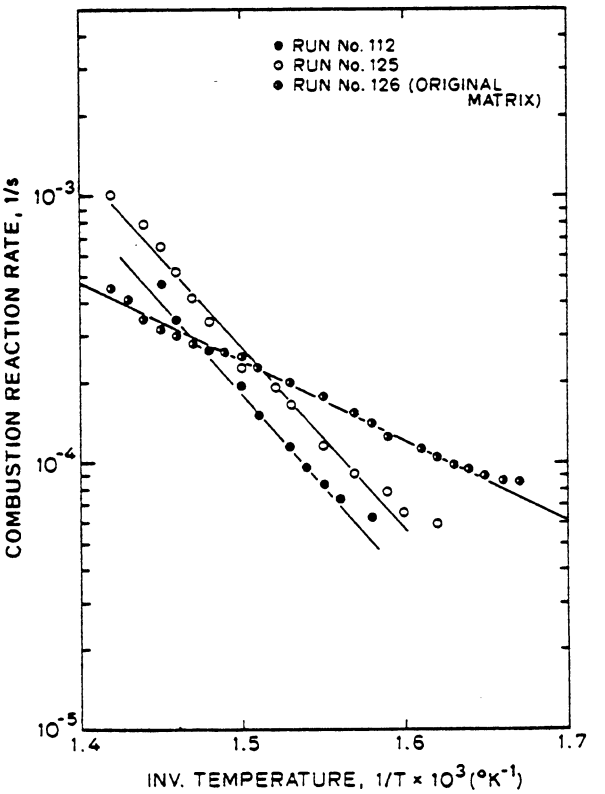

Fig. 12: ARRHENIUS PLOT FOR COMBUSTION REACTION (VENEZUELAN OIL)

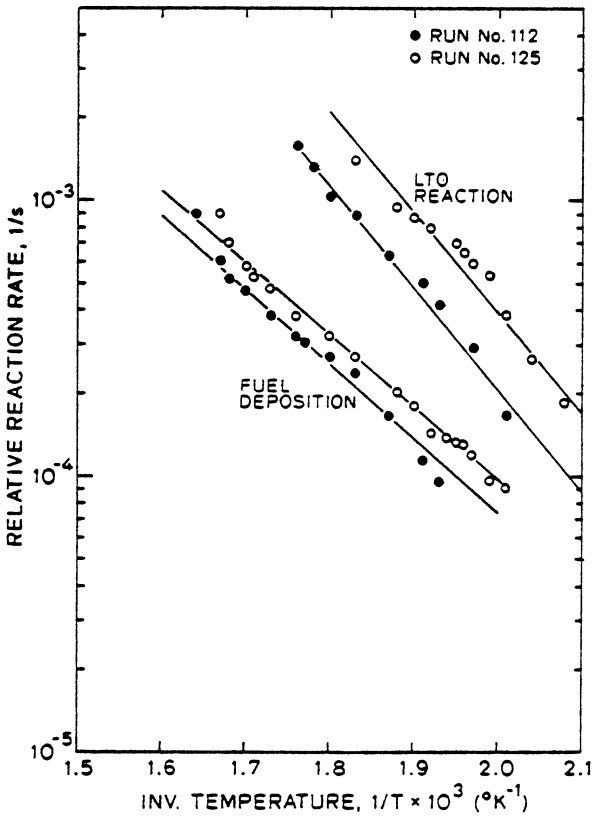

Fig. 13: ARRHENIUS PLOT FOR DIFFERENT REACTIONS (VENEZUELAN OIL)

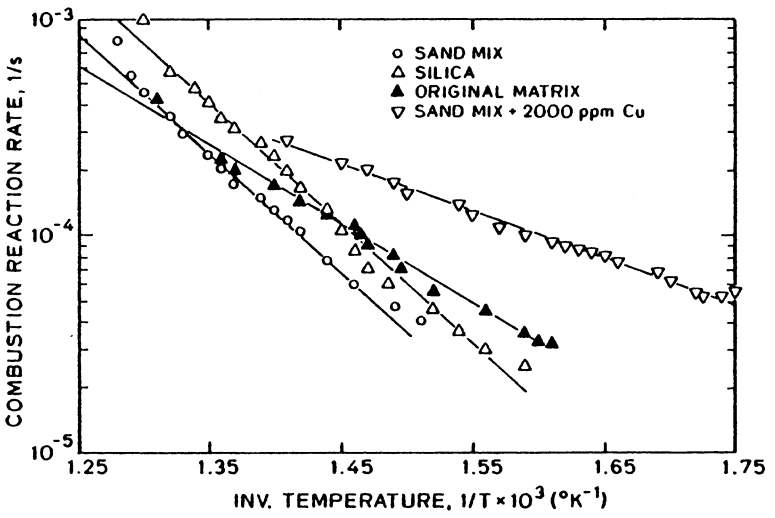

Fig. 15: ARRHENIUS PLOT FOR COMBUSTION REACTION (FRENCH OIL)

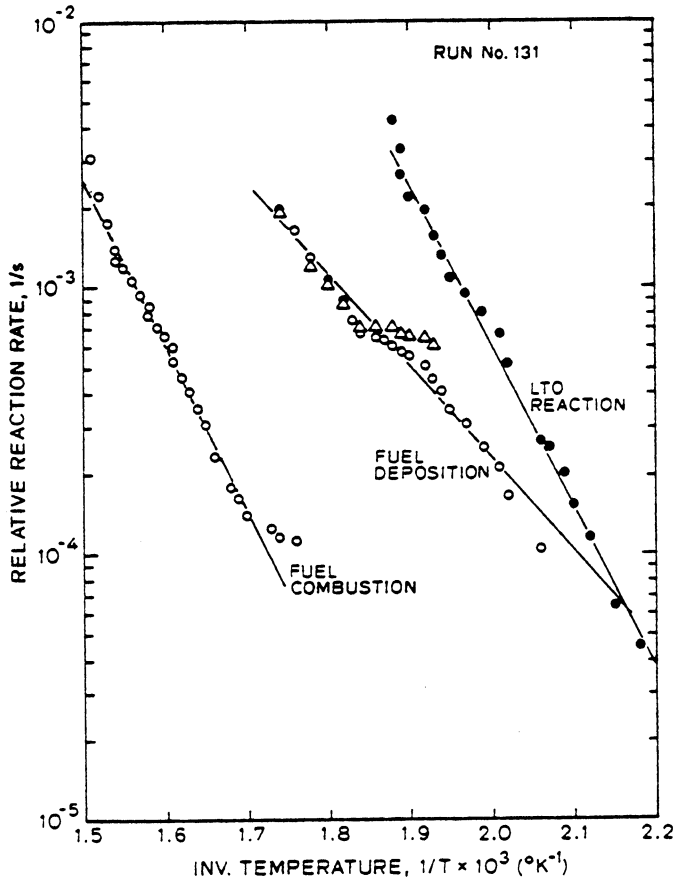

Fig. 14: ARRHENIUS PLOT FOR LYNCH CANYON OIL

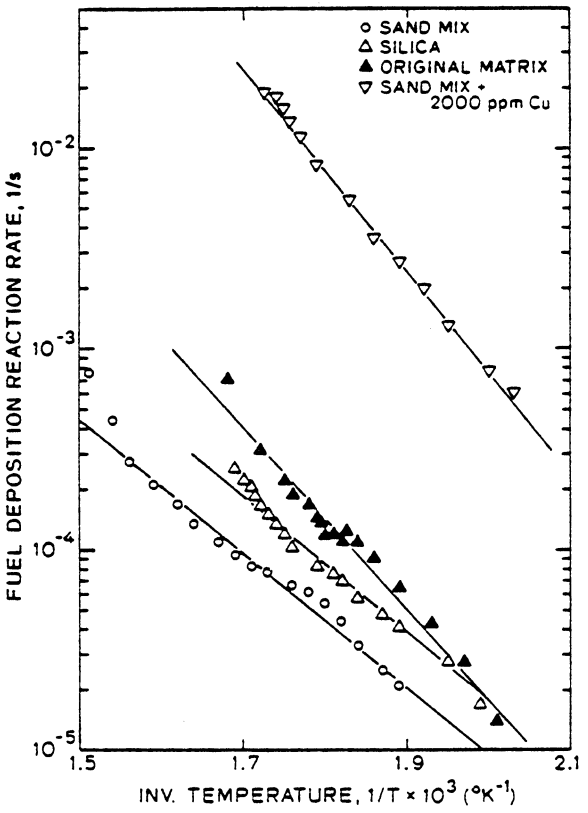

Fig. 16: ARRHENIUS PLOT FOR FUEL DEPOSITION REACTION (FRENCH OIL)

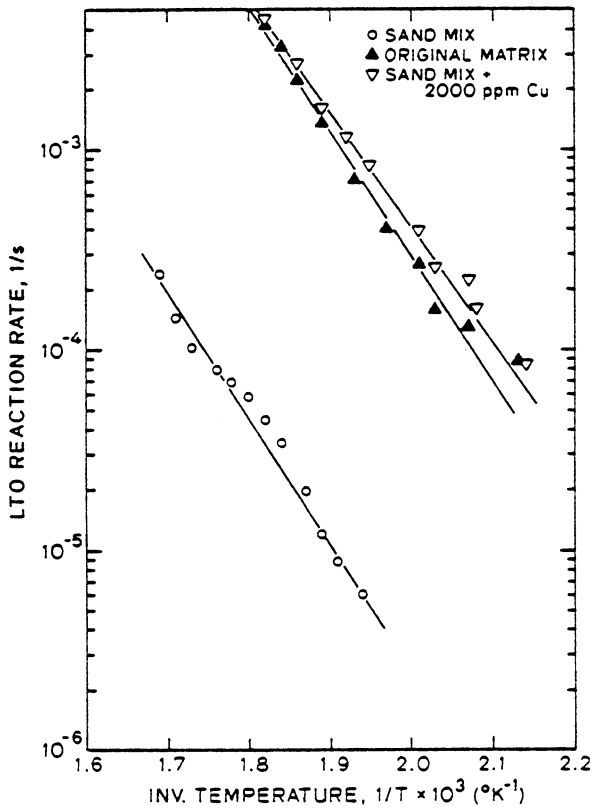

Fig. 17: ARRHENIUS PLOT FOR LTO REACTION (FRENCH OIL)

WILLIAMS HOLDING LEASE
STEAMFLOOD DEMONSTRATION PROJECT
CAT CANYON FIELD
SANTA BARBARA COUNTY, CALIFORNIA

By

Steven R. Loftus and Gary R. Adamson

Getty Oil Company
P. O. Box 811
Ventura, California 93002

ABSTRACT

The objective of this pilot program is to evaluate the efficiency and economics of the steam displacement process for future full-scale development of the Cat Canyon S1-B oil sand reservoir and in similar deep heavy crude oil reservoirs. The pilot consists of four inverted five-spot patterns on five-acre spacing. Initial steam displacement began in April, 1977. Except for brief down-time periods for well and generator maintenance, steam injection was continuous until February, 1980, when injection was halted in an attempt to de-water the pilot area. De-watering operations are substantially complete and the resumption of steam injection through insulated tubing is anticipated in August, 1981.

HISTORY OF PROJECT

This project was initiated June 25, 1976 with an anticipated completion date of May 1981. The total cost was anticipated to be $8,700,000 with DOE funding $2,000,000.

GENERAL PROJECT DESCRIPTION

Cat Canyon Field is located approximately eight miles southeast of the town of Santa Maria in Santa Barbara County, California, as shown in Figure 1. The S1-B sand of Cat Canyon Field is a relatively deep, heavy crude oil reservoir found at an average depth of 2,500 feet. It produces 9°API crude which has an estimated average oil viscosity of 25,000 centipoises at fully gas-saturated reservoir conditions. The S1-B sand is poorly consolidated with an average permeability of 2,800 md and porosity of 30%.

Prepared for DOE under Contract No. DE-AC03-76ET12058

On June 25, 1976, Getty Oil Company was awarded a cost sharing contract from the United States Energy Research and Development Administration (subsequently USDOE) to conduct a joint steamflood pilot on the Williams Holding Lease of Cat Canyon Field in the Santa Maria Basin. The original and current objective of this pilot program is to evaluate the efficiency and economics of steam displacement in the Cat Canyon Sl-B reservoir and in similar extremely viscous crude oil reservoirs. The pilot consists of four inverted five-spot patterns on five-acre spacing. Pilot configuration and location are shown in Figure 2.

Injection of displacement steam into the Williams Holding Pilot began in April, 1977. Intermittent steam stimulations of producing wells were conducted prior to and during displacement steam injection. Initial operating problems included repeated thermal packer failures and loss of sand control in the injectors. Both problems were solved with the removal of injection packers and the redesign of well completions. Normal operations resumed in mid-1978 although these operating problems delayed the initial response to the displacement phase of the project.

In late 1977, northernmost producer, WH/RF 204, and central producer, WH 205, began showing signs of displacement response. By mid-1978, flowline temperatures had increased to 350°F and fluid production rose dramatically. The high temperatures of the produced fluids resulted in severely reduced efficiency of the downhole pumps. Although larger pumping units were installed, pumping capacity was exceeded by fluid response, evidenced by 2,000' fluid levels. As fluid levels increased, oil production quickly decreased.

During the last half of 1978, two additional producers indicated displacement response. WH 25 and WH 26 showed much the same characteristics (high flowline temperatures, increased water production, increased fluid levels, and decreased oil production) as did WH/RF 204 and WH 205. Response in WH 25 occurred four months after nearby producer WH/RF 204 was shut-in. It appeared that by idling WH/RF 204, steam had been diverted to WH 25 from a common injector, WH 825.

Shortly after WH 25 began showing displacement response, all four responding producers were idled. This was done in order to divert steam to other non-responding pilot producers. This would distribute heat more evenly within the reservoir

and lower artificial lift requirements. The wells remained shut-in eight months during 1979 with no apparent success in diverting steam to other areas of the pilot.

In mid-1979, it was decided to drill thermal observation wells within the pilot area to investigate fluid paths and sweep efficiencies. In June, 1979, TO#1, located between the central producer and northernmost injector, was drilled and cored to below the displacement interval. A totally wet sand was found below the injection interval while near virgin oil saturations were found throughout the S1-B Zone. This prompted a computer simulation study to simulate the response characteristics and influence of the wet sand.

Three additional temperature observation wells (see Figure 2) were drilled to determine fluid and heat flow paths. Sidewall cores and log analysis showed zones within the S1-B of substantially reduced oil saturations in TO#2, TO#3, and to a lesser extent, TO#4. Subsequent temperature surveys showed no heat response in TO#1 which had shown near virgin oil saturations. However, TO#2 and #3 showed temperatures in excess of 300^{o}F while temperatures over 200^{o}F were found in TO#4. The zones of highest temperature corresponded well with the zones showing greatest oil saturation reduction, indicating steam channeling within the S1-B zone was responsible for the production problems noted earlier.

The computer simulation study was completed by December of 1979 and indicated that the wet sand was not acting as a thief zone. Instead, overinjection, channeling within the S1-B Zone, and low sandface steam quality were determined to be the factors causing high water and low oil production response. These findings led to a decision to return the four idle producers to production and lower the total steam injection rate to 1,150 BSPD in December, 1979.

Further simulation work indicated that halting steam injection entirely would accelerate the de-watering process and result in quicker oil production recovery. Consequently, the injection wells were idled in February, 1980, while all producers remained on production. Figures 3 and 4 show the production history of the total pilot and the central producer, WH 205. In addition, the displacement steam injection history and the cummulative pilot steam-oil ratio are shown in Figure 5.

PERFORMANCE ANALYSIS

The current pilot de-watering strategy has been largely successful. Gross fluid production for the pilot has decreased from a peak of 4,630 BFPD in January, 1980, to 1,115 BFPD in March, 1981. Pilot oil production simultaneously increased from 113 BOPD in January, 1980, to a peak of 321 BOPD in November, 1980. Pilot oil production declined from this peak, dropping to 163 BOPD by March, 1981.

The recent decline in oil production was anticipated and is taken as evidence that the pilot has been substantially de-watered. Further declines in oil production are expected until displacement steam injection is resumed. However, before returning the pilot to injection, we plan to solve the previously cited problem of poor sandface steam quality. This will require the installation of insulated tubing strings in the injection wells.

A study to determine the optimum thermally, mechanically, and economically acceptable insulated tubing string was initiated. The study has thus far concluded that prestressed concentric tubing with an insulated annulus will best meet the requirements. The final stages of design work and consultations with potential fabricators are presently underway. If there are no delays in obtaining the required materials, fabrication of the insulated tubing should be completed in July, 1981. Installation, testing, and the resumption of displacement steam injection should follow in August. A detailed description of the insulated tubing will be made available when initial fabrication problems are resolved and a final design determined.

It was decided to conduct a production test on a pilot injector while awaiting the fabrication of the insulated tubing. WH 826 was placed on production in April, 1981. Preliminary production results from the injector show an average gross fluid production of 400 BFPD and oil production of 50 BOPD. The relatively low initial gross production from the injector confirms that de-watering efforts have been successful. The immediate and fairly substantial oil production tends to confirm the severity of channeling problems and the absence of any piston-like displacement in the steamflood pilot. This, however, is not unexpected as the current understanding of the steamflood recovery mechanism is one of heat conduction from steam channels to surrounding reservoir rock with subsequent oil viscosity reduction and mobilization. Barring unforeseen difficulties, WH 826 will remain on production until insulated tubing is available to resume injection.

STACK GAS SO_2 SCRUBBER

Getty Oil Company successfully tested a stack gas scrubber for the removal of sulfur dioxide from emissions resulting from burning high sulfur crude oil as steam generator fuel. Many problems were encountered with the original scrubber design necessitating several modifications to the scrubber. These problems and modifications are discussed in the Third Progress Report - Williams Holding Lease Steamflood Demonstration Project.[1] The modified scrubber passed EPA emissions testing in March, 1979. However, in August, 1979, the Santa Barbara County APCD notified Getty that no operating permits would be issued unless continuous SO_2 monitoring of the stack gas was applied. This was not feasible, so it was negotiated that a permit would be issued if the scrubber liquor pH was continuously monitored and a one-week compliance test was performed quarterly. Subsequent quarterly compliance tests showed that SO_2 emissions were considerably lower than allowable maximums.

The Santa Barbara County APCD advised Getty that prior to the permitting of additional scrubbers, particulate emission data would be required. In December, 1980, tests were conducted firing high sulfur lease crude. Both the generator and SO_2 scrubber were monitored to determine inlet particulate loading to the scrubber and the particulate removal efficiency of the scrubber. The test data, submitted to the APCD, showed an average 56% particulate removal by the scrubber. The APCD, however, advised Getty that new scrubber permits would not be issued based on the particulate test data. The APCD will require that new scrubbers additionally remove 81% of particulate emissions. Getty is presently consulting with various manufacturers to determine equipment capable of meeting the new requirements.

ECONOMICS

Economic evaluations of pilot projects are inherently difficult due to the very nature of pilot operations. The pilot project is essentially an information gathering process involving much trial and error and thus costs are often difficult to extrapolate to field-wide operations. Ideally, the incremental cost of each incremental barrel of oil produced would be identified. However, in the Williams Holding Pilot, there is no accurate method of estimating incremental oil production due to steamflooding, although incremental costs of steamflooding could be reasonably estimated. For ease of interpretation, economics were

evaluated by estimating cumulative costs in 1981 dollars per barrel of oil produced since the project contract inception date of July 25, 1976. Non-fuel operating costs were inflated to 1981 dollars using the Consumer Price Index while fuel costs were estimated using a March, 1981, net cost of lease crude burned. The average non-fuel operating cost per barrel of oil produced in 1981 dollars is $10.50/Bbl. while fuel costs have averaged $8.00/Bbl. (total average cost of $18.50/Bbl). It is expected that with full-scale steamflood development, improved oil recovery, and the operating knowledge gained from this pilot, operating costs in any future steam displacement projects would be significantly lower.

FUTURE PLANS

Future operating plans are to continue producing from the pilot area until insulated tubing is installed in the pilot injectors. The production test of the pilot injector WH 826 should also continue until the insulated tubing is available, further de-watering the pilot area. Resumption of injection is presently anticipated in August, 1981, at a lower rate of 1,200 BSPD. Thus, with insulated tubing and a lower injection rate, adequate heat will be delivered to the formation without aggravating the previous overinjection problem as discussed in the General Project Description and History Section of this paper.

REFERENCE

[1] Hanzlik, E. J. et al, ed., Third Progress Report - Williams Holding Lease Steamflood Demonstration Project, Cat Canyon Field, U. S. DOE publication San/11884, 1979.

Figure 1

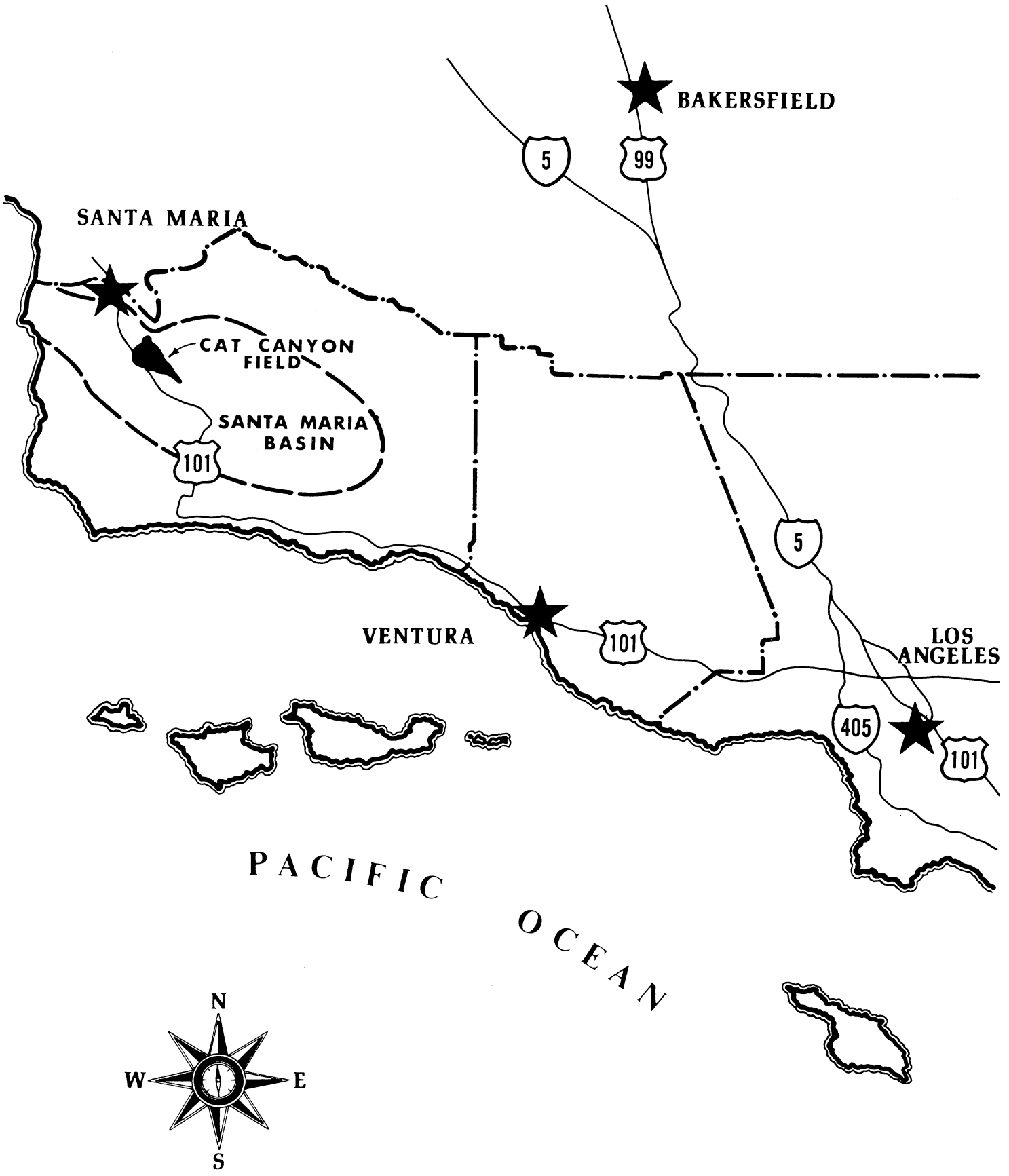
BAKERSFIELD
5
99
SANTA MARIA
CAT CANYON FIELD
SANTA MARIA BASIN
101
5
VENTURA
101
LOS ANGELES
405
101
PACIFIC OCEAN
N
W
E
S

Figure 2

WILLIAMS HOLDING
STEAMFLOOD PILOT CONFIGURATION

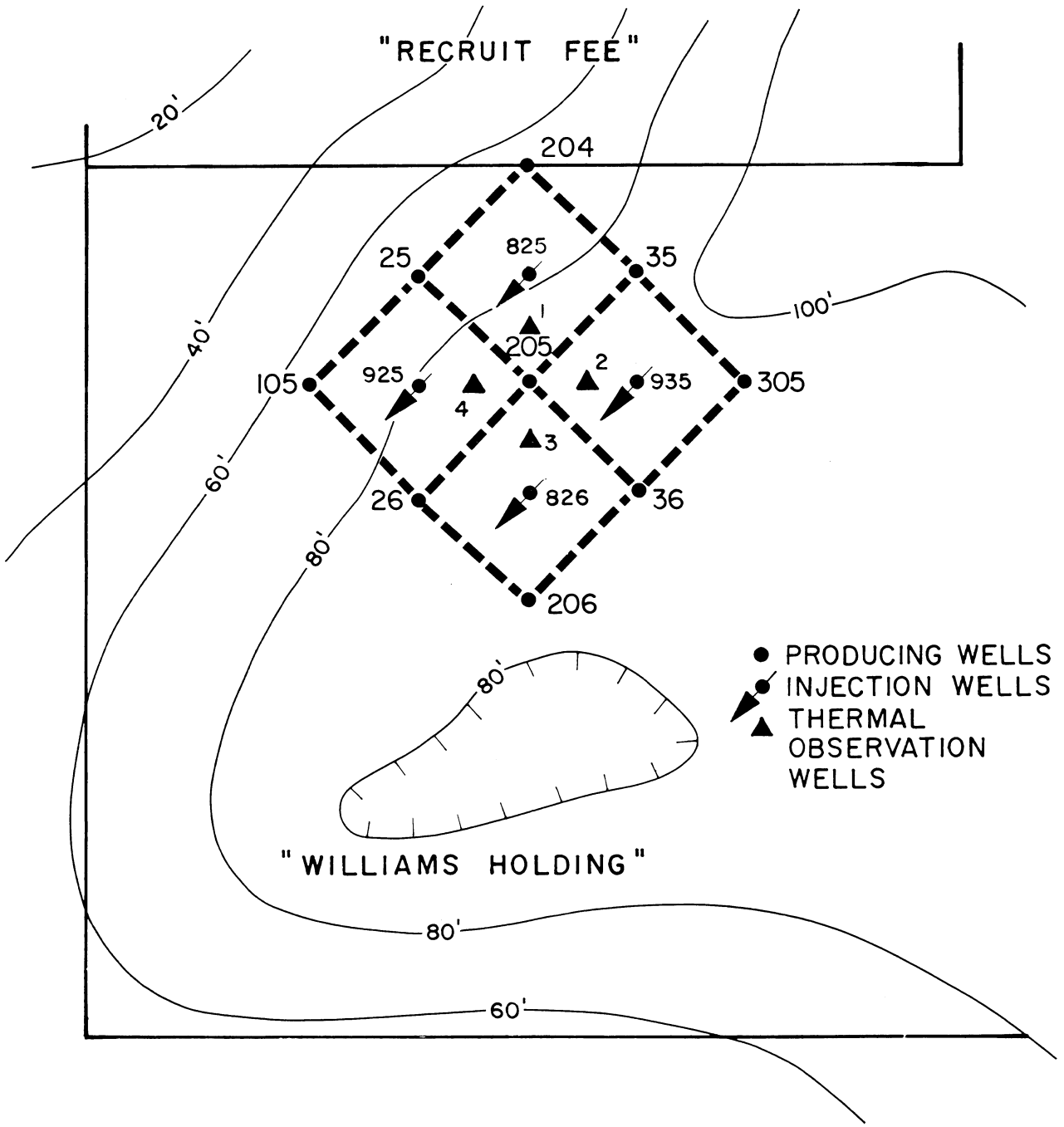

Figure 3

WILLIAMS HOLDING
STEAM DISPLACEMENT PILOT PRODUCTION PERFORMANCE

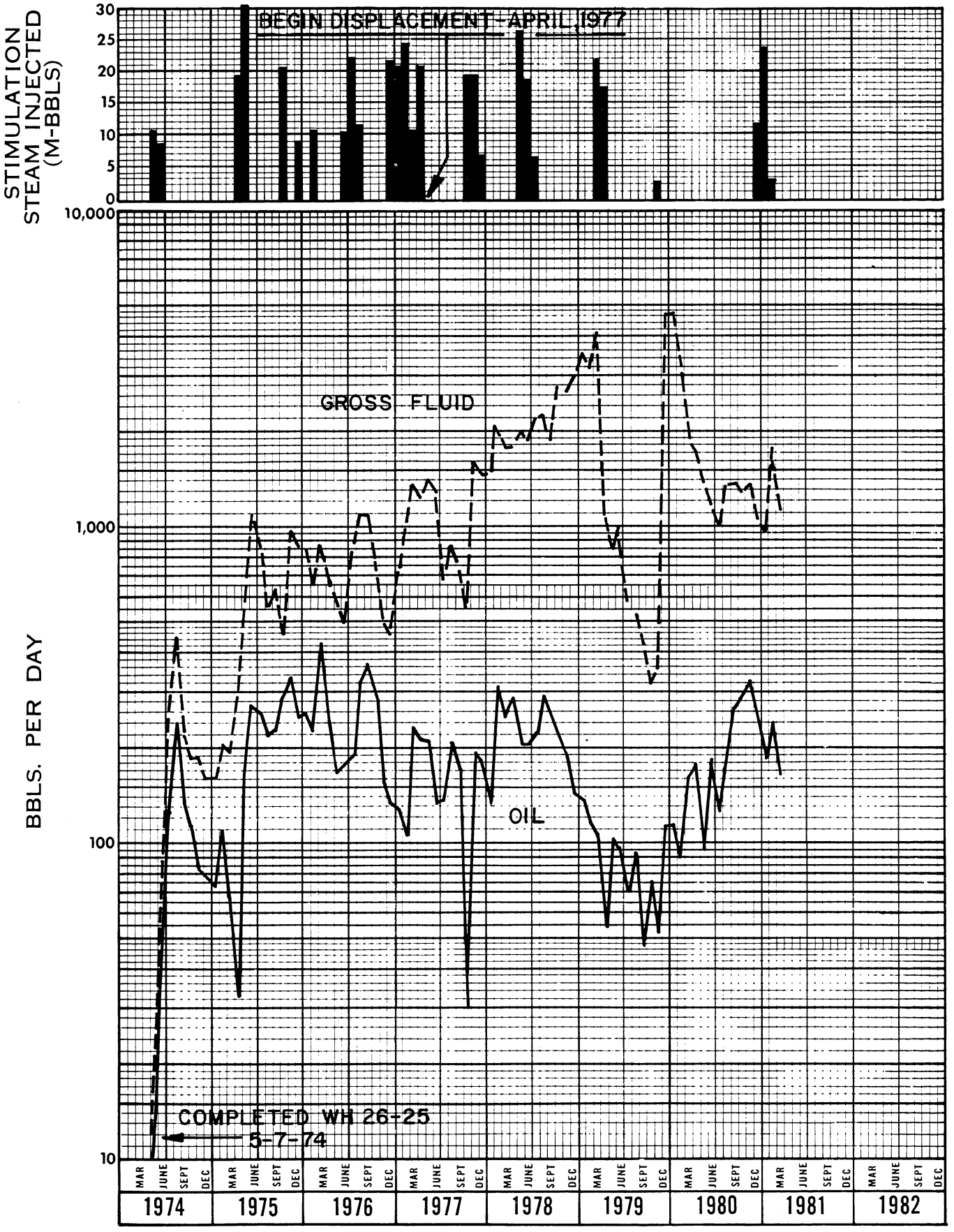

A1-M35

Figure 4

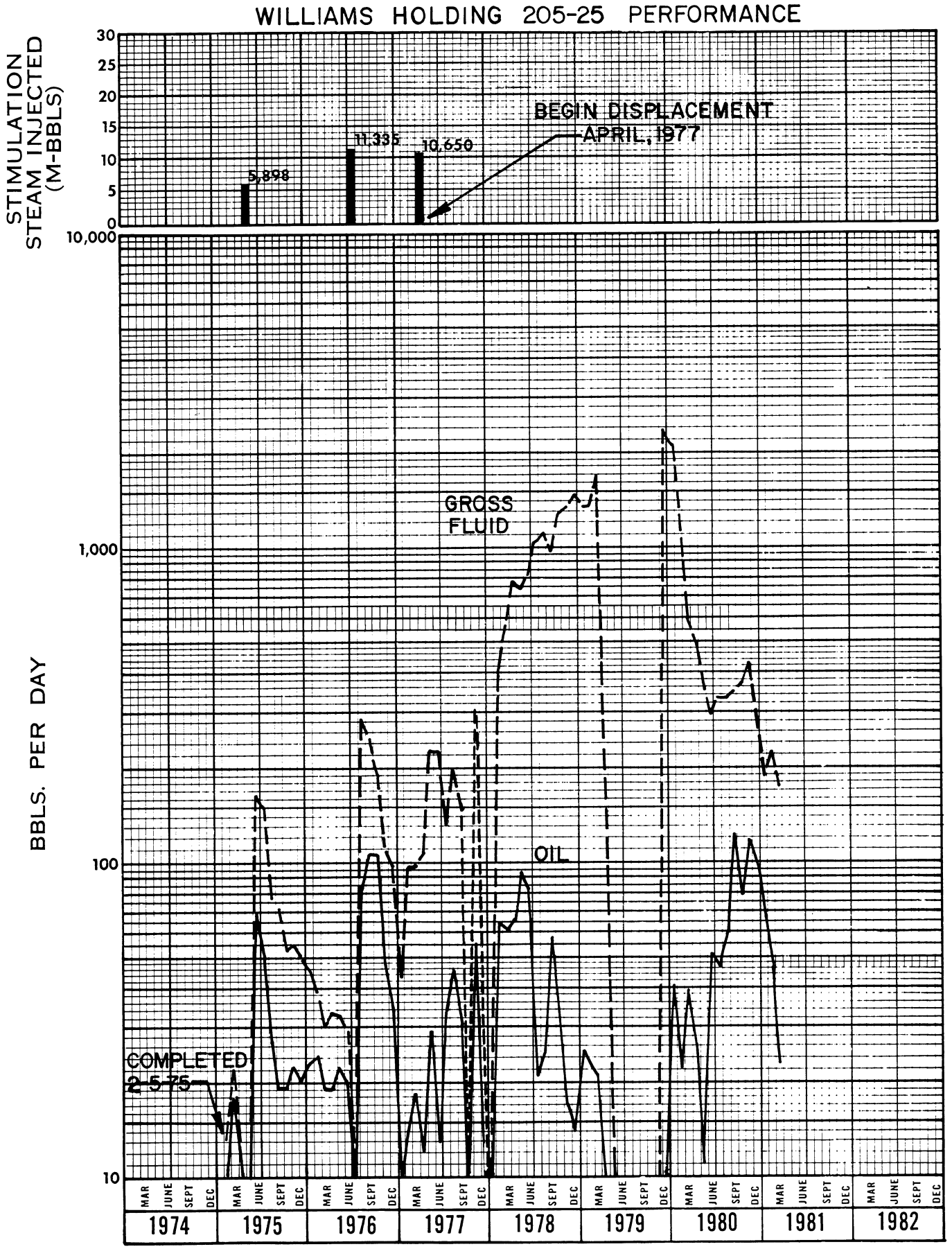

A1-M35

Figure 5

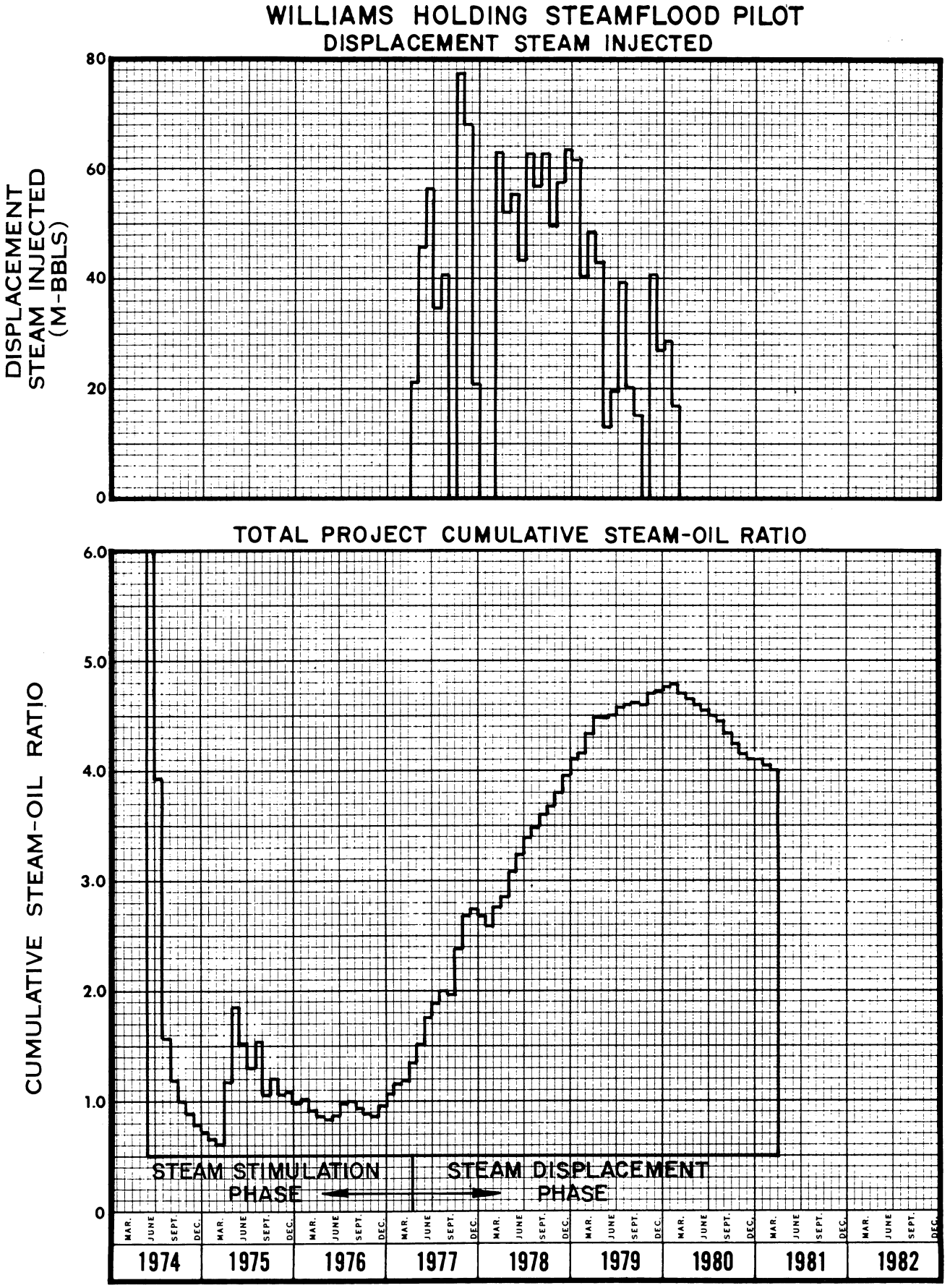

A1-M35

THE "200" SAND STEAMFLOOD DEMONSTRATION PROJECT

By

Willie O. Alford

SANTA FE ENERGY COMPANY - CHANSLOR DIVISION
10737 Shoemaker Avenue
Santa Fe Springs, California 90670

ABSTRACT

Steamflooding generally has been conducted in Midway-Sunset Field Field reservoirs which have responded favorably to cyclic steam stimulation in order to increase recovery and accelerate cyclic production. Numerous heavy oil pools in this field as well as other fields have not been adequately developed because of poor cyclic steam performance. The Demonstration Project was initiated in the "200" Sand Pool to demonstrate the operational, recovery, and economic aspects of steamflooding a typical heavy oil reservoir which had unfavorable response to cyclic stimulation. This pool, designated the "200" Sand, contains approximately 50 million barrels of oil-in-place in a structure that lies between 400 and 700 feet in depth. The reservoir produced very little primary oil production and responded poorly to cyclic steam stimulation.

The project is being conducted in two major phases. The first phase was a pilot test consisting of four (4) 2.35 acre inverted seven-spot steam drive patterns, which were not fully developed with producers (Figure 2). As a result of the response shown by the pilot, in April, 1980, the second phase was initiated by beginning work to expand the pilot area to a total of fourteen (14) fully developed 2.35 acre inverted seven-spot patterns (Figure 2). Expansion to a full-scale steamflood test consisted of drilling and completing 30 producing wells and 10 steam injection wells.

HISTORY OF PROJECT

The "200" Sand Steamflood Demonstration Project, a jointly funded venture between Santa Fe Energy Company - Chanslor Division (formerly Chanslor-Western Oil and Development Company) and the United States Department of Energy (DOE), is testing an enhanced steamflooding technique in the Midway-Sunset Field, Kern County, California. The project was initiated in July, 1975, by Santa Fe Energy Company - Chanslor Division (SFE) and was followed by the DOE Cost-Sharing Contract which commenced on June 16, 1976, and will expire on June 30, 1983. The total cost of the work to be performed under the contract is estimated to be $8,247,266. Of this estimated amount, the Government will fund a maximum amount of $1,700,000 (21%).

INTRODUCTION

The "200" Sand Steamflood Demonstration Project, a jointly funded venture between Santa Fe Energy Company - Chanslor Division (SFE) and the United States Department of Energy (DOE), is testing an enhanced steamflooding technique in the Midway-Sunset Field, Kern County, California (Figure 1). The project was initiated in July, 1975, by Santa Fe Energy Company - Chanslor

Prepared for the Department of Energy, under Contract No. DE-AC03-79ET12059

Division (SFE) and was followed by the DOE Cost-Sharing Contract which commenced on June 16, 1976. Estimated time required for the field trial is seven years.

The Midway-Sunset Field reservoirs may be generalized as having high oil viscosity, low reservoir pressure, shallow depth and high oil saturation, which are all favorable for thermal recovery techniques. However, steamflooding on Santa Fe Energy Company properties has been conducted only in reservoirs which have responded favorably to cyclic steam stimulation. The "200" Sand Reservoir was selected because of its poor response to cyclic steam stimulation. This pool produced virtually no primary oil production and responded poorly to cyclic steam stimulation. With the cyclic method, which is the principal thermal recovery technique used to produce the tar-like crude in this area, estimated ultimate oil recovery was virtually zero percent because of its ineffectiveness and unfavorable economics.

Pilots utilizing continuous steam have been monitored and evaluated in other parts of the field. Based on its predicted and actual performance in other heavy oil reservoirs, steamflooding is considered the most promising thermal recovery technique for this property. However, the high capital and operating costs of steamflooding made a pilot desirable to evaluate the process in this pool. Therefore, this project was initiated to demonstrate the operational, recovery, and economic aspects of steamflooding a typical heavy oil reservoir which had unfavorable response to cyclic steam stimulation.

PROJECT DESCRIPTION

Reservoir and Geological Data

The reservoir is located in Section 17, T32S, R23E, Midway-Sunset Field, Kern County, California. The Spellacy formation, designated the "200" Sand of Upper Miocene Age, contains approximately 50 million barrels of oil-in-place. The crude oil is very viscous with ambient viscosities in the range of 6500 centipoise. However, the oil viscosity reduces rapidly with elevated temperatures. Figure 3 shows as the temperature increases from 90°F (reservoir temp.) to approximately 200°F, the 12° API oil has an approximately 110-fold reduction in viscosity. With the same increased temperature, the oil-water viscosity ratio has a 35-fold reduction and an 18-fold mobility ratio reduction at original saturations.

The reservoir pressure in the "200" pool is very low, in the range of 20-60 psi. This pressure range does not provide sufficient energy for a producing mechanism. Most of the project area is located on top of a monoclinal structure where dips range from 5 to 15 degrees. With the low dips, gravity drainage does not provide an effective mechanism to obtain economical production rates and effectively deplete the reservoir. Herein lies the necessity of steamflooding, to not only reduce the oil viscosity, but also increase the displacement process, so the crude can flow to the wellbore.

Based on previous well data, and most recent drilling and coring data, the "200" Sand is a series of submarine fan-channels with the source area to the northwest of the project area. The reservoir consists of interbedded sands, conglomerates, silts and diatomite. Figure 4 is a south-north

cross-section map of the project. Contrary to initial analysis, these lower permeability layers of silts, diatomite or conglomerate, do not have continuity over long distances to allow the reservoir to be broken into discrete sand units. However, there are enough lower permeability layers so that lateral transmissibility is better than vertical transmissibility. Detailed correlation studies will be required to make sure all sand units are swept by the steam drive.

The sand is fine to medium grained, with scattered coarse to very coarse grains and pebbles. Usually the sand is clean and extremely friable with the grains being held together by the heavy viscous crude.

The average petrophysical properties for all productive sands are 2.250 millidarcies permeability, 30 percent porosity, and an oil saturation before steamflooding of 59 percent, equivalent to an average oil content of 1,373 barrels per acre foot. Table 1 has a summary of reservoir data obtained from the pilot wells and surrounding core holes in Section 17, T32S, R23E.

Well Completions

The pilot injection wells are completed with 5-1/2" O.D. casing strings cemented in 8-3/4" holes at total depth. To maintain good steam injection profiles, the steam drive interval was restricted to approximately the bottom 50 feet of the reservoir with selectively jet perforated 1/2" holes every 2 feet.

The expansion's injection wells have the same casing completions as the pilot's injection wells. However, to better control steam override, the bottom 20 feet was jet perforated with 1/2" holes every 2 feet.

Two types of producing well completions were used in the pilot area. All, except one, of the producing wells are completed with 7" O.D. casing cemented from surface to top of producing sand, and 5-1/2" O.D. liner 60 mesh, 2" slots, run from 9 feet above the 7" casing shoe to 2 feet off bottom. The liner is gravel flow packed with 6 X 9 gravel in a 9-7/8" hole. Producing conditions in unconsolidated sands generally require that producing wells be completed with sand control liners.

One producing well had a limited perforated cased-through completion. The well was completed with 7" cemented casing, jet perforated with four, 1/2" holes per foot. From the initial geologic study, the zone barriers were believed to be laterally continuous. Therefore, producing Well 255 was completed with a jet perforated cased-through completion to determine if steam injection could be confined to the drive interval by restricting production in a producer only to the steam drive interval. Since additional information indicates the silt interbeds are not laterally continuous, which prevent vertical flow between zones, this type of completion was terminated.

With the steam overriding almost as soon as it leaves the injector, it was more advantageous to complete the expansion's producing wells with 5-1/2" O.D. slotted liners open across the entire producing sand. Since the steam could not be confined to the 50' drive interval, Well 255 was reperforated over the entire sand and evaluation is being made

on the production and sanding problem under those conditions. The limited perforations did very well in controlling the sand production since it was put on production in 1975.

Project Facilities

Two 20-million Btu/Hr. steam generators were used in the pilot area, and the site for the generators was within the pilot area. The units provided approximately 1,800 B/D steam to the four injectors.

The pilot expansion will require an additional 5,500 B/D steam for 18 months, then the demand will be reduced to approximately 3,800 B/D steam. To make up the additional steam requirement, two new 50-million Btu/Hr. generators were installed. Each generator is capable of producing about 2,800 B/D steam. When the steam demand is reduced, at least one of the 20-million Btu/Hr. generators will be used elsewhere. The generators will be grouped together in the NW/4 of Section 17, T32S, R23E, as part of a central steam plant for this area.

Since the concentrations of sulphur dioxide by law cannot increase in the general area, 95% efficient SO_2 scrubber systems that can scrub two, 50-million Btu/Hr. and one, 20-million Btu/Hr. steam generators will be installed. The law requires that one of the two existing 20's be scrubbed. To make operation easier, each generator will have its own scrubbing system. The non-regenerative sulphur dioxide removal system can use aqueous solutions of sodium carbonate, sodium hydroxide or sodium sulfite as the scrubbing agent. At this time sodium hydroxide will be the chemical used. The disposal material will consist of sodium sulfite, sodium bisulfite and sodium carbonate. Design of the system will allow for expansion to accommodate more steam generators.

The project is supplied with fresh water from the West Kern Water District. Water with total dissolved solids of 246 parts per million (ppm) is treated at Santa Fe Energy's South Midway soft water plant located on Section 8, T32S, R23E, approximately 1-1/2 miles northeast of the project. This plant is capable of handling approximately 20,000 barrels of water per day. The water system services numerous oil production areas and has operated with only minor problems. The system allows the steam generators to be operated without any appreciable scaling problem.

With the additional steam requirement from the expansion, one new water softener that can handle about 5,500 barrels of water per day was installed. West Kern Water District will supply adequate water to be treated and used in the project.

The treating plant, located 1-3/4 miles northeast of the project on Section 9, T32S, R23E, has operated with minor problems throughout the project life. However, treating the fluid production is a major problem because an estimated 90% or greater of all Midway heavy

oil is produced as an emulsion. Between 5 and 10 percent of the oil is rejected and has to be pumped back through the treating system with emulsion breaking chemicals.

The pilot production and a significant amount of other SFE's production comes from the field to the treating plant, which was operating near maximum capacity. A heater treater and free water knockout have been installed and can handle 5,000 BFPD and 7,000 BWPD, respectively. This will accommodate an expected production increase of 1,100 B/D oil and 2,500 B/D water from the expansion project.

PROJECT PERFORMANCE

Steam Injection

Continuous injection was initiated in October, 1975. As of July 1, 1980, 2.09 million barrels of steam had been injected into the four injection wells at an average sand face injection temperature and quality of 350°F. and 72%, respectively. Steam at the generator outlets is 420°F. with 80% quality. The total project injection is shown in Figure 5.

In September, 1979, one of the two 20-million Btu/Hr. steam generators in the pilot was shut down. Since the operational, recovery, and economic performance had been determined, it was more advantageous to discontinue with the high injection rates that allows valuable BTU's to flow from the small pilot area. In June, 1980, the second steam generator was shut down and all steam injection will be suspended until May, 1980. The generators have been relocated at the South Midway centralized steam plant. Construction of the plant in the NW/4 of Section 17, T32S, R23E, is completed, and it will be able to accommodate expansion of the pilot area and other companies' projects as well.

Santa Fe Energy will resume steam injection during May, 1981, with a majority of the steam capacity going to stimulating the producers. It will take approximately two months to complete cyclic steaming the producers. Once that is achieved, all the steam will be going into the fourteen (14) injection wells at an average rate of 500 B/D per well. A smooth running steam plant is not expected for several months because, as with any new system, there will be minor system adjustments which will need to be worked out. This new steam plant will enable Santa Fe Energy to service the project in a more efficient manner.

During the period of suspended injection, temperature surveys ran in production and observation wells indicated that the average reservoir temperature have declined from approximately 200°F. to 140°F. After resumption of steam injection the heated pilot area will be re-established to its former extent in about six months.

Production

Total pilot area production is shown in Figure 6. Over half of the producers have shown very good response from the drive. The highest oil production rate was in Well 254 and its peak production was 67 B/D oil in March, 1978.

Since injection was reduced in September, 1979 and suspended in June, 1980, oil production from the pilot has shown a slight decline. Of course this was expected since a relatively flat formation doesn't allow for gravity drainage. Production also declined as a result of declining formation pressure after suspension of steam injection. With no surprises, several expansion producers have been on production due to heat that had flowed outside the small pilot area. The decline in the pilot is expect to continue until the new steam plant is completed and steam injection starts back up. Shortly after resumption of steam injection, the production rate will improve.

The discontinuous impervious layers have complicated the problem in predicting the reservoir performance. Had the barriers separating the sands been competent and laterally continuous, controlling the flood front and gravity override would have been easier, thus making production prediction less complicated. At the onset of the project, data from the small pilot area allowed us to believe that the reservoir was divided into separate zones by continuous barriers. However, additional drilling and coring have indicated the reservoir to contain many small discontinuous barriers. With these conditions, there is no known standard or proven method that can be used to describe and predict the oil recovery. Because of these factors, production rate and recovery are calculated from the empirical relationship between ultimate tertiary oil recovery and ultimate steam injection requirements.

Randomly distributed, discontinuous barriers will cause significant reduction in vertical transmissivity because of the tortuous path the fluid must follow. Yet while lateral transmissibility is better than vertical transmissibility, steam will eventually work around the discontinuous barriers and migrate upward to higher horizons. As the steam invades these regions, the oil will tend to flow vertically downward by gravity until it reaches the impervious rocks, whereto it will accumulate in a layer of high oil saturation. As the oil layer builds up above a barrier, it will begin lateral movement and move off the edge to lower regions. The driving force for lateral oil movement through the layer is the gravity head from the middle of the barrier where the oil layer is thicker. The oil layer will become thinner toward the edge of the barrier. Unfortunately, it is not known just how fast this oil will drain laterally and vertically from barrier to barrier after invasion from steam override. Since there is no conceptualization of the time involved, perforations are restricted in the expansion's injectors to the lower 20 feet of the sand. If recovery time becomes excessive, additional perforating will be considered.

Estimated steamflood and cyclic recovery for the total demonstration area is 4.5 million barrels of oil for the 200 foot sand reservoir. If the "200" Sand Steamflood Demonstration Project, which covers 32.9 acres, proves to be economically feasible, steamflooding can be expanded to the entire "200" Sand reservoir, which is approximately 250 acres and contains approximately 50 million barrels of oil-in-place. Likewise, methods and economics could be applied to other reservoirs in the Midway-Sunset Field as well as other fields with similar characteristics.

TABLE 1

SUMMARY OF RESERVOIR DATA

DEPTH, FEET	400-700
AREAL EXTENT, ACRES (EST.)	250
OIL GRAVITY, °API	12
RESERVOIR PRESSURE, PSI (EST.)	40
RESERVOIR TEMPERATURE, °F	90
AVERAGE FORMATION DIP, DEGREES	12
AVERAGE GROSS THICKNESS, FEET	200
AVERAGE NET THICKNESS, FEET	150
PERMEABILITY TO AIR, MD	1,050-3,440
AVERAGE POROSITY, PERCENT	30
AVERAGE OIL SATURATION, PERCENT	59
AVERAGE OIL CONTENT, BBL/ACRE-FT.	1,373
OIL VISCOSITY @ 90° F, CP	6,500
OIL VISCOSITY @ 212° F, CP	60

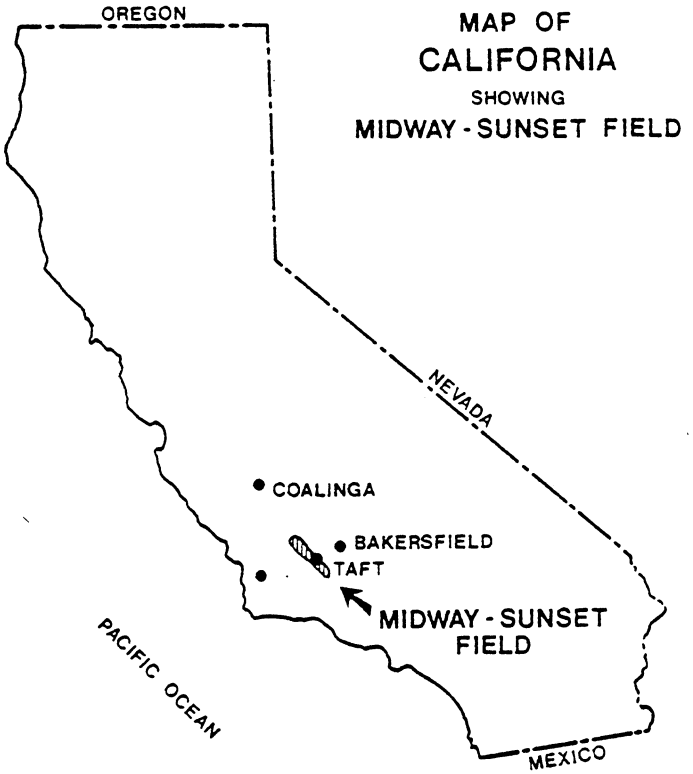

FIGURE 1

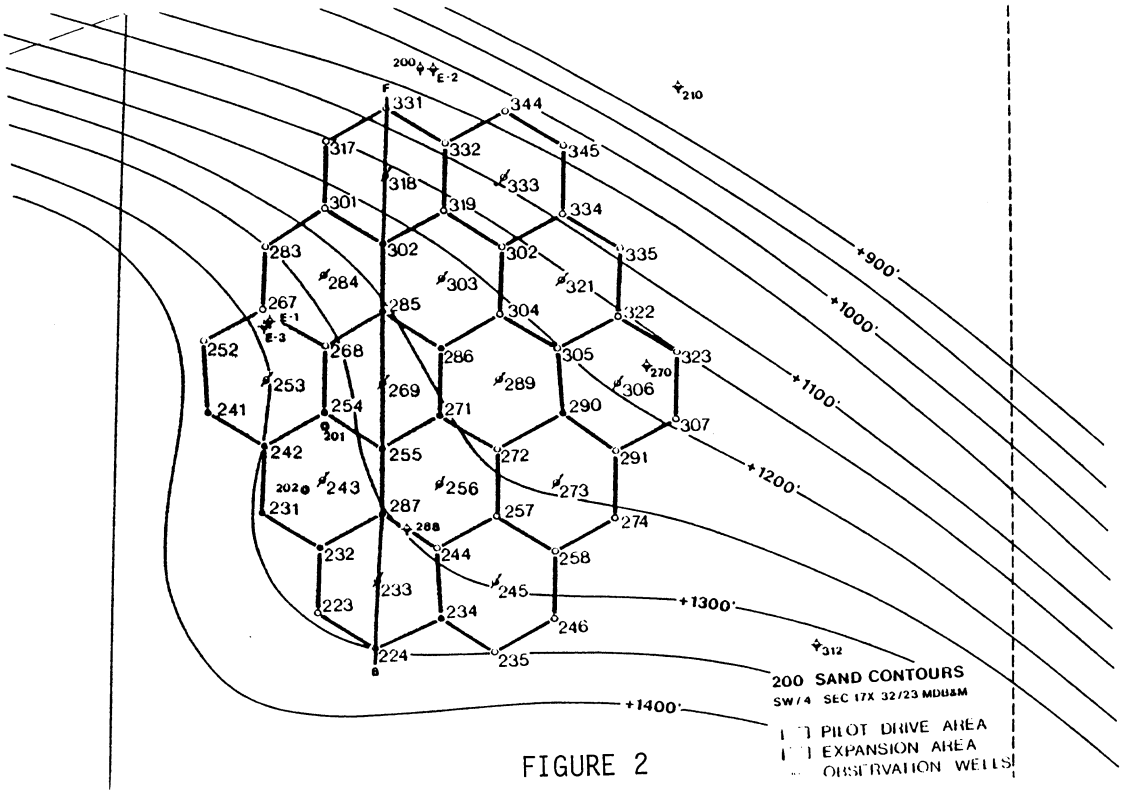

FIGURE 2

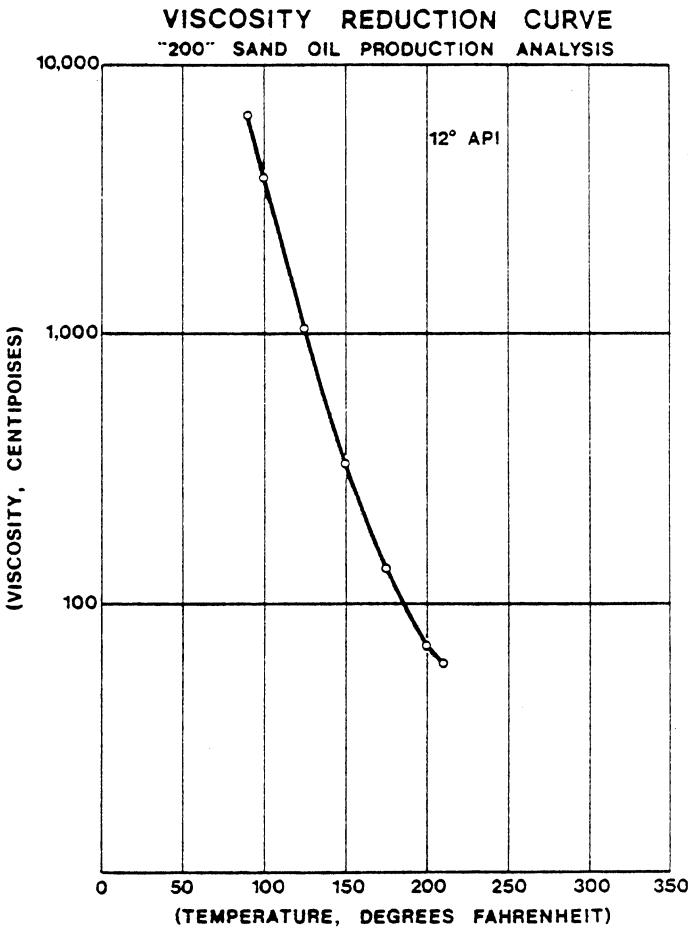

FIGURE 3

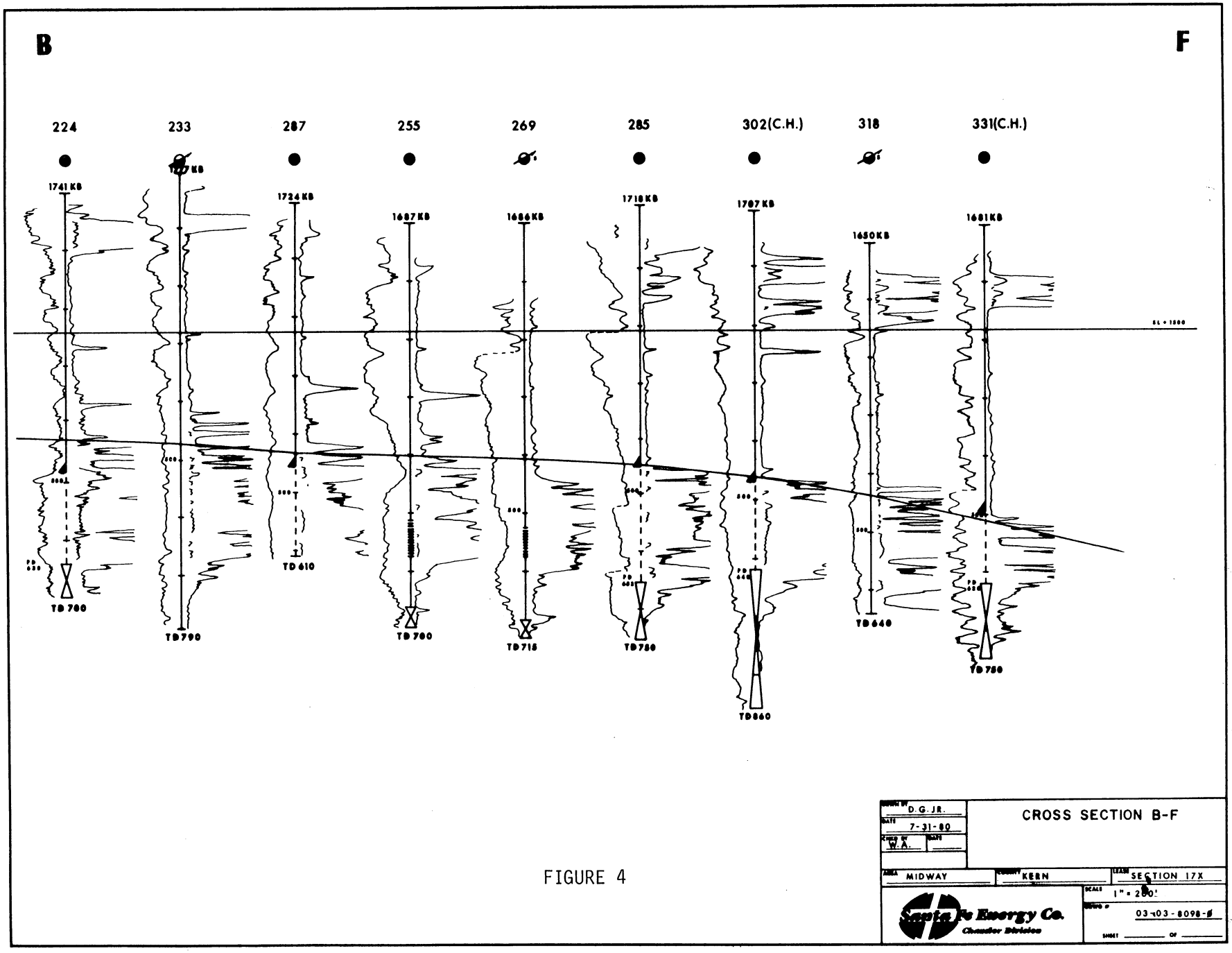
B
F
224
233
287
255
269
285
302(C.H.)
318
331(C.H.)
1741 KB
1724 KB
1687 KB
1686 KB
1718 KB
1707 KB
1650 KB
1681 KB
TD 700
TD 790
TD 610
TD 700
TD 718
TD 730
TD 660
TD 640
TD 750
D.G. JR.
7-31-80
W.A.
MIDWAY
KERN
SECTION 17X
1" = 200'
03-103-8098-#
Santa Fe Energy Co.
Chandler Division
CROSS SECTION B-F

FIGURE 4

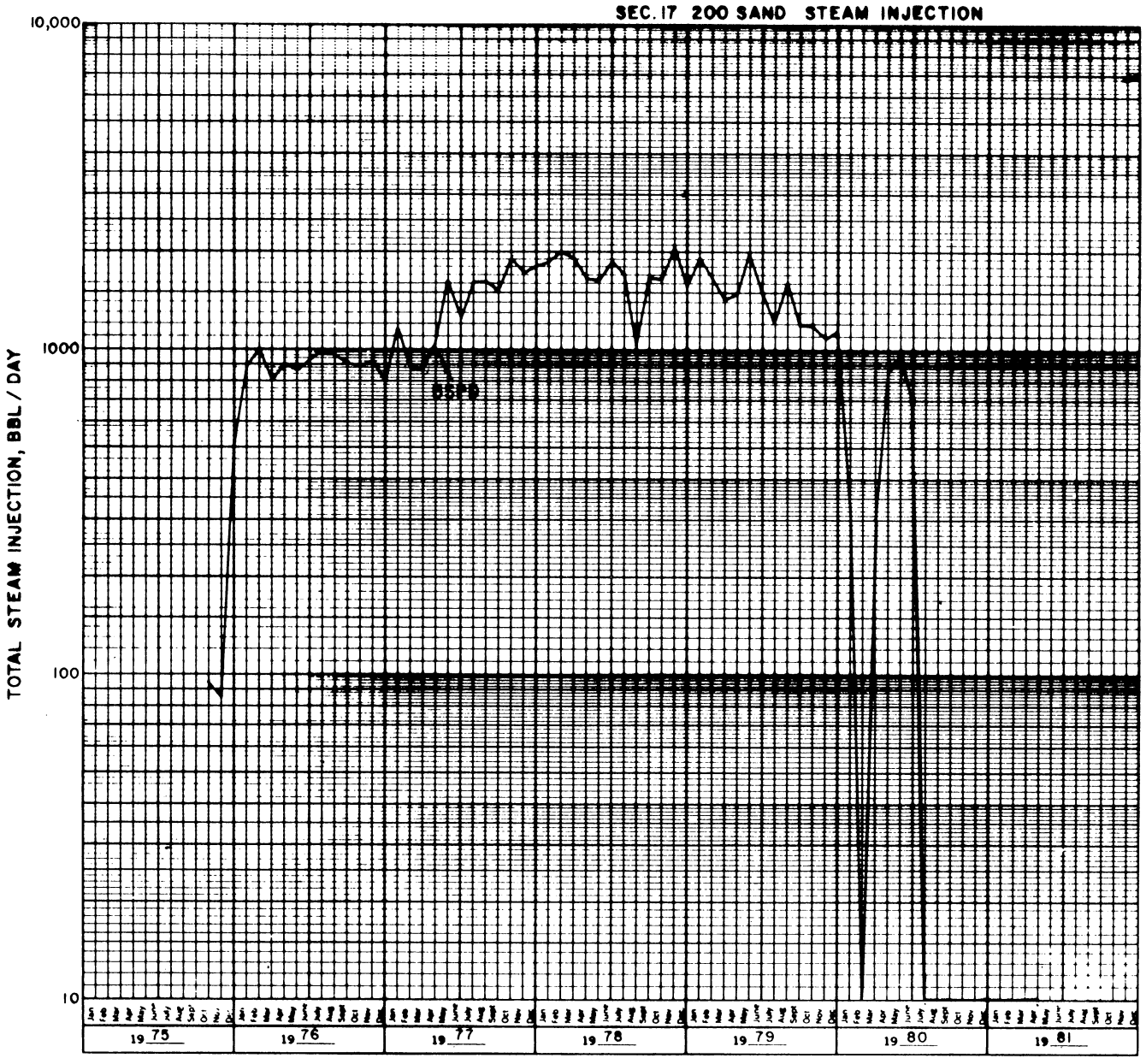
SEC. 17 200 SAND STEAM INJECTION
10,000
1000
100
10
TOTAL STEAM INJECTION, BBL / DAY
OSPD
19 75
19 76
19 77
19 78
19 79
19 80
19 81

FIGURE 5

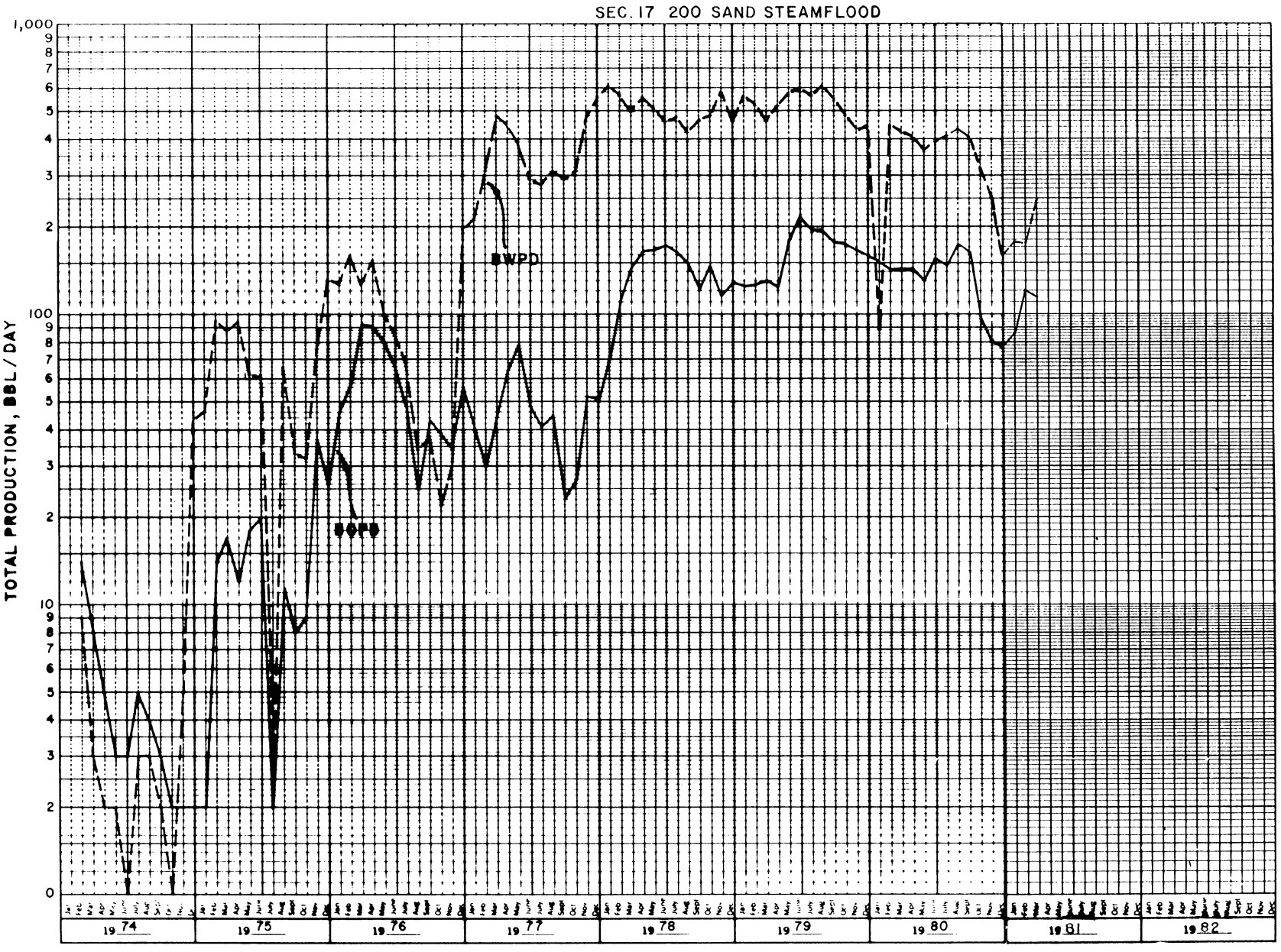
SEC. 17 200 SAND STEAMFLOOD
TOTAL PRODUCTION, BBL / DAY
1,000
100
10
0
BWPD
BOPD
1974
1975
1976
1977
1978
1979
1980
1981
1982

FIGURE 6

SCALED PHYSICAL MODEL STUDIES OF THE STEAM DRIVE FOR THE RECOVERY OF CRUDE OIL

T.M.DOSCHER, F. GHASSEMI, AND O. OMOREGIE

DEPARTMENT OF PETROLEUM ENGINEERING
UNIVERSITY OF SOUTHERN CALIFORNIA
LOS ANGELES 90007

I. ABSTRACT

Work on the physical scaled models of the steam drive have now continued into their third year. During the past year the work has been extended to the study of reservoir thickness, low viscosity fluids, the concurrent use of inert gas (nitrogen) and steam, and the equivalence of a high rate gas drive of low viscosity reservoir fluids to a steam drive of high viscosity fluids.

The studies have shown that reservoir thickness is not as critical a parameter in affecting the oil steam ratio as predicted by the results of analytical formulations which assume that the steam frontally displaces the reservoir fluids. Oil steam ratios in 26 foot sands are comparable to the oil steam ratios observed in 70 foot sands when gravity override dominates the process.

Low viscosity fluids are so much more efficiently displaced by steam (a smaller steam volume is required per volume of fluid displaced) that even when displacing residual oil saturations, the resulting oil steam ratios are sufficiently high for the process to be considered economic given ancillary favorable parameters.

The substitution of nitrogen for steam, concurrently or as sequential slugs, in a mature steam drive continues the production of oil with a resulting increase in the effective oil steam ratio of the process.

Model experiments using low viscosity fluids and high rate nitrogen injection confirmed that the relationship of the controlling parameters, viz., viscosity, permeability, etc. to displacement efficiency are virtually identical to those exhibited in the steam drive.

HISTORY OF PROJECT

The project was initiated October 1, 1979 and had a September 1980 completion date. The government award was $52,263.

Prepared for DOE under Contract DE-AS03-76SF00113

II. INTRODUCTION

Physical scaled model expriments on the steam drive have yielded information which appear to be in accord with the results of field operations, e.g., the occurrence of an optimum injection rate, and the dependence of the production rate on a fractional power of the oil viscosity at steam temperature. Conventional analytical models of the steam drive do not predict such effects of these parameters.

In the classic analytical derivation of the way in which a steam drive functions, attention is focussed on the development of a steam zone from which oil is assumed to be depleted to some naturally determined residual oil saturation. The fact is, however, that the pressure required to displace a viscous oil bank at an appreciable rate can rarely be developed in a real reservoir.

Reported field results have demonstrated that steam does not frontally displace heavy oil in a steam drive operation. Injected steam initially enters the formation through a depleted or wet interval, a fracture, or a fluidized interval. If the initial entry is not at the top of the oil section, then the steam will soon migrate to the top if there is any significant vertical permeability at all. Depletion of the oil to a very low saturation occurs in the inerval through which the steam is flowing, and with time the depletion extends downwards. In the scaled physical model studies, this vertical extension of the steam zone can be followed in some details. The production of oil occurs at an inerface which is continuously moving (downward). This stratified flow of steam is of course not unexpected in view of its very low density in comparison with the reservoir fluids. however, the unexpected result is that the steam , flowing over the oil column, is capable of decreasing oil saturation to extremely low values in a relatively short time period.

The interfacial tension of oil against saturated steam has been verified to be little different from that of oil against water, and therefore the only parameter to which the low residual can be attributed is the high velocity of the gas (steam vapor). It might be noted that the injection of 500 barrels per day of steam into a reservoir at an average pressure of 200 psi. is equivalent to the injection of 6 MM SCFD of an ideal gas (before condensation is considered). The resulting velocities on 2.5 to 6 acre spacing when less than half the reservoir is depleted are very high: of the order of 100 feet per day through a 25 foot depleted zone. Of course, a significant fraction of the injected steam condenses, but offsetting this somewhat is the fact that the production pressures are usually less than the average reservoir pressure and therefore the uncondensed steam has the opportunity of expanding and increasing its linear velocity through the reservoir.

Given that the foregoing description of the steam drive is valid, then there is no reason to anticipate a signficant effect of reservoir thickness on the process. The steam flowing through the reservoir, across the top of the oil column, sweeping or dragging a thin layer of heated oil along with it, does not interact with the base of the oil column for some time.

The earlier work with the physical models has also indicated a pronounced influence of the viscosity of the oil at steam temperature on the rate at which oil is displaced; the rate appearing to increase with the square root of the inverse of the oil viscosity at steam temperature. This result suggested that with low viscosity oils (with a viscosity at steam temperature of the order of that of water), the rate of displacement of both the oil and water in a watered out reservoir would be so great that a favorable oil steam ratio might be obtained despite the low saturation of the residual oil.

After significant depletion of the reservoir has occurred, the interval available for the flow of steam is quite large, and much of the steam merely circulates through the reservoir. A decrease in the rate of steam injection at that time would result in a greater utilization of the latent heat of the injected steam, but the decrease in the resulting gas velocity would decrease the rate at which oil could be displaced from the reservoir. Thus, there is an optimum rate of injection which will be a function of the amount of depletion that has already occurred and several of the fundamental parameters controlling the process. Substituting an inert gas for some of the steam in a mature steam drive should therefore be expected to maintain the production rate, and increase the oil steam ratio of the process. (Whether or not this would result in an economic gain will ultimately depend upon the relative costs of inert gas in comparison to steam.)

Finally, since so much of the steam drive process apears to be dependent upon the ability of the steam vapor to displace the hot oil (heated at the interface between the oil column and the steam zone), it appeared that a high rate gas drive in a reservoir saturated with low viscosity fluids, should show much of the same production characteristics of a steam drive in a heavy oil reservoir.

The work conducted during the past year on this project were intended to validate the preceding hypotheses which had been developed based on the scaled physical model studies conducted in prior years.

III. THE EFFECT OF RESERVOIR THICKNESS

Figure 1 shows the results obtained for a 26 foot prototype at three different steam injectiion rates. A comparison of this data with the results obtained earlier for the 70 foot prototype, Figure 2, indicates that the optimum steam injection rate is in the same range for both models; it is not dependent on the thickness of the formation. Figure 3 compares the performance of the optimum steam injection rate in the two models. (The initial, quite pronounced difference in the two runs is due to the fact that in the later work with the thinner reservoir the initial few hundreths of a pore volume of oil that was produced was not attributed to the steam drive.) Earlier conclusions based on field observations to the effect that the optimum rate is a function of the acre feet in the pattern area was probably due to the fact that all patterns had the same thickness.

The steam quality used in the 70 foot prototype runs averaged 45% whereas the steam quality for the 26 foot runs averaged 65%. Calculations based on frontal drive theory indicate the oil steam ratio in the first five years should be about 35% higher for the thick reservoir. Discounting the effect of quality, the results for for the two reservoirs would be virtually identical.

IV. EFFECT OF FLUID VISCOSITY

Figure 4 shows the results for the 26 foot thick prototype reservoir when the prototype reservoir fluid has a viscosity at steam temperature of 0.4 cp., slightly greater than water would have at the same temperature. A comparison of this production history with that of the more viscous reservoir fluid quickly shows that displacement of the low viscosity fluid by steam resuls in a much higher oil steam ratio.

Figure 5 shows the oil steam ratio as a function of viscosity of the oil at steam temperature. The data points for the three highest viscosity fluids were obtained in he earlier studies in a 70 foot model, and the data point for the lowest viscosity fluid is the one described in this study adjusted downwards because of the higher quality of steam that was used. It is apparent that for the same oil saturation, the oil steam ratio continues to increase as the viscosity of the reservoir fluid decreases.

A comparison of the steam (and therefore temperature) distribution in the reservoir for the displacement of a viscous fluid and one with a low viscosity is quite informative. Figures 6 and 7 show the temperature distribution for the displacement of the heavy oil and the mobile oil, respectively, after the injection of one half a pore volume of steam, and Figures 8 and 9 portray the distribution after the injection of 1.5 pore volumes of steam. The override of steam in the case of heavy oil displacement is very pronounced, and becomes somewhat attenuated in the case of the mobile oil. At a still lower viscosity of reservoir fluid, a piston like displacement by steam would be anticipated.

V. STEAM DRIVE OF A RESIDUAL OIL SATURATION

The relationship of the oil steam ratio to oil viscosity, Figure 5, indicates that a steam drive in a reservoir having a 33% porosity and saturated with water will produce the latter at a reservoir water/steam injected ratio of 0.7 after the injection of one pore volume of steam. Even higher, if the quality of the injected steam at the sand face is above 65% and the pressure is less than the prototype 200 psi. used in the experiment.

If the reservoir is not 100% saturated with water, but contains a residual, low viscosity crude oil which is displaced more or less in proportion to its saturation with the reservoir; then the resulting oil/steam ratio would be anticipated to be $(0.7s_{or}\cdot)$.

For a residual saturation of 0.25, or greater, the resulting oil steam ratio would be 0.18, or greater, as high or higher than the oil steam ratios experienced in the steam drive of heavy oils. The results of a model experiment with a residual oil saturation of 44% (unfortunate ly, the construction of the model did not permit the application of a sufficiently high pressure gradient to reduce the oil saturation to a true residual value) are shown in Figure 10. It is apparent that the hypothesis that the mobile oil is produced as efficiently as water is confirmed by the results of the portrayed experiment. Figure 11 shows that approximately 65% of the residual oil is produced at an oil/steam ratio of 0.28 after the injection of one pore volume of steam.

It is important to note that reaching such high oil steam ratios is dependent both on a suitably high steam injection rate and a sufficiently high porosity. Further, the mere fact that a high oil steam ratio is realized is not sufficient to indicate that an economic steam drive operation is feasible. Certainly, an economic operation would be at hand if no additional well drilling costs were to be ecountered in implementing the drive; however if many new wells had to be drilled in relatively thin sands (resulting in a high capital cost per recovered barrel) to carry out the operation, the advantages of the high oil/steam ratio might be overcome by the high investment costs.

VI. EFFECT OF CO-INJECTION OF NITROGEN AND STEAM

Figure 12 compares the performance of the steam drive of a viscous oil with that in two virtually identical reservoir situations in which the injection of steam and nitrogen was substituted for the injection of steam alone after one pore volume of steam had already been injected. In Run 36 steam and nitrogen were simultaneously injected and in Run 37 slugs of nitrogen are alternated with steam.

Comparing the results of Runs 36 and 37 with the control Run 38, it is apparent that oil production is being maintained even though the steam injecton is curtailed as a result of the ancillary effect of the injected inert gas. These results clearly show that in a steam drive operation the steam is playing a multiple role; one of heating the oil by the liberation of latent heat, and a second role of displacing the heated oil. The latter role can be taken over by an inert gas as shown by the results of the experiments.

At this time, it is not clear that there would be a marked economic gain in the substitution of an inert gas for some of the steam in a mature steam drive because of the unit cost of compressed, inert gas. However, this is not likely to be true in large installations at this time and may not be true at all in the future as the cost of energy continues to escalate. There is a far larger component of energy costs in the unit cost of steam than there is in the unit cost of an inert gas.

VII. HIGH RATE INJECTION OF NITROGEN INTO RESERVOIRS WITH LOW VISCOSITY OIL

The hypothesized equivalence of the steam drive process to a gas drive was further explored in scaled physical models by conducting

expriments in models saturated with a range of low to moderate viscosity fluids and injecting nitrogen at sand face velocities equivalent to those calulated for typical steam injection operations. The oil viscosities ranged from 1 cp. to 550 cps.

Figures 13 and 14 show the development of an override zone for the lowest viscosity fluids, 1 cp. and 15 cps., and the highest viscosity fluids, 140 and 550 cps. The numbers on the curves represent equal time intervals, and it is apparent that the displacement of crude by a gas drive is a function of oil viscosity. This is further borne out by Figure 15 in which the data has been replotted to show the relationship of recovery to injection time or volume.

Finally, in Figure 16 the production rate in these experiments is shown as a function of oil viscosity at different stages of depletion. The production rate decreases with degree of depletion as expected and in agreement with observations made in steam drive operations. Further, a calculation of the slopes of these curves, which reveal the dependence of the production rate on viscosity of the oil at any specified degree of production, shows that at low viscosities the rate of production is a linear function of the inverse of the oil viscosity. As the fluid viscosity increases, the production rate becomes dependent on a fractional power of the inverse of the viscosity; eventually approaching a fractional power of approximately 0.4. This compares very favorably with the 0.5 power observed for the range of crude oils used in the steam drive studies.

VIII. CONCLUSIONS

The continued study of the steam drive in scaled physical models has led to the following conclusions:

1. Thin reservoirs, in which steam communication between injector and producer can be secured early, will produce oil at oil steam ratios comparable to or greater than those ratios experienced in thicker reservoirs.

2. The residual oil in high porosity, water-flooded reservoirs, can be produced by steam drive at economic oil/steam ratios if high quality steam can be injected at high rates and moderate or low pressure.

3. An inert gas can be substituted for a significant fraction of the injected steam in a mature steam flood to maintain the production of oil and realize a higher oil/steam ratio. The economic advantage of such a substitution will become more signficant as the value of the crude oil itself increases.

4. High rate injection of an inert gas into a reservoir containing a low viscosity fluid will result in a production performance qualitatively similar to that of a steam drive into a heavy oil reservoir. The economic applicability of this scheme has not yet been evaluated but there is promise that such a scheme may have significant application.

5. A simple conceptual model for the steam drive progess which comprises the overlay of steam, the heating of the oil at the resulting oil steam interface, and the displacement of the heated oil by the gas drive accounts for virtually all of the observations made on steam drive operations in the field and in the laboratory scaled physical models.

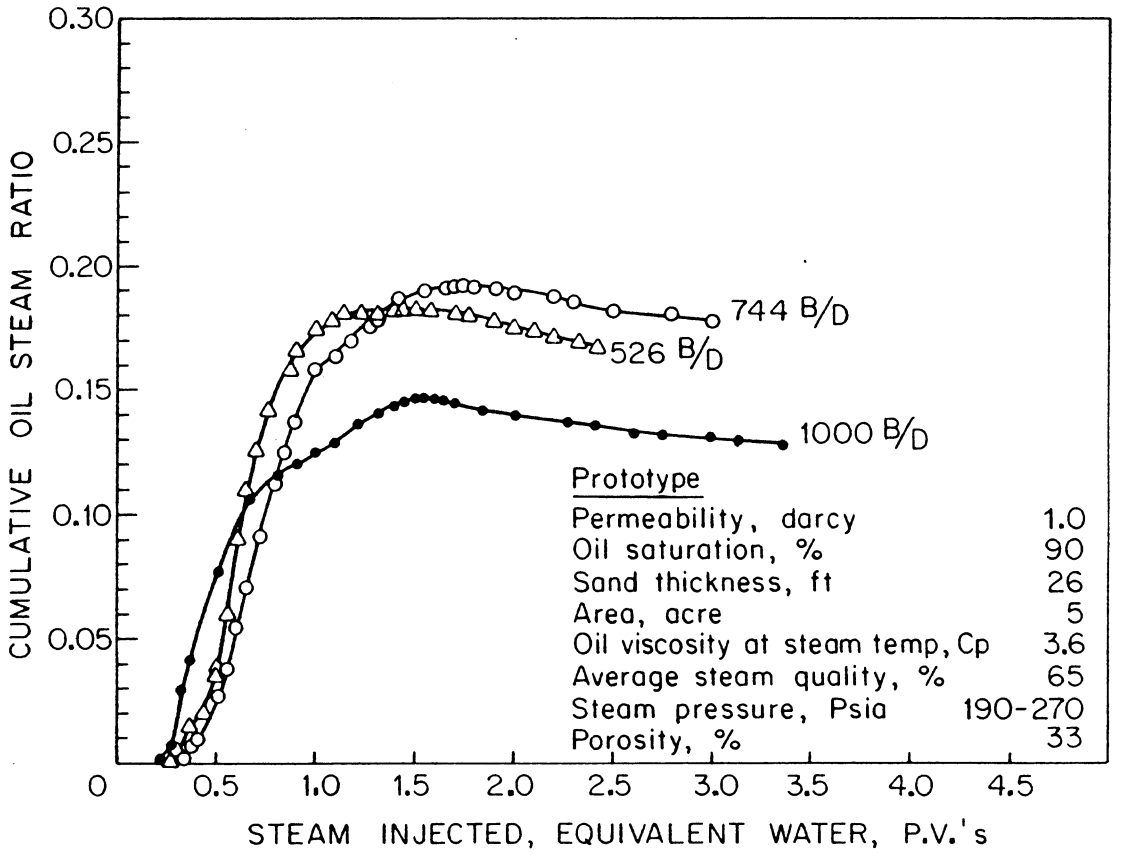

FIGURE 1. EFFECT OF INJECTION RATE ON THE OIL/STEAM RATIO

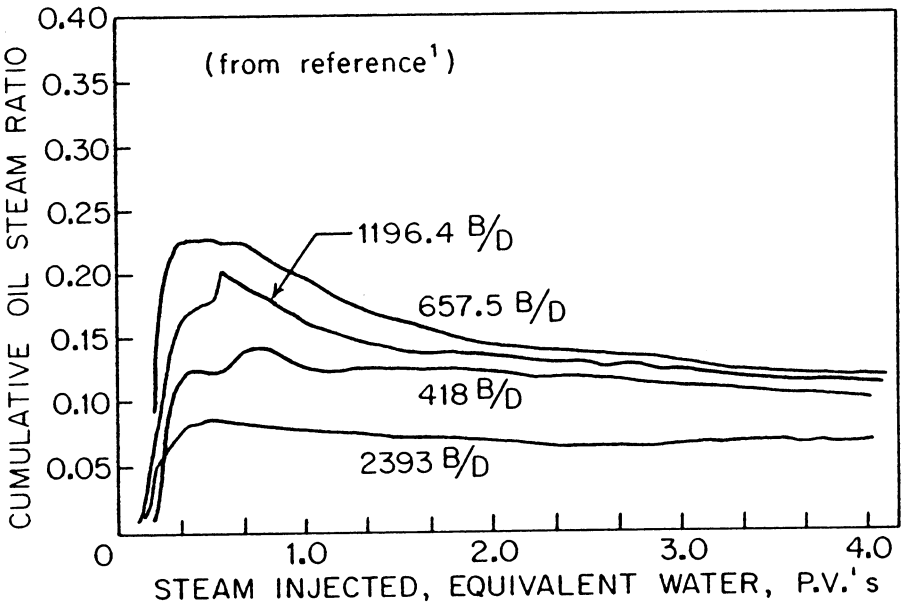

FIGURE 2. EFFECT OF INJECTION RATE ON OIL/STEAM RATIO

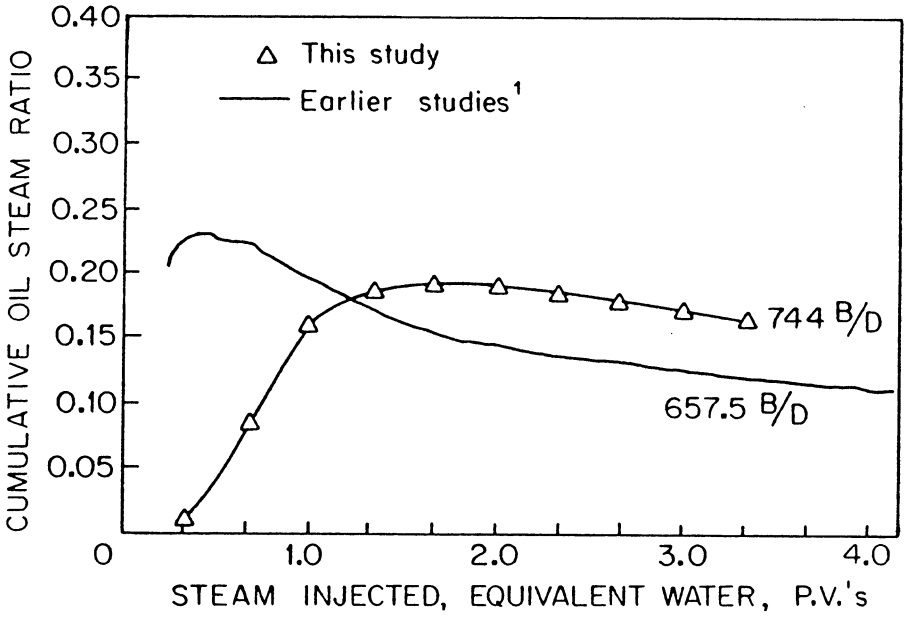

FIGURE 3. COMPARISON OF OIL/STEAM RATIO IN THICK AND THIN SAND

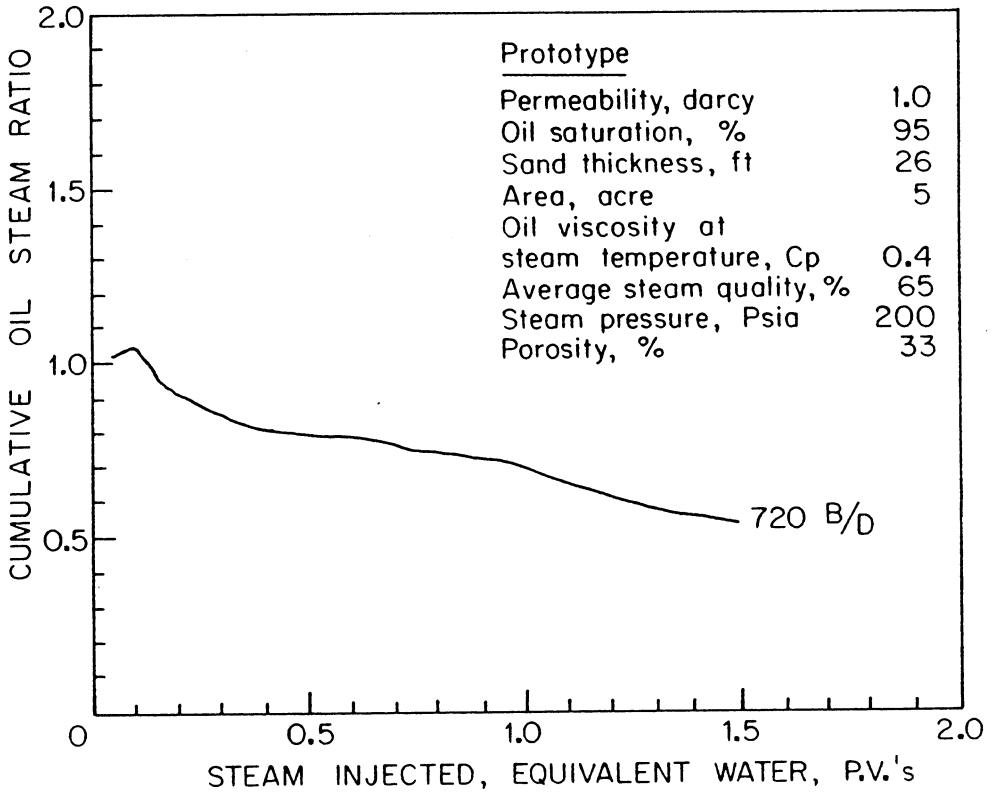

FIGURE 4. OIL/STEAM RATIO HISTORY FOR LOW VISCOSITY FLUID

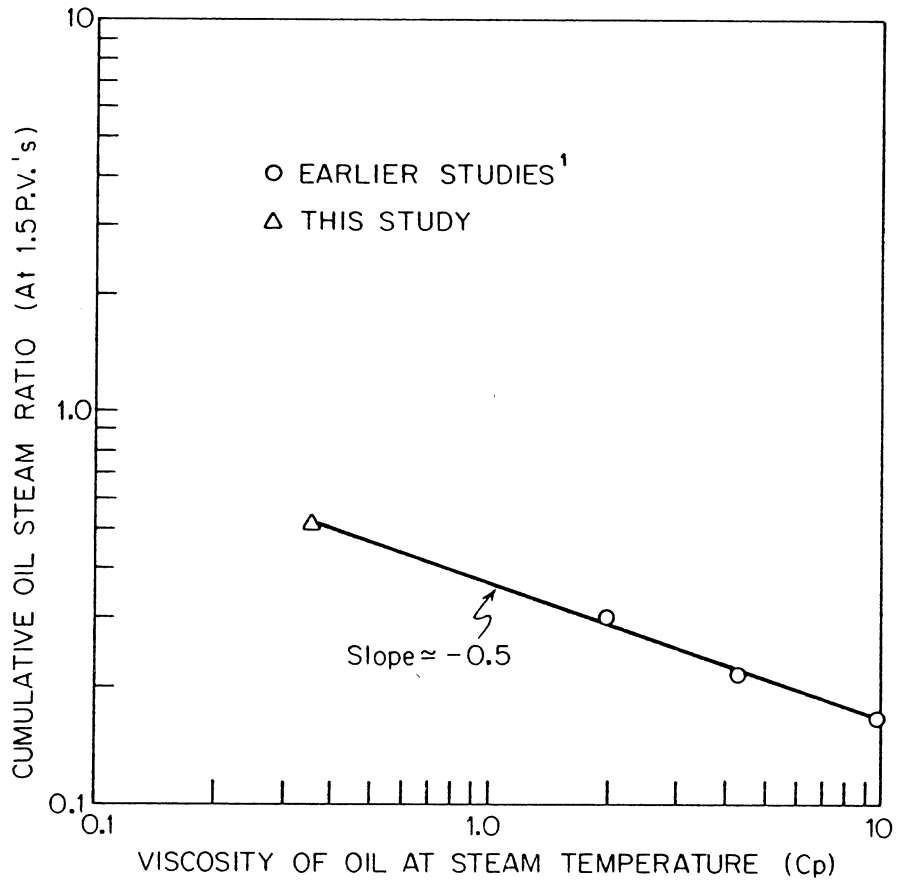

FIGURE 5. OIL/STEAM RATIO AS A FUNCTION OF RESERVOIR FLUID VISCOSITY

← FLOW DIRECTION

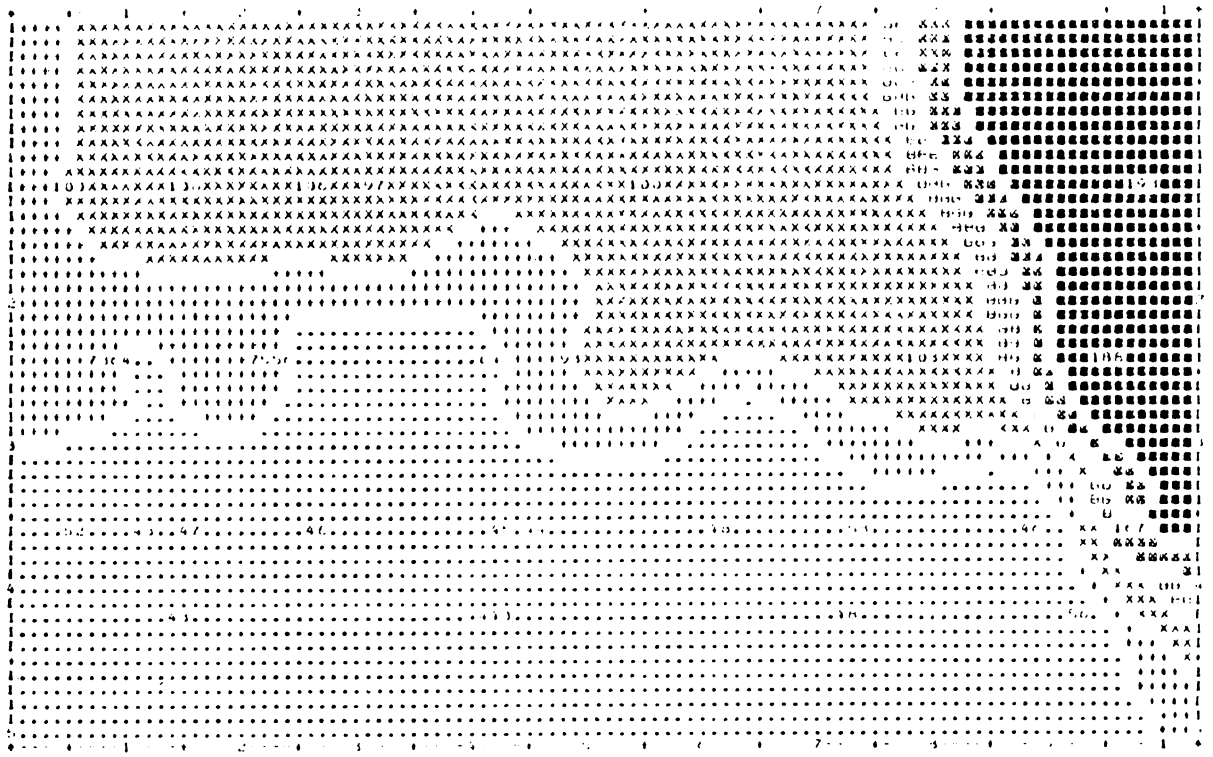

FIGURE 6. TEMPERATURE DISTRIBUTION FOR THE HEAVY OIL AFTER 0.51 P.V.'s OF STEAM INJECTED

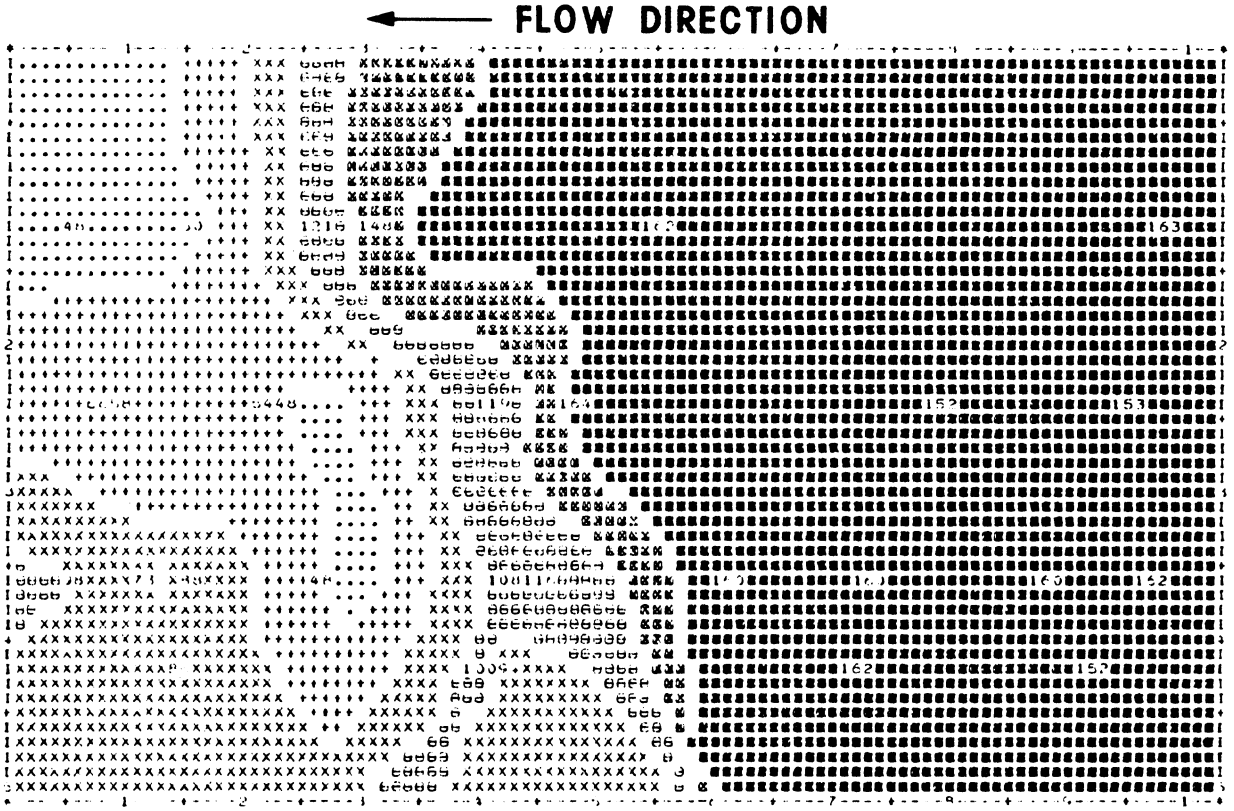

FIGURE 7. TEMPERATURE DISTRIBUTION FOR THE LIGHT OIL AFTER 0.5 P.V.'s OF STEAM INJECTED

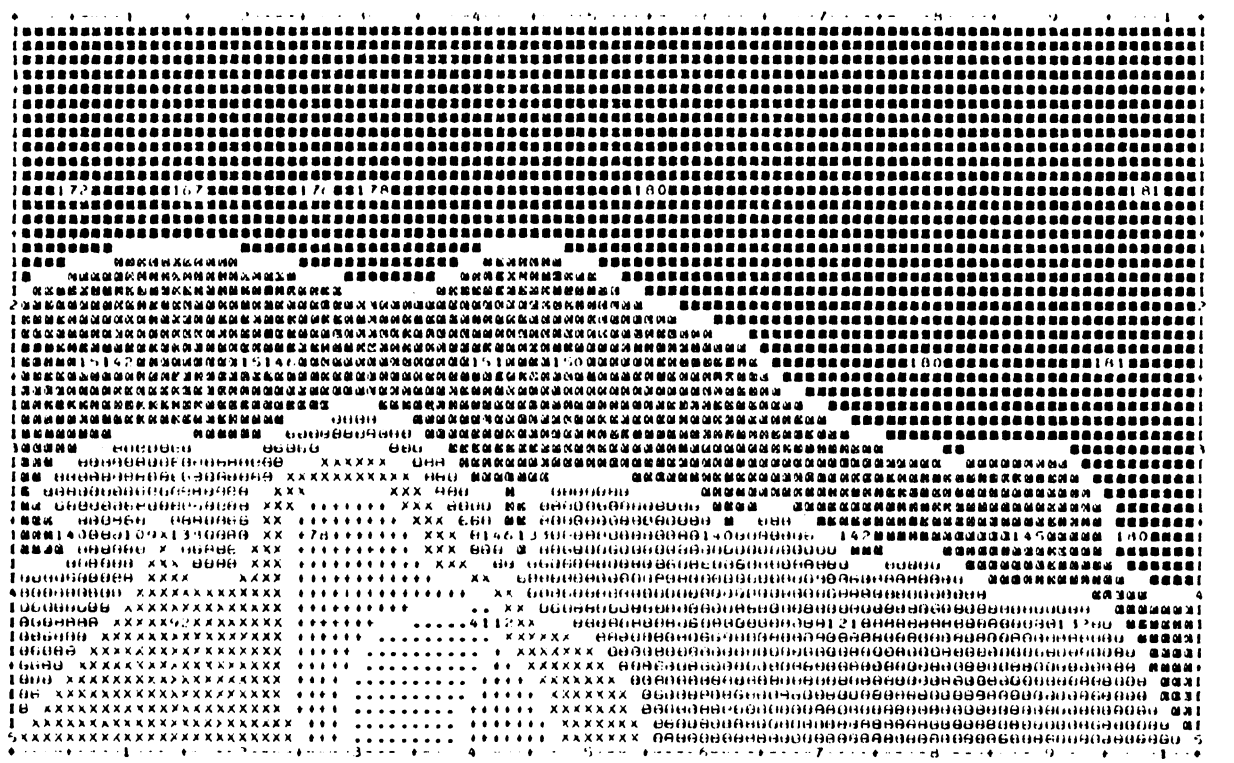

FIGURE 8. TEMPERATURE DISTRIBUTION FOR THE HEAVY OIL AFTER 1.5 P.V.'s OF STEAM INJECTED

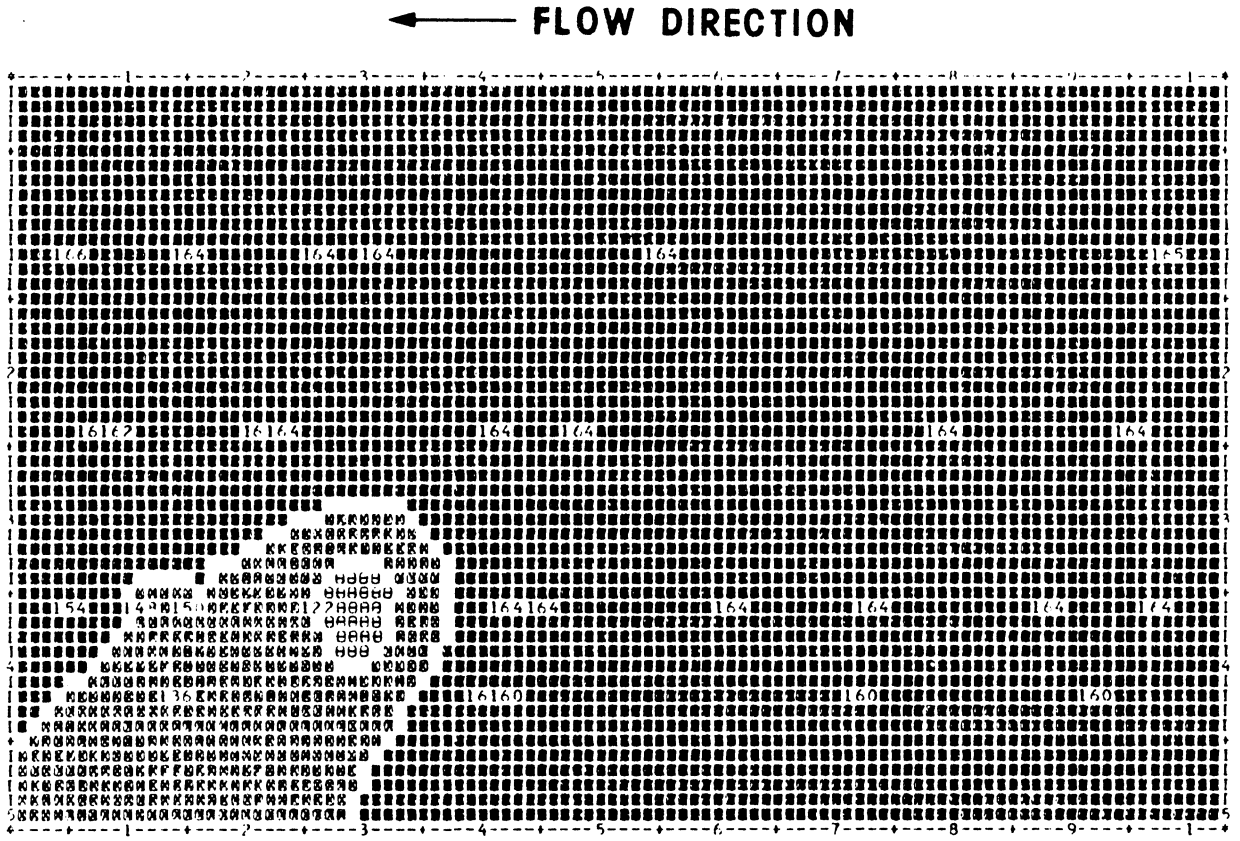

FIGURE 9. TEMPERATURE DISTRIBUTION FOR THE LIGHT OIL AFTER 1.5 P.V.'s OF STEAM INJECTED

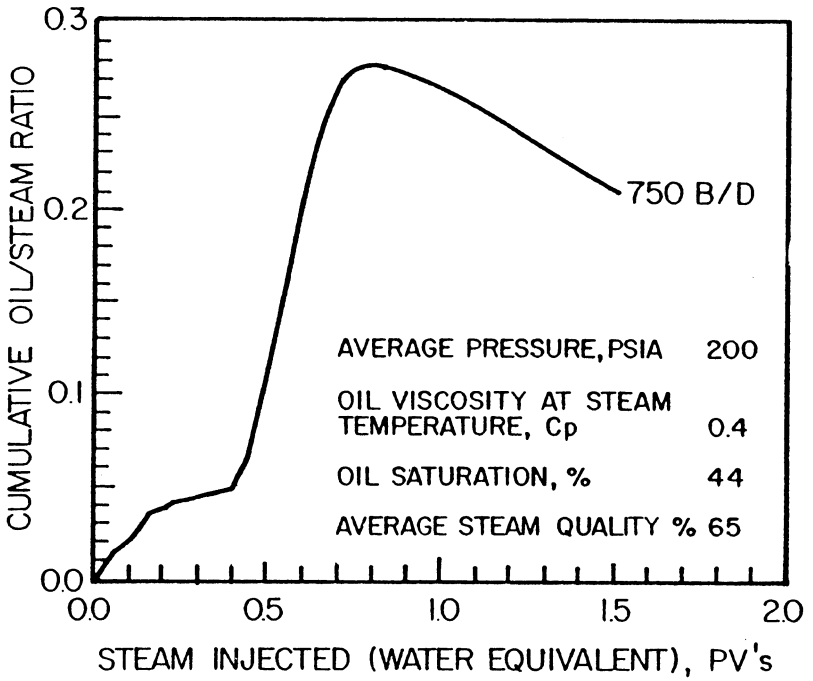

FIGURE 10

HISTORY OF CUMULATIVE OIL/STEAM RATIO VS PORE VOLUME STEAM INJECTED FOR THE LIGHT OIL

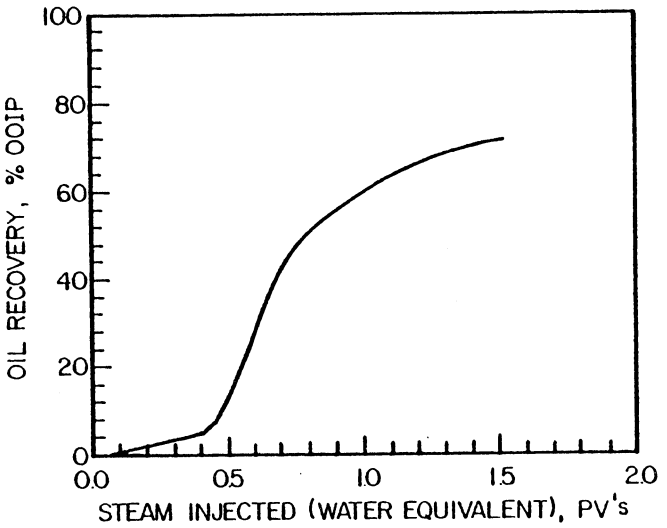

FIGURE 11

OIL RECOVERY VS PORE VOLUME STEAM INJECTED FOR THE LIGHT OIL

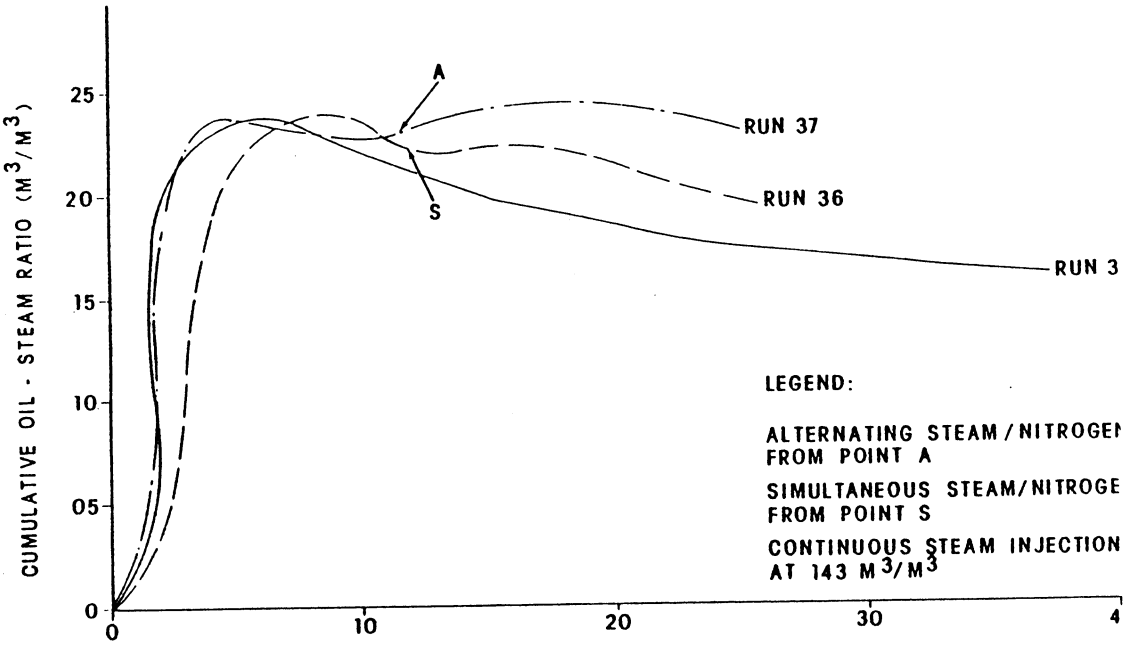

FIGURE 12. NITROGEN AS A STEAM ADDITIVE

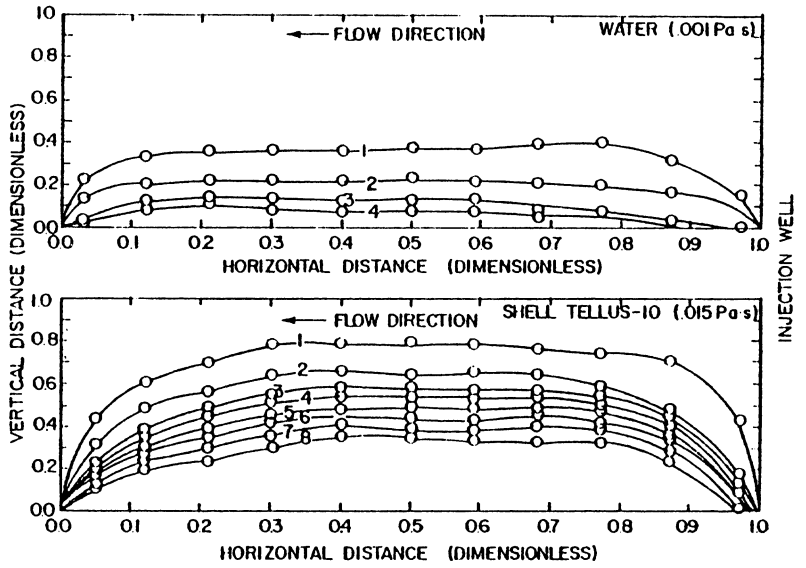

FIGURE 13. THE FLUID-GAS INTERFACE AS A FUNCTION OF TIME OF INJECTION

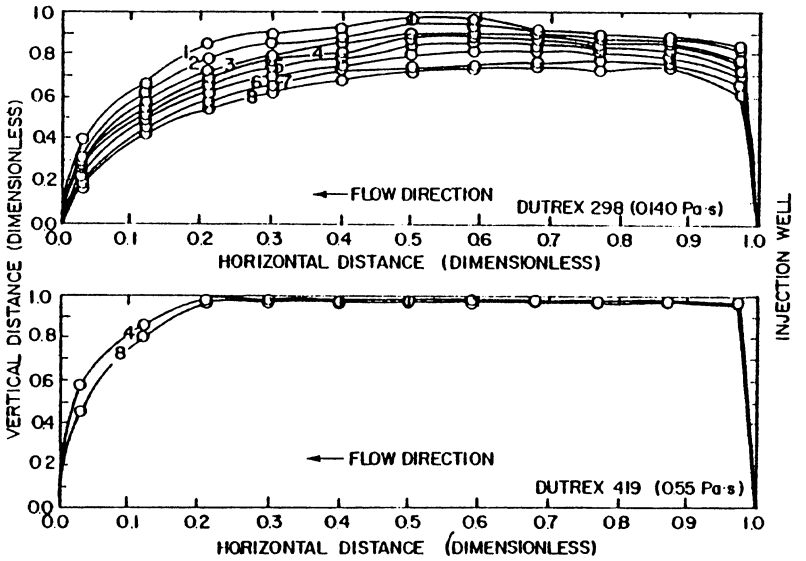

FIGURE 14. THE FLUID-GAS INTERFACE AS A FUNCTION OF TIME OF INJECTION

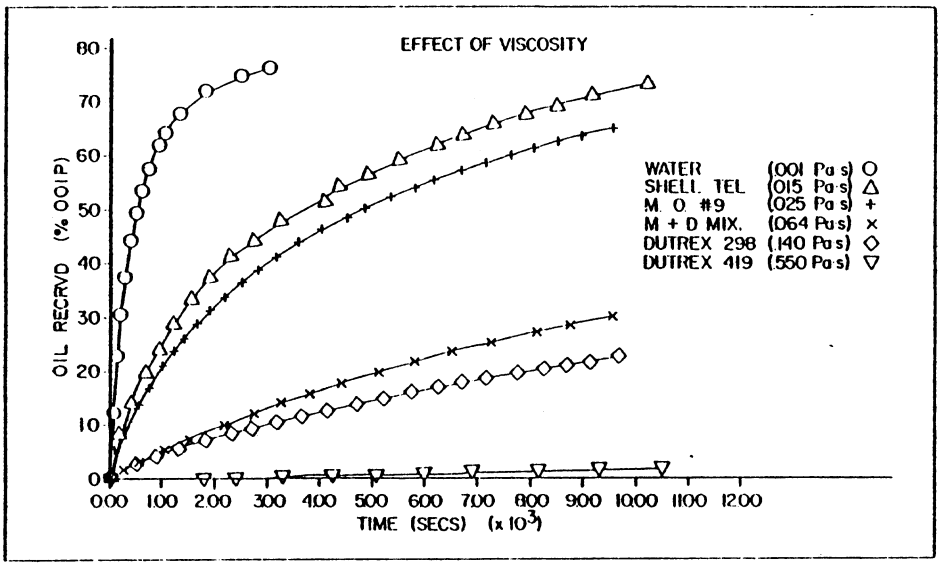

FIGURE 15. RECOVERY OF OIL OF DIFFERENT VISCOSITIES UNDER GAS DRIVE

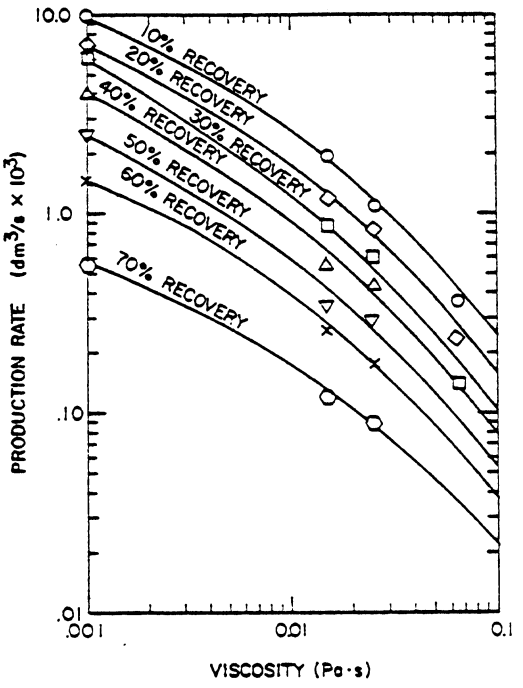

FIGURE 16. PRODUCTION RATE OF OIL OF DIFFERENT VISCOSITIES UNDER GAS DRIVE

COMPUTATION OF TRACER PRODUCTION CURVES FOR VARIOUS FLOODING PATTERNS

by

Maghsood Abbaszadeh-Dehghani and William E. Brigham
Stanford University Petroleum Research Institute (SUPRI)

ABSTRACT

The flow of a tracer slug in several homogeneous systems has been studied. The systems considered were the developed 5-spot, and both the staggered line drive and the direct line drive with various d/a ratios. In each system, the longitudinal mixing of the tracer slug in a general streamtube of the system was dealt with rigorously. A line integral along a streamline was derived, representing the length of the mixed zone. It was determined that substitution of the line integral into the mixing equation yields an expression for the concentration of tracer at any location within a streamtube. Furthermore, these expressions, integrated over the entire streamlines of the patterns, produce a set of equations describing the pattern effluent tracer concentration. This study shows that the effluent tracer concentration depends upon the geometry, size, and dispersion constant of the system.

HISTORY OF PROJECT

This report contributes to one of the five objectives of Contract DE-AC03-76ET12056 which was initiated in September 1976.

INTRODUCTION

Description of reservoir heterogeneity is of prime importance in recovery methods. In any fluid injection operation, the high permeability streaks and channels retain a considerable amount of the injected fluid, hence reducing the efficiency of the flooding and greatly increasing the cost of operation. Therefore, detection of highly permeable zones would be very helpful in understanding and increasing the efficiency of injection projects.

Injection of a tracer slug into a formation and subsequent analysis of the tracer concentration porfiles from output wells can furnish useful information about reservoir layering. Often, these tracer profiles are a combination of tracer responses from several of the layers which constitute the formation. Therefore, to analyze any of these tracer profiles, it is necessary to solve the inverse problem. To accomplish this, the tracer production curves must be deconvolved into several individual responses, each corresponding to a single layer. The constructed layer responses make it possible to compute the permeability, porosity and thickness of each layer (more precisely, kh and ϕh) (1).

The deconvolution process requires a precise knowledge of tracer flow behavior in homogeneous systems. In the past, several people have attempted

Prepared for DOE under Contract No. DE-AC03-76ET12056

to compute the tracer production curves for homogeneous systems theoretically. For example, Brigham and Smith (2) derived mathematical equations for the tracer concentration at the production well of a 5-spot pattern. They dealt with the mixing phenomenon of the tracer mathematically. Unfortunately, they made several simplifying assumptions which did not take into consideration the convergent effect of the flow on mixing. This detracted from the accuracy of their results.

Baldwin(3) divided one-eighth of the 5-spot pattern into 50 convergent-divergent triangular passages approximating the streamtubes of the pattern. He used the mixing equation in a radial system for each of the passages and computed the tracer concentrations. He utilized a trail and error method to fit the breakthrough curve of the 5-spot pattern as well as the tracer production curves obtained experimentally. This method is too combersome for regular use.

In this study, analytic equations were developed for the tracer concentration at the output well of not only a 5-spot pattern, but also of several other common flooding patterns. The equations are exact and, hence, the concentrations computed from them are precise.

DISCUSSION AND RESULTS

In a miscible displacement of one fluid by another fluid, the concentration of each fluid is a function of position. This is due to the mixing occurring between the two fluids. In the absence of viscous fingering, the equation defining mixing in a linear miscible displacement is (4,5):

$$\frac{c}{c_o} = \frac{1}{2}\,\mathrm{erfc}\left(\frac{x - \bar{x}}{\sqrt{2\sigma^2}}\right) \qquad (1\text{-a})$$

where

$$\sigma^2 = 2Kt + 2\alpha L \qquad (1\text{-b})$$

Equation 1-a still applies for a radial system (4,6); however, for this flow system, the equation for σ is:

$$\sigma^2 = Kt + \frac{2\alpha r}{3} \qquad (2)$$

Equation 1-a is valid for a system of any shape as long as a proper σ is defined for that shape. The following general equation has been derived to define σ:

$$\sigma^2 = 2\alpha v(\bar{s})^2 \int_o^{\bar{s}} \frac{ds}{v(s)^2} \tag{3}$$

(See Appendix A for the derivation.)

Consider a flooding pattern, e.g., the staggered line derived in Fig. 1. Suppose that a tracer slug is injected into this pattern, followed by a certain amount of displacing fluid which has the same mobility as the fluid ahead of the slug. The tracer slug will be distributed among the streamtubes. In a general streamtube, mixing will occur at both the leading edge and the trailing edge of the slug. The concentration of tracer at any location is the difference between two terms, each given by Eq. 1-a. This is:

$$\frac{c}{c_o} = \frac{1}{2}\,\mathrm{erfc}\left(\frac{s - \bar{s}_1}{\sqrt{2\sigma_1^2}}\right) - \frac{1}{2}\,\mathrm{erfc}\left(\frac{s - \bar{s}_2}{\sqrt{2\sigma_2^2}}\right) \tag{4}$$

See Fig. 1 for notations.

If the tracer slug size is small compared to the size of the system, Eq. 4 will take a differential form,

$$\frac{c}{c_o} = \frac{w}{\sqrt{2\pi\sigma^2}} \exp\left[-\frac{(s - \bar{s})^2}{2\sigma^2}\right] \tag{5}$$

In this equation, σ is given by Eq. 3. However, it is more convenient to express the above equation in volumetric terms rather than distances, by using the following two relationships:

$$s - \bar{s} = \frac{v\phi}{qh}(V - \bar{V}) \tag{6-a}$$

$$w = \frac{v}{q} t_r \tag{6-b}$$

Substitution of Eq. 6 in Eq. 5 results in:

$$\frac{c}{c_o} = \frac{t_r}{2q\sqrt{\pi\alpha I}} \exp\left[-\frac{(V - \bar{V})^2}{4\alpha q^2 I}\right] \tag{7-a}$$

where:

$$I = \int_o^{\bar{s}} \frac{ds}{v(s)^2} \tag{7-b}$$

Equation 7 defines the tracer concentration at any location within the streamtube. For example, for tracer concentration at the production well, the V term will be replaced by the total volume of the streamtube. These streamtube volumes can be replaced by pattern volumes using the expressions below.

$$\bar{V} = \frac{q}{Q} V_P \tag{8-a}$$

$$V = \frac{q}{Q} V_{PB} \tag{8-b}$$

The flow is radial around the wellbore, thus $Q = 2\pi\lambda h$. The pattern volumes in Eq. 8 are expressed in terms of pattern pore volumes,

$$\bar{V} = \frac{da}{\pi\lambda} V_{PD} \tag{9-a}$$

$$V = \frac{da}{\pi\lambda} V_{PBD} \tag{9-b}$$

In the early phase of this study, analytic expressions were derived for V_{PBD} for different patterns and were correlated (7). These expressions were defined in terms of various elliptic integrals.

By substituting Eq. 9 into Eq. 7 and noting that $t_r/q = T_r/Q$, the following expression is obtained:

$$\frac{c}{c_o} = \frac{\sqrt{K}\, K' \sqrt{\frac{a}{\alpha}}\, F_r}{\pi\sqrt{\pi Y}} \exp\left[- \frac{K\, K'^2\, \frac{a}{\alpha}\, (V_{PBD} - V_{PD})^2}{\pi^2 Y} \right] \tag{10}$$

where,

$$F_r = \frac{T_r}{2\phi shda}$$

The derivation of expressions for Y from Eq. 3 is illustrated in Appendix B. The above equation is the final expression that gives the tracer concentration at the exit end of an individual streamtube as a function of the volume injected into the pattern.

The output tracer concentration from the production well of the pattern is the sum of the concentrations from all the streamtubes. At the limit this is an integral given by:

$$\frac{\bar{c}}{c_o} = \frac{\int_o^{\frac{\pi}{4}} q \frac{c(\theta)}{c_o} \, d\theta}{\frac{Q}{8}} = \frac{4}{\pi} \int_o^{\frac{\pi}{4}} \frac{c(\theta)}{c_o} \, d\theta \qquad (11)$$

Substitute for $\frac{c(\theta)}{c_o}$ from Eq. 10:

$$\frac{\bar{c}}{c_o} = \frac{4\sqrt{K}\, K' \sqrt{\frac{a}{\alpha}}\, F_r}{\pi^2 \sqrt{\pi}} \int_o^{\frac{\pi}{4}} \frac{\exp\left\{ - \frac{K K' \frac{a}{\alpha}}{\pi Y(\theta)} \left[V_{PB}(\theta) - V_{PD} \right]^2 \right\}}{\sqrt{Y(\theta)}} \, d\theta \qquad (12)$$

Denoting $\frac{\bar{c}}{c_o F_r \sqrt{\frac{a}{\alpha}}}$ by $\bar{C}_D$ which is a dimensionless quantity, we get,

$$\bar{C}_D = \frac{4\sqrt{K}\, K'}{\pi^2 \sqrt{\pi}} \int_o^{\frac{\pi}{4}} \frac{\exp\left\{ - \frac{K K' \frac{a}{\alpha}}{\pi Y(\theta)} \left[V_{PB}(\theta) - V_{PD} \right]^2 \right\}}{\sqrt{Y(\theta)}} \, d\theta \qquad (13)$$

Equation 13, which describes the effluent tracer concentration at any pore volume, V_{PD}, of displacing fluid injected, is the final result of this study. This equation is exact for the 5-spot, staggered line drive and the direct line drive. Other patterns have the same form of expression with different constants. The authors have not yet investigated them in detail.

Figure 2 shows a plot of $\bar{C}_D$ vs V_{PD} for a staggered line drive with d/a = 1.5. As this graph shows, there are a series of curves which depend on a/α ratios. For a higher value of α, or an equivalently shorter

distance, the corresponding curve is broad. This is due to the high amount of mixing that occurs. Also, note that there is tracer production even at V_{PD} less than 0.85, which is the breakthrough sweep efficiency of this pattern. This is also the result of mixing.

Figure 3 illustrates tracer production curves of three different patterns for $a/\alpha = 500$. Again, early tracer production before the breakthrough sweep efficiency of the patterns is a characteristic of the mixing phenomenon.

Having defined the tracer production profiles from the homogeneous systems analytically, it is feasible to develop an algorithm based on the Yuen, et al.'s (1) method to deconvolve the tracer production curves from a multi-layered system into several responses each corresponding to a homogeneous layer. The physical parameters of the layers would be computed from these responses. This is the next goal of this research which will be done in the future.

CONCLUSIONS

1. Equations were derived which describe the mixing of the tracer slug with the contacted fluids in a general streamtube of the flooding pattern.

2. Analytic expressions have been obtained which define the tracer production curves of the different flooding patterns.

3. The study shows that the tracer production curves depend upon the geometry, size and dispersion constant of the formation.

4. It is postulated that the deconvolution of the tracer response profile from a multilayered system into several layer responses is possible by utilizing the results of this study.

NOMENCLATURE

a = distance between like wells, L

b = distance between unlike wells, L

c = concentration within the streamtube

$\bar{c}$ = concentration at the production well

c_o = initial tracer concentration

erfc = complementary error function

F_r = tracer slug size in terms of fraction of pattern pore volume

h = thickness of the system, L

k = permeability, L^2

$K(m)$ = complete elliptic integral of the first kind

$K'(m)$ = complementary complete elliptic integral

K = mixing constant, depends on diffusion coefficient and cementation factor, L^2/s

L = length, L

m, m_1 = parameters of elliptic integrals, $m + m_1 = 1$

q = flow rate in the streamtube, L^3/T

Q = total flow rate into the pattern, L^3/T

r = radius in a radial flow, L

s = distance along the streamline, L

$\bar{s}, \bar{s}_1, \bar{s}_2$ = distance along the streamline up to the front, L

sn, cn, dn = elementary Jacobian elliptic functions

t_r = volume of tracer injected into a streamtube, L^3

T_r = total volume of tracer slug injected into the pattern, L^3

v = velocity, L/t

$v(s)$ = velocity at the front, L/t

V = volume of streamtube up to any location, L^3

$\bar{V}$ = volume of streamtube up to the front, L^3

V_P = volume of displacing fluid injected into the pattern

V_{PB} = volume of displacing fluid injected into the pattern at breakthrough of a streamline, L^3

V_{PD} = pore pore volume of displacing fluid-injected, dimensionless

V_{PBD} = pore volumes of displacing fluid injected at breakthrough, dimensionless

x = distance, L

$\bar{x}$ = distance to the front, L

w = undiluted width of tracer slug in a streamtube, L

α = dispersion constant, L

λ = mobility of the fluid in a porous medium, k/μ

ϕ = porosity, fraction

$\sigma, \sigma_1, \sigma_2$ = standard deviation, measure of the length of the mixed zone, L

ψ = stream function

ACKNOWLEDGEMENT

The authors wish to thank DOE (contract number DE AC03 76 ET 12056) for support of this work. This support is greatly appreciated.

REFERENCES

1. Yuen, D. L., Brigham, W. E., Cinco, H. L.: "Analysis of Five-Spot Tracer Tests to Determine Reservoir Layering," DOE Report, Feb. 1979, 60.

2. Brigham, W. E., and Smith, D. H.: "Prediction of Tracer Behavior in Five-Spot Flow," Paper SPE 1130, 40th Annual Fall Meeting of SPE-AIME, Denver, Colorado, Oct. 1965.

3. Baldwin, D. E., Jr.: "Prediction of Tracer Performance in a Five-Spot Pattern," J. Pet. Tech., Apr. 1966, pp. 513-517.

4. Raimandi, P., Gardner, G. H. F., and Petrick, C. B.: "Effect of Pore Structure and Molecular Diffusion on the Mixing of Miscible Liquids Flowing in Porous Media," Paper 43, AIChE-SPE Joint Symposium, National AIChE Meeting, San Francisco, California, Dec. 6-9, 1959.

5. Brigham, W. E.: "Mixing Equations in Various Geometries," Paper SPE 4585, 48th Annual Fall Meeting of the Society of Petroleum Engineers of AIME, Las Vegas, Nevada, Sept. 30-Oct. 3, 1973.

6. Bentsen, R. G., and Nielson, R. F.: "A Study of Plane, Radial Miscible Displacement in a Consolidated Porous, Medium," Soc. Pet. Eng. J., March 1965, pp. 1-5.

7. Abbaszaden-Dehghani, M., Brown, L. S., Brigham, W. E.: "Tracer Related Studies," DOE Annual Heavy Oil/EOR Contractor Presentations, San Francisco, California, July 22-24, 1980, pp. 87-109.

8. Prats, M.: "The Breakthrough Sweep Efficiency of the Staggered Line Drive," J. Pet. Tech., December 1965, pp. 67.

9. Byrd, P. F., and Friedman, M. D.: "Handbook of Elliptic Integrals for Engineers and Scientists," Lange, Maxwell and Springer, Ltd., 1954, London.

APPENDIX A

Consider an arbitrary shape such as,

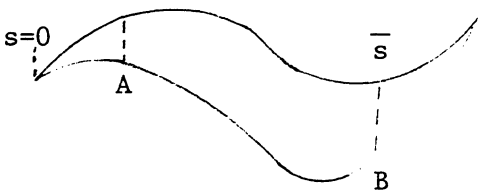

The change in σ from A to B is due to two effects (3,5):

a) The movement of fluid (the longer is the distance travelled, the wider is the mixed zone). This change is denoted by $d\sigma_x$.

b) The effect of geometry (the wider the passage, the narrower the mixed zone). This change is denoted by $d\sigma_g$.

Therefore, the total change in σ is given by,

$$d\sigma = d\sigma_x + d\sigma_g \qquad \text{(A-1)}$$

Equations for $d\sigma_x$ and $d\sigma_g$ are available in the literature (5). Assuming that the molecular diffusion is negligible in relation to the longitudinal dispersion, these equations reduce to,

$$d\sigma_x = \frac{\alpha v\, dt}{\sigma} \tag{A-2}$$

$$d\sigma_g = \sigma \frac{dv}{v} \tag{A-3}$$

Substitute the above formulas in Eq. A-1,

$$d\sigma = \frac{\alpha v\, dt}{\sigma} + \frac{\sigma dv}{v} \tag{A-4}$$

Multiply both sides by $\frac{2\sigma}{v^2}$ and note that $ds = v\, dt$,

$$\frac{2\sigma\, d\sigma}{v^2} - \frac{2\sigma^2\, dv}{v^3} = 2\alpha \frac{ds}{v^2}$$

$$d\left(\frac{\sigma^2}{v^2}\right) = 2\alpha \frac{ds}{v^2}$$

Integrate,

$$\frac{\sigma_B^2}{v_B^2} - \frac{\sigma_A^2}{v_A^2} = 2\alpha \int_A^B \frac{ds}{v^2} \tag{A-5}$$

If $\sigma A = 0$ at $s = 0$, i.e., at the entry, then the general equation for σ is,

$$\sigma^2 = 2\alpha\, v(\bar{s})^2 \int_o^{\bar{s}} \frac{ds}{v(s)^2} \tag{A-6}$$

APPENDIX B

Consider a staggered line drive pattern,

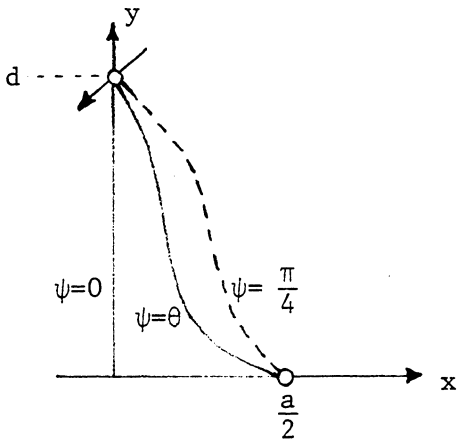


Injection

Production

The stream functions for this system are given by (8),

$$\psi = \tan^{-1}\left[f(w,m)\ f(z,m_1)\right] \tag{B-1.1}$$

$$f(w,m) = \frac{sn(w,m)\ dn(w,m)}{cn(w,m)} \tag{B-1.2}$$

$$w = \frac{2K(m)}{d}\ x \tag{B-1.3}$$

$$z = \frac{K'(m)}{d}\ y \tag{B-1.4}$$

$$\frac{K'(m)}{2K(m)} = \frac{d}{a} \tag{B-1.5}$$

The following equations facilitate evaluation of $I = \int_o^{\bar{s}} \frac{ds}{v(s)^2}$,

$$ds = \sqrt{(dx)^2 + (dy)^2} = dx\sqrt{1 + \left(\frac{dy}{dx}\right)^2} \tag{B-2.1}$$

$$v^2 = v_x^2 + v_y^2 \tag{B-2.2}$$

$$\frac{dx}{dy} = \frac{v_y}{v_x} \tag{B-2.3}$$

Using the above equations the line integral reduces to,

$$I = \int_o^{\bar{x}} \frac{dx}{v_x \sqrt{v_x^2 + v_y^2}} \tag{B-3}$$

In accord with the Cauchy-Riemann relationship the velocity components are related to stream functions,

$$v_x = \frac{\lambda}{\phi} \left.\frac{\partial \psi}{\partial y}\right|_{y=y(\psi,x)} \tag{B-4.1}$$

$$v_y = - \frac{\lambda}{\phi} \left.\frac{\partial \psi}{\partial x}\right|_{x=x(\psi,y)} \tag{B-4.2}$$

For a general streamline, ψ is a constant and Eq. B-1.1 yields,

$$f(w)\, f(z) = \sqrt{\eta} \tag{B-5}$$

where,

$$\eta = \tan^2 \psi = \text{constant}$$

Utilizing Eqs. B-1, B-2, and B-5, the following expression is obtained,

$$I = \frac{\phi s}{\lambda} (1 + \eta)^2 \frac{ad^2}{2KK'^2} \int_o^{\bar{w}} \frac{dw}{f(w)f'(w) \sqrt{[f(w)f'(z)]^2 + [f'(w)f(z)]^2}} \tag{B-6}$$

The following two equations, relating the derivatives to the functions, can be derived using the properties of elliptic integrals and Eq. B-1.3,

$$f'(z,m_1) = \sqrt{1 + f^4(z,m_1) + 2\beta f^2(z,m_1)} \qquad \text{(B-7.1)}$$

$$f'(w,m) = \sqrt{1 + f^4(w,m) - 2\beta f^2(w,m)} \qquad \text{(B-7.2)}$$

where,

$$\beta = m - m_1$$

Substituting for derivatives from B-7 and eleminating f(z) by Eq. B-5, Eq. B-6 reduces to,

$$I = \left(\frac{\phi s}{\lambda}\right)^2 (1 + \eta)^{1.5} \frac{ad^2}{2KK'^2} \int_o^{\bar{w}} \frac{f^2(w)dw}{\sqrt{[f^2(w) + \eta][f^4(w) + 2\beta\eta f^2(w) + \eta^2]}} \qquad \text{(B-8)}$$

Using a variable change, that $f^2(w) = t$, and using Eq. B-6.2, this equation simplifies to,

$$I = \left(\frac{\phi s}{\lambda}\right)^2 \frac{ad^2}{4KK'^2} Y \qquad \text{(B-9.1)}$$

$$Y = (1 + \eta)^{1.5} \int_o^{f^2(\bar{w})} \frac{\sqrt{t}\, dt}{\sqrt{(t^2 - 2\beta t + 1)(t^2 + 2\beta\eta t + \eta^2)(t^2 + \eta)}} \qquad \text{(B-9.2)}$$

It should be mentioned that at the production well the value of $f^2(w) = \infty$.

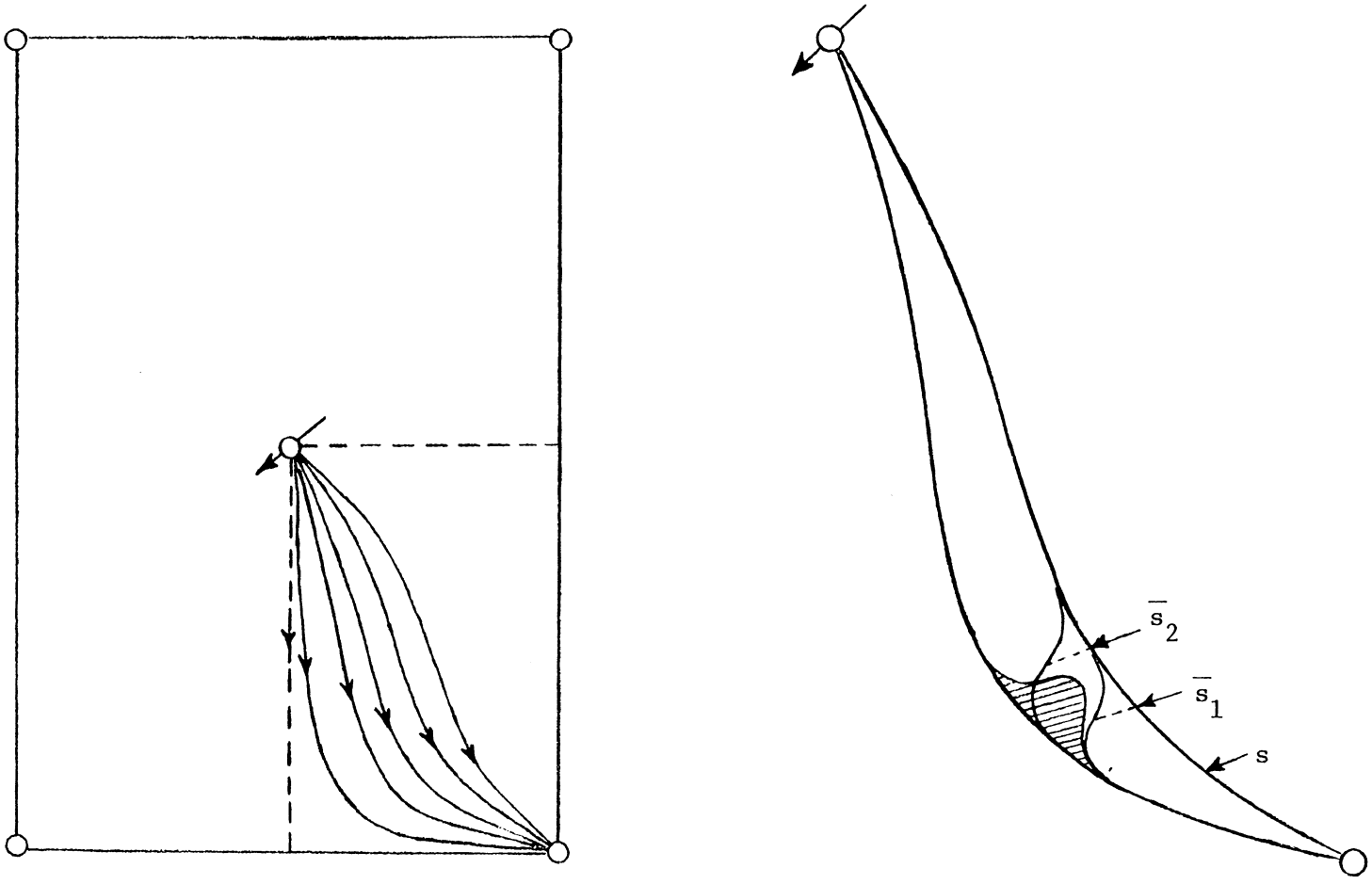

Fig. 1: STAGGERED LINE DRIVE WITH THE TRACER DISTRIBUTION PROFILE IN A STREAMTUBE

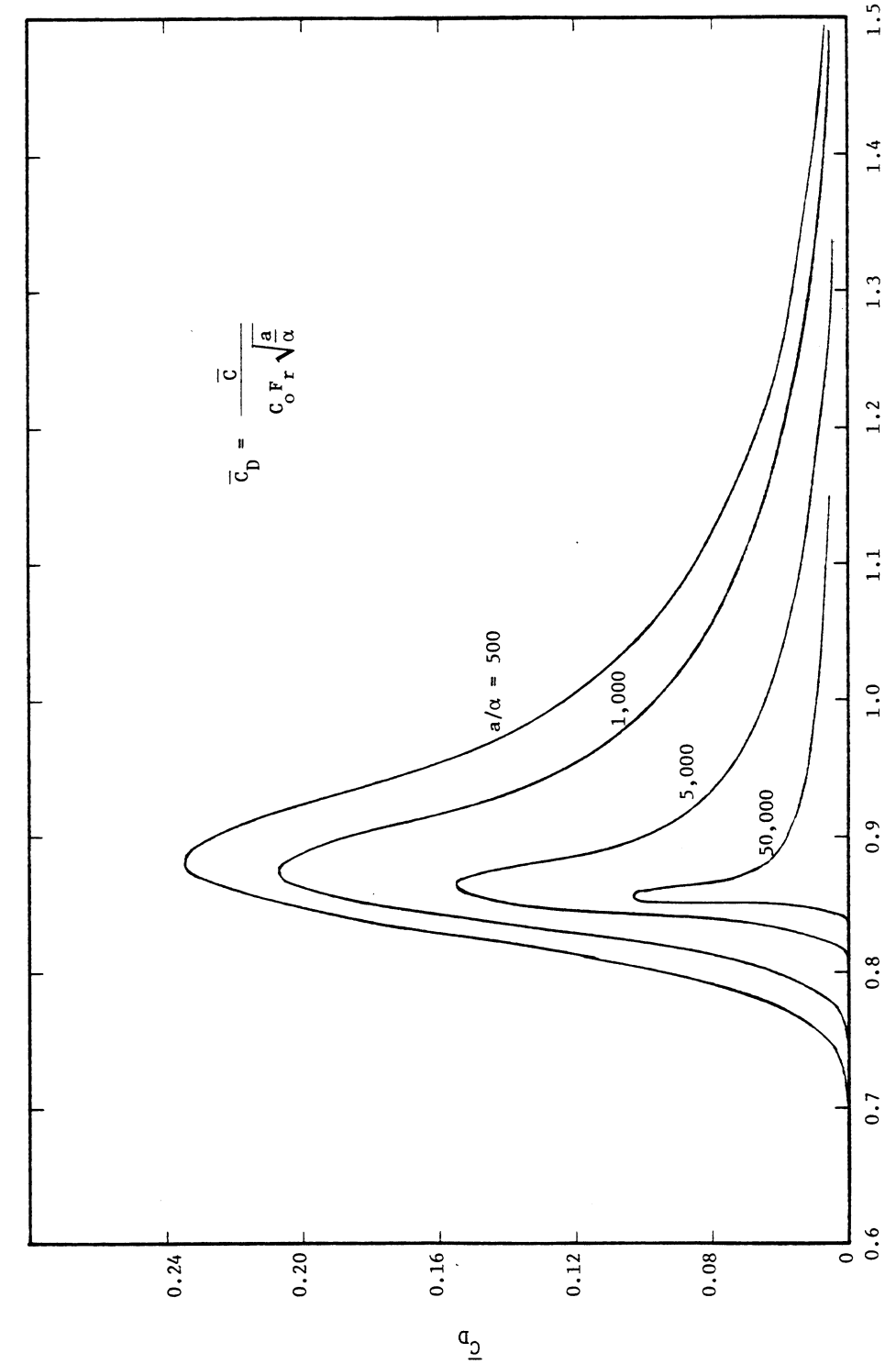

Fig. 2: TRACER PRODUCTION CURVES FOR A SMALL SLUG OF TRACER INJECTED INTO A HOMOGENEOUS STAGGERED LINE DRIVE, d/a = 1.5

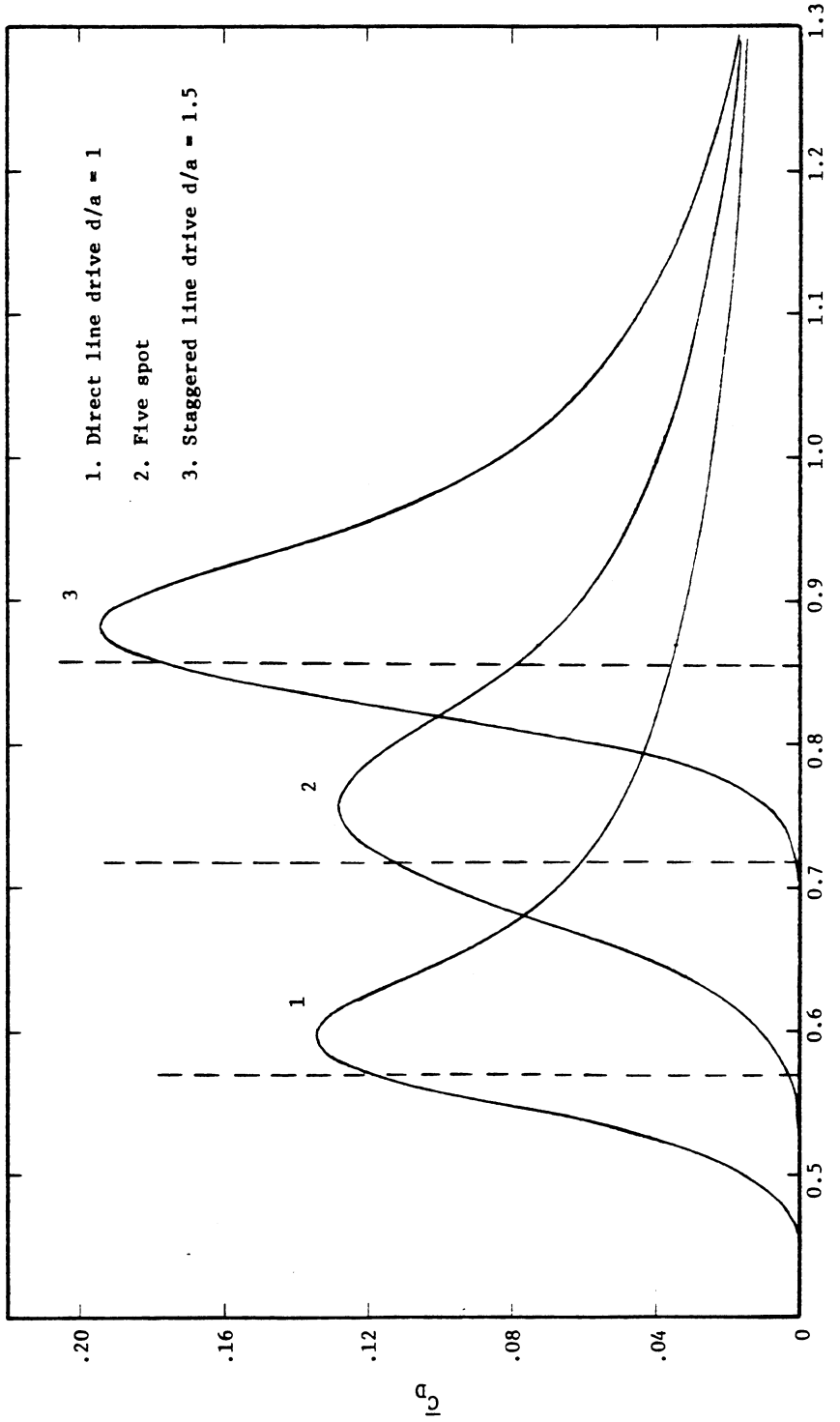

Fig. 3: TRACER PRODUCTION CURVES OF DIFFERENT FLOODING PATTERNS, $a/\alpha = 500$

CHEMICAL ASSISTED HOT WATERFLOOD: MODELING OF THE ADIABATIC CASE

by

Metin Karakas and Yanis C. Yortsos
Department of Petroleum Engineering
University of Southern California
Los Angeles, California 90007

ABSTRACT

The modeling of an adiabatic hot waterflood assisted by the simultaneous injection of chemical is presented. The process considered is one-dimensional, two-phase flow, with negligible effects of dispersion, heat conduction, and lateral heat losses. The model allows for the chemical to partition into the aqueous phase and to be adsorbed on the solid rock. The effects of temperature on the viscosity ratio and the adsorption kinetics and of chemical concentration on the fractional flow curves are included.

The theory of generalized simple waves (coherence) is used to develop solutions for the temperature, concentration, and oil saturation profiles, as well as the oil recovery curves. The results obtained show that in the adiabatic case the combined continuous injection of chemical and hot water considerably enhances the oil recovery. The sensitivity of the recovery performance to the adsorption parameters is discussed. It is shown that, for Langmuir adsorption kinetics, the chemical resides in the heated region of the reservoir if its injection concentration is below a critical value, and in the unheated region if its concentration exceeds this critical value.

HISTORY OF PROJECT

This report is part of a project "Chemical Additives with Steam Injection to Increase Oil Recovery." It was initiated September 15, 1976 with anticipated completion of October 15, 1981. The government award was $108,370.

INTRODUCTION

The displacement of a viscous crude oil by conventional recovery schemes operating at the reservoir temperature is not very effective due to the low mobility of the oleic phase. Taking advantage of the favorable alteration of the viscosity of the fluid phases achieved at high temperatures, various thermal processes have been successfully implemented for the economic recovery of heavy oils.[1] Steam injection, in-situ combustion, and, to a lesser degree, hot waterflood have been already established as commercially viable enhanced recovery schemes for such reservoirs. In an effort to further improve the recovery performance attained in such processes, it has been recently suggested[2] to aid the displacement mechanisms by the simultaneous injection of chemical additives.

The primary function of chemical additives in an enhanced recovery process is to alter the mobility characteristics of the fluid phases by reducing the interfacial tension between aqueous and oleic phases, thus increasing the relative permeability of oil to flow.[3] This effect, if acting in a synergestic way with the increased mobility achieved at higher temperatures, is expected to considerably enhance the recovery efficiency of standard thermal recovery processes. Although factors other than the above may play important roles at

Prepared for Department of Energy Under Contract No. DE-AC03-76SF00113

high temperatures,[4] it is the combined effect of changes in relative permeabilities and viscosity ratios that principally accounts for the enhancement in recovery.

Clearly, the viability of such a combined injection scheme rests on the hypothesis that the injected chemical additive asks its synergestic effect on the heated region of the reservoir, and particularly on the hot liquid region that precedes (any) advancing condensation fronts (e.g., in steam injection). Therefore, it is important to determine the region of residence of the chemical, with the ultimate objective to maximize the recovery performance by utilizing an optimum injection scheme. In an attempt to address this complex subject, we elect to study the simpler case of an adiabatic hot waterflood assisted by the simultaneous continuous injection of a chemical additive. Such a study will enable us to gain some insight on the rates or propagation of the chemical and heat fronts, and will provide considerable help in the analysis of the more complex process.

The process to be considered here is one-dimensional, two-phase flow, with negligible effects of dispersion, heat conduction, and lateral heat losses. The chemical is allowed to partition only in the aqueous phase and to be adsorbed on the solid surfaces following equilibrium adsorption. The important effects of temperature on the viscosity ratio and the adsorption kinetics, and of chemical on the relative permeabilities are included. With the above approximations the mathematical model of the process is cast into a system of hyperbolic equations. The latter is then solved by the method of generalized simple waves[5] (coherence[6]). From the results obtained a sensitivity analysis of the recovery performance with respect to the physical parameters follows with minimum computational requirements. The analysis is illustrated by example applications for typical injection and reservoir conditions.

MATHEMATICAL FORMULATION

The mathematical formulation of the system consists of the partial differential equations describing mass and energy balances in the reservoir. Since there are three species present, two independent mass balances can be written. By defining dimensionless time and space variables by

$$\tau = \frac{\int_o^t q\,dt}{\phi AL}, \qquad \xi = \frac{x}{L} \tag{1}$$

we obtain

(a) Chemical mass balance

$$\frac{\partial}{\partial \tau}[S_w \eta + g(\eta,T)] + \frac{\partial}{\partial \xi}[f_w \eta] = 0, \tag{2}$$

where,

$$g(\eta,T) = \left(\frac{1-\phi}{\phi}\right)\eta^R \tag{3}$$

Here, η is the volumetric concentration of the chemical in the aqueous phase, η^R the adsorbed concentration, g the adsorption isotherm. For Langmuir adsorption kinetics we have[7]

$$g(\eta,T) = \frac{\eta}{g_1\eta + g_2} \tag{4}$$

(b) Water mass balance

$$\frac{\partial S_w}{\partial \tau} + \frac{\partial f_w}{\partial \xi} = 0 \tag{5}$$

(c) Thermal energy balance

$$\frac{\partial}{\partial \tau}\left[(\rho_w C_{pw} S_w + \rho_o C_{po} S_o + \frac{(1-\phi)}{\phi}\rho_R C_{pR})(T-T_o)\right]$$

$$+ \frac{\partial}{\partial \xi}\left[(\rho_w C_{pw} f_w + \rho_o C_{po} f_o)(T-T_o)\right] = 0 \tag{6}$$

where T_o is the original reservoir temperature. In the above, the fractional flow of water f_w is assumed to be a function of T, η, S_w according to the expression[8]

$$f_w = \frac{1}{\left\{1 + \frac{\mu_w(T)}{\mu_o(T)} \cdot \frac{k_{ro}^{o}(T,\eta)}{k_{rw}^{o}(T,\eta)} \cdot \frac{(1-S)^n}{S^p}\right\}} , \tag{7}$$

where the exponents n, p may be functions of n, and S is the normalized water saturation

$$S = \frac{S_w - S_{wr}(\eta)}{1 - S_{wr}(\eta) - S_{or}(\eta)} . \tag{8}$$

In all of our subsequent numerical calculations we assumed constant k_{ro}^{o}, k_{rw}^{o} n, p, S_{wr}, while $S_{or}(\eta)$ was taken to vary according to the relationship[9]

$$S_{or}(\eta) = a_1 + a_2\exp(-\eta/a_3) . \tag{9}$$

Equations (2), (5), (6) are in the form of a conservative system and they are used later for the derivation of shock conditions. For mathematical purposes the three equations are linearly rearranged to the following convenient set. From (5), (6) we obtain,

$$\frac{\partial T}{\partial \tau} + \left(\frac{f_w + a}{S_w + b} \right) \frac{\partial T}{\partial \xi} = 0 \qquad (10)$$

where a,b are defined by

$$a = \frac{\rho_o C_{po}}{(\rho_w C_{pw} - \rho_o C_{po})} \quad , \qquad (10a)$$

and

$$b = \frac{\rho_o C_{po} + \frac{(1-\phi)}{\phi} \rho_R C_{pR}}{(\rho_w C_{pw} - \rho_o C_{po})} \quad , \qquad (10b)$$

From (2), (5), (6) we obtain,

$$\frac{\partial \eta}{\partial \tau} + \left(\frac{f_w}{S_w + \frac{\partial g}{\partial \eta}} \right) \frac{\partial \eta}{\partial \xi} - \frac{\frac{\partial g}{\partial T} (f_w + a)}{(S_w + \frac{\partial g}{\partial \xi})(S_w + b)} \frac{\partial T}{\partial \xi} = 0 \quad . \qquad (11)$$

The linearly rearranged equations (10), (11) along with equation (5) can be concisely written as the following vector equation

$$\frac{\partial \underline{U}}{\partial t} + \underline{\underline{A}} \frac{\partial \underline{U}}{\partial \xi} = 0 \quad . \qquad (12)$$

Here $\underline{U}$ is the vector of the dependent variables,

$$U = \begin{bmatrix} T \\ \eta \\ S_w \end{bmatrix} \qquad (12a)$$

and $\underline{\underline{A}}$ is the 3×3 coefficient matrix,

$$\underline{\underline{A}} = \begin{bmatrix} \dfrac{f_w + a}{S_w + b} & 0 & 0 \\ -\dfrac{\frac{\partial g}{\partial T}(f_w + a)}{(S_w + \frac{\partial g}{\partial \eta})(S_w + b)} & \dfrac{f_w}{S_w + \frac{\partial g}{\partial \eta}} & 0 \\ \dfrac{\partial f_w}{\partial T} & \dfrac{\partial f_w}{\partial \eta} & \dfrac{\partial f_w}{\partial S_w} \end{bmatrix} \tag{12b}$$

For later use, the eigenvalues λ_i of the matrix $\underline{\underline{A}}$ are needed. We obtain,

$$\lambda_1 = \frac{f_w + a}{S_w + b} \tag{13a}$$

$$\lambda_2 = \frac{f_w}{S_w + \frac{\partial g}{\partial \eta}} \tag{13b}$$

$$\lambda_3 = \frac{\partial f_w}{\partial S_w} \tag{13c}$$

Since all eigenvalues are real and distinct and the matrix $\underline{\underline{A}}$ is a function of $\underline{U}$ only, equation (12) defines a homogeneous, quasilinear, hyperbolic system.[5]

METHOD OF SOLUTION

The solution to the hyperbolic system (12) along with the appropriate initial and boundary conditions can be obtained by the method of characteristics.[10] Since λ_i's are functions of $\underline{U}$, this usually requires the use of numerical integration. However, for the particular case of continuous injection at a constant state into an initially uniform reservoir, of interest here, the solution can be obtained by the more tractable method of "generalized simple waves". The elements of this method have been outlined in Refs. 5, 10. According to this approach, it suffices to study the characteristics in the (T,η,S_w) space, construct the corresponding paths, and follow the variation of the eigenvalues along the paths. The solution route joins the constant injection and initial states by path segments in order of increasing space velocity (eigenvalues λ_i).

The path topology in the (T,η,S_w) space is examined in Ref. 11. Due to the qualitative difference adsorption introduces in the path topology we will discuss two distinct cases separately.

1. No Adsorption

When adsorption is neglected, the solution route follows the path $ABCDO_1$ (secondary flooding) or $ABDCO_2$ (tertiary flooding) (Fig. 1a). Along AB (constant T,η) the solution is continuous. At B the route shifts over to BC along which η is constant. Path ABC is identical to the route followed in an ordinary, hot waterflood. Path CDO_1 (secondary flooding) is identical to the route followed in an ordinary, dilute, chemical flooding.

The above lead to the following simple graphical construction of the solution: Three fractional flow curves $f_w^{o,o}$, $f_w^{o,i}$, $f_w^{i,i}$ corresponding to conditions $(T_o,0)$, (T_o,η_i), (T_i,η_i), respectively, are drawn on the same diagram (Fig. 1b). From point (-b,-a) a tangent is drawn to $f_w^{i,i}$. The point of tangency determines B, and the intersection with $f_w^{o,i}$ determines C. Point D is determined from the intersection of the straight line OC, with the curve $f_w^{o,o}$.

A schematic description of the temperature, concentration, and saturation profiles obtained for secondary and tertiary flooding are shown in Figure 1c. Note that in both cases the chemical front travels ahead of the temperature front. Thus, in the case of negligible adsorption, the chemical resides ahead of the heated region, and it breaks through the production end ahead of the temperature wave. Three saturation fronts develop, one due to ordinary waterflood, another due to dilute chemical flood at the original reservoir temperature, and a third front due to the reduction of the mobility ratio at the injection temperature and concentration. Recovery curves for typical conditions are discussed in the next section.

2. Adsorption Included

When adsorption is included, two distinct cases are examined depending upon whether

$$\eta_i < \eta_{cr}(T_i) \tag{14a}$$

(Case I), or

$$\eta_i > \eta_{cr}(T_i) \tag{14b}$$

(Case II). An approximate estimate of η_{cr} is furnished by the solution of the following equation[11]

$$\frac{1}{g_1\eta_{cr} + g_2} \simeq \frac{b - a + aa_1}{1+a} + \frac{aa_2}{1+a}\exp(-\eta_{cr}/a_3) \tag{15}$$

For simplicity, in the analysis below we will not consider the effect of temperature on the adsorption kinetics.

Case I, $\eta_i < \eta_{cr}$.

If at the injection point inequality (14a) is satisfied, the solution route lies initially on the constant temperature plane (ABC), then switches over to a path on the zero concentration plane (CDO_1 or CDO_2) (Fig. 2a). Due to adsorption, λ_2 is decreasing along BC, thus leading to the formation of shock. The path BC is then replaced by the integral path B'C' obtained from the Rankine-Hugoniot shock conditions.[11] Paths $C'DO_1$ (or $C'DO_2$) are determined as before.

The above lead to the following simple graphical construction of the solution: Three fractional flow curves $f_w^{o,o}$, $f_w^{i,o}$, $f_w^{i,i}$, corresponding to conditions $(T_o,0)$, $(T_i,0)$, (T_i,η_i), respectively, are drawn on the same diagram (Figure 2b). From the point $(-\frac{g_i}{\eta_i}, 0)$ a tangent is drawn to $f_w^{i,i}$. The point of tangency determines B', and the intersection with $f_w^{i,o}$ determines C'. Point D is determined from the intersection of the straight line connecting points (-b,-a) and C' with $f_w^{o,o}$. Paths DO_1 (or DO_2) are determined in a straightforward manner as discussed before.

A schematic description of the temperature, concentration, and saturation profiles obtained for secondary and tertiary flooding are shown in Figure 2c. Note that in contrast to the case of no adsorption, the chemical front travels behind the temperature front, while the temperature wave travels faster than in the previous case. In the present case, the chemical resides entirely in the heated region, and it breaks through the production end behind the temperature wave. This is clearly due to the magnitude of the rate of adsorption at the level of the injected concentration. Despite the fact that the chemical is present at a sufficient concentration to lower the residual oil saturation significantly, and the magnitude of adsorption is not at its maximum level, the rate by which the chemical is adsorbed on the rock is considerably high to retard the propagation of the chemical front. Three saturation fronts develop, one due to ordinary waterflood, another due to ordinary hot waterflood, and a third due to chemical flood at the injection temperature. Recovery curves for typical conditions are discussed in the next section.

Case II, $\eta_i > \eta_{cr}$.

If at the injection point inequality (14b) is satisfied, the solution route lies initially on the constant concentration plane (ABC), then switches over to a path on the original temperature plane (CDO_1 or CDO_2) (Fig. 3a). Along BC, λ_1 is constant, while along CD λ_2 is decreasing, thus leading to the formation of shock. The path CD is then replaced by the integral path CD' obtained from the shock conditions.[11] The remaining portion $D'O_1$ (of $D'O_2$) follows in a straightforward manner.

The above lead to the following simple graphical construction of the solution: Three fractional flow curves $f_w^{o,o}$, $f_w^{o,i}$, $f_w^{i,i}$, corresponding to conditions $(T_o,0)$, (T_o,η_i), (T_i,η_i), respectively, are drawn on the same diagram (Figure 3b). From the point (-b,-a) a tangent is drawn to $f_w^{i,i}$.

The point of tangency determines B, and the intersection with $f_w^{o,i}$ determines C. Point D' is determined from the intersection of the line connecting points $(-\frac{g_i}{\eta_i}, 0)$ and C with $f_w^{o,o}$. Paths $D'O_1$ (or $D'O_2$) are determined in a straightforward manner as discussed before.

A schematic description of the temperature, concentration, and saturation profiles obtained for secondary and tertiary flooding are shown in Figure 3c. Note that the chemical front travels ahead of the temperature front, although at a velocity lower than in case of negligible adsorption, while the temperature wave travels at the same velocity to the case of negligible adsorption. The chemical resides ahead of the heated region, and it breaks through the production end ahead of the temperature wave. Thus, although the magnitude of adsorption is considerably higher than in Case I, the rate of adsorption is not high enough to retard the chemical front behind the temperature wave. Recovery curves for typical conditions are discussed in the next section.

NUMERICAL EXAMPLES AND DISCUSSION

The mathematical model was subsequently used to simulate the recovery performance of a reservoir subjected to combined chemical-hot water injection at typical reservoir conditions. The reservoir was assumed to have an initial oil saturation $S_o = 0.80$ for the case of secondary flooding, a saturation $S_o = 0.40$ for the case of tertiary flooding, and an initial temperature $T_o = 100°F$. The injection temperature was set equal to $T_i = 200°F$. The corresponding value of the critical concentration $\eta_{cr}(T_i)$ was calculated to 6.9×10^{-3} (volume of chemical/volume injected). Thus, the injection concentration η_i was taken to be equal to 6.0×10^{-3} for Case I, and equal to 6.9×10^{-3} for Case II, respectively. Notice that in both cases the residual oil saturation at injection conditions is reduced to its asymptotic value which is approximately equal to 0.95. Table I lists the values of the reservoir and injection parameters used in the simulations.

The obtained recovery curves are shown in Figures 4, 5, 6. In Figure 4 we plot the cumulative recovery as a fraction of the OOIP for the combined chemical and hot water injection with negligible adsorption (denoted by CHO) for a secondary recovery process. Plotted also are the corresponding curves for the case of an isothermal chemical flood at 100°F and 200°F, (denoted by IC_o, IC_i, respectively) as well as the unassisted hot waterflood. A substantially higher recovery efficiency is shown to result in the combined injection as compared to either pure hot waterflood or pure chemical flood at the original temperature. At 2PV of injection the increase in the recovery is higher by about 25% of the OOIP to the recoveries obtained in the unassisted cases. Beyond the time of temperature breakthrough ($\sim$2PV), the combined injection is essentially an isothermal chemical flood at 200°F, thus the recovery curve rapidly approaches the maximum recovery efficiency.

The effect of adsorption in the combined injection process is illustrated in Figure 5. As expected, the chemical breaks through the production end at a considerably shorter time in CHO than in the case of adsorption for both Case I (CH1) and Case II (CH2). The temperature breakthrough time is approximately the same for all three cases. Before this time the recovery efficiency is highest for the case of no adsorption (CHO) and lowest for Case I (CH1),

as expected. After the temperature breakthrough, however, the recovery for CH1 is noticeably higher than the recovery for both CH0 and CH2. This result is clearly attributed to the fact that in Case I the chemical resides entirely in the heated region of the reservoir, in contrast to both other cases. The driving mechanism is more efficient due to the synergestic effect of relative permeability and viscosity reduction alteration, thus the recovery curve overtakes the two other recovery curves. All three curves approach asympototically the same limit. This effect is expected to be more pronounced as the viscosity ratio reduction becomes higher (e.g., as the injection temperature is higher or the original oil is more viscous), and to be less pronounced as the viscosity ratio reduction becomes smaller.

The results for tertiary flooding are plotted in Figure 6. Similarly to the secondary flooding the resulting recovery in the combined injection process is higher than the recoveries obtained in the unassisted cases. Beyond the time of temperature breakthrough ($\sim$2PV) the combined injection process becomes essentially an isothermal chemical flood at 200°F, and the recovery curves rapidly display such a behavior with the notable exception of CH1. In this case ($\eta<\eta_{cr}$) it is observed that the recovery curve overtakes not only the recovery curves for CH0 and CH2 but also the recovery curve for the isothermal chemical flood IC$_1$. This result is to be attributed to the retardation of the chemical front beyond the temperature front experienced in Case I. The oil bank resulting from the combined displacement mechanism has size and propagation characteristics such that the obtained recovery efficiency is higher than in any of the other cases. This effect is expected to be strongly dependent on the viscosity ratio reduction, thus on the level of the injection temperature and the original viscosity. The sensitivity of the recovery performance to these operational parameters is currently under investigation.

CONCLUSIONS

In this study a simplified mathematical model that describes the combined injection of chemical additive and hot water into a reservoir has been developed. In order to obtain a tractable solution the assumptions of negligible dispersion, heat conduction, and lateral heat losses have been made. The first two assumptions can be justified at large flow rates where sharp fronts are expected to develop. By contrast, neglecting lateral heat losses is not as easily justifiable and it would certainly lead to optimistic oil recovery rates, for a combined injection process. Nevertheless, the results obtained here provide considerable insight into the important aspects of more complex chemical assisted thermal processes, such as steam injection.

The preliminary results obtained from the mathematical model indicate that, at least for the continuous injection, adsorption plays a decisive role in determining the rate of propagation of the chemical relative to the temperature wave. In the absence of adsorption, or in cases where adsorption in included but the injected concentration lies above the critical value η_{cr}, the chemical travels ahead of the temperature, thus a significant portion of the injected chemical resides in the unheated region of the reservoir. By contrast, when adsorption is included and the injected concentration is below η_{cr}, the chemical resides entirely in the heated region of the reservoir, resulting into a more efficient displacement mechanism. This effect is expected to be more pronounced under conditions of higher injection temperature

and more viscous oil. It is also expected that similar results would be obtained in the case of chemical slug injection. The recovery efficiency of slug injection processes is currently under investigation.

An analysis of the recovery efficiency in a typical heavy oil reservoir indicates that the combined injection is a viable enhanced recovery process. The preliminary results suggest that the recovery efficiency is maximized if the process is used in a reservoir already subjected to secondary recovery, and if the injection concentration lies below the critical value. A more extensive study of the sensitivity of the process parameters is presently undertaken.

REFERENCES

1. Prats, M.: "A Current Appraisal of Thermal Recovery," paper SPE 7044, presented at the 5th Symposium on Improved Methods for Oil Recovery, April 16-19, 1978, Tulsa, Oklahoma.

2. Gopalakrishnan, P., Bories, S.A., and Combarnous, M.: "An Enhanced Oil Recovery Method -- Injection of Steam with Surfactant Solution," report of Group d'Etude IFP-IMF sur les Millieux Poreux, Toulouse, France (1977).

3. Larson, R.G., Davis, H.T., and Scriven, L.E.: "Elementary Mechanisms of Oil Recovery by Chemical Methods," paper SPE 8840, presented at the First Joint SPE/DOE Symposium on Enhanced Oil Recovery at Tulsa, OK (April 20-23, 1980).

4. Ziegler, V.M., and Handy, L.L.: "Effect of Temperature on Surfactant Adsorption in Porous Media," Soc. Pet. Eng. J. (April 1981) 218-228.

5. Jeffrey, A.: Quasilinear Hyperbolic Systems and Waves, Pitman Publishing Limited, London (1976).

6. Helfferich, F.: "Theory of Multicomponent, Multiphase Displacement in Porous Media," Soc. Pet. Eng. J. (Feb. 1981) 51-62.

7. Adamson, A.W.: Physical Chemistry of Surfaces, 3rd Ed., Wiley Interscience Publications, New York (1976).

8. Larson, R.G., and Hirasaki, G.J.: "Analysis of the Physical Mechanisms in Surfactant Flooding," Soc. Pet. Eng. J. (Feb. 1978) 42-58.

9. Dezabala, E.F., Vislocky, J.M., Rubin, E., and Radke, C.J.: "Theory of Linear Alkaline Flooding," paper SPE 8997, presented at the SPE Fifth International Symposium on Oilfield and Geothermal Chemistry, Stanford, California (May 28-30, 1980).

10. Aris, R., and Amundson, N.R.: Mathematical Methods in Chemical Engineering, Prentice-Hall, Inc., Englewood Cliffs, NJ (1973).

11. Karakas, M., and Yortsos, Y.C., in preparation.

TABLE I

Parameter $a_1 = 0.05$

Parameter $a_2 = 0.35$

Parameter $a_3 = 1.77 \times 10^{-4}$

Heat Capacity of Oil = $Cp_o = 0.5$ Btu/lb°F

Heat Capacity of Rock = $Cp_R = 0.2$ Btu/lb°F

Heat Capacity of Water = $Cp_w = 1.0$ Btu/lb°F

Parameter $g_1 = 100$

Parameter $g_2 = 0.01$

Parameter $k_{ro}^{o} = 1.0$

Parameter $k_{rw}^{o} = 0.1$

Parameters, $n = p = 1.5$

Original Temperature = $T_o = 100°F$

Injection Temperature = $T_i = 200°F$

Residual Water Saturation = $Sw_r = 0.20$

Viscosity of Water at Original Temperature = $\mu_w = 0.65$ cp

Viscosity of Oil at Original Temperature = $\mu_o = 680$ cp

Viscosity of Water at Injection Temperature = $\mu_w = 0.30$ cp

Viscosity of Oil at Injection Temperature = $\mu_o = 50$ cp

Density of Oil = $\rho_o = 50$ lb/cu ft

Density of Rock = $\rho_R = 167$ lb/cu ft

Density of Water = $\rho_w = 62.4$ lb/cu ft

Porosity = $\phi = 0.30$

NO ADSORPTION SOLUTION

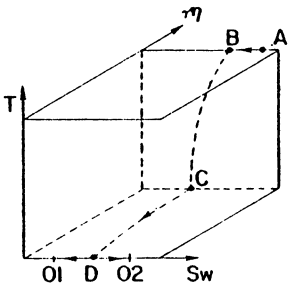

FIGURE 1A

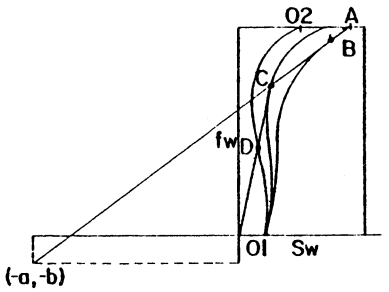

FIGURE 1B

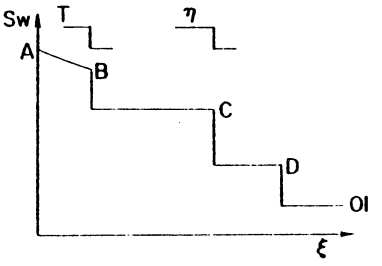

FIGURE 1C

CASE I

$\eta_i < \eta_{CR}$

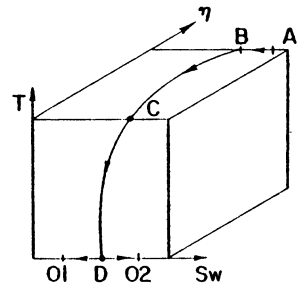

FIGURE 2A

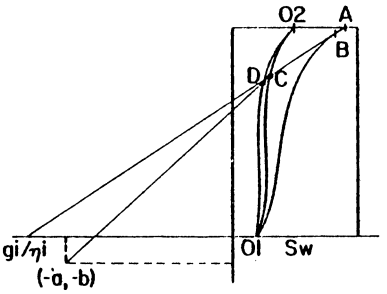

FIGURE 2B

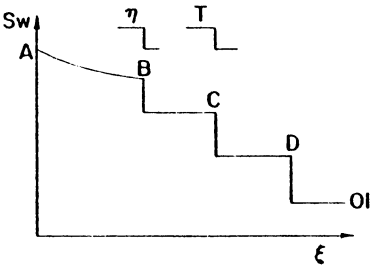

FIGURE 2C

CASE II

$\eta_i > \eta_{CR}$

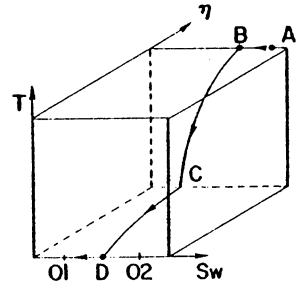

FIGURE 3A

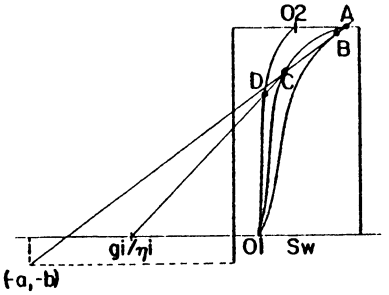

FIGURE 3B

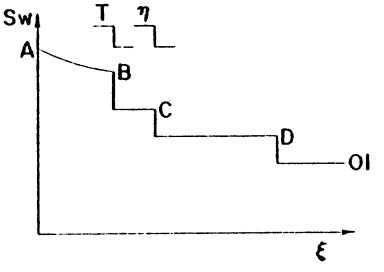

FIGURE 3C

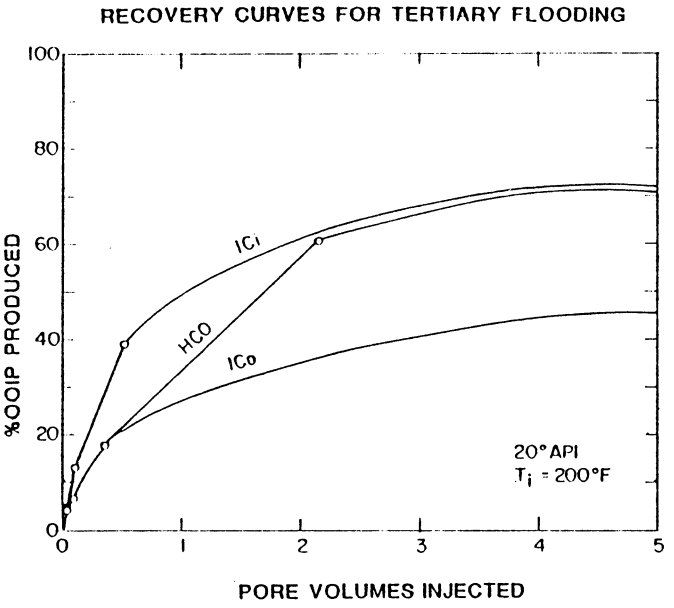

FIGURE 4

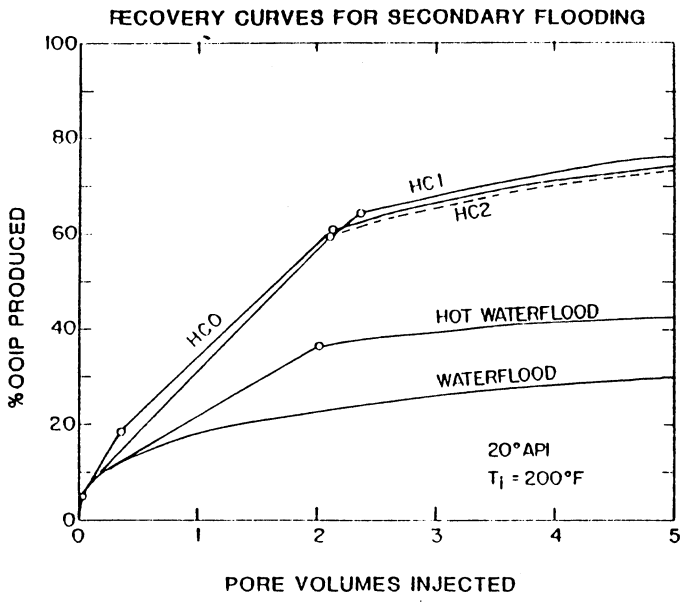

FIGURE 5

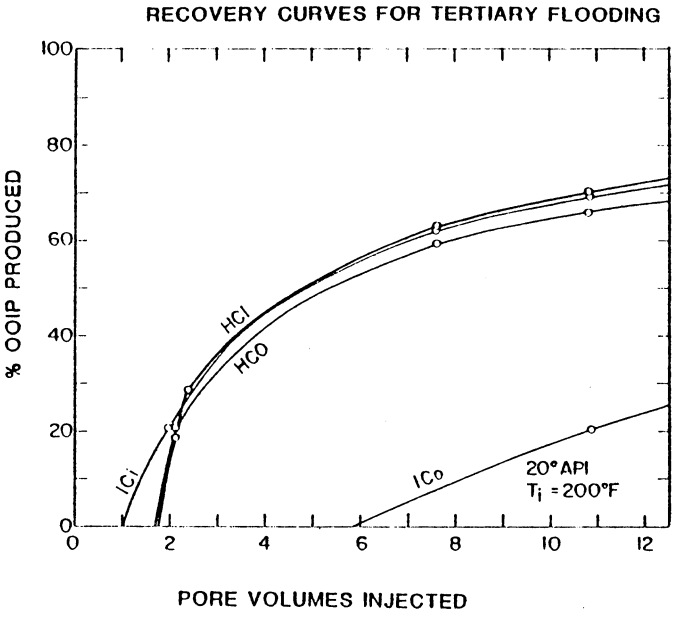

FIGURE 6

TEMPERATURE EFFECTS ON LOW TENSION SURFACTANT FLOODING EFFICIENCY IN CONSOLIDATED SANDS

by

M. O. Amabeoku and L. L. Handy
Department of Petroleum Engineering
University of Southern California
Los Angeles, California 90007

ABSTRACT

A heavy oil recovery process that has attracted considerable attention and is widely practiced is the injection of saturated steam into an oil reservoir. In the steam injection model a significant amount of the injected heat is lost to the overburden stratum. This is because steam overrides the top of the formation in a thin layer. Below this zone is a region of condensed water in which a hot water drive occurs.

The concurrent injection of surfactant with steam has been proposed to improve the oil recovery efficiency of the steamflood process. This mode of injection will give rise to a low tension process supplemental to the steam drive which, because of its nature, affects that portion of the reservoir where the condensed water is flowing.

In low tension flooding the surfactant reduces the interfacial tension between the aqueous surfactant phase and the oil phase and alters the capillary number significantly. This substantially releases residual oil in porous media. In surfactant flooding many parameters, namely, relative permeabilities, viscosities, interfacial tensions, dispersion, adsorption and, in this case, temperature, are coupled. An attempt has been made to decouple these parameters and identify the operative mechanisms.

To accomplish this objective several flooding experiments have been performed with Berea sandstones. The surfactants used were Witco TRS 10-80 and Stepan Petrostep 465, both of which are anionic. Flood temperatures were 25°C, 82.2°C and 177°C. Core floods included sequences wherein a core was flooded to residual oil saturation with hot water followed by surfactant to further displace oil that would otherwise not be recoverable without the lowering of the interfacial tension between the residual oil and injection fluid. Also reported are floods in which the surfactant solution was used as the primary injection fluid so as to compare this mode of injection with other sequences.

Water-oil relative permeability ratios were calculated at the flood temperatures. No definite temperature correlation was established, but it was observed that relative permeability to oil increased with increasing temperature while relative permeability to water was almost insensitive to changes in temperature.

HISTORY OF PROJECT

This report is part of a project "Chemical Additives with Steam Injection to Increase Oil Recovery." It was initiated September 15, 1976 with anticipated completion of October 15, 1981. The government award was $108,370.

Prepared for the Department of Energy under Contract No. DE AS03 76SF00113

INTRODUCTION

Of the three common thermal processes to recover oil after waterflood or primary depletion -- steam injection, hot water injection, and in-situ combustion; steam injection has proven to be the most attractive.

Laboratory studies[1] and field pilot tests[2,3] have indicated there is a marked improvement in oil recovery by steam injection compared with recovery by water injection in the same system. Residual oil saturations in the steam-flooded zone can be 8% or less, but below the steam zone saturations can be as high as 35%. The remarkable success of the steamflood process is attributed to the reduction in the viscosities and the swelling of the heavy oils with increasing temperature. Additionally, steam distillation, related gas drive and solvent extraction contribute to the recovery mechanism.

An inherent problem is heat losses during steam injection from the point of exit at the steam generation system through the piping and on to the sand face. At the point of injection steam quality has been drastically reduced. Gravity override of the steam higher up in the formation occurs because of the density difference between the steam and the resident fluids in the formation. A schematic diagram of a developed steamflood profile is shown in Figure 1. Gravity override in steamflood, as measured by vertical sweep efficiency,[4] depends mostly on mass injection rate and the steam zone volume is a function of the formation thickness.

In porous media whose void space is filled with a moving fluid, the three basic modes of heat transfer may manifest themselves in any of the following ways:[5]

1. Heat transfer through the solid phase by conduction.
2. Heat transfer through the liquid phase by conduction.
3. Heat transfer through the liquid phase by convection.
4. Heat transfer through the liquid phase by dispersion (i.e., by heat dispersion) due to the presence of grains and an interconnected pore system.
5. Heat transfer from the solid phase to the liquid phase.

In the region of the reservoir not swept by steam, the drive mechanism is a combination of hot waterflood and a cold waterflood. Oil in this region is trapped in a ganglia-type distribution and prevented from being recovered by capillary forces. Very high pressure gradients would be required to mobilize this oil. To circumvent this problem Atkinson[6] proposed the injection of aqueous surfactant solutions to decrease the interfacial tension between the oil and water phases. This decrease in interfacial tension will result in a reduction in pressure drop across the oil-water interface and, consequently, improve waterflood performance. Brown et al.[7] and Gopalakrishnan et al.[8] have proposed the concurrent injection of surfactant with steam to improve on the recovery efficiency of steam drive. From the relative rates of the hot water front and surfactant front Ziegler[9] confirmed results of earlier work,[10] involving chemical additives in steamflood, that the injected surfactant will travel through that portion of the reservoir being flooded by hot water. Technical feasibility of surfactant injection with steam can be established

if the surfactant can satisfy certain criteria. These criteria should help to determine what surfactants are best suited for this purpose. The screening process should include:

1. Surfactant stability under steamflood conditions. The surfactant is expected to move in the hot water zone at steam temperature over the life of the flood.
2. Temperature effects on the interfacial tension between oil and the injected aqueous phase. This is particularly important because lowering IFT is the basic premise of low tension flooding at normal pressure gradients to mobilize trapped oil.
3. The effect of temperature on surfactant adsorption in porous media. The interaction between the solid surface of the porous matrix and the liquid may take several forms: adsorption of surfactant onto the solid surface, partitioning of the surfactant into the oil phase, deposition, solution, ion exchange, etc. All these phenomena cause changes in the injected fluid's density and viscosity, and these, in turn, affect the flow regime, i.e., velocity distribution that depends on these properties.
4. Effect of temperature on surfactant flood performance.

Thermal stabilities of some ionic and nonionic surfactants have been reported by Handy et al.[11] Hill et al.[12] and Handy et al.[13] have shown that interfacial tension between oil and aqueous surfactant is decreased at elevated temperatures. The degree to which this phenomenon is observed depends on many factors. These include surfactant concentration, the constitution of the oil, and the temperature level. Murtada et al.[14] and Ziegler et al.[15] have reported work on surfactant adsorption at elevated temperatures. If a surfactant is obtained which is stable under steamflood conditions and also reduces interfacial tension between the oil phase and the aqueous phase, a beneficial effect will be obtained by injecting surfactant with steam. However, adsorption and other loss mechanisms and the degree to which these inhibit the effectiveness of surfactant as a recovery agent have to be identified. The minimum amount of surfactant to inject into the reservoir to satisfy the losses and still recover economically additional oil that would otherwise not be recoverable needs to be determined.

At the time of this study information has not been published on surfactant adsorption in porous media at elevated temperature in the presence of an oleic phase. All studies to date have excluded oil in the core sample. Low tension floods at temperatures ranging from room temperature through steam temperature have been conducted on cores that have been extensively waterflooded and also on oil-saturated cores prior to waterflooding.

EXPERIMENTAL SETUP AND PROCEDURE

A. MATERIALS

1. Oils

The oil used was a Sonneborn white oil marketed under the brand name of Kaydol. It is a homogeneous mixture of completely saturated aliphatic and

alicyclic hydrocarbons and is entirely free of aromatics. It is chemically and biologically inert and also nonpolar. At 25°C this oil has a viscosity of 22×10^{-3} Pa.s. During the experimental program higher viscosity oils were required. White oils in such a viscosity range could not be obtained. In order to avoid the problem of interpreting experimental data obtained with different oil compositions and to enhance the delineation of operative parameters during a flood sequence, a procedure was developed to boost the viscosity of the white oil while still maintaining its basic characteristics. This was achieved by mixing the mineral oil with Chevron Polybutenes. Chevron Polybutenes are manufactured by Chevron Chemical Company. They are pale colored, chemically inert oils of moderate to high viscosity and tackiness. They are permanently fluid, nondrying and resistant to chemical attack, oxidation and photodegradation. Polybutenes are soluble in petroleum solvents, chlorinated hydrocarbons and some esters but essentially insoluble in oxygenated solvents. They are compatible with a wide variety of organic materials, most synthetic hydrocarbon polymers and natural products. The Polybutene used was No. 128. Its average molar mass is 3000. It has a flash point of 238°C, a pour point of 27°C and viscosity of about 3600×10^{-3} Pa.s at 99°C. Mixed with mineral oil No. 9, viscosities in the range of 22×10^{-3} Pa.s to 3000×10^{-3} Pa.s can be obtained, depending on the mixing ratio.

2. Porous Media

The porous medium used in all the experiments was consolidated Berea sandstone. The core samples were cut to size without any cutting fluid with the aid of reinforced silicon carbide masonry cutoff blades to within 3.2 mm tolerance and polished with motor driven sandpaper. To negate the deleterious effect of clays upon saturation with water due to particulate plugging the samples were fired in a furnace for 24 hours at 500°C.

3. Surfactants

Two surfactants were used in this study. Both are anionic surfactants. The first of these commercially available petroleum sulfonates is Petronate TRS 10-80 from Witco Chemical Corporation. In its crude form TRS 10-80 has unsulfonated oil, water, sodium sulfate and a reasonable amount of active sulfonate with an average relative molecular mass of 415. It was purified to 100% active component by liquid chromatography. It is a mixture of sodium alkylbenzene sulfonates. It has a critical micelle concentration (CMC) of 48 μmol/L in distilled water at 25°C.

The second surfactant is Petrostep 465 manufactured by Stepan Chemical Corporation. According to Stepan, Petrostep 465 has 59.4% active component, 14.7% unsulfonated oil, 22.7% associated water and 3.2% of salts. The average molar mass is 465. This surfactant was purified for use by liquid chromatography, also. In distilled water is has a CMC of 160 μmol/L.

Interfacial tensions between the aqueous surfactant solutions and oils were measured at three temperatures with the spinning drop method. Portions of the surfactant solutions were mixed with the oils and allowed to equilibrate over a period of 24 hours. This allowed for partitioning of the surfactant between the aqueous and oil phases. This also reduced the spinning time required to attain equilibrium in the measurement of IFT. El-Gassier[16] has documented the procedures for measuring interfacial tensions at elevated

temperatures. Interfacial tension values via the spinning drop method were calculated using either the Vonnegut[17] equation (approximate solution) or the exact solution as dictated by the experimental conditions.

$$\sigma = \Delta\rho\omega^2 y^3/4 \qquad \text{(approximate solution)}$$

$$\sigma = \Delta\rho\omega^2/4.0c \qquad \text{(exact solution)}$$

where

σ = interfacial tension

$\Delta\rho$ = density difference $(\rho_w - \rho_o)$, g/cc

ω = rotational speed, rad/sec.

y = one-half the minor axis of the drop, cm

c = f(drop shape).

Results generated with all three oils and Petrostep 465 are displayed in Figure 2.

B. FLOW EXPERIMENT

1. Equipment

A schematic diagram of the flood equipment is shown in Figure 3.

2. Core Mounting

Teflon heat-shrinkable roll cover served as the protective sleeve for the sandstone core. The nominal diameter of the Teflon sleeve was 5.08 cm. It had a maximum diameter of 5.33 cm and a minimum of 4.32 cm, which it attained upon shrinking due to the application of heat. The sleeve was etched with Tetra Etch, a fluorocarbon etching solution by brushing the solution on to dry and clean sleeve surface. After a noticeable color change of the surface which occurred in a few minutes, the surface was washed in an organic solvent such as methanol or acetone and then in water to remove all residue. The sleeve was rolled over the sandstone core. A high temperature, high strength, General Electric RTV 159 sealant was thinly applied to the overlapping ends of the sleeve and end plugs to provide the bond required between the sleeve and the plugs. The end plugs had machined grooves for even distribution of fluids. A heat gun with power in excess of 1000 watts was used to blow hot air around the sleeve in order to shrink it onto the core and end plugs while they were tightly clamped together.

3. Experimental Procedure

Prior to connecting the core holder to the flow network, the porosity was determined by gas expansion. This method is based on Boyle's Law, which states that under isothermal conditions the product of the volume of a gas and its associated pressure is constant. After the porosity and pore volume of the core had been obtained, carbon dioxide was flowed through the core to displace air. The core was then evacuated and saturated with brine solution.

Against a back pressure of 1034 kPa several pore volumes of brine were injected to ensure complete saturation. The brine solution injected had the same sodium chloride concentration (10.0 g/L) as that in the surfactant solution. And besides being the resident brine in the core it removed any multivalent cations by the process of cation exchange to condition the core. Permeability measurements were conducted during this stage of flow. Several pore volumes of oil were pumped through the core to displace the brine. The amount of brine displaced was measured. Thus the initial oil saturation and the connate water saturation were determined. The core was then reconnected to the flooding equipment and allowed to equilibrate at the test temperature. Floods were conducted at three temperatures; 25°C, 82°C and 177°C.

Two flooding schemes were used:

a. Waterflood followed by surfactant flood.

b. Surfactant flood with no prior waterflood.

In the first scheme brine having the same concentration as the connate water was injected to displace oil as in a conventional waterflood. This was continued until no oil was produced upon continued brine injection. The oil was collected in graduated cylinders. Surfactant solution, having a concentration of 2.5 g/L in brine solution of concentration 10 g/L, was injected to displace oil left in the core after waterflood.

The second sequence was one that entailed the injection of surfactant from the beginning of the flood without first waterflooding the core to residual oil saturation.

The above schemes were conducted at three different temperatures with four oils having different viscosities. Back pressures in excess of the saturation pressures of the fluids were maintained on the core to essentially simulate the hot water region of the reservoir profile during a steamflood. In this work the minimum back pressure maintained was 1380 kPa. Changes in pressure during the runs were recorded on the chart recorder.

Cores were prepared for reruns by flushing with toluene to remove the oil; with isopropyl alcohol to remove the water, toluene and surfactant; and, finally, with fresh water. They were then resaturated with brine and oil to reestablish saturations for the next runs. On many occasions fresh cores were used.

In order to estimate adsorption of surfactant in the presence of oil a fresh core was saturated with brine and oil. The oil was displaced by brine to the residual oil saturation. Surfactant was injected and the effluent surfactant concentrations were monitored continuously from time of injection to the end of the flood sequence. The UV spectrophotometer was used to study the absorbance of the produced surfactant. Its concentration was determined from a calibration curve that was prepared using several concentrations of stock surfactant solutions.

EXPERIMENTAL RESULTS AND DISCUSSION

The ultimate objective of this research was to study the possible benefits in additional oil recovery of the synergism between high temperature

and low tension. Injection of steam into an oil reservoir reduces the viscosity of the oil and makes it mobile. Introduction of surfactant into an oil reservoir reduces the interfacial tension between the oil and the aqueous injected phase. This results in the release of discontinuous oil following a waterflood. The two effects, working simultaneously, contribute to improve the recovery of the residual oil. This objective has been accomplished.

Results are presented in this chapter that confirm the existence of such a synergistic effect. Two surfactants were used, TRS 10-80 and Petrostep 465. However, only the effectiveness of Petrostep 465 was studied extensively. The reason for this, among other considerations, was its stability at elevated temperatures. No sacrificial agents were used to adsorb preferentially onto the Berea sandstone in order to preserve the integrity of the injected surfactant slug. Although it was not requisite to conduct adsorption studies, a run was made with the sole intent of understanding adsorption of chemical species onto reservoir rock in the presence of oil. It was also hoped that this attempt would emphasize the need for more detailed studies which include the effects of adsorption at the water-oil interface.

Floods were performed with four oil formulations with viscosities ranging from 22×10^{-3} Pa.s to 2100×10^{-3} Pa.s.

The first of these oils had a viscosity of 504×10^{-3} Pa.s at 25°C. The core was waterflooded to residual oil saturation. A surfactant solution of 2.50 g/L Petrostep 465 and 10.0 g/L NaCl concentration was injected to displace the residual oil in the core. The viscosity of the oil was 36×10^{-3} Pa.s at 82.2°C and at 177°C it was 2.15×10^{-3} Pa.s. The flood performance at each of these temperatures is shown in Figure 4. Total oil recovery at 82.2°C was 75.6% of original oil-in-place. Waterflood recovery was 66% and additional recovery due to the surfactant was 9.6%. This represents 14.5% over waterflood performance. At 177°C total oil recovery was 89.8%. Recovery over waterflood at this temperature was 33.3%.

Water-oil ratio plots at the two temperatures are given in Figure 5. With increasing temperature the water-oil ratio (WOR) plots shift rightward. After breakthrough the WOR tended to infinity. When surfactant was injected oil production resumed and the water-oil ratio decreased sharply. As oil production continued WOR gradually increased and at the second plateau in the recovery plots, it tended to infinity again.

Welge type calculations were made to obtain the water-oil relative permeability ratios (k_w/k_o) for each flood. This is shown in Figure 6. Data from the waterflood prior to surfactant injection were used to calculate the relative permeability ratios. With increasing temperature the relative permeability ratio shifts toward increasing water saturation. A rise in temperature at any value of water saturation led to an increase in the relative permeability to oil; but there was no clear effect of temperature change on the relative permeability for water. The effect of temperature on waterflood performance was greater than that due solely to the reduction of the viscosity ratio. However, no definite correlation between temperature and relative permeability ratios has been established. With an increase in temperature, the mobility of the oil increases and the interfacial tension between the oil and water decreases. Due to wettability alteration, probably to a condition that favored oil recovery, an increase in oil recovery was observed. All these may have

resulted in the decrease in the relative permeability ratio between oil and water. Fraction of water in the produced stream (f_w) for each temperature is plotted in Figure 7.

The next flood was performed with an oil of viscosity 2100×10^{-3} Pa.s at 25°C. This is shown in Figure 8. Because of the high viscosity of this oil at lower temperatures flood was performed only at 177°C. Waterflood recovery with this oil was 73.4%. Additional oil recovery due to surfactant injection was 12.7%. This represents a 17.3% recovery over waterflood. The oil viscosity at 177°C was 4.3×10^{-3} Pa.s. The corresponding WOR, k_w/k_o and f_w plots for this oil are given in Figures 9, 10 and 11, respectively.

Comparison between waterflood and surfactant flood

A core saturated with 74×10^{-3} Pa.s oil was waterflooded at 26.7°C. The same core was resaturated with the same oil and flooded with surfactant. The results are shown in Figure 12. The purpose of this was to compare only flood performance while eliminating any interference of other parameters. Recovery with surfactant was 70.9% whereas the oil recovery during waterflood was 66.7% of original oil-in-place. Recovery over waterflood was significant, and would have been better if adsorption of surfactant had been minimized by the use of sacrificial agents. A second run with this core was conducted at 82.2°C. At this temperature the surfactant-oil interfacial tension was 0.35 mN/m, and recovery was 78.4%. These flood results prove the benefits obtained from the synergism between interfacial tension reduction and viscosity reduction. When the core was waterflooded, about 0.37 pore volume of oil was recovered. During surfactant flooding oil recovery was 0.47 pore volume. This represents an increase of 0.1 pore volume attributed to interfacial tension reduction. Oil recovery with surfactant flooding at 82.2°C was about 0.52 pore volume. This incremental recovery was due to reduction of the oil viscosity at the higher temperature. The combined effect is manifested by the oil recovery of 0.15 pore volume over waterflood performance. The water oil ratio plots are given in Figure 13.

Surfactant loss by adsorption/retention and partitioning

A probable reason for obtaining less oil recovery with an initial surfactant flooding without a prior waterflooding than would be predicted from the reduction in interfacial tension was because of loss of surfactant. This loss occurred through adsorption of the surfactant onto the sand surface. Even at higher temperatures, recoveries were not as high as would be predicted. Temperature affects not only adsorption but also the solubility of the adsorbate. Generally, adsorption from solution decreases with increasing temperature. If the solubility of the adsorbate increases with temperature, adsorption decreases. But if solubility decreases with increasing temperature, depending on whether solubility effect or temperature effect is more dominant, adsorption may increase or decrease. The temperature effect is also referred to as the exothermicity effect. The solubility component of adsorption would have been dominant over the exothermicity effect and so adsorption was still increasing with temperature increase. When the cores were cleaned out with toluene, alcohol and fresh water, and resaturated for second runs, recoveries improved substantially. This was observed for all reconstituted cores. The obvious inference is that surfactant was retained in the cores and it did not take much surfactant to satisfy adsorption the next time around. This is

illustrated in Figure 14. Another explanation is that the wettability of the core may have been altered as a result of surfactant retention. If this change in wettability was to a favorable condition that allowed a continuous distribution of oil, recovery would improve. The second flood on the same system did better than when the core was used the first time. It should be mentioned here that the very high recoveries presented earlier, at the higher temperatures, were obtained with cores that had been exposed to surfactant in preceding floods.

To investigate more thoroughly the above postulates a fresh core was saturated with oil. It was waterflooded to residual oil saturation and then flooded with surfactant. The surfactant concentrations in the effluent fractions were monitored and compared to injection surfactant concentration. A striking phenomenon was observed. With increasing surfactant injection the concentration of surfactant in the effluent aqueous phase increased for a while and then flattened out. This plateau in concentration was observed in the region where more of the oil was being produced. Oil production peaked in the region where the concentration ratio remained constant. This is illustrated by the plot of the fraction of oil in the effluent stream. The concentration ratio started rising again after oil production ceased. This is represented in Figure 15. A plausible explanation is that we were losing surfactant not only by adsorption but also through partitioning of the surfactant into the oil phase. All adsorption studies have excluded oil in the system consciously to idealize the situation. Partitioning, although recognized to be a factor in surfactant flooding, has often been neglected in discussion of low tension recovery work and neglected in numerical simulation and other model studies. It was beyond the scope of this work to carry out elaborate study of adsorption. But because it was deemed necessary to identify the causes of problems in interpreting our surfactant flood performance, this digression was made. However, this should be considered a preliminary study. Much work still has to be done to determine when the oil and surfactant are produced. Material balance calculations would be required to account for surfactant loss to both adsorption and partitioning.

The Capillary Number (Nc) Correlation

Capillary numbers were calculated for the fluid systems. These were related to both the microscopic displacement efficiency, Em, defined by Melrose and Bradner[18] and the normalized residual oil saturation, Sorc/Sor, defined by Stegemeier.[19] Another attempt was made to calculate the capillary number group, F, defined by Abrams.[20] In this grouping Abrams includes corrections for the effect of viscosity ratio in flood performance. The plot presented here was calculated by the method of Melrose and Bradner. It is given in Figure 16. With increasing Nc the displacement efficiency increased. This is well in agreement with observations of other authors. If the capillary number is high enough, it is theorized, the microscopic displacement efficiency will tend to 100 percent. Foster[21] contends that Berea sandstone has a residual oil saturation of zero at a capillary number of about 7×10^{-2}. This is a reasonable range as can be seen in the Em plot. The scatter in the experimental data is not unusual. Foster represented the range of the data by a band. The scatter in data is even worse when consolidated Berea sandstone is used. The reasoning is that in consolidated sands there is a wide pore size distribution. This variation in pore shape and other parameters associated with pore geometry influence the trend and scatter of the data. Instabilities in the flow, in

terms of viscosity, precipitation and redissolution of chemical species are likely to contribute to the data scatter.

CONCLUSIONS

The effect of temperature on surfactant flooding in consolidated Berea sandstone has been evaluated. From the observations the following conclusions have been arrived at:

A. Both Petrostep 465 and TRS 10-80 gave additional oil recoveries beyond those obtained by waterflooding at all temperatures. Total recoveries of the original oil-in-place varied between 44 percent at 25°C and 93 percent at 177°C for Wtico TRS 10-80 and between 55 percent and 98 percent for Petrostep 465 over the same temperature range.

B. The effect of temperature on waterflood recoveries is greater than would be predicted from the effect of temperature on the water-oil viscosity ratios only.

C. The synergism between interfacial tension reduction by surfactant and oil viscosity reduction at elevated temperature has been established. Oil recoveries are improved significantly by this effect.

D. The oil viscosities in these experiments are substantially lower than would be expected in steamfloods. However, the observed trend is expected to hold in heavier oils.

E. Significantly higher oil recoveries were observed with cores that had previously been flooded with surfactants although the cleaning procedure between floods should have removed all the surfactant. Since the oil recoveries were up to 98 percent of the original oil-in-place, it is of considerable interest to determine what mechanism is giving these high recoveries.

F. Water-oil relative permeability ratios show no definite correlation with temperature. However, relative permeability to oil increases with temperature.

G. Partitioning of surfactant into the oil phase has been observed to be a possible surfactant loss mechanism during the surfactant flood mechanism, depending on the relative solubility of the surfactant in water and oil.

H. Interfacial tensions attained were between 0.0447 and 3.355 mN/m. In this range oil recoveries were found to be high. If ultra-low IFT is defined to be much lower, then it was not attained as to achieve such recoveries.

I. As a result of surfactant precipitation and redissolution in-situ IFT may have been lower than the values measured.

J. Only two surfactants were used. Cosurfactants may be necessary to maintain solubility of surfactant in high brine concentrations and to give low interfacial tensions.

REFERENCES

1. Willman, B.T., Valleroy, V.V., Runberg, G.S., Cornelius, A.J., and Powers, L.W.: "Laboratory Studies of Oil Recovery by Steam Injection," Trans., AIME (1961) Vol. 222, 681-690.

2. Bursell, C.G., and Pittman, B.M.: "Performance of Steam Displacement in the Kern River Field," J. Pet. Tech. (Aug. 1975) 997-1004.

3. Blevins, T.R., and Billingsley, R.H.: "The Ten-Pattern Steamflood, Kern River Field, California," J. Pet. Tech. (Dec. 1975) 1505-1514.

4. Baker, P.E.: "Effect of Pressure and Rate on Steam Zone Development in Steamflooding," Soc. Pet. Eng. J. (Oct. 1973) 274-284.

5. Bear, J.: Dynamics of Fluids in Porous Media, American Elsevier Publishing Co., Inc., New York (1972).

6. Atkinson, H.: U.S. Patent 1 651 311 (1927).

7. Brown, A., Carlin, J.T., Fontaine, M.F., and Hayes, S.: "Methods for Recovery of Hydrocarbons Utilizing Steam Injection," U.S. Patent 3 732 926 (May 1973).

8. Gopalakrishnan, P., Bories, S.A., and Combarnous, M.: "An Enhanced Oil Recovery Method-Injection of Steam with Surfactant Solutions," Report of Group d'Etude IFP-IMF sur les Millieux Poreux, Toulouse, France (1977).

9. Ziegler, V.M.: The Effect of Temperature on Surfactant Adsorption in Porous Media, Ph.D. Dissertation, University of Southern California (March 1980).

10. Robinson, R.J., Bursell, C.G., and Restine, J.L.: "A Caustic Steamflood Pilot-Kern River Field," SPE 6523 presented at California Regional Meeting of SPE of AIME, Bakersfield, CA (April 1977).

11. Handy, L.L., Amaefule, J.O., Ziegler, V.M., and Ershaghi, I.: "Thermal Stability of Surfactants for Reservoir Application," SPE 7867 presented at 1979 SPE of AIME International Symposium on Oilfield and Geothermal Chemistry, Houston, Texas (Jan. 1979).

12. Hill, H.J., Reisberg, J., and Stegemeir, G.L.: "Aqueous Surfactant Systems for Oil Recovery," J. Pet. Tech. (Feb. 1973) 186-194, Trans., AIME, Vol. 255.

13. Handy, L.L., El-Gassier, M., and Ershaghi, I.: "Interfacial Tension Properties of Surfactant-Oil Systems Measured by a Modified Spinning Drop Method at High Temperatures," SPE 9003 presented at SPE Fifth International Symposium on Oilfield and Geothermal Chemistry, Stanford, CA (May 1980).

14. Murtada, H., and Marx, C.: "Evaluation of Low Tension Flood Process for High Salinity Reservoirs-Laboratory Investigation Under Reservoir Conditions," SPE 8999 presented at SPE Fifth International Symposium on Oilfield and Geothermal Chemistry, Stanford, CA (May 1980).

15. Ziegler, V.M., and Handy, L.L.: "The Effect of Temperature on Surfactant Adsorption in Porous Media," SPE 8264 presented at 54th Annual Fall Technical Conference and Exhibition of SPE of AIME, Las Vegas, Nevada (Sept. 1979).

16. El-Gassier, M.M.: The Effect of Temperature on Interfacial Tension of Surfactant-Oil Systems, Ph.D. Dissertation, University of Southern California (Aug. 1980).

17. Vonnegut, B.: "Rotating Bubble Method for the Determination of Surface and Interfacial Tensions," Rev. Sci. Instr. (1942) 13, 6.

18. Melrose, J.C., and Bradner, C.F.: Role of Capillary Forces in Determining Microscopic Displacement Efficiency for Oil Recovery by Waterflooding," J. Can. Pet. Tech. (Oct.-Dec. 1974) 54-62.

19. Stegemeier, G.L.: "Mechanisms of Entrapment and Mobilization of Oil in Porous Media," Improved Oil Recovery by Surfactant and Polymer Flooding, Ed. D.O. Shah and R.S. Schechter, Academic Press, Inc., NY (1977).

20. Abrams, A.: "The Influence of Fluid Viscosity, Interfacial Tension and Flow Velocity on Residual Oil Saturation Left by Waterflood," Soc. Pet. Engr. J. (Oct. 1975) 437-447.

21. Foster, W.R.: "A Low Tension Waterflooding Process," J. Pet. Tech. (Feb. 1973) 203-210.

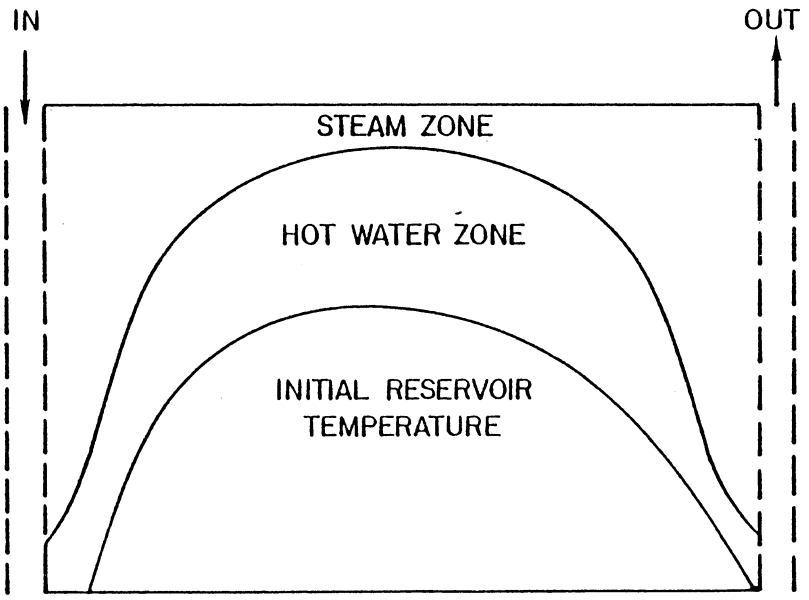

Figure 1. Schematic of a well-developed steamflood pattern

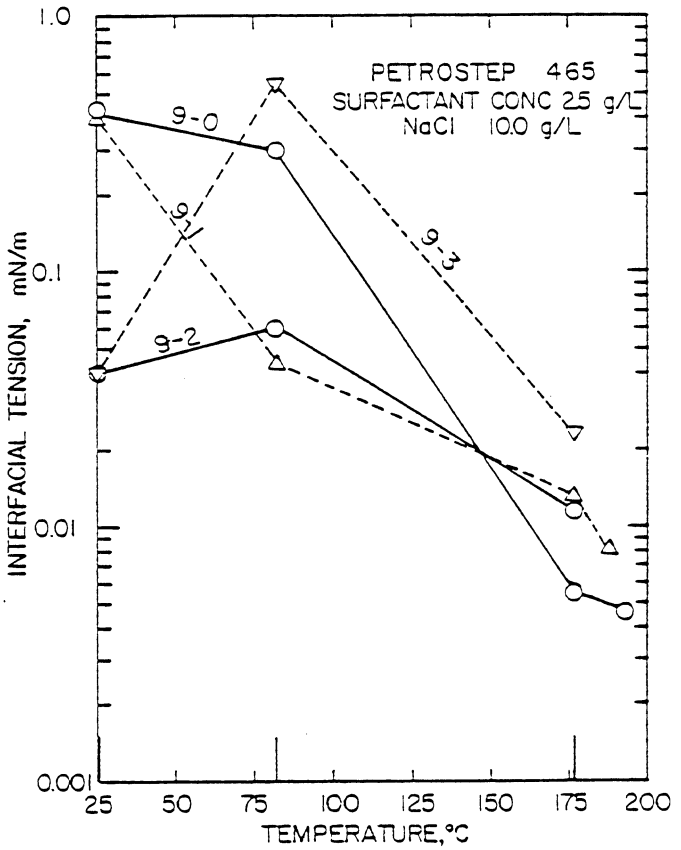

Figure 2. Interfacial tension measurements for surfactant/oil systems

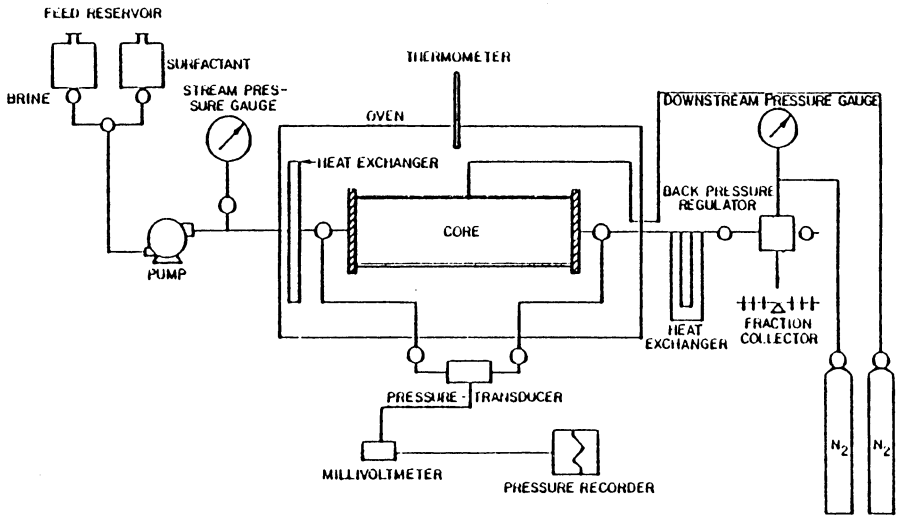

Figure 3. Schematic of the flooding equipment

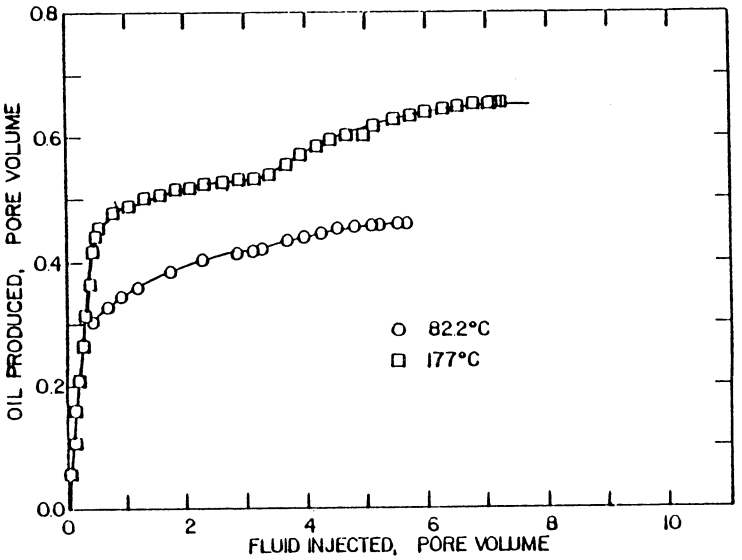

Figure 4. Oil displacement with Petrostep 465, sequence 1, oil 9-1

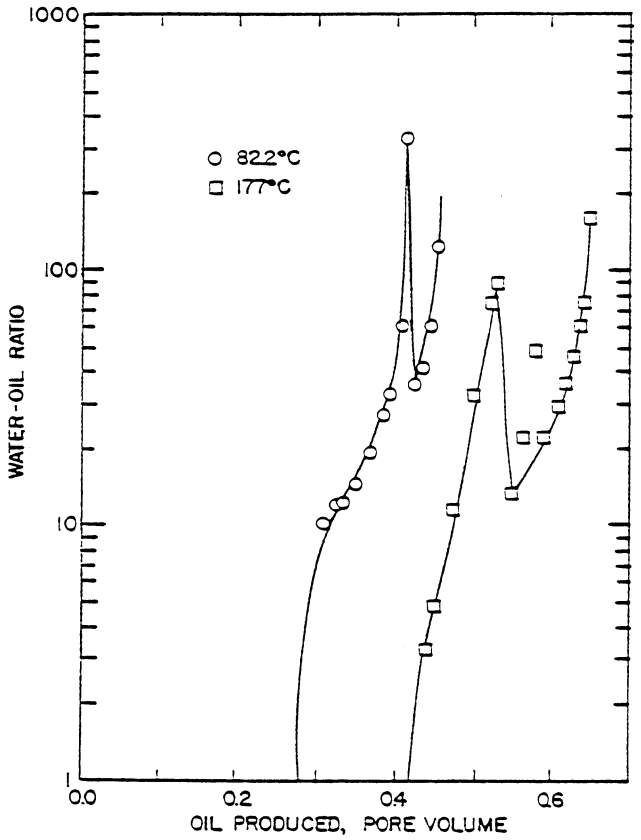

Figure 5. Water-oil ratio, oil 9-1

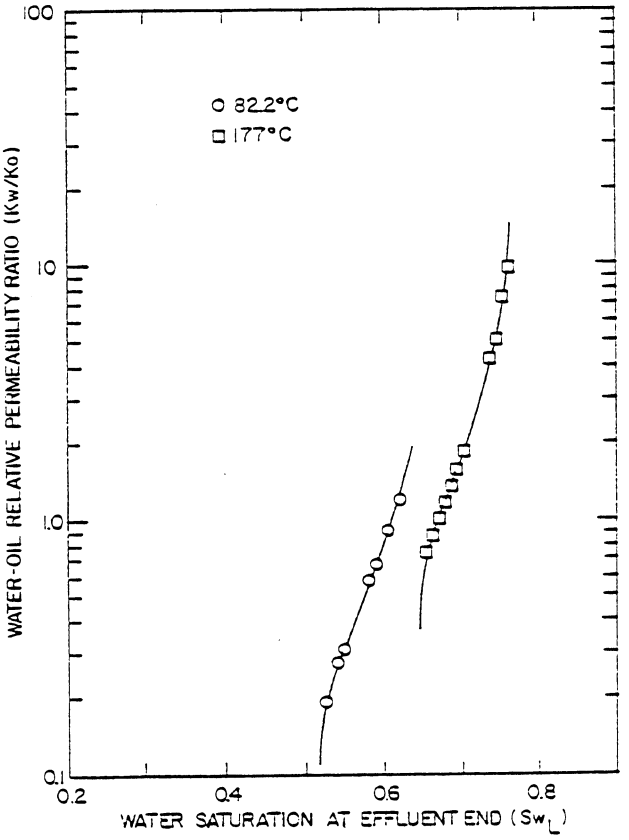

Figure 6. Water-oil relative permeability ratio, oil 9-1

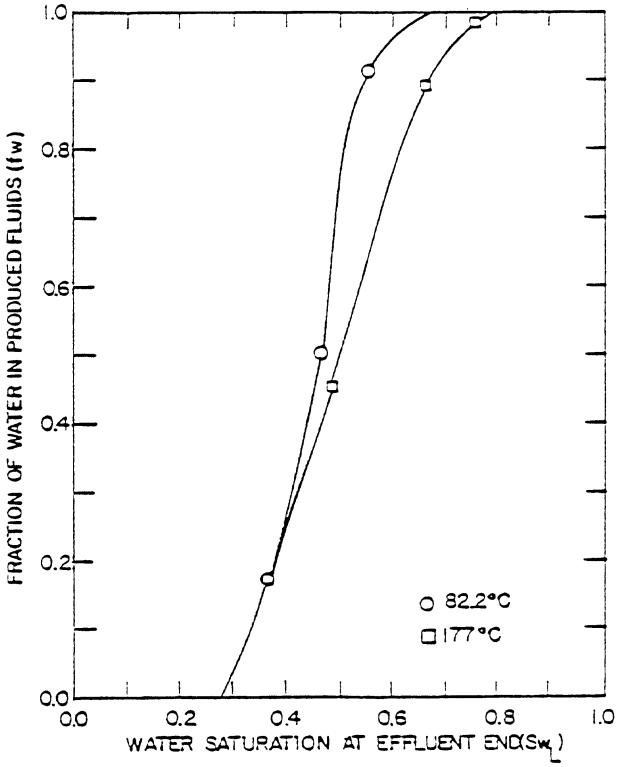

Figure 7. Water fractional flow curves, oil 9-1

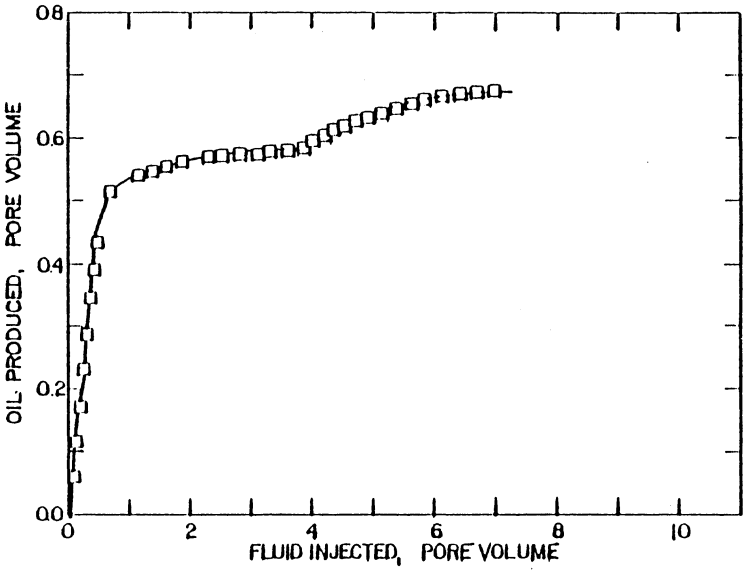

Figure 8. Oil displacement with Petrostep 465, oil 9-3, temperature 177°C

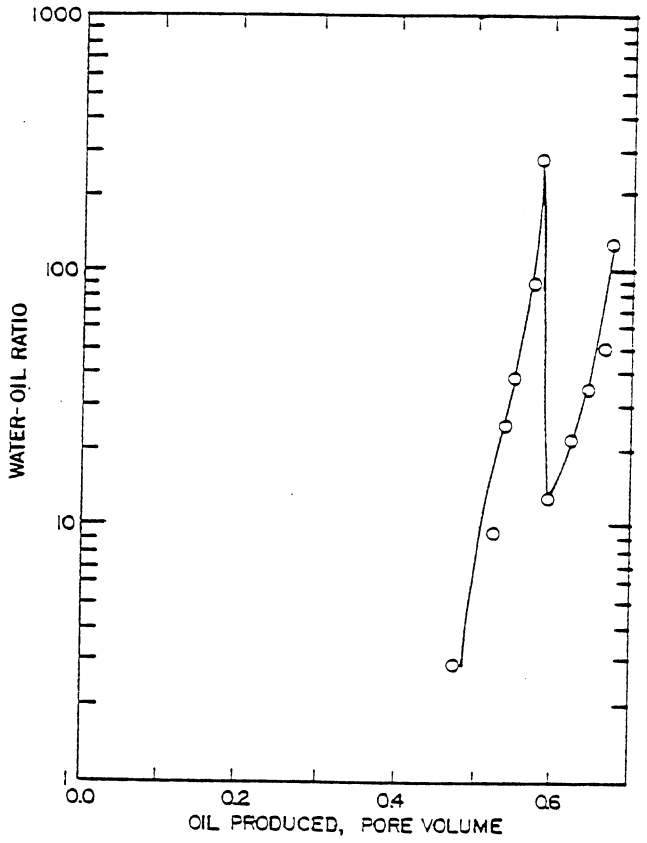

Figure 9 Water-oil ratio, oil 9-3

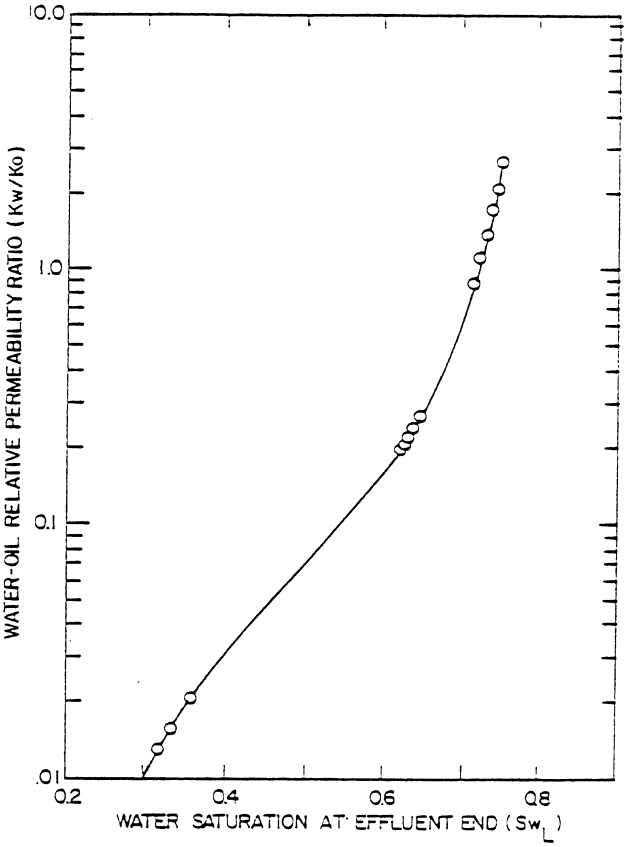

Figure 10. Water-oil relative permeability ratio, oil 9-3

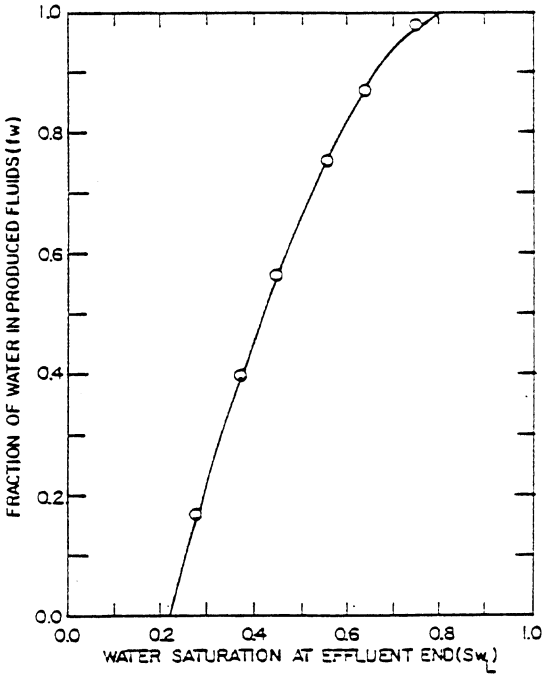

Figure 11. Water fractional flow curve, oil 9-3

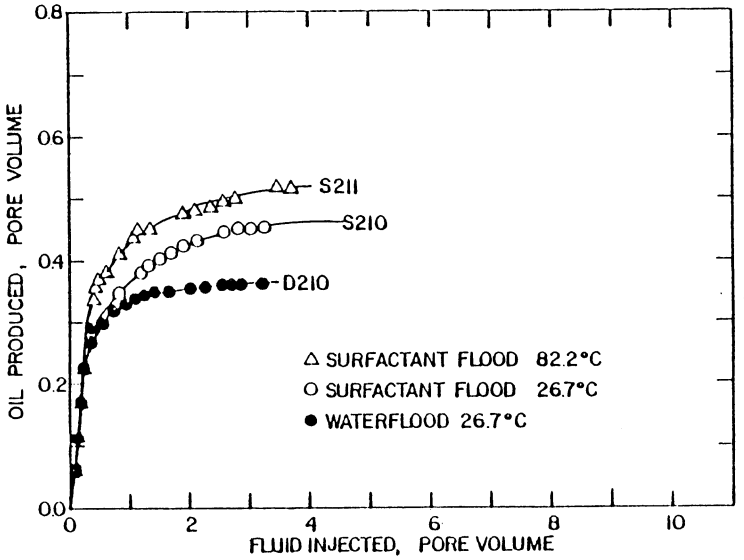

Figure 12. Comparison between waterflood and surfactant flood; Petrostep 465, oil 9-1

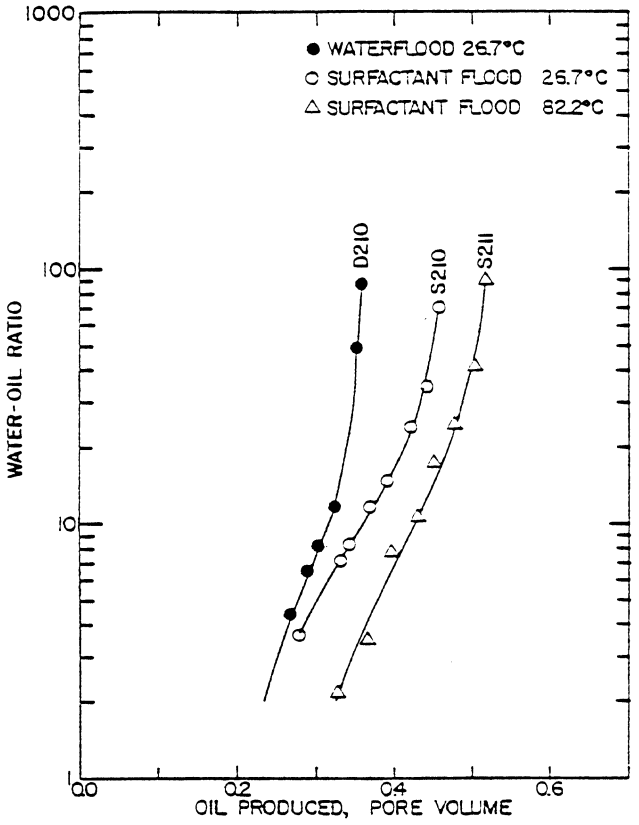

Figure 13. Comparison of water-oil ratio plots

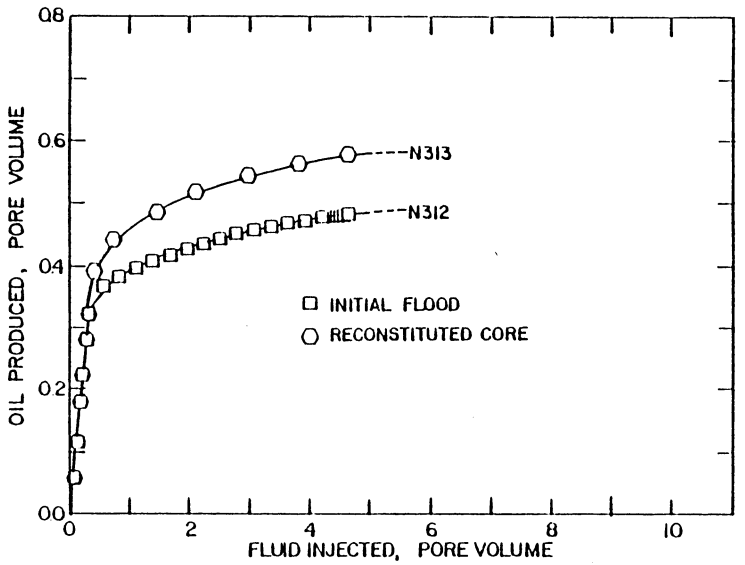

Figure 14. Effect of surfactant retention on flood performance, sequence 2

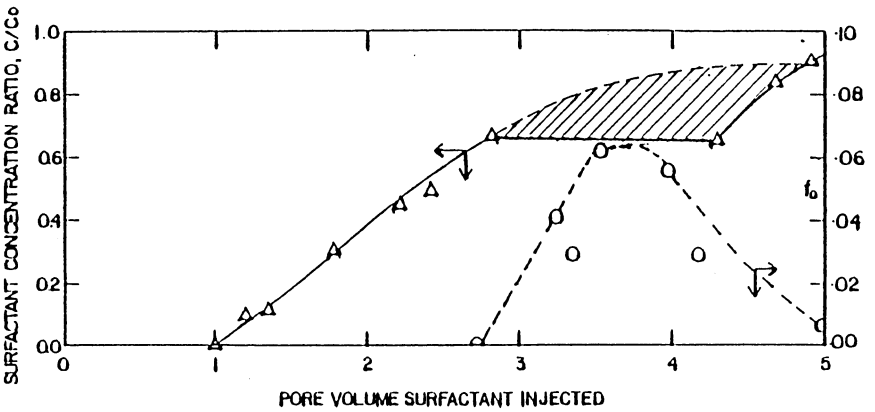

Figure 15. Demonstration of partitioning of surfactant into oil phase

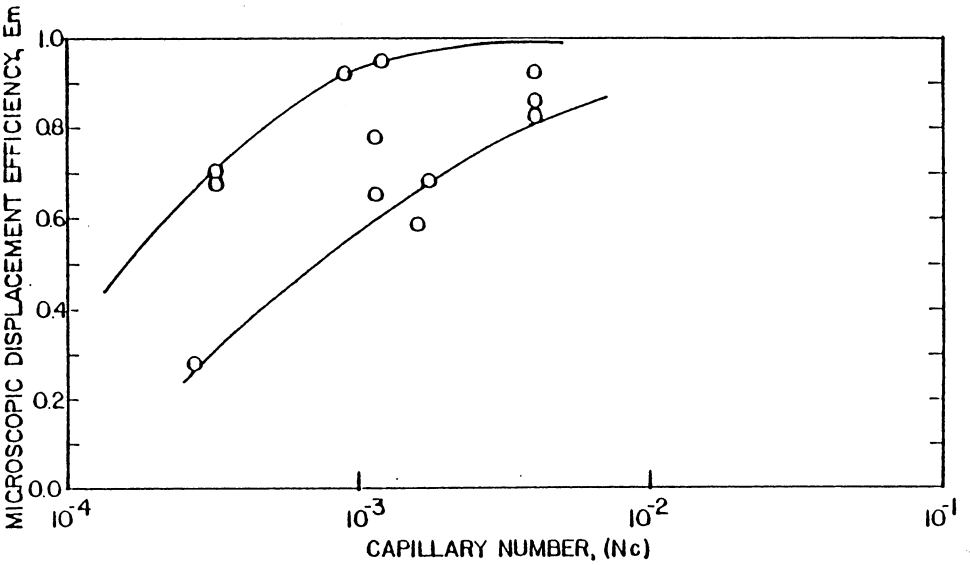

Figure 16. Capillary number correlation

ENVIRONMENTAL CONSTRAINTS TO THERMAL OIL PRODUCTION

Radian Corporation

ABSTRACT

In December 1978, President Carter decontrolled the price of heavy oil in order to stimulate U.S. heavy oil production. Natural forces (the primary production method) and conventional water flooding (secondary production method) have been only able to produce a few percent of the heavy oil reserves. However, thermal enhanced oil recovery (TEOR) technologies are expected to substantially increase heavy oil production with oil price decontrol. A large percent of the crude oil must be burned to produce the heavy oil by the two conventional TEOR technologies - steam injection and in situ combustion. One-tenth to one-half of the produced crude oil must be burned in package steam generators to produce the heavy oil by the steam injection methods. The package steam generators can release large qualities of sulfur dioxide (SO_2), nitrogen oxides (NOx), and particulate matter (PM), to the atmosphere. The wellhead vents, if not controlled, can release large quantities of hydrocarbons to the atmosphere. Large amounts of crude oil must be burned in the reservoir for in situ projects. In order to maintain the combustion of crude oil in the reservoir, vast quantities of combustion air must be compressed and injected into the reservoir. The compressors are typically driven by natural gas or diesel fired engines, which emit primarily NOx, SOx, and PM to the atmosphere.

Ninety percent of the future U.S. TEOR production is expected to be from heavy oil reserves in Southern California, Louisiana, Texas, and Arkansas. In recent years, stringent air pollution control regulations and preconstruction review processes have been established in these areas in response to the 1977 Amendments to the Clean Air Act. These regulations and review processes are expected to significantly constrain U.S. TEOR production in spite of the increased prices for the heavy oil.

In this presentation, the impact of air pollution control regulations and permitting processes on costs of current TEOR production are estimated along with their impact on future TEOR production. The air pollution regulations and permitting processes are described for representative TEOR production areas. Then the availability and cost effectiveness of air pollution control systems are presented. Using extremely optimistic assumptions on the achievable control levels and costs, the regulatory requirements, and the permitting processes, the maximum potential TEOR production levels are presented for key TEOR production areas. The costs are then calculated for the air pollution control systems needed to achieve the maximum TEOR potential production levels. The regulatory, technical, and cost constraints involved in achieving the maximum potential TEOR production by 1990 are summarized. Finally, the potential TEOR production that can realistically be expected by 1990 is presented.

Prepared for DOE under Contract No. DE-AC03-78SF01863

FORMATION EVALUATION IN THERMAL RECOVERY--RECENT WORK

by

S. L. Brown, J. W. Walsh, Jr.,
W. J. O'Brien, H. J. Ramey, Jr., and S. K. Sanyal
Stanford University Petroleum Research Institute

ABSTRACT

This paper will discuss current work of two SUPRI projects concerning formation evaluation. These projects are well-test evaluation and well log analysis.

The work in well-testing has been in the development of an analysis technique for pressure buildup and drawdown tests on wells being produced by steam drive or in-situ combustion. This well-test only takes a few hours and obtains the volume burned for in-situ combustion and the swept volume for a steam drive. Both parameters are important for determining the economic feasibility of a process. Field examples are shown for both a steam drive and an in-situ combustion process.

Work in well log analysis is being done to try: 1) to quantify, if possible, interpretations of the carbon/oxygen log; and 2) to write hand-held calculator programs for various log combinations to allow the engineer quick calculations of reservior parameters at the well site. The programs have been written for the analysis of shaly gas sands for the determination of R_o and TDS, and for matrix/fluid identification. A discussion will be given of the problems encountered when trying to analyze the Dresser-Atlas C/O log. These problems led to the computation of log responses for various idealized reservoir systems. These expected responses are now being correlated with Dresser-Atlas log data from the Kern River field.

HISTORY OF PROJECT

This report contributes to one of the objectives of contract DE AC03 76ET12056 which was initiated in September 1976.

INTRODUCTION

Eggenschwiler, et al. (1) have presented a method for measuring the gas-filled swept volume in an in-situ combustion or steamflood operation. The swept volumes may be measured by a short pressure transient test at the injection well. Calculation of the fuel concentration for a combustion operation or the cumulative heat loss from a steamflood was possible once the swept volume was known. This study discusses the analytical basis of this work and presents two field examples.

Prepared for the Department of Energy under Contracts DE AC03 76ET12056 and DE AC03 80SF11459.

ANALYTICAL BASIS

A steamflood or combustion process is modeled as a two-region reservoir, with an inner swept region surrounding the injection well and an infinitely large unswept region beyond the front. Figure 1 shows both top and side views of the system. The diffusivity equation for both regions is solved analytically using the appropriate boundary conditions. The injection well is considered to have both wellbore storage and a skin effect. The problem was solved by Laplace transformation with numerical inversion (1). A computer program was written to simulate a pressure transient test at the injection well using this model. Figure 2 illustrates a sample buildup test generated by the program.

The wellbore storage effect ceases almost immediately after shut-in. A semilog straight line develops rapidly, indicating the conductivity of the swept zone. From the slope of the line, the permeability-thickness in the swept zone, kh, and the skin factor, s, may be computed as follows:

$$kh = \frac{162.6\ qB\mu}{m} \tag{1}$$

and:

$$s = 1.1513 \left[\frac{p_w - p_{1hr}}{m} - \log \frac{k}{\phi \mu c_t r_w^2} + 3.23 \right] \tag{2}$$

where m was the computed slope and p_{1hr} was the extrapolated pressure at one hour shut-in time on the semilog straight line. Equation 2 is written for a pressure falloff test. The slope m is taken as positive. The parameters B, ϕ, μ, and c_t correspond to rock and fluid properties in the swept volume, and r_w is the radius of the well. All symbols are standard Society of Petroleum Engineers symbols and are defined at the end of this report.

After the semilog straight line, the system starts to feel the effect of the radial discontinuity. Due to the high mobility contrast, the front behaves like an impermeable boundary. A transition period is apparent, as pressures rise above the straight line, as seen in Fig. 2. During this transition period, the system approximates pseudosteady-state flow, as shown in the Cartesian pressure graph (Fig. 3). This is an important finding in that it allows calculation of the pore volume in the swept zone. Previously, it had been thought that one semilog straight line simply bent towards another semilog straight line.

The pore volume is related to the slope of the pseudosteady-state straight line as follows:

$$V_1 = \frac{5.615\ qB}{m_1 c_t} \tag{3}$$

Even though a radial front is assumed in developing the model, Eq. 3 applies for any swept volume shape. The concept of approximate pseudosteady-state involves a material balance calculation correct for any swept volume shape. The pore volume of the swept region determined from a Cartesian graph of pressure versus time actually is independent of the geometry of the swept zone.

After the Cartesian straight line, another transition zone lasts for a long time, and then the system behaves like an infinite reservoir, as shown in Fig. 2. In principle, the permeability for the unswept region can be computed using Eq. 1 and evaluating rock and fluid physical properties for conditions in the unswept zone. In fact, it is likely that the outer boundary effects would interfere with the second semilog straight line. The interference would probably prevent identification of a proper slope in most cases. There are other complications in applying this simple, single-phase flow model to thermal recovery systems. In the case of combustion oil recovery, only air flows in the swept zone, but multi-phase flow occurs ahead of the front. In steam injection, the steam totally condenses by the time it reaches the swept zone front. One example is the steam plateau region ahead of the combustion front. Study of such problems is the main focus of current study. The purpose of this report is to review findings to date. We turn now to potential applications of field determination of swept volume: calculation of fuel concentration or vertical heat loss.

The fuel concentration can be calculated from the volume of the swept zone as follows:

$$C_F = \frac{\phi\ Q_t}{AFR\ V_1} \tag{4}$$

where C_f is the fuel concentration in lbs of fuel/cu ft of rock, Q_t is the total volume of injected air in scf, and AFR is the air-fuel-ratio, scf of air/lb of fuel. The air-fuel-ratio (AFR) can be calculated from the analysis of the produced gases:

$$AFR = \frac{1805\left(1 + \frac{x}{4} - \frac{f}{2}\right)}{12 + x} \tag{5}$$

where:

f = fraction carbon gasified to carbon monoxide, and

x = atomic ratio of hydrogen to carbon in the fuel.

For air injection:

$$x = \frac{4\left(\frac{21}{79}\,\%N_2 - \%CO_2 - \frac{1}{2}\,\%CO - \%O_2\right)}{(\%CO_2 + \%CO)} \tag{6}$$

$$f = \frac{\%CO}{\%CO + \%CO_2} \tag{7}$$

$\%N_2$, $\%CO_2$, %CO, and $\%O_2$ are the respective percentages of nitrogen, carbon dioxide, carbon monoxide, and oxygen in the produced gas. We turn now to steam injection.

In a steamflood, knowledge of the steam-swept volume will permit the calculation of the vertical heat loss. From the average temperature in the steam zone, the amount of heat remaining in the swept pore volume can be calculated. The total heat injected into the system can be found from the total amount of injected steam. Thus, the heat loss from the steam zone is the total heat injected minus the amount of heat still in the swept volume. It is necessary to estimate the residual oil and water saturations in the swept zone, however.

DISCUSSION

Before Eq. 3 can be used to calculate the pore volume, the gas formation volume factor and total compressibility of the swept region must be known. These two parameters can be estimated from the average reservoir pressure and temperature in the swept zone. Methods for finding the average pressure and average temperature will be discussed in this section.

The average reservoir pressure can be found from the semilog graph of pressure vs time in Figure 2. After the initial wellbore storage and skin effect have ceased, the pressure in the wellbore almost stabilizes, and is equal to the pressure in the swept region: This is because the high mobility in the swept region causes a low semilog straight line in the swept region. Note the early, nearly horizontal straight line in Fig. 2. Therefore, the average reservoir pressure behind the front can be approximated by the early-time flattening of the pressure on the semilog graph.

The average reservoir temperature is crucial for calculating the correct pore volume. In Eq. 3, the ratio of B/c_t is a function of both pressure and temperature. However, the pressure effects tend to cancel, thus only an approximate average pressure is needed to calculate the pore

volume. On the other hand, the ratio is a function of temperature also. The accuracy of the calculated pore volume is proportional to the accuracy of the average temperature in the swept zone.

For steam injection, the average temperature may be estimated from the average temperature correcting for the partial pressure of steam in the swept zone. The problem is not that straight forward for combustion oil recovery tests.

The average swept volume temperature for combustion can be estimated in a number of ways depending on the information available and the degree of accuracy needed. The average temperature should lie between the injected air temperature and the pack combustion temperature. A reasonable method would be to do heat balance and find the average temperature that corresponds to the amount of heat behind the front. Several authors (2-5) have published temperature profiles for the combustion process from which the average temperature might be found by integrating the temperature profile over the swept volume. Combustion simulators may be used for the same purpose. Another method is to use the thermal efficiency of the process [see Prats (6)], and then calculate the average temperature corresponding to the amount of energy remaining in the reservoir. Thus, several methods are available for calculating the average reservoir temperature.

Most of the methods cited above require prior knowledge of the swept volume to estimate average temperature. Therefore, a trial and error procedure must be used to find the swept volume. First, assume an average temperature. Second, calculate fluid and rock properties and the swept volume. Third, calculate the average temperature using one of the above methods. Repeat the last two steps until the swept volume and average temperature do not change significantly from the previous iteration.

The estimation of fuel concentration for combustion oil recovery or vertical heat loss for steam injection from a short pressure transient test could have immense operational importance to field operations. This possibility was discovered by analysis of a simple flow model which does not match either process in detail. Although it is obvious that a reasonably complete finite-difference thermal simulator could be prepared to provide a better test, it was decided to search field case history data for evidence of the approximate pseudosteady-state regions.

A pseudosteady-state straight line has been observed in every field test studied. Two examples follow which demonstrate the information that can be calculated from thermal pressure transient tests.

Case A

The first example involves a combustion project in an inverted nine-spot pattern. All pertinent reservoir and fluid data are listed in Table 1. Figure 4 shows the semilog graph of a falloff test taken at the injection well. As seen in the figure, the flattening of the curve occurs at a pressure of 1640 psig. Therefore, the average reservoir pressure in the swept volume was 1640 psig. The average reservoir temperature was assumed to be 500°F.

The first semilog straight line began at about 0.07 hours and lasted until 0.5 hours. From Fig. 4, the slope of the straight line was 5.5 psi/cycle. Using Eq. 1 to calculate the permeability-thickness:

$$kh = \frac{(162.2)(2.8 \times 10^6)(0.016)(0.04)}{(5.615)(5.5)}$$

$$kh = 9435 \text{ md-ft}$$

If the average thickness of the swept region was known, the effective permeability to air of the formation could be calculated. If the permeability to air was known, the average thickness of the swept zone could be calculated. This permeability should be very close to the absolute permeability of the rock.

Just before shut-in, the downhole flowing pressure, p_w, was 1734 psig. Using Eq. 2 to compute the skin effect, s:

$$s = 1.1513\left(\frac{1785 - 1634}{5.5} - \log\frac{9435}{(.20)(0.4)(25)(604 \times 10^{-6})(.04)^2} + 3.23\right)$$

$$s = 23.0$$

This is a very large skin effect as evidenced by the large pressure drop between the flowing wellbore pressure and the average pressure in the swept zone. Large skin effects such as this one have been observed in other thermal pressure transient tests, such as the Belridge combustion project. In the Belridge project, the high skin effect was caused by lube oil from the compressors. However, several pressure falloff tests have been observed which have almost no skin effect and start directly with the semilog straight line.

Plotting the transition period on a Cartesian graph, a pseudosteady-state straight line is observed (Fig. 5). The straight line lasts from 2 to 7.5 hours. The slope of the line is 4.8 psi/hr. With an average reservoir pressure of 1640 psig and an average temperature of 500°F, the air formation volume factor is 0.0085 ft^3/scf, and the total compressibility is 604×10^{-6} psi^{-1}. Using Eq. 3 to find the pore volume:

$$V_p = \frac{(2.8 \times 10^6 \text{ scf/day})(0.016 \text{ ft}^3/\text{scf})}{(4.8 \text{ psi/hr})(24 \text{ hr/day})(604 \times 10^{-6} \text{ psi}^{-1})}$$

$$V_p = 644{,}000 \text{ ft}^3$$

The produced gas analysis shows 80 percent nitrogen, 10 percent carbon dioxide, 6 percent oxygen, and 2 percent carbon monoxide. From Eq. 6, the atomic ratio of H to C is:

$$x = \frac{4\left(\frac{21}{79}\,(80) - 10 - \frac{1}{2}\,(2) - 6\right)}{(10 + 2)}$$

$$x = 1.4$$

Using Eq. 7, the fraction of carbon converted to carbon monoxide is:

$$f = \frac{2}{2 + 10}$$

$$f = 0.17$$

From Eq. 5, the air-fuel-ratio, AFR, is:

$$AFR = \frac{\left(1 + \frac{1.4}{4} - \frac{0.17}{2}\right)\ 1805}{12 + 1.4}$$

$$AFR = 170.4 \text{ scf/lb of fuel}$$

The total injected air at the time of the test was 2.8×10^9 scf. Therefore, using Eq. 4 to calculate the fuel concentration:

$$C_F = \frac{(0.20)(2.8 \times 10^9 \text{ scf})}{(170 \text{ scf/lb of fuel})(660{,}000 \text{ ft}^3)}$$

$$C_F = 4.99 \text{ lb of fuel/ft}^3 \text{ of rock}$$

In laboratory combustion tube runs performed to evaluate this combustion project, the fuel concentration was 1.5 lbs of fuel/ft^3 of rock. This pressure test method results in a much higher fuel concentration. Almost no oil was produced in this test. However, it is not known with certainty that excessive fuel consumption was real in this case. This example is shown mainly for purposes of illustration of the potential of this procedure.

To summarize results of Example A, the following were calculated from a thermal pressure transient test: swept pore volume, permeability-thickness of the swept zone, damage around the wellbore, swept volume, and fuel concentration. We turn now to a steam injection case history.

Case B

The second example involves a steamflood project. Figure 6 shows a semilog graph of a pressure falloff test taken at the injection well. Detailed projection and reservoir data are not available for this test, but a qualitative analysis is possible.

The flattening of the curve at 1175 psia is the average pressure in the steam zone. The average reservoir temperature for a steamflood is roughly equal to the steam saturation temperature at the average pressure. The steam saturation temperature at 1175 psia is 565°F. The semilog straight line lasts from 0.3 to 0.6 hours, has a slope of 7.3 psi/cycle. The permeability-thickness, kh, of the swept zone may be found from Eq. 1, and the skin effect from Eq. 2.

The transition period is shown in Fig. 7. The pseudosteady-state straight line begins immediately after the semilog straight line ends, and lasts for over six hours. The slope of the line is 26.9 psi/hr. From the slope, the steam-filled pore volume can be calculated using Eq. 3 if the steam injection rate before shut-in is known.

To summarize the results of field Example B, the average swept zone reservoir pressure and temperature are evident, the slope of the semilog straight line permits calculation of the steam permeability-thickness product in the swept zone, and the slope of the approximate pseudosteady-state line was observed, from which the steam-filled pore volume could be calculated.

In the preceeding, the approximate swept volume was described, realizing that flow across the front affects the result. Approximate correlation factors have been developed by Tang (7). Other pertinent reports have been issued (8,9).

FUTURE WORK

In the combustion example, the calculated pore volume was directly related to the average reservoir temperature in the swept region. The assumed temperature of 500°F produced a pore volume of 644,000 cu ft. If the average temperature had been 400°F, the calculated pore volume would have been only 577,000 cu ft. Thus, an accurate method of estimating the average temperature is needed. Current work is being done investigating such methods. The method of calculating the thermal efficiency of the process seems to be best suited for these calculations.

One of the questions that has arisen from this work involves the calculated pore volume in a combustion operation. Is this pore volume the total air volume behind the front, or does it also include the gas volume in the steam zone ahead of the front? The pressure response is dependent upon the relative permeabilities of the fluids. If the gas

saturation in the steam zone is small, the gas relative permeability will be small, and the pore volume calculated is the pore volume behind the front. However, if the gas saturation in the steam zone is large, its relative permeability will be large, and the calculated pore volume may include both the swept volume and the gas volume in the steam zone. Further research is being done to determine the answers to these and similar conditions.

CONCLUSIONS

An analysis of the pressure transient falloff testing of thermal injection wells based on a simple, approximate model has produced a surprising and potentially important result. A long transition zone between the two semilog straight lines for the swept and unswept regions contains an approximate pseudo-state region based on the swept volume near the injection well.

Although the model is ideal and includes all the usual simplifying assumptions, the concept of pseudosteady-state is a material balance concept and independent of the actual dimensions and regularity of the swept volume.

The pressure transient test required to identify the approximate pseudosteady state region is of short duration: 1 to 10 hours at most. This is an almost ideal pressure transient test.

The pseudosteady state region actually yields an estimate of the swept volume storage volume in units of standard volumes of gas per psi pressure change. To compute the swept zone pore volume requires an estimate of the mean temperature and pressure in the swept zone. Estimation of mean pressure is not difficult. Estimation of mean temperature for combustion oil recovery can be a problem.

An examination of a large number of field case histories for both combustion and steam injection oil recovery reveals pseudo-steady linear pressure-time data immediately following an initial semilog straight line for every case. The potential importance of this finding for field operations is immense. Research to develop methods to interpret pressure transient falloff tests for thermal wells is continuing. This method should also be applicable to other enhanced oil recovery operations, involving high mobility contrasts across the swept region. Applications have already been made to boiling liquid geothermal systems and cold water injection in geothermal steam systems (10).

WELL LOG ANALYSIS WORK

Work involving well log analysis has been done in two main areas: development of hand calculator programs, and improving upon the current methods of analysis for the carbon/oxygen log. Four hand-held calculator programs have been written for the Texas Instrument 59 calculator. Three of these have been published.

Two of the programs were written for shaly gas sand analysis. These programs follow Poupon and others (11) work of describing shale as

dispersed, laminar, or structural. Both programs need the neutron and density logs to obtain porosity and the amount of each type of shale. Water saturation can then be calculated once resistivity data is entered. One of the programs [Gobran and others (12)] uses water saturation of the flushed zone, S_{xo} (e.g., derived from a shallow-investigation resistivity log), and gives the total volume of shale. The other program [Saldana and others (13)] requires a shale indicator (e.g., the gamma ray log) and finds S_{xo} by an iterative method.

Another program [Gobran and others (14)] finds the resistivity of a water zone, and the total dissolved solids for that zone from any of the following logs or combination of logs: spontaneous potential log, resistivity and porosity logs, laterolog, or thermal decay time log.

The final program is currently being completed. This analysis uses three porosity tools--neutron, density, and sonic logs--to identify the matrix and fluid of a zone. An analysis technique for matrix identification was worked out by Clavier and Rush (15). They defined apparent matrix values of the density (obtained from the density and neutron logs) and sonic (obtained from the sonic and neutron logs) values to obtain the mineral content of a zone. This crossplot is called the Matrix Identification Plot (MID). Bateman (16) described another crossplot, Fluid Identification Plot (FID), based upon these apparent parameters and mud properties to determine if a formation is clean, wet, shaly, or shaly with gas.

Based upon these methods, a computer algorithm has been written. Three separate programs are used. One finds the apparent matrix density from density and neutron data; also, from this program, porosity and lithology are found, assuming either a sandstone-limestone or a limestone-dolomite system exists. Charts used to find these values are provided by the logging service companies, and an example is shown in Fig. 8. Similarly, another program finds the apparent matrix sonic time, porosity and lithology by using sonic and neutron log data. The third program uses these apparent values and mud data to obtain the type of lithology, assuming a sandstone-limestone-dolomite system, type of fluid and presence of shale.

In general, these hand-calculator programs have turned out to be very practical for quick, well-site estimates of reservoir parameters. Considering the insignificant amount of budget devoted to the development of these programs, the effort has been rewarding.

Work continues to be done on the carbon/oxygen log. This project was begun because little work has been done in developing a quantitative analysis for this tool. Also, an analysis technique that can help estimate the oil saturation in a cased-hole can greatly aid enhanced oil recovery projects.

Lawrence (17) presents a paper which gives several possible techniques for analysis of the carbon/oxygen log. Several of these techniques will be shown with data from Kern County, Ca., to illustrate some likely problems in analysis. The well chosen for analysis has been

cyclic-steam flooded since 1969. This well is now receiving sequential slugs of a steam-foam-polymer combination and has been doing so since March 1979.

The zone of interest for the examples is a sandstone from 1550-1574' (see Fig. 10). The average log values (logged September 1980) from this zone are C/O = 1.52 and Si/Ca = 1/39. Porosity for this zone is approximately 35%. The crude oil is fairly heavy with a gravity of 13°API, or a density of .9792 g/cc. Whole core samples taken in January, 1980 show oil saturation varying in this zone from forty to seventy percent.

Oil saturation will now be calculated for this zone using several equations which Lawrence (17) presents. One method uses a C/O vs Si/Ca crossplot, shown in Fig. 9 with a water line defined by him and one which may be more appropriate for this particular well. To find oil saturation be presents the following linear equation:

$$S_o = \frac{C/O - (C/O)_{water}}{(C/O)_{oil} - (C/O)_{water}} \tag{8}$$

He further defines a water line and oil line for high porosities and obtains,

$$S_o = \frac{C/O + .8\ Si/Ca - 2.3625}{.2} \tag{9}$$

Water saturation is found to be 0.99. This is much too high so an attempt was made to redefine the water line described by the crossplot (see Fig. 9). This gives:

$$S_o = \frac{C/O + .45\ Si/Ca - 1.93}{.2} \tag{10}$$

with S_o = 0.88 for the zone. This is still high so corrections Lawrence presents were applied. To correct for porosity,

$$S_o = \frac{C/O + m\ Si/Ca - I_w}{.6\ \phi^{1.11}} \tag{11}$$

Given a porosity of 0.35, S_o = 1.06 using the water line in Eq. 9 and S_o = 0.94 using the water line in Eq. 10. Therefore, the porosity values were not properly changing the oil saturation and were even causing unrealistic values.

Lawrence presents an empirical equation which relates the C/O values for oil and water zones by,

$$S_o = 7.52 \left(1 - \frac{(C/O)_{water}}{C/O}\right) \qquad (12)$$

Taking the C/O value from a water zone as 1.42, $S_o = 0.49$. This is an improvement over the other methods as S_o is a realistic value. However, the oils Lawrence used for all previous equations were light crude oils. He does provide a correction for different oils,

$$S_o^{1.11} = \frac{.865\ S_{oa}^{1.11}}{\rho_{he}} \qquad (13)$$

where S_{oa} was found by the previous equations and

$$\rho_{he} = \frac{14n\ \rho_h}{12n + m} \qquad \text{(molecule of } C_n H_m\text{)}$$

Assuming $m = 1.5n$ and a molecular weight of 310, $S_o = 0.42$. This value is still realistic but lower than core values.

Another method commonly used for qualitatively finding oil zones is the overlay technique. Dresser uses a rather arbitrary method based upon their oil and water line. For water sands, the curves should come together, and this could provide a means for redefining the water line.

From the values of S_o some of the techniques tried do not appear applicable for the example well. Neuman and Oden (18) point out that the window size Dresser-Atlas uses for counting the different elements may not be the best to use. In fact, they find a high correlation between the silicon/calcium ratio and oil saturation. In order to gain a better understanding of the carbon/oxygen tool and Dresser Atlas' manipulation of that data, the basic priniples for the tool are being studied.

Figure 11 shows two log readings for this zone, one taken in Sept. 1980 and one in Feb. 1981. The C/O values have decreased as they should if they are an indicator of oil saturation as the well produces over time. Please note that although the Si/Ca curve is not constant for the zone of interest, it does appear to be constant with time.

At this point an attempt is made to try to describe these ratios. A mass balance for the chemical ratios can be written using coefficients which denote the amount of that element in a particular medium. The general equations describing the two ratios are as follows:

$$C/O = \frac{a\phi S_o + \sum_i^n b_i V_i}{c\,\phi\,(1 - S_o) + \sum_i^n d_i V_i} + \varepsilon_1 \qquad (14)$$

$$Si/Ca = \frac{\lambda_e e\phi(1 - S_o) + \sum_i^n f_i V_i}{\lambda_g g\phi(1 - S_o) + \sum_i^n h_i V_i} + \varepsilon_2 \qquad (15)$$

where λ denotes the amount of silicon or calcium in the water and ε describes borehole effects and tool anomalies. Please note that although ε is shown here as an additive effect that is not necessarily the case.

For a low salinity sandstone, these equations become,

$$C/O = \frac{.0768\ \phi\ S_o}{0.556\ \phi(1 - S_o) + 0.882(1 - \phi)} + \varepsilon_1 \qquad (16)$$

$$Si/Ca = \frac{e(1 - \phi)}{0} + \varepsilon_2 \to \infty \qquad (17)$$

So, theoretically a sandstone should have a constant Si/Ca ratio and the oil saturation should be a function of the C/O ratio and porosity only. A graph of C/C+O vs S_o was constructed for a sandstone using Eq.16 and different porosities (Fig. 12).

To correct the log values, ε_1 was taken to be the minimum value on the log, C/O = 0.21 and Si/Ca = 0.156. Looking at Fig. 12, the oil saturation is 0.41. This is again low, but a more accurate indication of ε_1 could provide more accurate oil saturation values. Hearst (19) suggested that an empirical correlation between C/O atomic ratio and the C/O count ratio might be possible through test pit data.

Dresser (17) has presented some test pit data with 100% oil and water saturations. Curves were generated for C/O vs Si/Si+Ca for several porosities and an oil saturation of zero and one. Figure 13 shows these curves for various porosity and varying amounts of sandstone and limestone. These curves are similar to those presented by Dresser by the negative slopes and spread between the saturation curves. Also, the S_o = 100% curve decreases as porosity decreases. However, Dresser did not take enough points to show that the curves are indeed nonlinear. The similarities show that the equations being used here are behaving similarly to data found from test pits.

Work is now being done to create curves for sandstone-limestone systems and to correlate these curves. The Si/Ca ratio is difficult to correlate. For our zone which is almost all sand, the corrected Si/Si+Ca curve should be around 1.0, not 0.135. A better understanding of how Dresser measures that ratio should help in determining the correct value.

A study is just beginning at SUPRI to search the physics literature to obtain information on how the tool works and to find, if possible, correlations which can describe the window technique Dresser uses. If spectra data can be obtained by either Dresser or Schlumberger, a study to analyze the logs can begin in a similar way to the method that Schlumberger is presently using (20).

NOMENCLATURE

Well-Testing

AFR = air/fuel ratio (scf/lb fuel)

B = gas formation volume factor in swept zone (RV/STV)

C_F = fuel concentration (lb fuel/ft^3 bulk volume)

c_t = total system compressibility in swept zone (psi^{-1})

f = fraction of carbon gasified to carbon monoxide

h = net thickness of swept region (ft)

k = effective permeability to gas in the swept region (md)

m = semilog straight line slope in swept zone (psi/cycle)

m_1 = Cartesian slope (psi/day)

p_{1hr} = semilog straight line pressure at 1 hour shut-in (psi)

p_w = injection pressure on shut in (psi)

q = injection rate (std bbl/day)

Q_t = total air injected (scf)

r_w = well radius (ft)

S = skin effect (dimensionless)

V_1 = swept pore volume (ft^3)

x = atomic hydrogen-carbon ratio of fuel

μ = gas viscosity in swept zone (cp)

ϕ = porosity of swept zone (fraction)

Well-Logging

a = amount of carbon in oil (# of molecules/medium)

b = amount of carbon in lithology

c = amount of oxygen in water

d = amount of oxygen in lithology

e = amount of silicon in water

f = amount of silicon in lithology

g = amount of calcium in water

h = amount of calcium in lithology

m = water line slope

C/O = carbon/oxygen ratio

I_w = water line slope

Si/Ca = silicon/calcium ratio

S_o = oil saturation

S_{oa} = apparent oil saturation

V_i = bulk volume of a particular lithology

ε = borehole effects and tool anomalies

λ = percentage of an element in water

ϕ = porosity

ρ_h = hydrocarbon density

ρ_{he} = effective hydrocarbon density

ACKNOWLEDGEMENTS

The authors would like to thank DOE (contract numbers DE AC03 76 ET 12056 and DE ACT03 80 SF 11459) and INTEVEP for support of this work. Also, the helpful advice on the Carbon/Oxygen log by Tony Lawrence of Atlantic Richfield was greatly appreciated.

REFERENCES

1. Eggenschwiler, M., Ramey, H. J., Jr., Satman, A., and Cinco-Ley, H.: "Interpretation of Injection Well Pressure Transient Data in Thermal Oil Recovery," presented at "VI Journadas Tecnicas de Petroleo" Meeting, Maracaibo, Vene., Oct. 28-Nov. 3, 1979.

2. Ramey, H. J., Jr.: "Transient Heat Conduction During Radial Movement of a Cylindrical Heat Source--Applications to the Thermal Recovery Process," Trans., AIME (1959) Vol. 216, 115.

3. Bailey, H. R., and Larkin, B. K.: "Conduction-Convection in Underground Combustion," Trans., AIME (1960) Vol. 219, 320.

4. Couch, E. J., and Selig, F. F.: "The Significance of Heat Transport for Underground Combustion Processes," Erdoel Kohle (July, 1962) 515.

5. Chu, C.: "Two-Dimensional Ananalysis of a Radial Heat Wave," Soc. Pet. Eng. J. (June, 1964), 85.

6. Prats, M.: "The Heat Efficiency of Thermal Recovery Processes," Jour. Pet. Tech. (March, 1969) 323.

7. Tang, R.: "Transient Pressure Analysis in Composite Reservoirs", Master's thesis at Stanford University (June, 1980).

8. Eggenschwiler, M., Satman, A., Ramey, H. J., Jr., and Cinco-Ley, H.: "Interpretation of Injected Well Pressure Transient Data in Thermal Oil Recovery," presented at the California Regional Meeting of the SPE in Los Angeles, CA. (April, 1980).

9. Satman, A., Eggenschwiler, M., Tang, R., and Ramey, H. J., Jr.: "An Analytical Study of Transient Flow in Systems with Radial Discontinuities," presented at the Annual Meeting of the SPE in Dallas, Tx (Sept., 1980).

10. Horne, R. N. and Satman, A.: "A Study of Drawdown and Buildup Tests in Wells with Phase Boundaries," Geothermal Resources Council, Trans., Vol.4, September, 1980.

11. Poupon, A., Clavier, C., Dumanoir, J., Gaymard, R., and Misk, A.: "Log Analysis of Sand-Shale Sequences - A Systematic Approach," Journal of Petroleum Technology (July, 1970).

12. Gobran, B., Saldana, M., Brown, S., and Sanyal, S.: "A Comprehensive Mathematical Approach and a Hand-Held Calculator Program for Analysis of Shaly Gas Sands," The Log Analyst (September-October, 1980).

13. Saldana, M., O'Brien, W., Brown, S., Gobran, B., and Sanyal, S.: "An Algorithm for the Analysis of Shaly Gas Sands," presented at the California Regional Meeting of the SPE in Bakersfield, CA (March, 1981).

14. Gobran, B., Brown, S., and Sanyal, S.: "A Hand-held Calculator Program for Estimating Water Salinity from Well Log," submitted to the Log Analyst for publication.

15. Calvier, C., and Rust, D.H.: "Mid Plot: A New Lithology Technique," The Log Analyst (November-December, 1976)/

16. Bateman, R.: "The Fluid Indentification Plot," SPWLA Transactions (1977).

17. Lawrence, T.: "Continuous Carbon/Oxygen Log Interpretation Techniques," presented at the Annual Fall Technical Meeting of the SPE in Las Vegas, NV (September, 1979).

18. Neuman, C., and Oden, A.: "Cased-Hole Measurement of Residual Oil - San Joaquin Valley, California," presented at the California Regional Meeting of the SPE in Bakersfield, CA (March, 1981).

19. Hearst, J.: "Laboratory Studies of an Improved C/O Log," The Log Analyst (November-December, 1978).

20. Westaway, P., Hertzog, R., and Plasek, R.: "The Gamma Spectrometer Tool Inelastic and Capture Gamma-Ray Spectroscopy for Reservoir Analysis," presented at the Annual Fall Technical Meeting of the SPE in Dallas, TX (September, 1980).

Table 1. Reservoir and Fluid Data for Example A.

Air Injection Rate, q	2.8×10^6 SCF/day
Porosity, ϕ	.20
Wellbore Radius, r_w	.04 ft
Total Injected Air, Q_t	2.8×10^9 SCF/day
Produced Gas Analysis	
Nitrogen, N_2	80%
Carbon Dioxide, CO_2	10%
Oxygen, O_2	6%
Carbon Monoxide, CO	2%

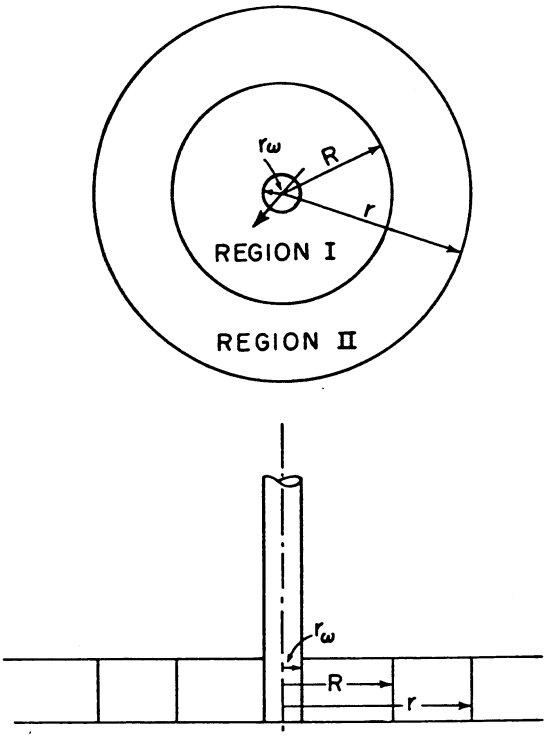

Fig. 1 - Idealization of the porous medium.

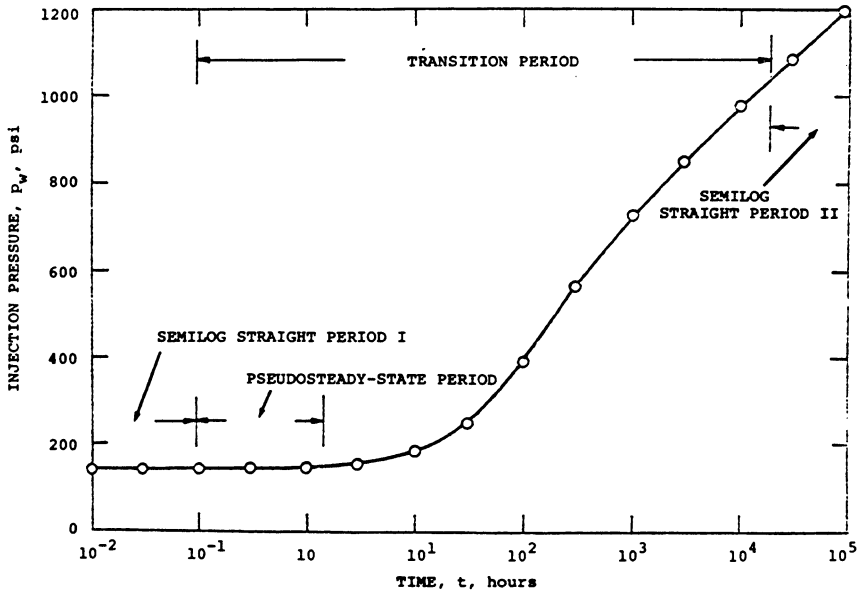

Fig. 2 - Bottomhole pressure vs time for in-situ combustion injection.

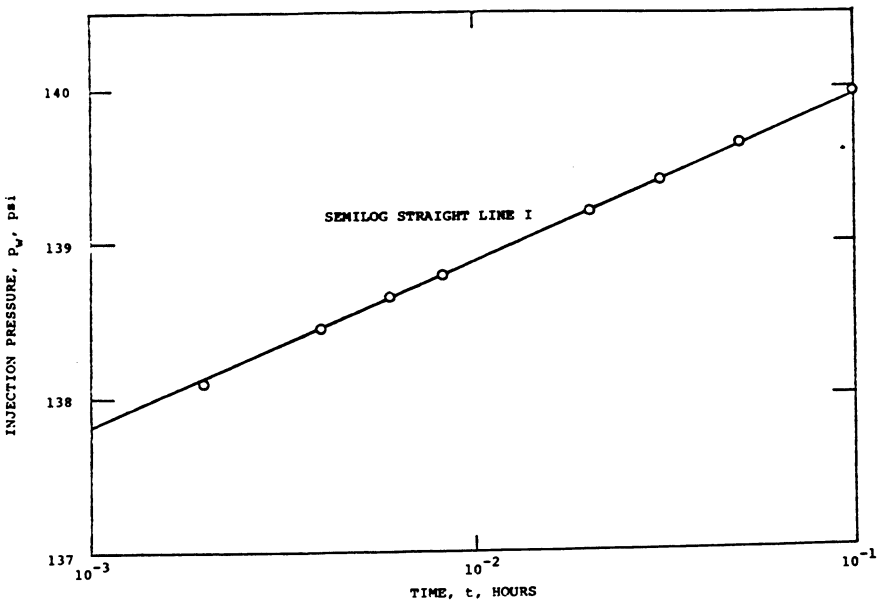

Fig. 3 - Bottomhole pressure vs time for in-situ combustion injection.

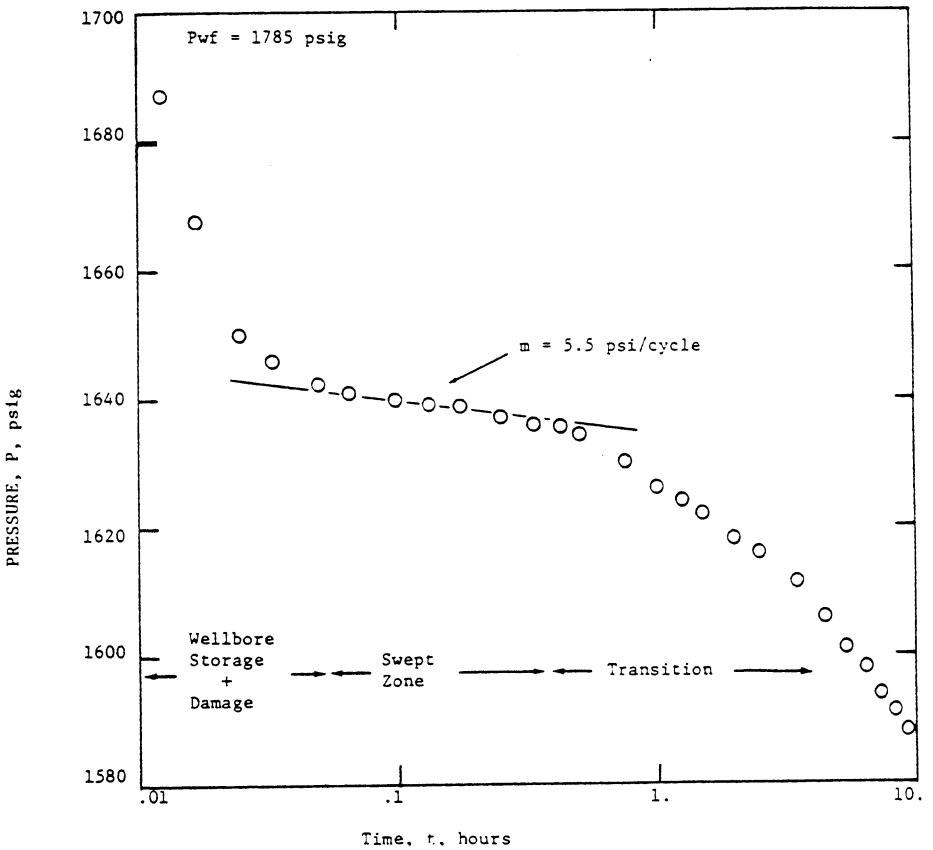

Fig. 4 - Bottomhole Shut-in Pressure vs log time for example A, in-situ combustion

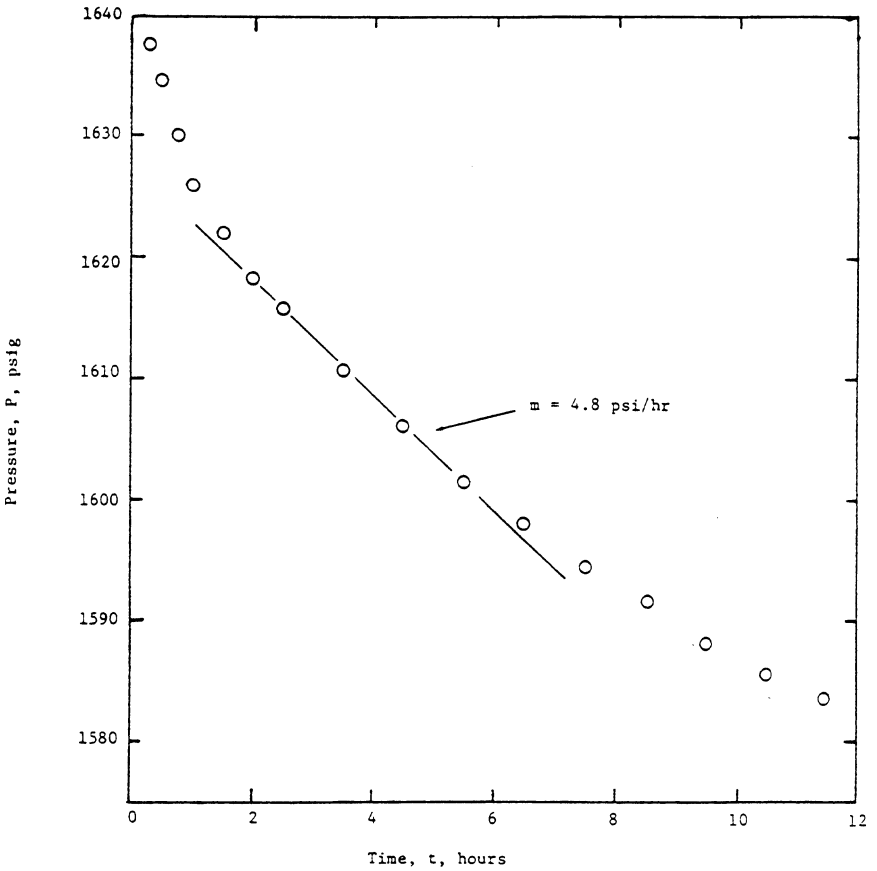

Fig. 5 - Pseudosteady-state for example A, in-situ combustion

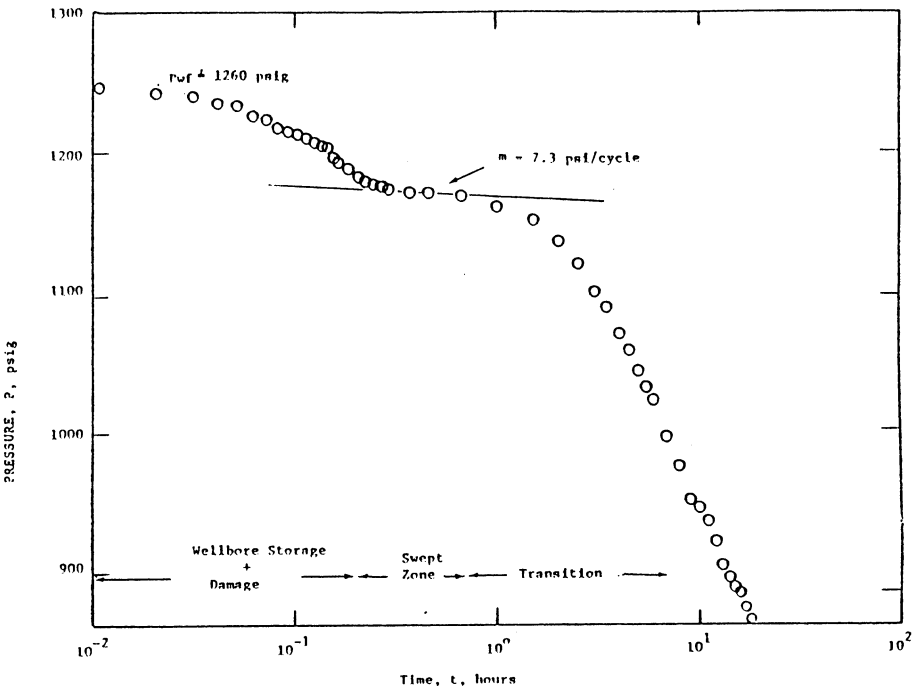

Fig. 6 - Bottomhole Shut-in Pressure vs Log Time for example B, steam injection

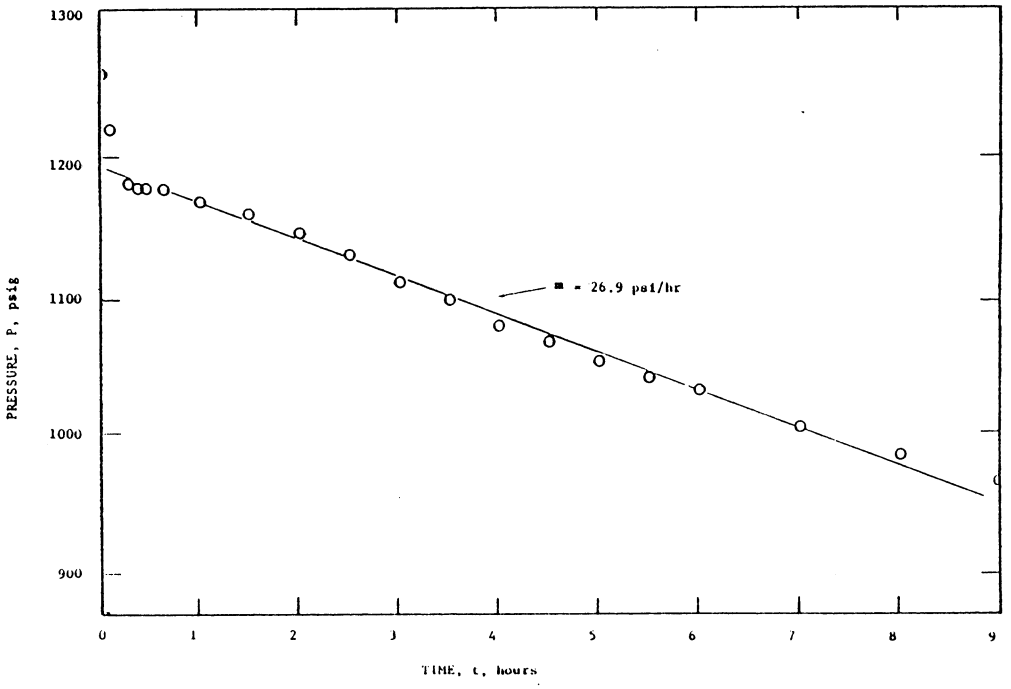

Fig. 7 - Pseudosteady-state for Example B, Steam Injection

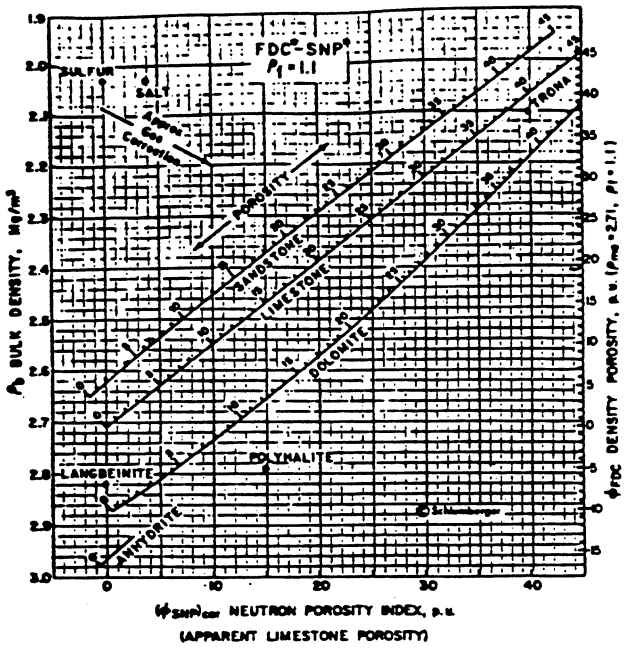

Figure 8. Example Plot from 1979 Schlumberger Chart Book.

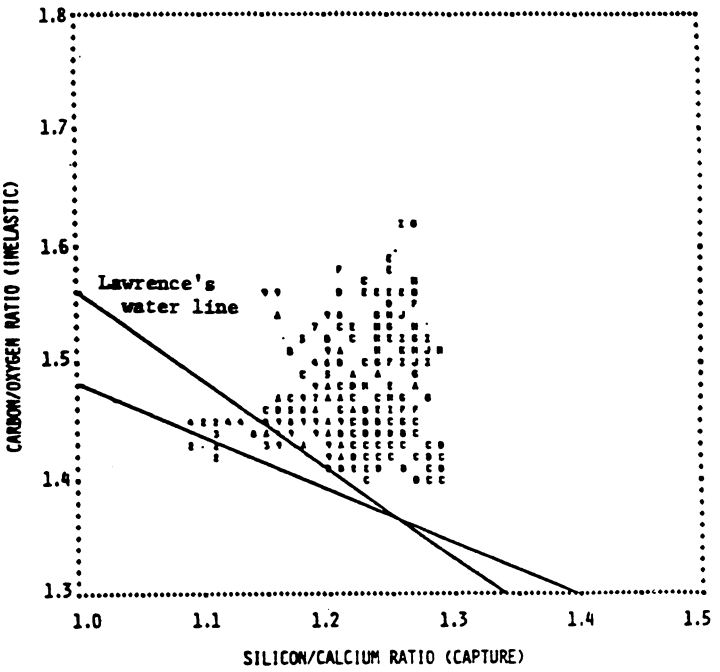

Figure 9. Crossplot of Si/Ca vs C/O.

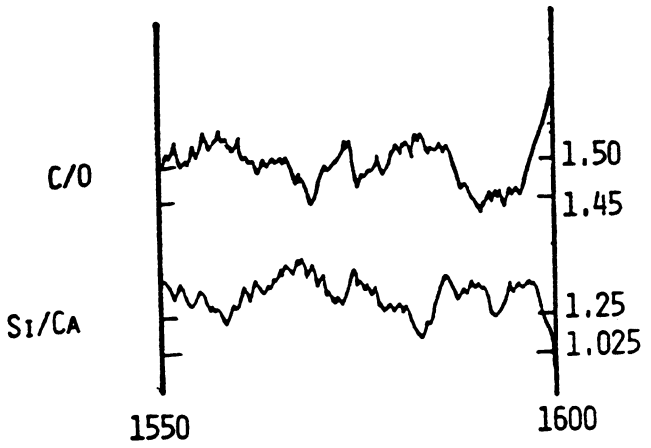

Figure 10. Log Example.

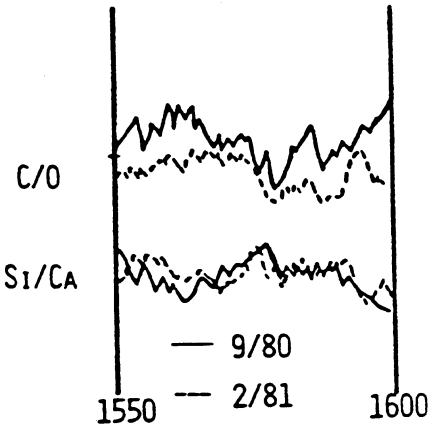

Figure 11. Log Changes with Time.

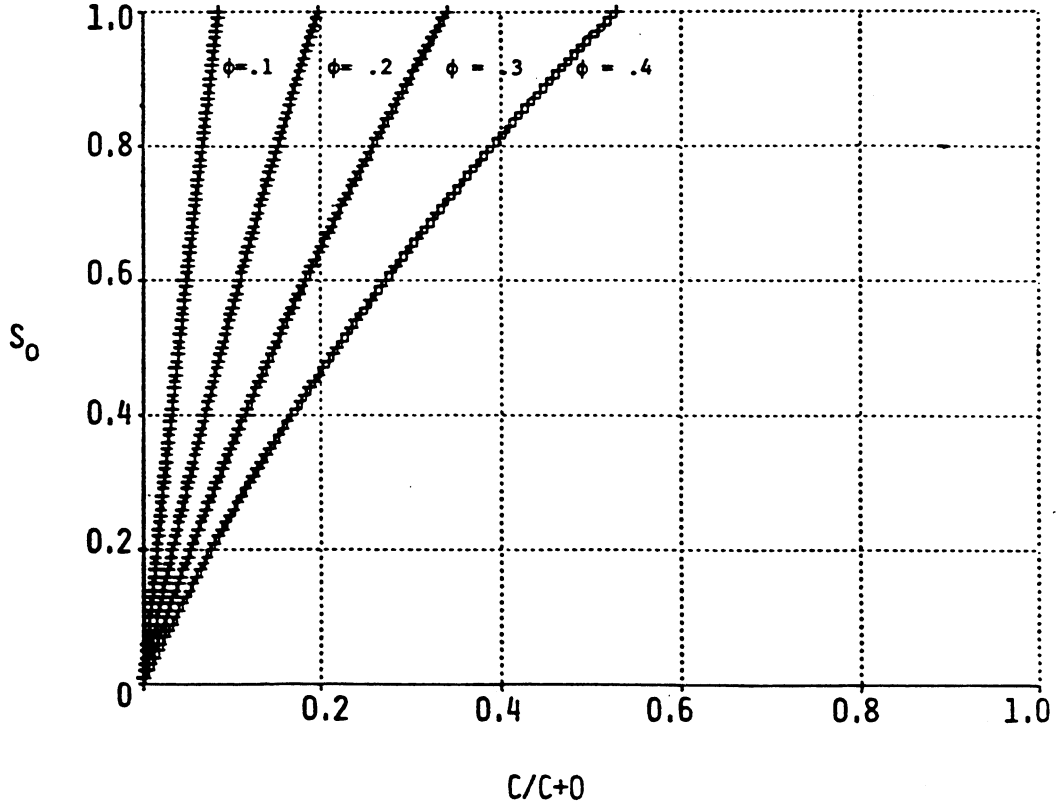

Figure 12. Plot of S_o vs C/C + O.

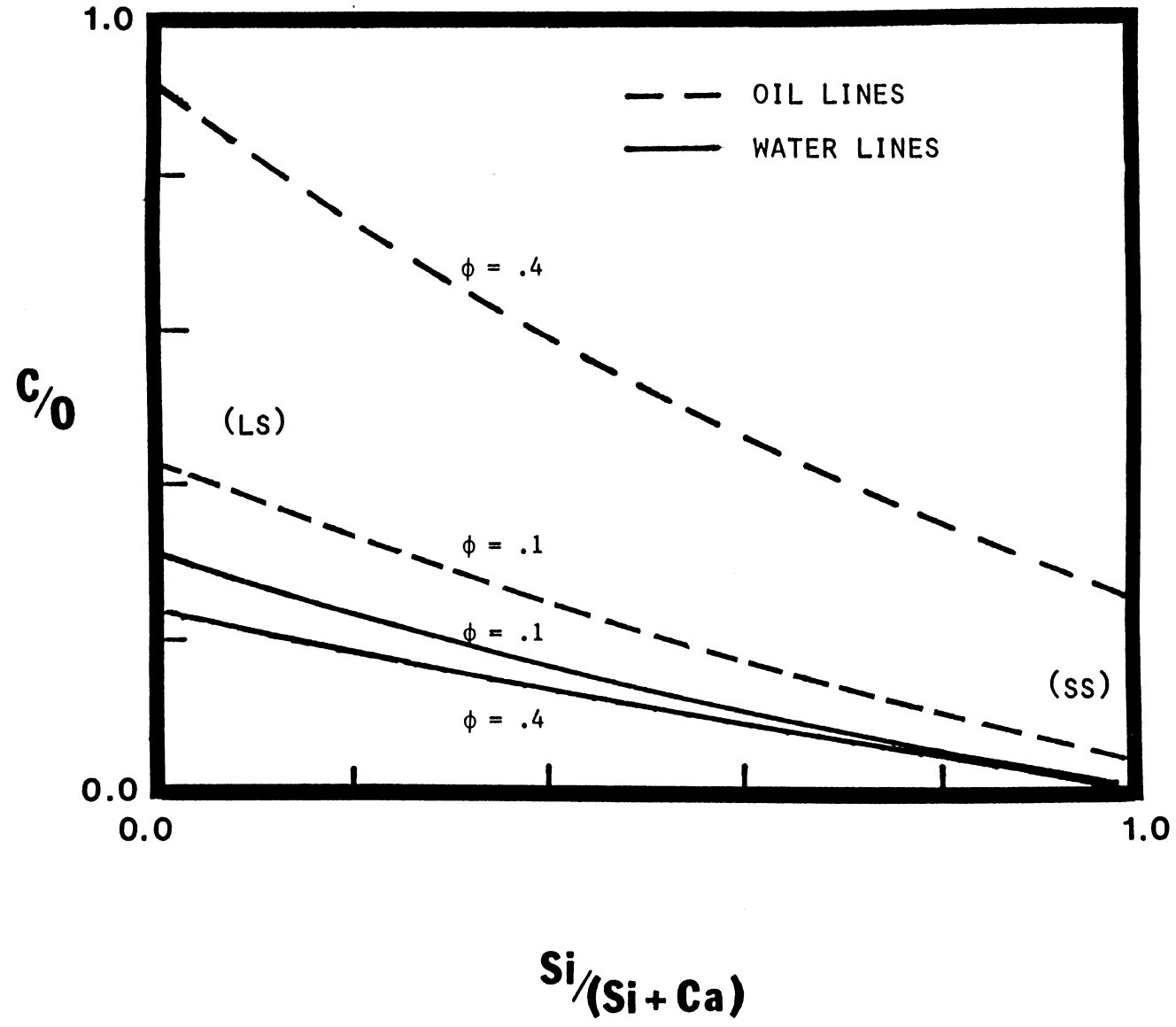

Figure 13. C/O vs Si/Si + Ca for a Limestone-Sandstone System.

PROJECT DEEP STEAM

by

R. L. Fox and D. P. Aeschliman

Sandia National Laboratories

Albuquerque, New Mexico

ABSTRACT

Evaluations of thermal packers and insulated delivery strings have been completed at the Tacoma facility of General Electric. Field tests of insulated delivery strings have been initiated at the Lloydminster test site of Husky Oil Co. A low-pressure combustion generator is being developed by Rockwell and a high-pressure combustion generator by Foster-Miller. Surface field tests in cooperation with Chevron are complete, and further tests are underway in cooperation with the City of Long Beach.

HISTORY OF PROJECT

The Project started March 7, 1978. Based on a 5-year plan, it is expected to be completed in 1983.

OBJECTIVES

The objectives of Project DEEP STEAM are to examine modified well completions for surface injection into deep reservoirs, develop economic downhole steam generators, and examine existing reservoir models for modifications required for steam injection into deep heavy-oil reservoirs. The project is designed to make deep steam drive a conventionally applied technique for producing low-gravity reservoirs.

MODIFIED WELL COMPLETIONS

In order to quantitatively evaluate techniques for the thermally efficient delivery of steam to deep reservoirs, a simulation test tower has been constructed under contract with General Electric at Tacoma, Wash. The thermal simulation test facility consists of a 73-foot-high tower which encloses a standard 7-inch well casing, with a vented annulus.

Testing in this facility was initiated in FY 1980, and a series of evaluations of thermal packers and insulated delivery strings have been completed. The tests which have been carried out to date were focused on tubular insulations including two designs based on calcium silicate, mineral wool, and two multilayered insulations. The expansion of testing to include non-tubular insulations is in process. Non-tubular insulations which will be examined include Ken-Pac and perlite.

Prepared for DOE under Contract No. DE-AC04-76DP00789

FIELD TESTING OF INSULATED INJECTION STRINGS

Field tests of the performance of insulated delivery strings have been initiated in cooperation with Husky Oil Co. The test site is located near Lloydminster, Canada. The test well was installed with a series of three small tubulars attached to the outside of the casing, as shown in Fig. 1. These tubulars are used to measure the casing temperature with a traveling thermocouple. Insulations which will be examined in the test well will be those which have provided promising performance in simulation tests at the Tacoma facility. Initial measurements using a bare tubular injection string have been carried out. The bare string test section has been removed and replaced with a calcium silicate insulated string. The delivery tubulars are instrumented with thermocouples and heat flux gages which are attached to the outer walls of the strings.

DOWNHOLE STEAM GENERATION

Two approaches to downhole steam production are under development as part of Project DEEP STEAM. The two systems are designated as a high-pressure combustion generator and a low-pressure combustion generator. Both steam generator systems utilize hydrocarbon fuels. The low-pressure combustion generator is being developed under contract with Rockwell International Corp., Rocketdyne Division. This design incorporates the transfer of energy from high-temperature, low-pressure combustion gases to high-pressure water via a downhole heat exchanger. The high-pressure combustion generator is being developed under contract with Foster-Miller Associates and at Sandia National Laboratories. This design carries out the combustion at pressures sufficient to inject the exhaust gases into the reservoir with the steam.

FIELD TESTING

A systematic series of field tests has been designed to support development of the downhole steam generator and to provide definitive evaluation of the system. The initial field test was carried out in FY 1980 in cooperation with Chevron, USA in the Kern River Field near Bakersfield, Calif. The initial test utilized a compact steam generator (6-inch diameter by 30-inches long) on the surface to inject steam and combustion gases into a shallow (800-ft) reservoir. This initial testing was completed in May 1980.

The next field examination of the downhole steam generator will be conducted in cooperation with the City of Long Beach, Calif., and Long Beach Oil Development Co. The test in Long Beach is in the 2,200-foot-deep tar zone of the Wilmington Field. The initial testing of the downhole generator in Long Beach began in May 1981. The test includes comparative recovery operations with air-fired and oxygen-fired generators. For the early stages of testing, the oxygen-fired generator will be located on the surface with the air-fired generator installed downhole in a nearby injection pattern.

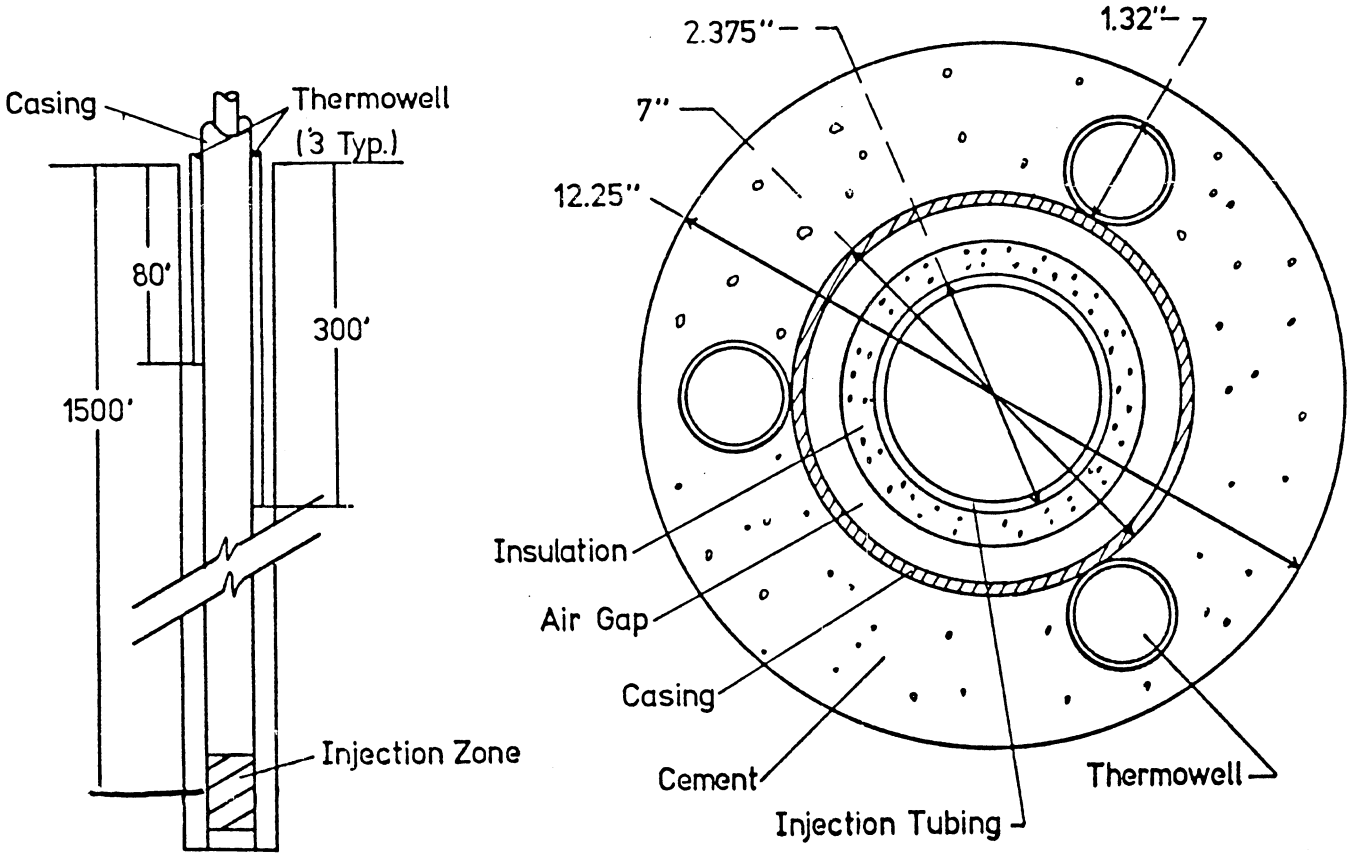

Figure 1. Test Well Profile and Cross Section

A SIMULATION STUDY OF DETERGENT FLOODING IN A VERTICAL CROSS SECTION

by

Guillermo C. Dominguez, Elmer L. Dougherty
and Lyman L. Handy
University of Southern California
Los Angeles, California 90007

ABSTRACT

A two-dimensional numerical model for simulating detergent flooding was developed. The model considers simultaneous flow of oil and water in a vertical cross section. The detergent (considered to be insoluble in oil) introduced in the injected water distributes itself between the water phase and the rock surface according to an equilibrium Langmuir type adsorption curve. The effect of dispersion on the distribution of detergent is considered. The model considers the typically observed relation between detergent concentration in the water phase and interfacial tension, with this relation exhibiting a strong minimum at the critical micelle concentration. The relation between interfacial tension (plus flow velocity and water viscosity via the capillary number) and relative permeability and residual saturation of both oil and water is considered in turn; the relationship used was derived from recent laboratory studies at University of Southern California.

The results obtained to predict effect of various parameters on oil recovery, from a system initially containing water and oil with the latter at residual saturation, are presented. Parameters considered include location of injection interval, slug size, surfactant concentration, oil viscosity and injection rate. Increase in injection rate was found to result in significant increase in oil recovery. For smaller fixed total amount of detergent used in a flood, the model predicts recovery to be insensitive to slug size, but for larger total amounts of detergent, larger slug sizes yield significantly higher recovery.

HISTORY OF PROJECT

This report is part of a project "Chemical Additives With Steam Injection To Increase Oil Recovery." It was initiated Sept. 15, 1976, with anticipated completion of Oct. 15, 1981.

INTRODUCTION

The initial objective of this research effort was to develop computer methods for predicting the behavior of a complex but potentially productive technique, injection of steam containing a surface active chemical component. The sheer magnitude of the task caused us to stop short of this objective. Although the equations were formulated and computer programs written for solving the combined process, the programs were debugged, tested and applied only to isothermal detergent flooding in a vertical cross section.

The incentive for the combined process derives from the nature of steam flooding itself. Steam injection is currently by far the most important enhanced oil recovery method. It has been used in various field conditions, but has been most successful with viscous, heavy oils which yeild very low recovery with any other recovery process.

Prepared for the Department of Energy Under Contract No. DE-AS03-76SF00113

Aspects of the combined steam and chemical injection process have recently been studied in the laboratory (1,2). The effect of temperature on adsorption of surfactant on the rock surface and on surfactant degradation has been researched (3,4), and has the effect of temperature on interfacial tension (5,6) and in turn on relative permeabilities of oil and water (7). Our study was targeted to proceed in parallel with these experiments. The objective was to build a numerical simulation model of the combined steam-chemical process incorporating the laboratory findings, and to conduct a series of recovery predictions with it using parameter values derived from such experimental results.

In consonance with this objective a set of equations describing the combined process was formulated, a numerical procedure for solving these equations was devised, and a system of FORTRAN computer programs for carrying out the required calculations was written. This system of programs was partially debugged and tested. However, midway through this effort it became apparent that the time required to fully complete the initial targeted objective was going to be considerably greater than was initially estimated. Therefore, our sights were lowered to allow completing a significant piece of the initial target in the time available. The piece selected was to simulate isothermal chemical flooding in a two-dimensional vertical cross section. As a result only this portion of the FORTRAN programs were completely checked out and used.

MATHEMATICAL FORMULATION OF CHEMICAL FLOODING

In this section the mathematical equations describing isothermal chemical flooding are presented. The assumptions pertaining to this system are listed as are the initial and boundary conditions specifying the problem actually solved. Data required to generate solutions for this numerical simulator are also given.

Assumptions

The following is a list of the more important assumptions made in developing the isothermal checmical flooding model:

1. Flow is two phase, oil and water.
2. Darcy's law applies to each phase.
3. Gravity effects are included but capillary effects are neglected.
4. The surfactant, a single chemical component, is insoluble in oil.
5. Surfactant concentration on the rock surface and in the water phase are in physical equilibrium, and the governing relationship is of the Langmuir type.
6. The surfactant does not react chemically with the rock, water or oil.
7. The dispersion coefficient of the surfactant is independent of velocity.
8. The interfacial tension between oil and water is a function of surfactant concentration. Interfacial tension decreases rapidly with concentration until the critical concentration is reached; above the latter interfacial tension increases, rapidly at first but more slowly as concentration becomes much greater than the critical value.
9. Changes in interfacial tension result in predictable changes of relative permeability of oil and water.
10. For interfacial tension values less than a critical value residual saturation of oil and water decrease. For any interfacial tension less than the critical value the residual saturation of each phase decreases as fluid velocity increases.

Equations Describing Isothermal Chemical Flooding

Given these assumptions the following equations describe the behavior of isothermal chemical flooding.

Oil Mass Balance:

$$\frac{\delta}{\delta x}\left[\rho_o \frac{k_o}{\mu_o}\frac{\delta \Phi_o}{\delta x}\right] + \frac{\delta}{\delta z}\left[\rho_o \frac{k_o}{\mu_o}\frac{\delta \Phi_o}{\delta z}\right] + Q_o\rho_o = \frac{\delta}{\delta t}(\phi \rho_o S_o) \tag{1}$$

Water Mass Balance:

$$\frac{\delta}{\delta x}\left[\rho_w \frac{k_w}{\mu_w}\frac{\delta \Phi_w}{\delta x}\right] + \frac{\delta}{\delta z}\left[\rho_w \frac{k_w}{\mu_w}\frac{\delta \Phi_w}{\delta z}\right] + Q_w\rho_w = \frac{\delta}{\delta t}(\phi \rho_w S_w) \tag{2}$$

Surfactant Mass Balance:

$$\frac{\delta}{\delta x}\left[\phi S_w D_x \frac{\delta C}{\delta x}\right] + \frac{\delta}{\delta x}\left[C \frac{k_w}{\mu_w}\frac{\delta \Phi_w}{\delta x}\right] + \frac{\delta}{\delta z}\left[\phi S_w D_z \frac{\delta C}{\delta z}\right] + \frac{\delta}{\delta z}\left[\phi S_w D_z \frac{\delta C}{\delta z}\right] +$$

$$\frac{\delta}{\delta z}\left[C \frac{k_w}{\mu_w}\frac{\delta \Phi_w}{\delta z}\right] + Q_w C = \frac{\delta}{\delta t}(\phi C S_w) + \frac{\delta}{\delta t}\left[(1-\phi)\ \Sigma\ \rho_r C_r\right] \tag{3}$$

Initial And Boundary Conditions

Inspection of the above equations reveals that they contain three independent variables; x, z and t, and three dependent variables; P, C and S_w (or So). The initial and boundary conditions must specify values of the dependent variables at the problem boundaries sufficiently to determine the solution.

Initial Conditions The values of P, C and S_w at all points in the permeable strata at t = o must be specified, viz.,

$$P(x,z,0) = P_i\ (x,z)$$
$$C(x,z,0) = C_i\ (x,z)$$
$$S_w(x,z,0) = S_{wi}(x,z)$$

Boundary Conditions Conditions must be given at the injection and production wells and at the interface with the overburden and overburden.

Injection Well Water injection rate is constant.

$$J \cdot \frac{\delta P}{\delta x}(0,z,t) = q_{w,inj}$$

For those segments of the injection well which are closed to flow, $q_{w,inj} = 0$

Concentration of surfactant in the injected water is a known function of time.

$$C(0,z,t) = C_o(t)$$

Production Well Pressure at the effluent face is constant for producing segments:

$$p(L,z,t) = p_{wf}$$

For nonproducing segments there is no flow; i.e.,

$$\frac{\delta p}{\delta x}(L,z,t) = 0$$

There is no transfer of surfactant across the effluent boundary by dispersion:

$$\frac{\delta C}{\delta x}(L,z,t) = 0$$

Reservoir Rock And Fluid Parameter Values

The data used in this study of isothermal chemical flooding is presented in Table 1. Most of these data are self explanatory, and we will only consider here the basis and means of describing the effect of surfactant concentration on the critical flow properties, relative permeability and residual saturation of the oil and water phases.

Very little has been published on the quantitative relation between surfactant concentration and oil and water relative permeabilities. To construct the required relationships for our study we used a procedure recently presented by Amaefule (7), based upon laboratory studies conducted at USC in parallel with our work. In this procedure the residual saturation of oil and water are each related to capilllary number, defined as:

$$N_c = \frac{\mu v}{\sigma} \tag{4}$$

Since N_c contains interfacial tension, a relation between S_{or} and S_{wr} is thus established. The actual equations used in our study were:

$$S_{or}(\sigma) = S_{or}(\sigma_o)\left(\frac{N_c}{N_{co}}\right)^{-0.5213} \quad ; \quad S_{wr}(\sigma) = S_{wr}(\sigma_o)\left(\frac{N_c}{N_{co}}\right)^{-0.1534}$$

where

$$S_{or}(\sigma_o) = 0.2$$
$$S_{wr}(\sigma_o) = 0.4$$
$$N_{co}(\sigma_o) = 1.44\times10^{-4}$$

The value of S_{or} or S_{wr}, as shown in Figure 1, defines the end point of the corresponding relative permeability curve, so that the above equations establish a relation between σ and the end points. Given the end points the following analytical relation was selected to define relative permeabilities at intermediate saturation values:

$$k_{ro} = 5.0[S_{or}(\sigma)(S_o^*)^2 - S_{or}(\sigma)(S_o^*)] + S_o^* \tag{5}$$

$$k_{rw} = 2.5[S_{wr}(\sigma)(S_w^*)^3 - S_{wr}(\sigma)(S_w^*)] + S_w^* \tag{6}$$

where:

$$S_o^* = \frac{1.0 - S_w - S_{or}(\sigma)}{1.0 - S_{wr}(\sigma) - S_{or}(\sigma)}; \qquad S_w^* = \frac{S_w - S_{wr}(\sigma)}{1.0 - S_{wr}(\sigma)}$$

Relative permeability curves such as are depicted in Figure 2 were derived from these equations and input into our program in the form of tables. Values of k_{ro} and k_{rw} at intermediate values of N_c were obtained in the program via given equations 5 and 6.

The relation between interfacial tension and surfactant concentration used is shown in Figure 3. This curve represent the general characteristics of most surfactants reported by various laboratory investigators.

DESCRIPTION OF CHEMICAL SIMULATOR

The simulator can be, and has been run with either one or two-dimensional grids, and numerous features and options have been included which enhance the utility of the system. The following is a list of these features:

(1) A different value may be input for porosity and absolute permeability in each cell thereby allowing the possibility of evaluating effect of reservoir heterogeneity on process behavior.
(2) Grid dimensions; x, y, z, may all be different.
(3) A different value may be input for initial saturation in each cell.
(4) The size of the time step can be changed as many times as needed during a run.
(5) Fluid and rock properties can be input in two ways: Analytical functions or tables. The tables contain coefficients of a quadratic polynomial fitted to segments of the data using the fitting program discussed above. The fitting program, which is fast and easy to use is run independently and the results input for use by the simulator.
(6) Relative permeability of the oil and water phases may depend on interfacial tension, viscosity, and fluid velocity, this latter dependence arising through dependence on the capillary number. The relations used are derived from recently reported laboratory data. An alternate relative permeability procedure could be easily implemented.
(7) A new procedure is incorporated to compute surfactant concentration which has proven to be very effective in eliminating unrealistic numerical smoothing of sharp concentration profiles. This procedure includes three parameters for a particular case, should this prove necessary.
(8) The simulator uses a very efficient sparse matrix code to solve the equations on each time step which results in considerably less CPU time than would otherwise be required.
(9) Because the simulator uses a fully implicit finite difference scheme, larger time steps may be used without sacrificing accuracy than would otherwise be the case.

A system flow diagram for the isothermal chemical flooding simulator is shown in Figure 4.

A 3×7 grid was used for the two-dimensional cross sectional studies, as shown in Figure 5. A number of calculations were performed using a one-dimensional

grid containing 20 cells. These latter cases, which included conventional water flooding and slugs followed by water injection through systems containing some immobile oil (with and without adsorption), were mainly made to check on the accuracy of the simulator.

The simulator, all of whose programs are written in FORTRAN, is prepared to use more cells if the user so requests. The restrictions on use of finer grids are computer memory requirements and required computing time. All of our runs were made using a DEC KL-1090 computer; on this machine an average of 0.12 seconds CPU time was required for each cell during an iteration. In the usual case 2 or 3 iterations were required to converge to a solution. Coats (8) reported a similar number for a black oil simulator.

EFFECT OF SEVERAL PARAMETERS ON THE SURFACTANT INJECTION PERFORMANCE

A sensitivity analysis on some parameters involved in a chemical flood process was performed. The effect of varying them is presented and discussed here. All simulations runs were conducted using data given in Table 1, unless otherwise specified. Some parameters values were selected within a range trying to find optimum values for the system used. In some cases, the parameter values chosen were only one or two since their effect is pretty well known and no additional information could be expected about the system behavior. Mineral balances on oil, water and surfactant were exceptionally good in all runs with an error less than one percent. In all cases run the iterative procedure reached convergence in pressure within 0.1 psi in 2 - 3 iterations per time step. The average CPU time observed was 0.12 second per iteration per cell in the system.

Location Of The Injection Interval

The effect of location of injection interval was first investigated to define a base system to compare with. Several run were made comparing injection at the top of the formation against injection at the bottom. In both cases the production well was completed at the top of formation studied. It was observed that injection at the bottom gives better enhanced oil recoveries in this system.

When injection is done through the upper portion of the interval studied a strong effect of the gravitational forces is observed. Since oil moves to the top of formation because of gravity, an earlier initial production is observed when comparing with the case of bottom injection. However, final recovery is lower as can be observed on figure 6.

Once the advantages of injecting at bottom part of reservoir was established, at least with the system used, a sensitivity analysis was undertaken on some of the parameters which were believed to have an effect on the expected oil recovery.

Surfactant Slug Size

The effect of slug size used is obvious if values of surfactant concentration used are close to the optimum. In this system, enhanced oil recovery would be better using larger slug size. This is true when injection concentration is 1.5 g/L which is the surfactant concentration that gives a minimum interfacial tension between oil and water, as it is shown in figure 3. Results from using different slug size of surfactant are given in fig. 7, 8 and 9.

Slug size selection is very important but it is closely related to the concentration of surfactant. A better correlation could be made if one sees this effect considering total amount of surfactant injected. As given in figure 10, for different injection rates, a plot can be made for equal amount of surfactant used depending on slug size. This implies that for higher slug size a smaller surfactant concentration has to be used to comly with equal total amount of surfactant injected. The observed effect is that using low amounts of surfactant to carry out the displacement process would show little or not change in the expected oil recovery, no matter what the slug size used is. This is true if one uses a minimum surfactant concentration close to the optimum value.

Surfactant Concentration

The effect of this parameter on oil recovery has already been mentioned in discussing the slug size selection. For a fixed small slug size used, less than 0.35 pore volume, the higher surfactant concentration injected the better the expected final oil recovery. This is observed in figures 11 and 12, and its explanation is again related to slug dispersion. Small slug sizes are easily deteriorated by dispersion no matter what surfactant concentration is used. However, as slug size is increased together with surfactant concentration, displacement would take place at higher surfactant values and slug will not be dispersed enough to allow chemical to lower interfacial tension and to reduce the residual oil saturation. This may be observed in figure 13, which clearly shows the poor recovery obtained using a large slug size and high surfactant concentration.

An important relationship we investigated in this research was if one could have an optimum combination of slug size and surfactant concentration. In figure 14 contour maps are shown to support that optimum combination. These enhanced oil recovery contour maps are presented as a function of slug size in pore volumes and surfactant concentration in g/L.

It is important to point out that this type of analysis may help in field application of the process. A few computer runs may save money on the field or even more they could make the difference between a successful and unsuccessful enhanced recovery project.

Injection Rate

Injection rate play an important role on the outcome of a chemical flood process, as shown in Figure 15. This is because of capillary number relationship ($v\mu/\sigma$). It has been observed on the model that not only low interfacial tensions are important to mobilize residual oil, but high displacement velocities are required. In some of the runs made in this study it was observed a highly efficient surfactant flood in terms of reaching reservoir zones of high residual oil saturation, but with a poor final outcome due to low fluid displacing velocities, mainly because of water finding easier paths to travel in the reservoir.

Oil Viscosity

One effect that we were interested to investigate was the consequences of adverse mobility ratios on enhanced oil recovery. This would be the typical case when using steam and chemical flooding as a combined recovery process. Some runs were made with oil viscosities of 3 and 5 cp, although most of the runs used 1 cp as

oil viscosity. The observed effect of higher oil viscosities was what we would expect; the higher the oil viscosity, the lower oil recovery obtained. This may be observed in figure 16. It is also observed that when higher oil viscosities are used, there is a delay on the time when oil production starts which is also what we would expect for an oil-water system like this.

Dispersion

Dispersion has an effect on the chemical flooding process. It has the effect of degrading surfactant slug in both edges, leading and trailing. In this research such effect has been observed, but no attempt was made to establish its magnitude. The model uses constant dispersion coefficient. Dispersion coefficient values used were those typical of petroleum reservoir problems and as noted in figure 17, a very small effect is observed when dispersion coefficient is set equal to zero.

NOMENCLATURE

C - Surfactant concentration in aqueous phase, g/L

Co - Surfactant injection concentration in aqueous phase, g/L

Cr - Surfactant adsorption on the solid phase, g/cm^2

D_x - Dispersion coefficient in x-direction, ft/day

D_z - Dispersion coefficient in z-direction, ft/day

ϕ - Porosity, fraction

$k_{o,w,g}$ - Effective permeability, mD

$\Phi_{o,w,g}$ - Potential, psi, i.e. $\Phi_o = p_o - g\rho_o h$
where:
h - Depth, measured downward, ft

$p_{o,w,g}$ - Fluid pressure, psi

p_{cow} - Oil-water capillary pressure, psi

ρ - Fluid density, mole/Bbl

S_{or} - Residual oil saturation at interfacial tension σ, Fraction

$S_{o,w,g}$ - Fluid saturation, Fraction

S_{wr} - Residual water saturation at interfacial tension σ, Fraction

v_x - Fluid velocity in X-direction, cm/sec

v_z - Fluid velocity in Z-direction, cm/sec

μ - Fluid viscosity, cp

ρ_r - Rock density, lb/ft^3

$S_{or}(\sigma_o)$ - Residual oil saturation in high tension σ_o system, Fraction

$S_{wr}(\sigma_o)$ - Residual water saturation in high tension σ_o system, Fraction

σ - Interfacial tension, mN/m

N_c - Capillary number, dimensionless

x - X-direction

y - Y-direction

z - Z-direction

t - Time, days

J - Well productivity index, Bbl/day/psi

C_1 - Unit convertion factor

A - Area of low into well, ft^2

H - Thickness of open interval, ft

pwf - Well flow pressure, psi

k_{rw} - Water relative permeability, fraction

k_{ro} - Oil relative permeability, fraction

Qo,g,w - Flow rate per unit volume, i.e., $Qo = qo/\Delta x \cdot \Delta y \cdot \Delta z)$

qo,g,w - Volumetric rate, Bbl/day

Øi - Porosity at pressure p_i, fraction

Σ - Surface area, ft^2

a,b - Constants used in Langmuir type adsorption equatio, i.e., $C_r = \frac{aC}{1+bC}$

$\lambda_{o,w,g}$ - Fluid molibity, mD/cp

q_{winj} - Water injection rate, Bbl/day

SUBSCRIPTS

i - Initial conditions

ℓ - Iteration

g - Gas

o - Oil

r - Rock

n - old time

REFERENCES

1. Gopolakrishnan, P., Bories, S.A. and Combarnous, M.: "An Enhanced Oil Recovery Method - Injection of Steam With Surfactant Solutions," Report of Group d'Etude IFP-IMF sur les Millieux Poreux, Toulouse, France (1977).

2. Handy, L.L., Amaefule, J.O., Hsu, J., Ershaghi, I.: "The Use of Chemical Additives with Steam for Oil Recovery," presented at the Fourth Annual Department of Energy Symposium on Enahcned Oil and Gase Recovery and Improved Drilling Methods, held at Tulsa, Oklahoma, August 1978.

3. Ziegler, V.M.: The Effect of Temperature on Surfactant Adsorption in Porous Media, Ph.D. Dissertation, University of Southern California (March 1980).

4. Handy, L.L., Amaefule, J.O., Ziegler, V.M., and Ershaghi, I.: "Thermal Stability of Surfactants for Reservoir Application," SPE-7867 presented at SPE of AIME International Symposium on Oilfield and Geethermal Chemistry, Houston, Tx. (January 1979).

5. Handy, L.L., El-Gassier, M.M., Ershaghi, I.: "Interfacial Tension Properties of Surfactant-Oil Systems Measured by a Modified Spinning Drop Method at High Temperaturs," SPIE-9003 presented at Fifth International Symposium on Oilfield and Geothermal Chemistry, Stanford, Ca. (May 1980).

6. El-Gassier, M.M.: The Effect of Temperature on Interfacial Tension of Surfactant-Oil Systems, Ph.D. Disseration, University of Southern California (August 1980).

7. Amaefule, J.O.: The Effect of Interfacial Tensions on Relative Oil-Water Permeabilities of Consolidated Porous Media, Ph.D. Dissertation, University of Southern California (February 1981).

8. Coats, K.H.: "A Fully Implicit Steamflood Model," SPE-6105 presented at 51st. Annual Fall Technical Conference, New Orleans, Louisiana (October 1976).

TABLE 1

BASIC MODEL AND RESERVOIR DATA USED

Blocks in x - direction	7	Water saturation, fraction	0.30
Blocks in y - direction	1	Oil compressibility, psi - 1	0.1×10^{-4}
Blocks in z - direction	3	Water compressibility, psi - 1	0.35×10^{-5}
Reservoir length, ft	350.0	Rock compressibility, psi - 1	0.3×10^{-5}
Reservoir thickness, ft	150.0	Initial oil density, mole/Bbl	1.5316
Reservoir width, ft	50.0	Initial water density, mole/Bbl	19.448
Well radius, ft	0.5	Initial pressure, psi	500.0
Skin factor in production well	0.0	Pressure at production well, psi	490.0
Absolute permeability in x-direction, md	300.0	Water viscosity, cp	1.0
Absolute permeability in z-direction, md	300.0	Oil viscosity, cp	1.0
Initial porosity, fraction	0.38	Dispersion coefficient, ft/day	1.0
Reservoir temperature, ^{o}F	90.0	Residual oil saturation after water-flooding, fraction	0.2
Oil saturation, fraction	0.20	Oil-water capillary pressure, psi	0.0

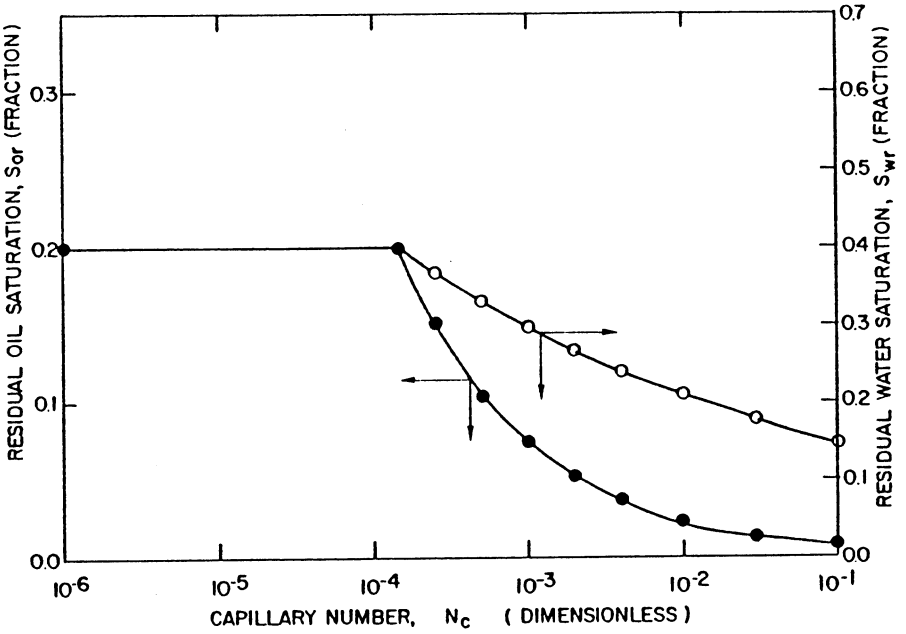

Fig. 1 Typical oil and water residual saturations as function of capillary number

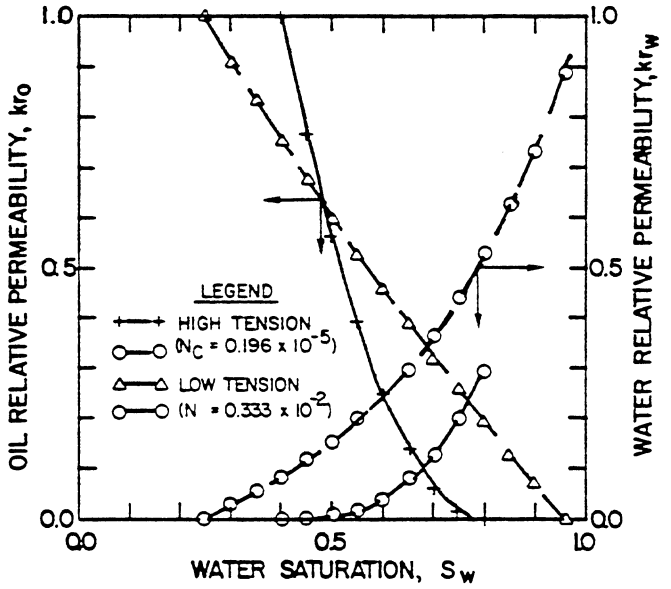

Fig. 2 Typical oil-water relative permeabilities at low and high interfacial tension

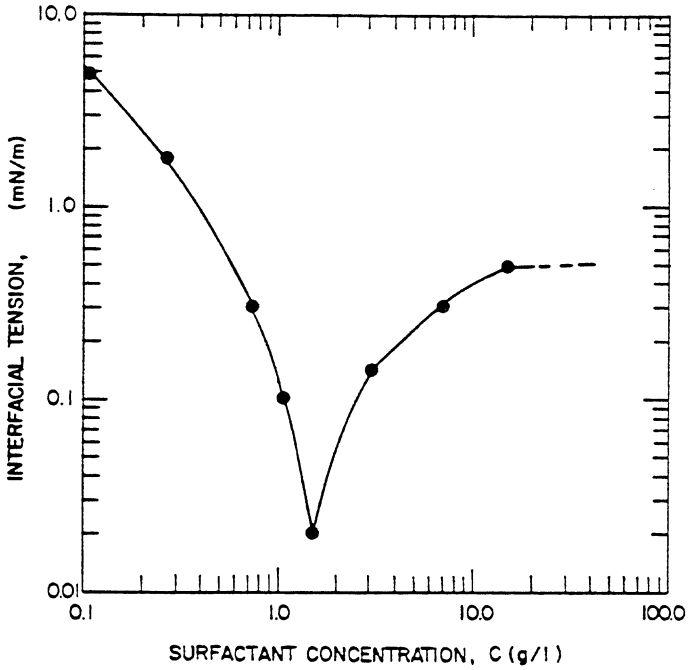

Fig. 3 Typical interfacial tension as function of surfactant concentration

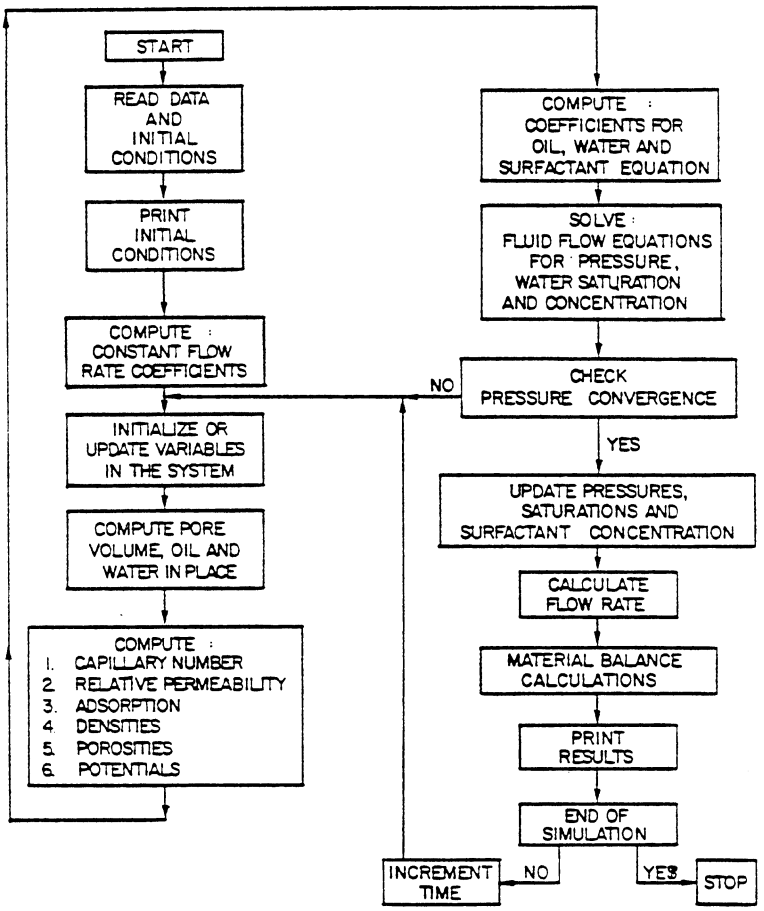

Fig. 4 Numerical simulator flow chart

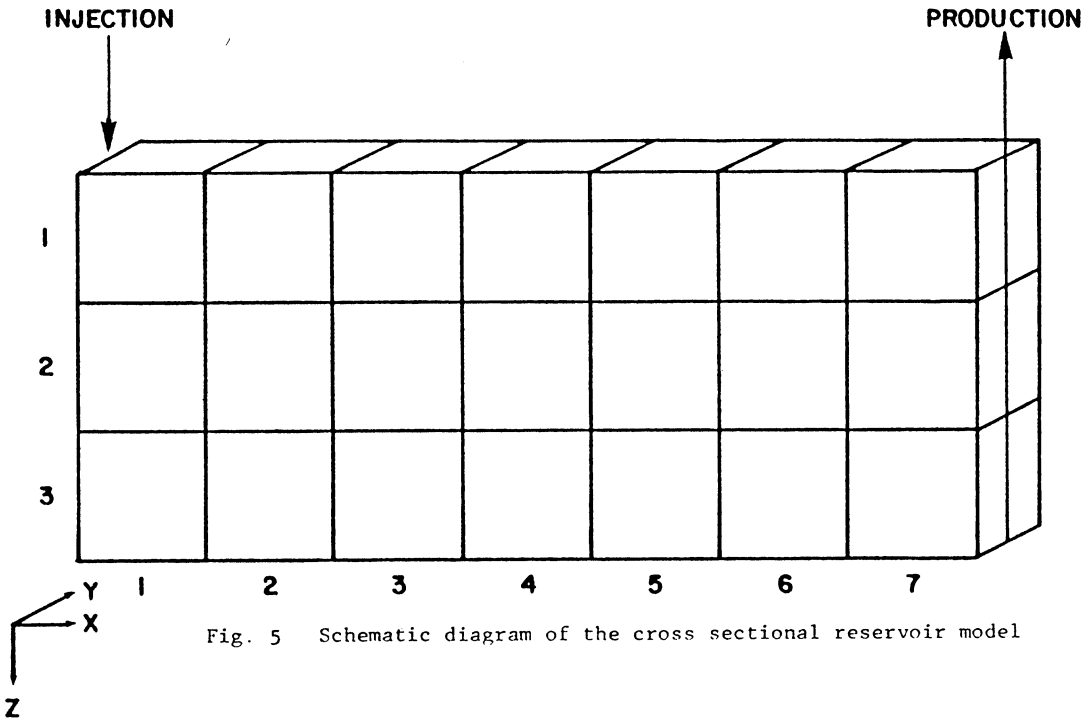

Fig. 5 Schematic diagram of the cross sectional reservoir model

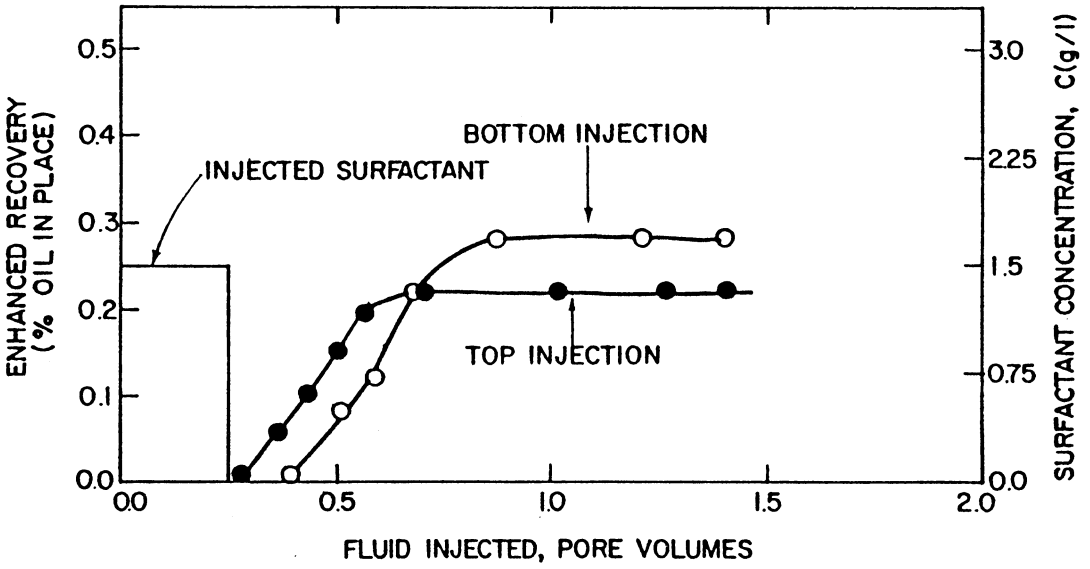

Fig. 6 Effect of location of injection interval on enhanced oil recovery as function of pore volumes injected, for a slug size of 0.25 pore volume and C_o = 1.5 g/L

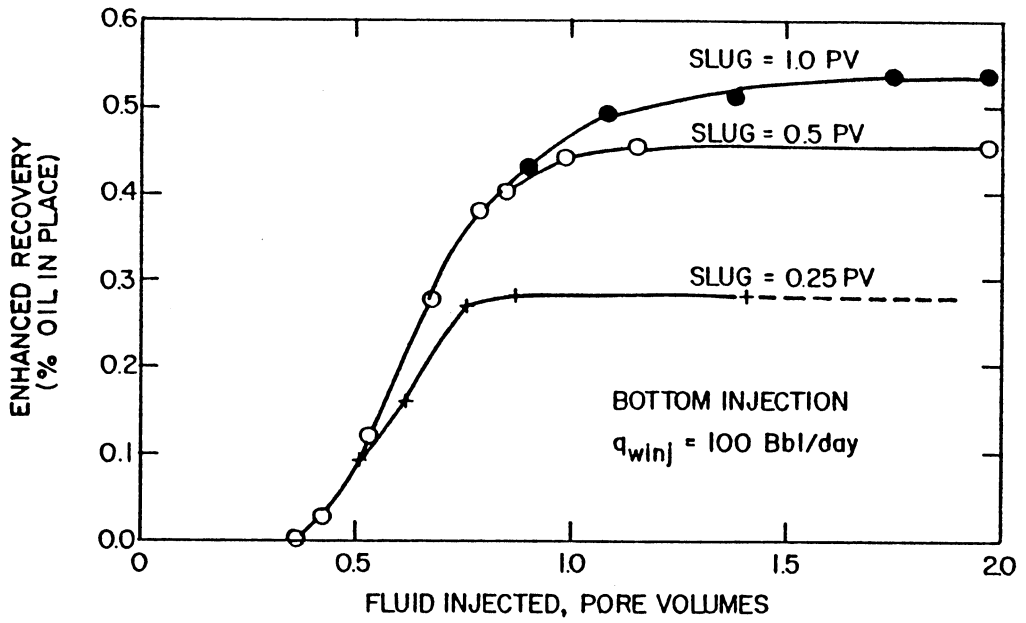

Fig. 7 Effect of surfactant slug size on enhanced oil recovery as function of pore volumes injected. C_o = 1.5 g/L

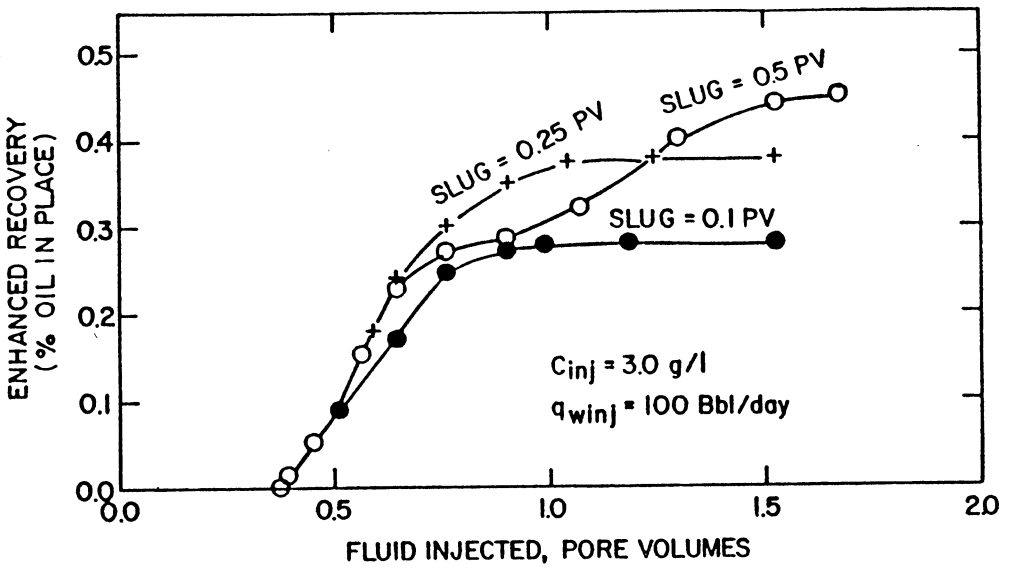

Fig. 8 Effect of surfactant slug size on enhanced oil recovery as function of pore volumes injected. C_o = 3.0 g/L

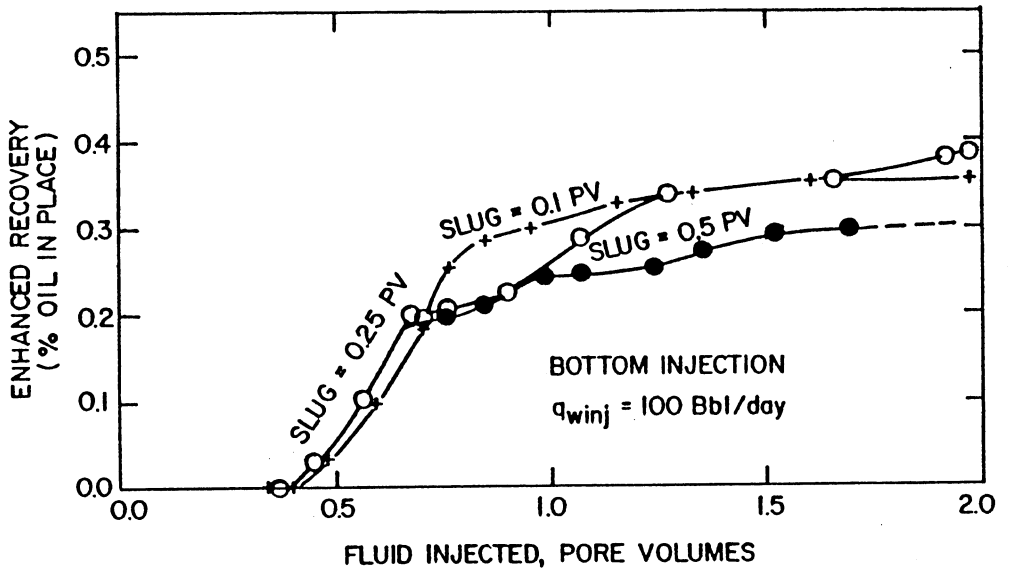

Fig. 9 Effect of surfactant slug size on enhanced oil recovery as function of pore volumes injected. C_o = 6.0 g/L

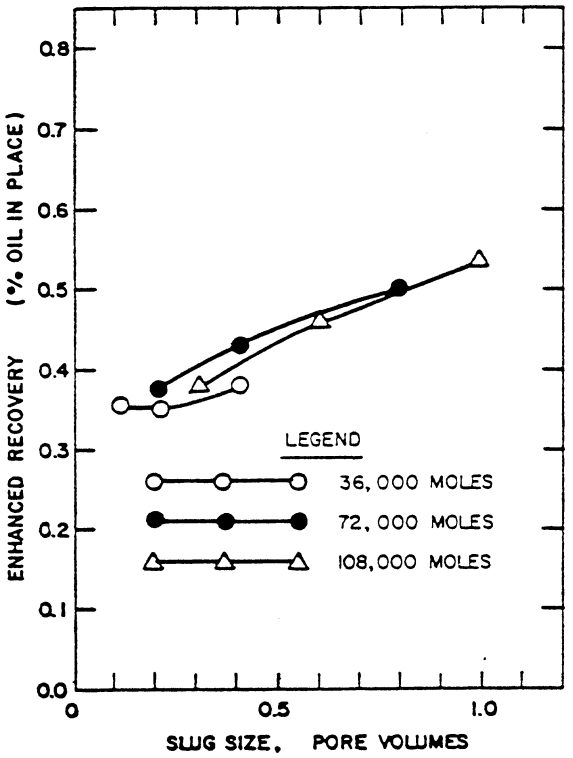

Fig. 10 Effect of amount of surfactant injected on enhanced oil recovery as function of pore volumes injected. qw_{inj} = 100 Bbl/day

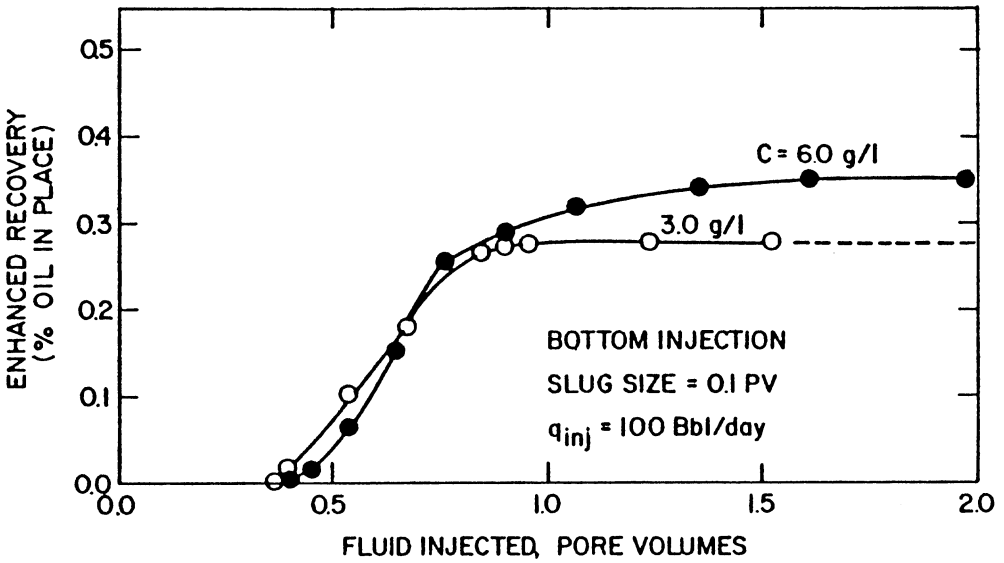

Fig. 11 Effect of surfactant concentration on enhanced oil recovery as function of pore volumes injected. Slug size = 0.1

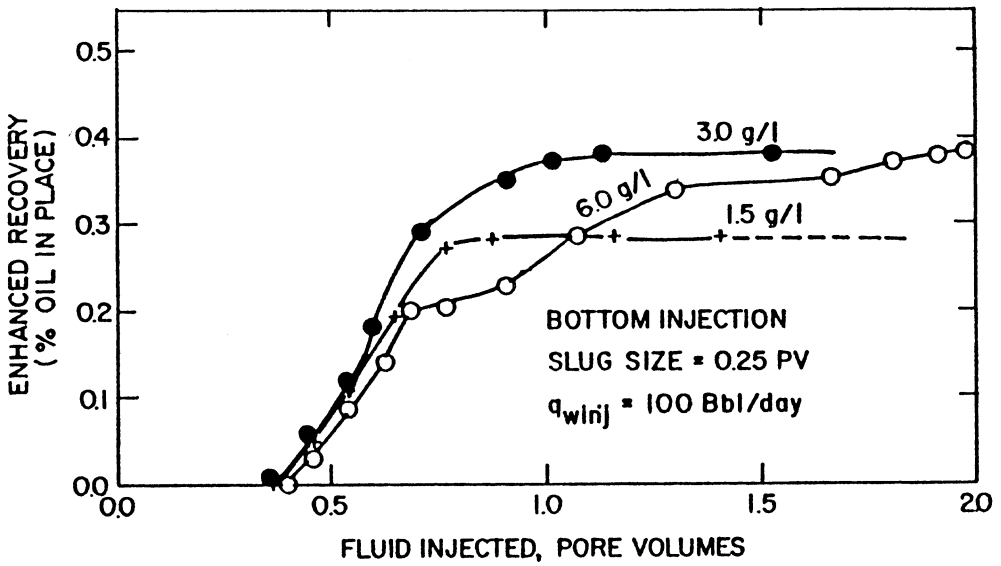

Fig. 12 Effect of surfactant concentration on enhanced oil recovery as function of pore volumes injected. Slug size = 0.25

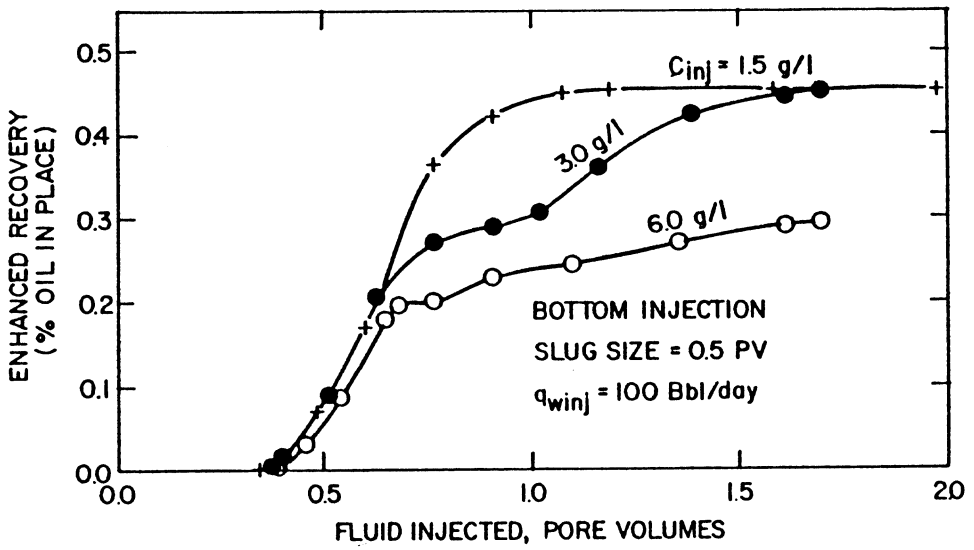

Fig. 13 Effect of surfactant concentration on enhanced oil recovery as function of pore volumes injected. Slug size = 0.5

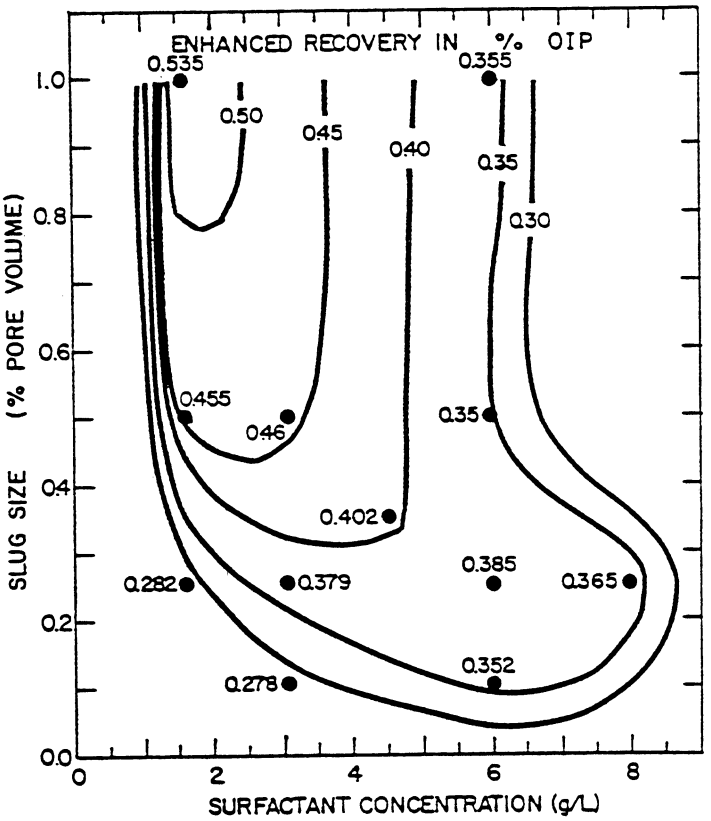

Fig. 14 Contour map of enhanced oil recovery as function of surfactant slug size and surfactant concentration. qw_{inj} = 100 Bbl/day

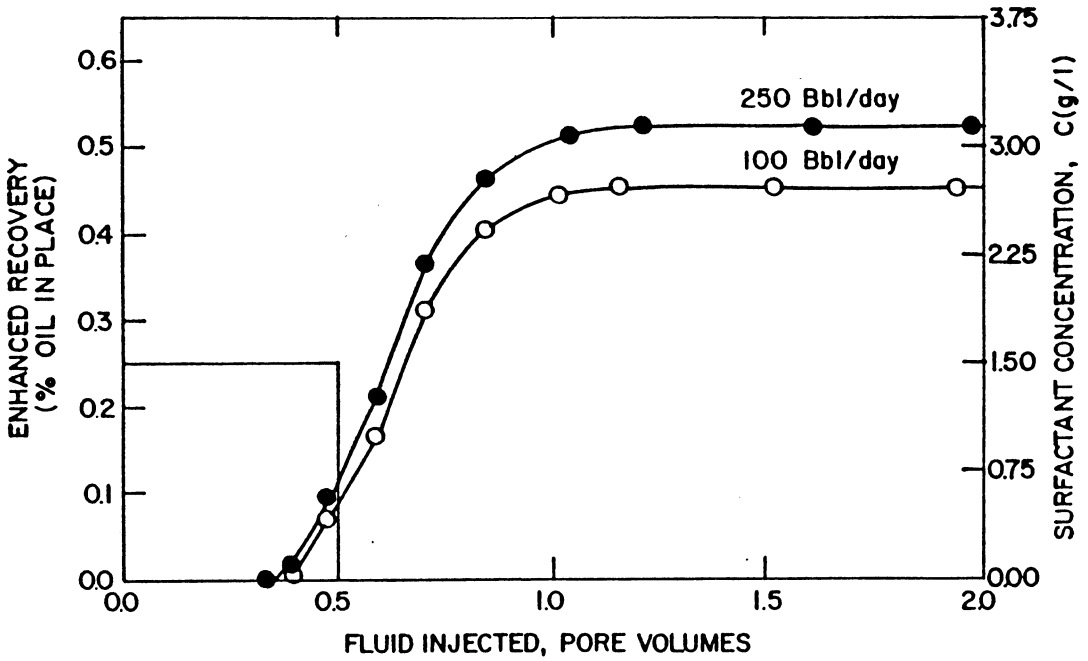

Fig. 15 Effect of injection rate on enhanced oil recovery as function of pore volumes injected. Slug size = 0.5, C_o = 1.5 g/L

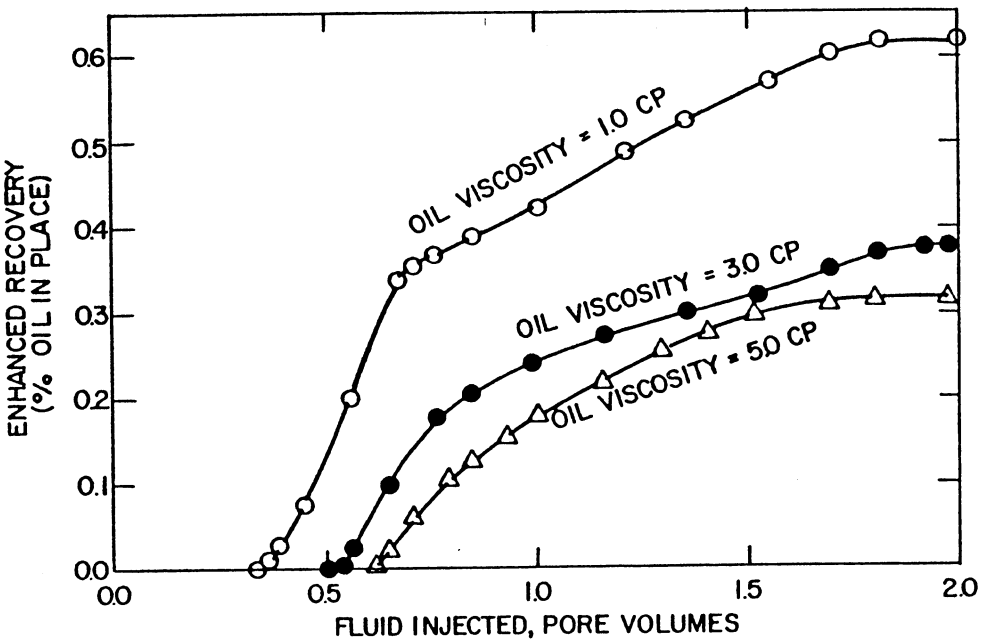

Fig. 16 Effect of oil viscosity on enhanced oil recovery as function of pore volumes injected. Slug size = 0.5, C_o = 3.0 g/L, qw_{inj} = 250 Bbl/day

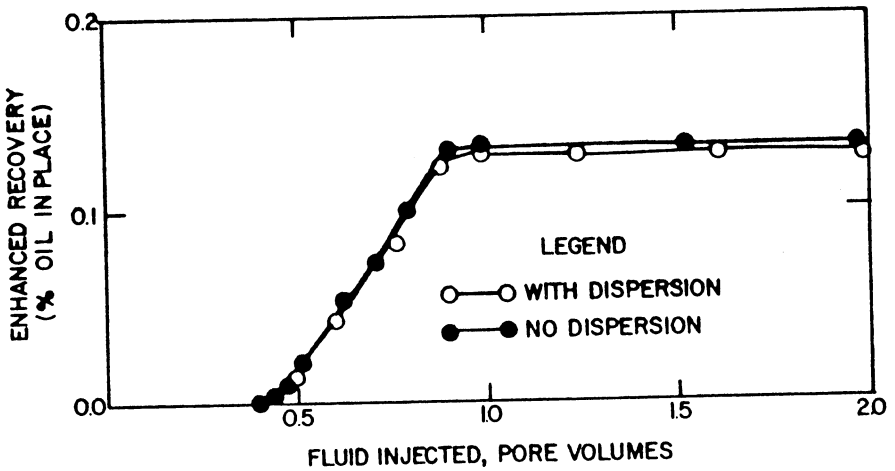

Fig. 17 Effect of surfactant dispersion on enhanced oil recovery as function of pore volumes injected. Slug size = 0.1, C_o = 1.5 g/L, qw_{inj} = 250 Bbl/day

FIELD DEMONSTRATION OF THE CONVENTIONAL STEAM DRIVE PROCESS WITH ANCILLARY MATERIALS

by

Rodney L. Eson
Chemical Oil Recovery Company for Petro-Lewis Corporation

ABSTRACT

Since steam injection became a viable recovery technique nearly three decades ago, the problems of gravity segregation and poor areal and vertical sweep efficiencies have limited recoveries in many heavy oil reservoirs. In many instances the injected steam prematurely breaks through into producing wells creating steam channels. It is believed that overall recoveries of a steam drive can be improved if the steam channeling can be controlled. This report documents efforts under a Department of Energy cost sharing contract to reduce steam channeling in a conventional steam drive using ancillary materials.

A steam foam solution and a steam foam encapsulated in a polymer gel are being introduced in four steam injection patterns in the North Kern Front Field near Bakersfield, California. The ability of the ancillary materials to improve recovery will be determined through injection profiles, chemical tracer surveys, casing vent gas analysis, core and log data, and residual oil saturation data, as well as through temperature and production data.

It has been shown that in-situ steam foams can be used to alter the steam injection profiles to prevent excessive steam channeling. The results of early production data have indicated that as much as 100 B/D of incremental oil is being produced by the four chemically treated patterns.

HISTORY OF PROJECT

The contract was initiated September 28, 1979, for completion by October 15, 1982. The total cost was estimated at $4,142,772 with DOE furnishing $2,508,813.

INTRODUCTION

Steam injection in the North Kern Front Leases, currently operated by Petro-Lewis Corporation, began in January 1978. Within a year a total of six producing wells had been converted to steam injection wells creating six 10-acre inverted nine-spot steam drive patterns which are fully developed with producers. Initially high injection rates of 850 B/D, combined with extreme variations in vertical permeability, adverse structural dip and an edgewater drive mechanism caused steam channels and premature steam breakthrough.

This early steam breakthrough was accompanied by a decline in oil production rates and an adverse steam/oil ratio. In an attempt to block the steam channels and improve oil recovery, two injection patterns were selected to receive periodic chemical injections of a steam foam (COR-180) and two injection patterns were selected to receive periodic chemical injections of a steam foam encapsulated in a crosslinked polymer gel (COR-GEL). A complete monitoring program, including the drilling of observation wells, was devised to determine the ability of the ancillary

Prepared for the Department of Energy under Contract No. DE-FC03-79SF10762

materials to improve the areal and vertical sweep efficiencies. The ultimate test, however, will be determined by the cost incurred to produce an incremental barrel of oil.

Steam Drive Problems

In the steam drive process, steam is continuously introduced into injection wells which theoretically propagates a steam bank through the reservoir to displace the heavy oil towards producing wells. When steam is injected into the reservoir, heat is transferred to the oil-bearing formation, the reservoir fluids and some to the adjacent cap and base rock. As a result, some of the steam condenses which yields a mixture of steam and hot water flowing through the reservoir. The composition of this mixture will depend on many variables such as radial distance from the wellbore, thickness of the reservoir, injection rate and quality of the injected steam.

The steam drive works by driving the water and oil to form an oil bank ahead of the steamed zone. Ideally this oil bank remains ahead, increasing in size until it is produced by the wells offsetting the injector. In addition to the movement of an oil bank, recoverability is increased due to the steam lowering the oil viscosity, thus improving oil mobility.

Displacement of oil by steam flooding is controlled by factors such as well spacing, reservoir heterogeneity, properties of the reservoir and crude oil, gravity segregation, reservoir pressure and temperature, relative permeabilities, steam quality, mobility ratio and fluid saturations in the formation. These factors contribute to the overall recovery, which is primarily dependent upon the vertical and areal sweep efficiencies experienced in the project.

The areal sweep efficiency depends primarily on two factors, the flooding pattern and the mobility ratios of the fluids in the reservoir. Mobility of a fluid is defined as the ratio of the permeability of the formation to a fluid divided by the fluid viscosity. Adverse mobility ratios which result promote fingering of the steam through the more viscous reservoir fluids and can reduce the oil recovery efficiency.

Vertical sweep efficiency of a process depends primarily upon the vertical distribution of permeabilities within the reservoir, on the mobility of the fluids involved and on the density differences between flowing fluids. In many cases, permeability stratification has a dominant effect on behavior of the steam flood.

In addition to reservoir heterogenities, gravity segregation is usually a serious problem. Hot water which separates from the injected steam tends to sweep through the bottom portions of the heated interval while the steam vapor tends to override the hot water because of differences in densities of the two fluids.

Field Description

The North Kern Front Leases, currently operated by Petro-Lewis Corporation of Denver, Colorado, are located approximately eight miles north of Bakersfield, California, in the San Joaquin Valley, where 80 percent of the United States' thermally recovered oil is produced.

The properties have been heavily developed since the introduction of cyclic steam stimulation in 1969. At this time there are approximately 180 wells completed on the Petro-Lewis Corporation North Kern Front properties, with the majority of the steam floodable sections drilled on 2.5 acre spacing. When existing production wells were converted to injection wells, 10 acre inverted nine-spot patterns were created. The main productive sand is the Chanac of Upper Miocene age, however Etchegoin sands of Pliocene age are evident.

The characteristics of the reservoir lend themselves very well to cyclic stimulation and steam displacement processes. With an average net sand thickness of 42'-52' the project area contained nearly 3,344,000 barrels of oil in place at the beginning of the field demonstration. The 13° API oil is extremely viscous with small volumes of gas produced in conjunction with the crude. High porosity (33%) and original oil saturations of 64% yield 1640 barrels of oil per acre-foot originally in place. Permeabilities average approximately 2210 md, but can vary from 15 to 12,000 md in a single producing interval. The trapping mechanism of the reservoir is a structural-fault with an edgewater drive.

TREATMENTS

To properly study the effects of the ancillary material additives to the conventional steam drive process, six steam injection patterns were selected (FIGURE 1). Each pattern contains eight producing wells and encompasses 10 acres. Two patterns (Mitchel 65 and Witmer B2-3) are treated with sequential slugs of steam foam (COR-180) and two patterns (Mitchel 63 and Witmer B2-5) are treated with sequential slugs of steam foam-polymer combination (COR-GEL). The remaining two patterns (Mitchel 67 and Witmer A2-7) will remain untreated and shall be referred to as control patterns.

Even though the severity of the existing steam channeling in the two COR-180 steam foam treatment wells varied from extremely severe (Witmer B2-3) to moderate (Mitchel 65), it was decided that the initial steam foam treatment size (or slug size) would be the same in each. An initial treatment size of 110 gallons per week of aqueous solution of COR-180 was selected. This aqueous solution, containing approximately 60% active foaming agents, is injected into the injection well at the wellhead using small injector pumps at rates between 2.0 and 2.5 gallons per minute. The vapor phase of the steam present at the wellhead begins to react immediately with the aqueous solution, thus initiating the in-situ foaming process.

The steam containing the foaming agent being injected is entering high permeability areas and as the foaming process continues it begins to decrease the permeability in the channels. When the permeability of this previously high permeable zone decreases sufficiently, the steam will then enter other portions of the injection interval. Since these sections have not been adequately swept by the steam they will be higher in oil saturation and thus improve the recoverability of the steam drive process through improved vertical sweep efficiency.

After breakthrough, the steam travels to the producing well(s) according to the paths of least resistance. Once the foam has been activated in-situ it begins diverting the steam which follows the treatment slug into normally lesser permeable zones. Again the steam will seek the paths of least resistance, which could be (and hopefully will be) an alternate producing well in the pattern, thus improving the areal sweep efficiency of the pattern.

The steam foam used (COR-180) in the first two test patterns is designed to begin breakdown after approximately three to five days. As it breaks down it once again becomes an aqueous solution. This solution moves along with the steam drive products and is produced at the producing wells. This liquid by-product is completely biodegradable and thus will not cause any adverse effects upon the environment. In addition, no emulsion or other treating problems have been experienced. The first slug treatment of COR-180 steam foam was injected on January 21, 1980, in Mitchel 65. The second steam foam well, Witmer B2-3 began slug treatments on March 11, 1980.

Since the steam foam reacts almost immediately when it contacts the vapor phase of the steam, a delaying action is required if an attempt is to be made to displace the steam foam further into the reservoir. To delay the foaming action until the steam foam is approximately 15 feet into the reservoir the steam foam (COR-180) is mixed with a crosslinked gel solution of CMC-9 (carboxymethyl cellulose with a number 9 substitution factor). The polymer coats the steam foam preventing activation until the gel begins to break down due to the extreme temperatures of the steam drive. The COR-GEL is injected in the injection well at the wellhead in the same manner as the COR-180. Weekly slugs of 165 gallons of COR-GEL began in March 1980 for Mitchel 63 and in May 1980 for Witmer B2-5.

FIELD DATA COLLECTED

Production/Temperature Data

To better understand the data collected, the physical positioning of the injection patterns should be explained. The field demonstration project is divided into two separate sets of patterns (FIGURE 1) with three injection wells in each set. One set of patterns is referred to as the Mitchel patterns and the other as the Witmer patterns. Each set is comprised of 18 producing wells and 3 injection wells with each injection well serving 8 first line production wells.

The primary objective of any steamflood is to maximize production while controlling operating costs. One of the key factors to watch during a steamflood is the producing wellhead temperatures. For this reason, prior to any treatments the production rates and producing temperatures for the two groups of steam injection patterns were obtained and plotted. Two items were found to repeat throughout each of the patterns.

First, there does not appear to be a significant amount of steam (heat) moving to the west from the injection wells. In every instance there is a significant temperature increase in the producing well directly to the east of the steam injection wells. Second, is that severe casing blow and specific temperature increases indicate that steam has already begun to channel; thus, reduced sweep efficiencies are being experienced.

In the group of steam injection patterns on the Witmer leases some steam is moving in the north and south direction from the injectors. This is evidenced by the elevated temperatures found in producing wells Witmer B2-2 (210° F), Witmer B2-4 (210° F) and Witmer A2-8 (110° F). The exact quantity and direction of the injected steam, however, cannot be determined by production and temperature data alone - tracer surveys must be obtained and analyzed in conjunction with core data.

To understand the data obtained, an in-depth reservoir structural study was completed. The log data were collected and several sets of cross sections were created to better understand the reservoir and steam flow. In both groups of patterns there is between 30 and 55 ft. of vertical subsea variation in the formation between adjacent wells in the east-west direction, with the easterly wells being located upstructure. The vertical variation in the north-south direction varied less than 5 ft. in adjacent wells. The heavy structural updip to the east and the fact that water is encroaching from the west substantiates the conclusions regarding reduced sweep efficiencies based on production and temperature data.

Chemical Tracers

To determine the steam path in each injection pattern prior to any chemical treatments, it was necessary to run a chemical tracer survey on each injection pattern. Produced fluid samples from each production well in every injection pattern were taken (total of 36 wells) and analyzed for background element levels of nitrate, bromide, iodide, and thiocyanate. Once these levels were established, the proper amount of tracer chemical (sodium nitrate, sodium bromide, sodium thiocyanate or potassium iodide) for each injection well was determined and introduced into the steam injection well. Produced fluid samples were then taken at predetermined intervals and analyzed for the element ion(s) introduced into the injection wells. The background level of each element ion was subtracted from these levels, and the data were tabulated and plotted. In June and July 1980 (four months after treatments had begun) the second set of chemical tracer surveys was obtained on each pattern according to the same method previously described. The ion concentration versus time plots vary slightly from the pretreatment tracer surveys, but it is too early to determine if any significant changes in areal sweep efficiencies have occurred.

Injection Profiles

During October and November 1979, the first injection profile for each of the six injection wells was obtained using both gas and water soluble radioactive Iodine (I-131). These profiles were used to establish injection data prior to the use of ancillary materials in the test patterns. The profiles brought to light several details that will be beneficial in establishing overall project sweep efficiencies. In the Kern Front reservoir there are a number of "lens-type" sands making up the body of the Kern Front oil sand. These lenses are in some areas separated by shale and in other areas are overlapping such that they appear as one sand. The injection profiles indicate that each lens (when present in the injection well) accepts the steam at a different rate. If unaltered by the ancillary material, the steam entering only one of the lenses will quickly deplete that lens while not reducing the residual oil saturation in the other lenses.

Additional injection profiles obtained indicated that there is definite vertical movement of the injected steam after a slug treatment of the diverting agents. The profile alteration lasts a minimum of two days, but the elevated injection pressures give credence to the idea that the foam continues to divert further from the wellbore for up to a week.

A series of injection profiles was obtained in June 1980 on Mitchel 63 injection well. An injection profile of steam was obtained prior to a slug treatment of 165 gallons of COR-GEL, followed by daily injection profiles until the profile returned

to the pretreatment mode. The profiles indicate a definite change in the injection profile after a slug treatment, thus improving the vertical sweep efficiencies. It was noted that injection pressures remained above normal even after the injection profile returned to the pretreatment mode. This indicates that the COR-GEL is still acting to divert the injected steam deeper in the formation but is not active directly at the wellbore.

Casing Vent Gas Measurements

In mid-September 1979, operators of steam drive projects were required by the California Air Pollution Control Districts to monitor casing vent gas emissions in an effort to comply with new air quality regulations. Data collected on first line producing wells were used to design proper casing vent recovery systems. Analysis of these data indicated that the rates and constituents of the gases evident at the casing vents had a direct relation to the efficiency of the steam drive in progress. More precisely, it helped to identify existing steam channels.

These tests will be repeated several times throughout the life of the field demonstration. The exact frequency and scope of the test will be adjusted during the demonstration in an effort to maximize data collection but minimize costs.

WELL COMPLETIONS

Production and Injection Wells

Production conditions in unconsolidated sands, present in the operator's North Kern Front Field, usually require gravel packed open hole completion with slotted liners. The average depth of the wells is 1570 feet and normally can be drilled and completed with 7" casing and $5\frac{1}{2}$" liner in three and one-half days.

The injection wells were converted from production wells. To convert the well to injection the surface equipment, the subsurface pump and the rods are removed. In addition, a thermal packer is run on the tubing and set in the 7" casing approximately 2'-5' above the top of the port-collar adapter on the liner. This prevents the upper portion of the casing and casing cement from being under continual thermal stresses which could cause damage and require a workover or shutting in the well.

Observation Wells

In an effort to properly determine the effects of the ancillary materials to steam on the vertical and areal sweep efficiencies, it was decided that observation wells would be drilled and monitored. The best method for determining the effectiveness of the processes tested is by observing the changes in oil saturation with time. To accomplish this the following plan was established:

1) Determine observation well locations.
2) Prepare drilling programs and obtain government permits.
3) Drill to the top of the steam flood zone.
4) Core through the steam flood zone.
5) Obtain open hole logs.

6) Run casing.
7) Obtain cased hole Carbon-Oxygen Logs.
8) Repeat cased hole logs every 3-5 months.
9) Drill final data wells adjacent to observation wells (at end of 3 years).
10) Core final data wells through the steam flood zone.
11) Obtain open hole logs.
12) Correlate final data with initial data and periodic Carbon-Oxygen data.

After review of the pretest data, specifically chemical tracer, water influx, and structural maps, it was determined that it would be virtually impossible to divert a significant amount of steam in the westerly direction. Therefore, the six observation well locations were selected to encompass a 180° sweep from north to south through the east. One observation well per injection pattern was drilled in a direct line between the injection well and a producing well, one-third the distance to the producing well. One observation well was drilled to the north, one to the south, one along the north-east diagonal, one along the south-east diagonal, and two to the east of the injection wells. The observation well drilling phase of the project was completed prior to the first chemical slug injections.

CORING AND LOGGING OF OBSERVATION WELLS

Cores

Conventional cores and sidewall samples were taken through the entire producing interval (42'-52' Net). A polymer base mud was used for minimal core infiltration and flushing. Initial coring was attempted with a drag bit, but less than desired recovery and excessive rig time prompted the decision to try a specially designed rock bit. This bit, combined with extreme care in operating pumps and monitoring of bit weights, improved recoveries of these unconsolidated sands to nearly 90%. Previous attempts at coring in this area showed recoveries below 35%.

A direct comparison of core samples and sidewall samples was obtained on each of the observation wells. Almost without exception the permeabilities obtained from the conventional core samples were 2-3 times greater than those obtained from sidewall samples. Oil saturations obtained from the sidewall samples were 5-10% below the oil saturations obtained from the conventional core samples. Porosities remained very close, but sidewall analysis was slightly lower than conventional analysis.

Open Hole Logging

The following open hole logs were obtained: Dual Induction, Compensated Neutron, Compensated Density, Gamma Ray, Dielectric and Temperature.

Cased Hole Logging

To monitor the change in residual oil saturation during the life of the field demonstration, Carbon-Oxygen Logs will be obtained every 3-5 months. The Carbon-Oxygen Log employs a 14 mev (million electron volts) neutron source and a receiver in the logging tool which measures the energy output from the carbon and oxygen nuclei as they are bombarded by the high-energy neutrons.

INITIAL PRODUCTION RESULTS

Review of the injection pattern production curves (FIGURES 2 through 7) shows that since the beginning of the ancillary material addition to the steam in the four treatment patterns between 9,500 and 16,500 incremental barrels of oil have been produced. The figures of incremental oil vary widely due to the fact that the decline curves are difficult to project caused by the short time interval being evaluated. It is certain that between 50 and 100 barrels per day of incremental oil were produced during the month of August 1980.

Both patterns being treated with COR-GEL (Mitchel 63 and Witmer B2-5) have responded exceptionally well. The treatment chronology data records indicate a good (20-60 psi) injection pressure increase during each treatment. In addition, the established decline curve was arrested within 30 days of the initial slug treatment of COR-GEL and production is continuing to increase each month. With incremental production of these patterns possibly over 70 BOPD (FIGURES 2 and 6) and the current reduced injection rates the profitability of these patterns has improved dramatically.

In August through September, 1980, Witmer B2-3 pattern has begun to show a substantial amount of incremental oil (FIGURE 5). In March 1980, weekly slug treatments of COR-180 began. Almost immediately the injection rates were decreased. The treatment chronology indicates adequate pressure increases to properly divert the steam. Injection profiles, however, give rise to the possibility of over treatment (the treatment slugs were based on the higher injection rates). To evaluate this possibility the slug size was reduced by 50%. Pressures and production will be monitored in an effort to evaluate this change.

The second well being treated with COR-180 is Mitchel 65. Immediately following the initial treatments production began to increase (FIGURE 3). In April 1980, the injection rates were severely reduced and the production returned to the original decline curve. According to the treatment chronology report through August 1980, it did not appear as though there was adequate steam quality at Mitchel 65 to activate the foam at the lower injection rates. A physical observation made at this injection well substantiated this suspicion. When standing next to this well liquid could be heard flowing through the flow line. A new (much shorter) flow line was installed near the end of September and the quality of the injected steam has improved considerably.

The control pattern, Mitchel 67, has been in a steady production decline (FIGURE 4) during 1981 and in October 1980 is 83 BOPD for the 8 producing wells. Knowing that the residual oil saturation in Mitchel 67M observation well was found to be greater than 60% there is a considerable amount of residual oil in this pattern.

It is extremely difficult to define a specific decline rate for control pattern Witmer A2-7 because steam injection was stopped for nearly 5 months (hole in casing) causing an abnormal production decline (FIGURE 7). Then after steam injection resumed in May 1980, the production responded positively. A new decline trend is expected to be noticeable within a year.

CONCLUSIONS

1. The North Kern Front reservoir is susceptible to the same basic problems as other steam driven reservoirs: namely, gravity segregation and poor areal and vertical sweep efficiencies.

2. Ancillary materials can be used in conjunction with the conventional steam drive process to augment production.

3. The ancillary materials being evaluated do not adversely affect normal production, water treating or oil treating procedures.

4. A steam foam can be encapsulated in a polymer gel for better penetration into the reservoir without adversly affecting the foaming properties of the steam foam.

5. Steam foams can sucessfully alter the injection profile of steam injection wells for several days after injection of the steam foam, giving credence to the suspicion that foam can be created in-situ, relying on the vapor phase of the steam to activate the foaming process.

6. Casing vent gas emissions caused by severe steam channeling can be decreased, and possibly even eliminated, when reducing the steam flow in the channels through the introduction of steam foams.

7. Variations of residual oil saturations with time can be monitored in observation wells in the steam drive pattern through periodic Carbon-Oxygen cased hole logs.

8. Based on early economic evaluations, the use of ancillary materials in a steam drive is encouraging enough to continue the injection treatments and data monitoring as described in this paper.

REFERENCES

1. Ali, S. M. Farouq and Meldau, R. F.: "A Current Appraisal of Steam Injection Field Projects," SPE 7183.

2. Clampitt, R. L.: U. S. Patent No. 3,993,133.

3. Fitch, Jon P. and Minter, Rick B.: "Chemical Diversion of Heat Will Improve Thermal Oil Recovery," SPE 6172.

4. Needham, R. B.: U. S. Patent No. 3,412,793.

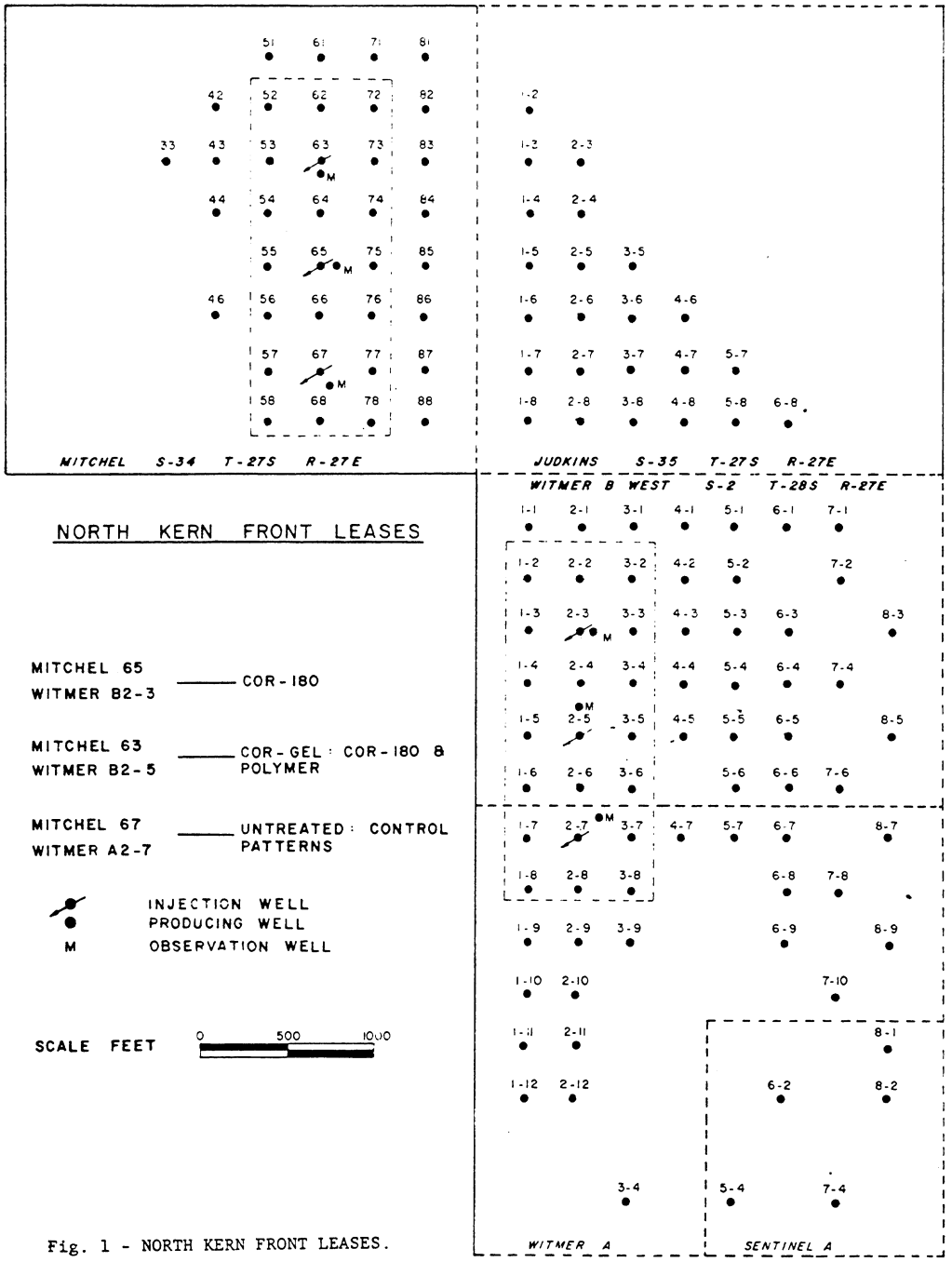

Fig. 1 - NORTH KERN FRONT LEASES.

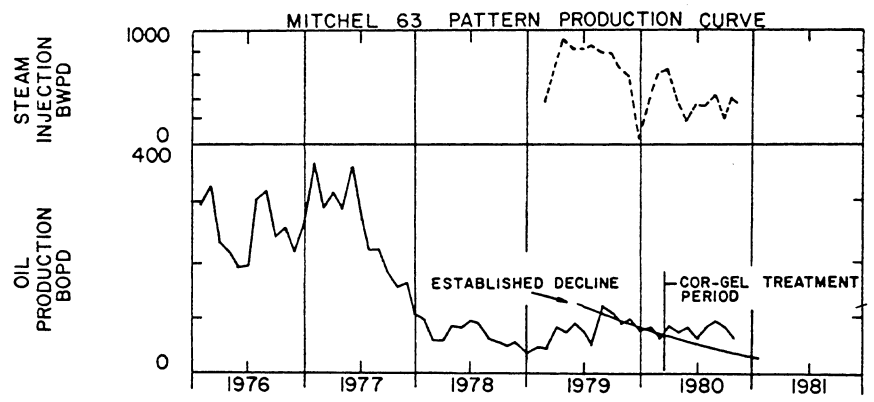

Fig. 2 - MITCHEL 63 PATTERN PRODUCTION CURVE.

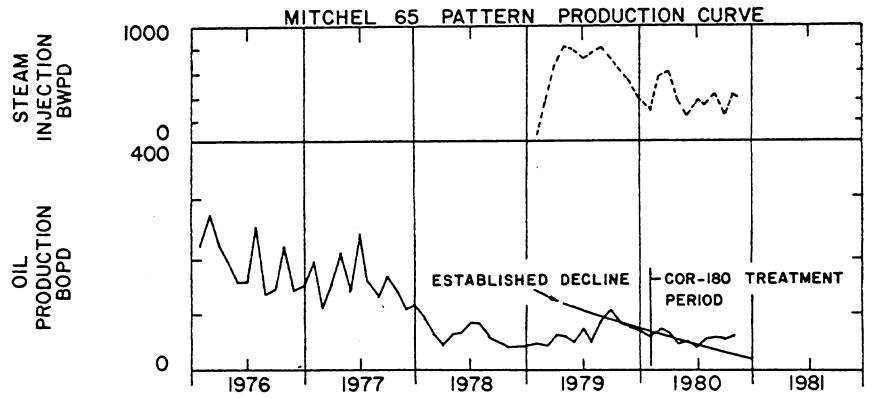

Fig. 3 - MITCHEL 65 PATTERN PRODUCTION CURVE.

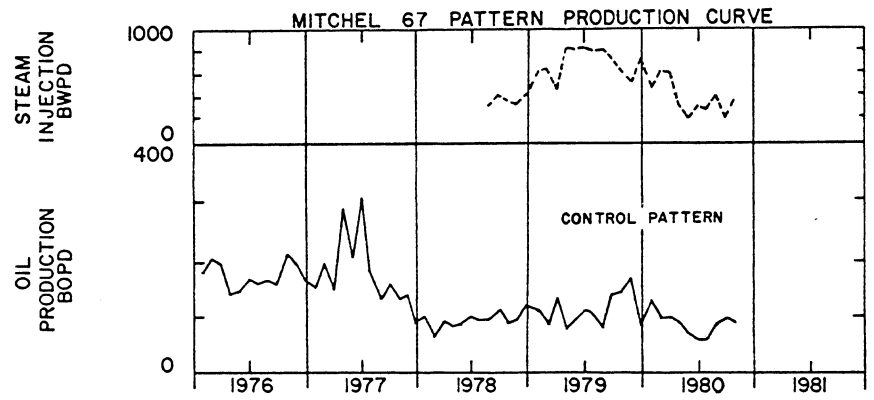

Fig. 4 - MITCHEL 67 PATTERN PRODUCTION CURVE.

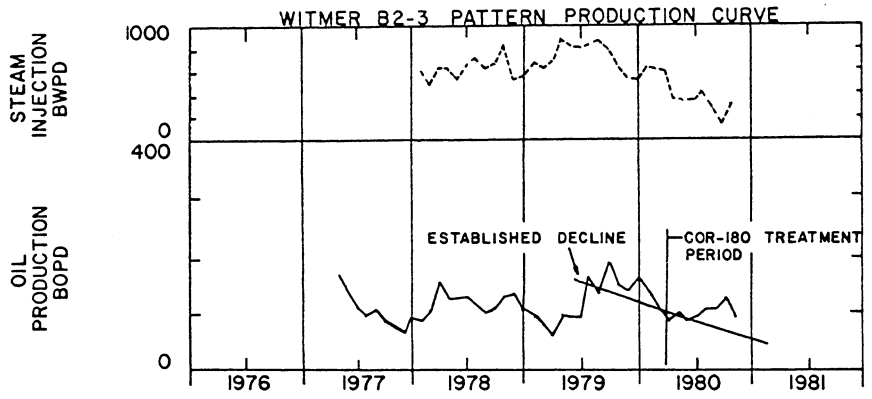

Fig. 5 - WITMER B2-3 PATTERN PRODUCTION CURVE.

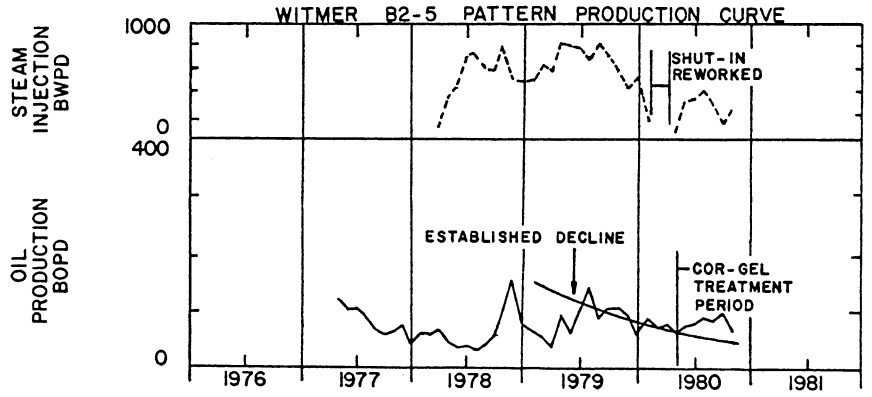

Fig. 6 - WITMER B2-5 PATTERN PRODUCTION CURVE.

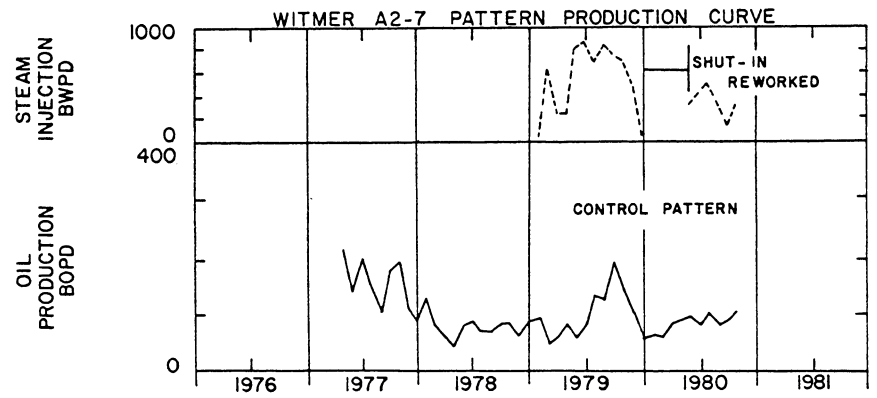

Fig. 7 - WITMER A2-7 PATTERN PRODUCTION CURVE.

FIELD DEMONSTRATION OF STEAM DRIVE

WITH ANCILLARY MATERIALS

CLD GROUP INC.

BY

T. M. Doscher, R. W. Bowman and C. G. Horcher

ABSTRACT

CLD Group, Inc. is conducting field demonstration tests together with DOE on the use of ancillary materials to improve the efficiency of conventional steam drive. During the past year, laboratory tests were conducted to identify surfactants with the best blocking potential, as well as optimum techniques for injecting the foaming materials. The first field test of foam injection using a 5-spot pattern in the Midway Sunset Field is complete. Radioactive tracers were employed to determine the extent of the thief zone before and after injecting surfactant.

HISTORY OF PROJECT

This two-year project was initiated October 1979 for the purpose of conducting five field tests using channel blocking foams. The cost of the project was $2,923,680 with DOE paying $1,748,680.

I. INTRODUCTION

The CLD Group Inc. entered into a contract with the United States Department of Energy to test the applicability of foams to effect some degree of mobility control and/or permeability reduction of injected steam in steam drive operations.

The entire project is to comprise five individual tests. At this time final arrangements have been made with Santa Fe Energy to conduct two tests in the Midway Sunset Field, with Conoco for one test in the Cat Canyon Field, and with Texaco for two tests in the San Ardo Field.

The test locations were chosen so that the two major reservoir problems that are encountered in steam drive operations were to be addressed: the transmission of steam through "thief" zones or other channels that exist at the outset of initiating operations, and the progressive increase in channelling of steam through the oil-depleted, steam swept zone.

The initial laboratory testing was aimed at screening foam chemicals for thermal stability, and later was concerned with the emplacement of the foam systems in porous media. The final bench tests were done in a sixteen foot sand pack in order to verify the compatibility of the emplacement techniques and the chemical system itself in effecting a significant measure of mobility control to injected steam. The work with these systems has been reported in the Annual Report and in SPE/DOE Paper 9777 presented at Tulsa, April 1981.

Prepared for DOE under Contract DE-FC03-79SF10761

Additional laboratory work will be done to attempt to optimize the process following the evaluation of the early field results. Some of the optimization work will involve the addition of polymers and other additives to seek greater longevity to the effected mobility reduction. The first field test at Midway Sunset is now completed, and testing has begun at the Conoco site. The second Midway Sunset test will be started in late June, and the Texaco tests in late summer.

II. PROCESS CONCEPT

The initial concept of the way in which the foams might work to control the mobility of injected steam was abandoned when it was appreciated that a foam in which the gaseous phase was steam could not be considered a stable system. Heat losses would of course result in the collapse of the foam, and constant rejuventation would be required. This was confirmed by laboratory work, and as a result it was necessary to reformulate the systems including a non-condensible gas.

Also, the initial concept of the process was based on emplacing a foam of sufficient stability and resistance so that the channel would be more or less completely blocked. However, reviewing the way in which steam effects displacement of oil, it was obvious that if such complete blocking occurred the displacement of oil would cease. It would be necessary to establish another interval into which to inject steam since permissible injection pressures do not permit the frontal displacement of heavy oil. Hence, it was now apparent that the foam had to contain some non-condensible gas and in addition be co-injected or serially injected with steam. The basic goal is to effectively increase the viscosity of the steam, and thus retard its flow through existing channels.

Although eventually cost competitive supplies of nitrogen were located, initially air had to be used as the non-condensible gas because of availability and cost. Steam and air cannot be injected simultaneously because of the potentially dangerous corrosive environment resulting from such a combination. Hence, when using air the foams had to be injected as slugs alternating with steam. When eventually nitrogen supplies were obtained; continuous, simultaneous injection of foams and steam became possible.

Thus, the initial test at Midway Sunset employed alternating slugs of air-based foams and steam. It was anticipated that increases in well head (injection) pressure would give an early indication of the effect of the foam on reducing the mobility of steam. The ultimate measure of success, of course, being an increase in oil production rate or marked decrease in the water cut at the immediately offsetting producing wells.

III. MIDWAY SUNSET TEST NO. 1.

The location and subsurface features of the test location have already been described in previous project reports.

A. FACILITIES PROBLEMS

The initial test location was reputed to be beset with a channeling problem resulting from naturally occurring intervals of high permeability. Several unexpected problems in equipment and procedure arose immediately. These ranged from the delivery of hardware (the compressor) to difficulty in pumping the viscous foam chemicals. The chemical was therefore diluted with water to form a 6% (2.5% active) solution and co-injected with steam. Extreme hammering occurred at the well head because of the condensation of steam when contacting the cool solution. This was corrected by installing a heat exchanger at the well head to raise the temperature of the aqueous solution of the chemical. Problems were also encountered in controlling the steam injection rate to the one experimental well when several other wells were on line at the same time. Eventually, the facilities problems were all corrected or controlled well enough for the test to proceed.

B. THE INITIAL TEST PROCEDURE IN THE MIDWAY SUNSET FIELD.

Initially, it was intended to monitor the progress of the foam injection test by monitoring the pressure required to maintain injection at the well head. However, the supply of steam at the well head was not sufficiently steady to permit using the well head pressure as a guide to reservoir response.

Therefore, reliance had to be put on the measured water cuts, the temperature profile surveys run before and after the test, and the oil production at the wells offsetting the central injection well of the pattern. Oil production from these pattern wells has been quite erratic and here too it soon developed that it would be possible to use oil production data as a guide to the effectiveness of the foams only if something like three months moving averages were employed. Since the historical data was not in a form that permitted this to be done quickly, the only immediate guide to reservoir response is the produced water cuts. (The three months moving averages will be developed for the next report.) Subsequently, the comparison of the before and after temperature profile surveys shed further light on the activity of the injected foams.

The procedure ultimately adopted for injecting the foam comprised injecting a slug of twenty barrels of the diluted surfactant (see above) into the steam flow line while continuously injecting steam, then shutting down the steam flow and injecting air at the rate of 420,000 SCF/Hr. for a period of one hour. Finally, steam injection was resumed.

An increase in well head pressure ıe order of 50 psi. was usually observed following the injection r and the resumption of steam injection. The dosage was repeated fourth day if steam was available; otherwise on the first day ther that it was again made available.

Because of the unsteady delivery of steam to the well head, it was not feasible to monitor the progress of the test by analsis of the history of the well head pressure; water cuts and oil production were the only parameters that could be used for evaluating the test performance.

C. THE WATER CUTS IN OFFSETTING WELLS

Figures 1 and 2 show the location of the pilot operation and arrangement of the wells in the pilot pattern. Pre-pilot studies indicated that wells 194 and 23 were the principal wells towards which steam was flowing from the injection well, 590.

The data in Table 1 records the water cut from the four offsetting pattern wells. A marked effect is observed on wells 194 and 23, the two wells that had been showing the greatest response to steam injection. Both of these wells also showed a signficant amount of nitrogen (residual from the injected air) breakthrough although the measurements of nitrogen production were not made sufficiently routinely to demonstrate any unique juxtaposition of increased nitrogen content and changes in the water cut.

The other two pattern wells, 24 and 194, did not show any significant change in water cut. Well 24 did show a nitrogen blow, however, and did show some increased oil production after the nitrogen appeared in January.

D. OIL PRODUCTION

As already noted, the oil production from the pattern wells was far too erratic for single measurements to have too have much significance. However, as seen in Table 2 the oil production from Well 194 did increase markedly in April and May, and both Well 24 and Well 23 showed signficant, but somewhat less marked increases in oil production during the same period. Well 209, which showed no affect of the foam injection as judged by water cut or nitrogen breakthrough, showed a small, probably statistically unreliable, drop in production.

E. TEMPERATURE RESPONSE

The temperature response in Wells 23 and 194 were very marked as a result of the foam injection. Well 23 exhibited a broadened zone of high temperature, expanding from approximately 50 feet to 150 feet following the injection of the foam, see Figure 4. In Well 194 the high temperature band had already covered the entire interval before the injection of the foam, but afterwards was found to have risen approximately 20°F., to over 260°F., Figure 5.

The 75 feet of the producing zone that had already been affected in

Well 24 showed a marked increase in temperature, increasing over 50°F. to over 320°F. The observed increase in oil production from this well, despite the absence of a change in water cut, is apparently in keeping with this marked increase in bottom hole temerature.

It is to be noted that the two wells which were affected by the foam injection were also the two wells which showed major response to injected fluid before the foam job. Well 23 is definitely up-dip of the injection well, but 194 appears to be on strike. Well 24 is downdip and 209, again, is on strike. Hence, there doesn't appear to be any singular structural control to the direction away from the injector which was primarily affected by steam injection.

However, Wells 60 and 294, one location removed from the pattern producers, and somewhat updip from the injector continued to show significant nitrogen production for a month or two after ceasing the injection of air into Well 590 although the production of nitrogen from the pattern wells stopped almost immediately (within less than the month between successive readings) after air injection was halted. There is a suggestion in these observations that the flow of nitrogen towards Wells 60 and 294 caused the diversion of steam to the closer wells, 23, 24 and 190. The production data from the outside pattern wells is inadequate for any conclusion to be reached on this matter at this time.

F. PLAN FOR TEST NO. 2 IN MIDWAY SUNSET FIELD.

Larger quantities of the chemical and larger quantities of air will be used on the forthcoming test at Midway Sunset. It will be initiated in late June.

IV. CAT CANYON TEST

This test, on the Conoco lease in the Cat Canyon Field is still in progress at the time of preparing this report. The project area is shown in Figure 8, and the wells immediately surrounding the test injection well are shown in Figure 9. Figure 10 is a composite log of the section, and Figure 11 shows the presence of the heated (thief ?) zone at the well closest to the injection well.

A. TEST PROCEDURE

During the first 12 days of the test, 560 gal of 10v.% aqueous solution of Thermophoam BW-D was injected along with a slug of nitrogen that averaged about 8,000 SCF. This was followed by the continuous injection of nitrogen and steam at an average rate of 75 SCF of the former and a constant daily rate of steam injection of 300 B/D. The steam quality during this entire period averaged about 82 %, and varied between 78 % and 88 %. During a final 7-day period, the size of the surfactant slug injected each day was half of the earlier slug volume, or 280 gal, and the continuous injection of nitrogen was also reduced to about 50% of the previous rate.

TABLE I

WELLHEAD TEMPERATURE AND WATER CUT

DATE (1980)	WELL # 194-21N		WELL # 23-21N		WELL # 209-21N		WELL # 24-21N	
	TEMP. °F	WATER % v/v	TEMP. °F	WATER % v/v	TEMP. °F	WATER % v/v	TEMP. °F	WATER % v/v
10/9	220		142		118		216	
10/10	220	80	142	84	116	97	214	99
10/11	220		142		116		212	
10/12	220		140		116		210	
10/13	220	82	140	84	116	96	210	98
10/14	215	72	134	19	114	98	210	97
10/15	210	83	130	71	114	99	205	99
10/16	210	82	128	70	114	99	205	99
10/17	208	82	126	72	113	99	205	99
10/20	212	91	126	57	113	99	213	99
10/21	218	75	124	64	111	99	203	100
10/22	228	85	125	61	112	99	216	99
10/23	225	93	124	60	112	99	214	99
10/24	220	85	124	62	112	99	210	99
10/27	212	77	123	58	112	99	213	99
11/5	234		134		110		220	
11/7	232		144		110		222	
11/10	233		134		108		220	
11/11	234	97	129	55	108	99	220	99
11/12	234	92	128	54	108	98	215	99
11/13	232	94	132	78	108	99	214	99
11/14	230	99	134	60	108	99	214	99
11/17	225	86	140	72	110	99	218	96
11/18	225	98	140	80	110	99	215	90
11/19	225	89	140	80	110	99	216	99
11/20	230	84	138	74	110	98	220	99
11/24	227	86	144	94	108	99	210	99
11/25	226	90	140	92	108	98	212	99
11/26	224	84	140	80	110	99	214	99
12/1	235	96	134	74	108	94	190	99
12/2	235	98	138	80	110	99	210	99
12/3	232	94	134	72	108	96	212	99
12/4	228	96	130	78	110	86	214	99
12/8	224	98	126	84	108	99	210	99
12/29	230	96	138	82	106	99	221	99
12/30	230	94	135	76	104	99	218	99
12/31	232	96	138	84	108	99	220	99
1981								
1/2	234	80	137	71	108	97	223	99
1/5	234	86	136	78	110	96	222	99
1/6	235	92	138	72	110	99	224	99
1/7	234	88	138	76	110	93	222	99
1/8	235	82			110	96	224	99
1/14	232	99	134	78	110	99	222	99
1/15	234	99	136	82	108	99	222	99

TABLE I)cont'd)

WELLHEAD TEMPERATURE AND WATER CUT

DATE (1980)	WELL # 194-21N		WELL # 23-21N		WELL # 209-21N		WELL # 24-21N	
	TEMP. °F	WATER % v/v	TEMP. °F	WATER % v/v	TEMP. °F	WATER % v/v	TEMP. °F	WATER % v/v
1/16	232	92	134	72	108	99	216	99
1/19	232	96	136	84	108	99	NOT PUMPING	
1/20	232	96	134	91	106	99	148	93
1/21	232	93	136	84	108	96	188	95
1/22	235	94	136	78	110	99	192	99
1/23	236	92	138	74	110	96	210	99
1/26	238	94	140	78	110	94	216	97
1/27	236	98	140	84	110	99	218	99
1/28	236	97	140	92	112	99	219	99
1/29	232	94	138	88	112	99	218	99
1/30	232	98	138	84	110	94	214	99
2/2	235	99	146	94	108	98	218	99
2/3	228	95	146	92	108	99	218	99
2/4	228	89	145	80	108	99	218	98
2/5	226	92	142	82	108	99	217	99
2/6	222	88	140	76	108	99	217	96
2/9	218	81	137	70	106	99	216	94
2/10	216	76	136	57	106	99	216	97
2/11	216	78	134	62	106	99	215	97
2/12	220	82	136	66	106	99	218	99
2/16	220	73	128	46	102	99	204	99
2/17	222	75	130	49	102	99	208	97
2/18	222	72	128	56	104	99	210	99
2/19	220	75	127	38	92	99	192	99
2/20	220	74	126	42	91	99	190	99
2/23	224	78	128	48	94	99	194	99
3/2	NOT PUMPING		126	38	102	99	210	99
3/3	NOT PUMPING		126	34	102	99	208	99
4/7	220	66	122	78	88	95	192	87
4/8	219	66	121	77	87	99	188	89
4/9	220	74	130	77	87	96	192	99
4/10		80		75		98		95

TABLE II

PRODUCTION FIGURES

WELL #	194-21			209-21			23-21			24-21		
DATE	BOPD	BWPD	% OIL	BOPD	BWPD	% OIL	BOPD	BWPD	% OIL	BOPD	BWPD	% OIL
JUNE 1980	7	150	4.5	7	13	35	2	23	8	3	74	4
JULY 1980	6	130	4.4	6	8	42.9	4	16	20	3	42	7
AUG. 1980	2	240	0.8	6	15	28.6	7	16	30	3	64	4
SEPT. 1980	4	165	2.4	11	19	36.7	2	18	10	2	62	3
OCT. 1980	2	175	1.1	8.5	13	39.5	1	32	3	0	72	0
NOV. 1980	10	130	7.1	2	11	15.4	2	24	8	5	39	11
DEC. 1980	6	120	4.8	2	20	9.1	7	21	24	3	52	5
JAN. 1981	4	100	3.8	2	5	28.6	4	18	18	0	19	0
FEBR. 1981	2	34	5.6	1	7	12.5	10	10	50	10	35	22
MARCH 1981	28	110	20	1	6	19	14	14	50	7	50	12
APRIL 1981	44	125	26	3	7	30	1	19	5	3	53	5

WELL #	60-21			179-21			210-21			20-21		
DATE	BOPD	BWPD	% OIL	BOPD	BWPD	% OIL	BOPD	BWPD	% OIL	BOPD	BWPD	% OIL
JUNE 1980	2	30	6.3	17	33	34.0	5	4	55.6	8	10	44.4
JULY 1980	2	24	7.7	38	26	59.4	6	8	42.9	3	2	60.0
AUG. 1980	1	18	5.3	15	7	68.2	9	17	34.6	2	1	66.7
SEPT. 1980	1	14	6.7	8	4	66.7	10	40	20.0	9	10	47.4
OCT. 1980	0.7	19	3.6	7	4	63.6	11	105	9.5	11	26	31.0
NOV. 1980	0.7	8	8.0	8	1.8	81.6	4	60	6.3	4	30	11.8
DEC. 1980	0.7	10	6.5	12	5	70.6	3	40	7.0	11	30	26.8
JAN. 1981	2	28	6.7	12	5	70.6	1	30	3.2	7	27	20.6
FEBR. 1981	2	7	22.2	12	8	60.0	1	22	4.3	4	40	9.1
MAR. 1981												
APR. 1981												

WELL #	294-21			61-21			195-21			25-21		
DATE	BOPD	BWPD	% OIL	BOPD	BWPD	% OIL	BOPD	BWPD	% OIL	BOPD	BWPD	% OIL
JUNE 1980	8	3	72.7	26	26	50	1	13	7.1	4	8	33.3
JULY 1980	9	2	81.8	14	15	48.3	3	20	1.3	5	7	41.7
AUG. 1980	8	3	72.7	4	70	5.4	2.2	34	6.1	1	120	0.8
SEPT. 1980	6	3	66.7	1	95	1.0	1	48	2.0	1	125	0.8
OCT. 1980	10	10	50.0	4	70	5.4	1	40	2.4	0.8	128	0.6
NOV. 1980	14	15	48.3	22	44	33.3	3	20	13.0	9	100	8.3
DEC. 1980	8	8	50.0	3	60	4.8	5	18	21.7	20	65	23.5
JAN. 1981	2	1	66.7	6	53	10.2	2.5	30	7.7	10	70	12.5
FEBR. 1981	8	21	27.6	14	48	22.6	1	30	3.2	5	95	5.0
MARCH 1981												
APRIL 1981												

WELL #	208-21			75-21			193-21		
DATE	BOPD	BWPD	% OIL	BOPD	BWPD	% OIL	BOPD	BWPD	% OIL
JUNE 1980	6	5	54.5	4	270	1.5	14	65	17.7
JULY 1980	6	3	66.7	6	270	2.2	37	25	59.7
AUG. 1980	6	3	66.7	6	7	46.2	37	30	55.2
SEPT. 1980	1	3	25.0	6	6	50.0	49	34	59.0
OCT. 1980	12	110	9.8	3	32	8.8	52	34	60.5
NOV. 1980	3	36	7.7	10	47	17.5	46	30	60.5
DEC. 1980	11	60	15.5	33	21	61.1	75	38	66.4
JAN. 1981	1	10	9.1	33	20	62.3	57	27	67.9
FEBR. 1981	6	9	40.0	67	52	56.3	50	34	59.5
MARCH 1981									
APRIL 1981									

TABLE III

CASING GAS ANALYSES OF PRODUCING WELL

WELL NUMBER	DATE 1981	SELECTED COMPONENTS: MOLE % CARBON DIOXIDE	NITROGEN	OXYGEN	METHANE
23-21N	1/10	74.17	14.90	ND	10.93
23-21N	3/12	84.02	ND	ND	15.94
23-21N	4/10	84.44	ND	ND	15.55
23-21N	5/19	89.26	ND	ND	10.74

TABLE IV

CASING GAS ANALYSES OF PRODUCING WELL

WELL NUMBER	DATE 1981	SELECTED COMPONENTS: MOLE % CARBON DIOXIDE	NITROGEN	OXYGEN	METHANE
194-21N*	1/10	90.68	3.20	ND	6.12
194-11N*	3/12	67.75	0.99	ND	11.13
194-21N*	4/10	78.41	1.90	ND	17.73
194-21N	4/28	48.86	34.55	10.10	5.20
194-21N	5/19	84.98	0.09	ND	11.01

* Casing was shut in on these dates.

TABLE V

CASING GAS ANALYSES OF PRODUCING WELL

WELL NUMBER	DATE 1981	SELECTED COMPONENTS: MOLE % CARBON DIOXIDE	NITROGEN	OXYGEN	METHANE
24-21N	1/10	16.25	53.36	ND	30.39
24-21N	3/12	32.00	ND	ND	67.74
24-21N	4/10	32.72	ND	ND	67.28
24-21N	4/28	38.06	ND	ND	61.94
24-21N	5/19	42.59	ND	ND	50.41

TABLE VI

CASING GAS ANALYSES OF PRODUCING WELL

WELL NUMBER	DATE 1981	SELECTED COMPONENTS: MOLE % CARBON DIOXIDE	NITROGEN	OXYGEN	METHANE
209-21N	1/10	76.17	6.01	ND	9.82
209-21N	3/12	81.08	0.02	ND	18.14
209-21N	4/10	87.70	ND	ND	12.16
209-21N	4/28	93.83	ND	ND	6.18
209-21N	5/19	84.98	ND	ND	11.01

TABLE VII

CASING GAS ANALYSES OF PRODUCING WELLS

SURROUNDING STEAM INJECTION WELL # 590-21N

WELL NUMBER	DATE 1981	SELECTED COMPONENTS: MOLE %			
		CARBON DIOXIDE	NITROGEN	OXYGEN	METHANE
60-21N	1/10	80.90	ND	ND	19.10
60-21N	3/12	53.43	30.75	ND	13.34
60-21N	4/3	66.31	27.49	ND	6.20
60-21N	4/10	65.54	27.33	ND	7.13
60-21N	4/28	25.11	61.69	7.61	10.88

TABLE VIII

CASING GAS ANALYSES OF PRODUCING WELL

WELL NUMBER	DATE 1981	SELECTED COMPONENTS: MOLE %			
		CARBON DIOXIDE	NITROGEN	OXYGEN	METHANE
61-21N	1/10	70.78	ND	ND	29.22
61-21N	3/12	69.53	0.31	ND	30.16
61-21N	4/3	42.26	0.04	ND	57.70
61-21N	4/10	42.31	0.01	ND	57.68
61-21N	4/28	42.34	ND	ND	57.66

TABLE IX

CASING GAS ANALYSES OF PRODUCING WELLS

SURROUNDING STEAM INJECTION WELL # 590-21N

WELL NUMBER	DATE 1981	SELECTED COMPONENTS: MOLE %			
		CARBON DIOXIDE	NITROGEN	OXYGEN	METHANE
294-21N	4/28	25.11	61.69	7.61	10.88

TABLE X

CASING GAS ANALYSES OF PRODUCING WELL

WELL NUMBER	DATE 1981	SELECTED COMPONENTS: MOLE %			
		CARBON DIOXIDE	NITROGEN	OXYGEN	METHANE
62-21N	4/28	65.01	ND	ND	34.99

TABLE XI

CASING GAS ANALYSES OF PRODUCING WELL.

WELL NUMBER	DATE 1981	SELECTED COMPONENTS: MOLE %			
		CARBON DIOXIDE	NITROGEN	OXYGEN	METHANE
180-21N	4/28	44.29	ND	ND	55.71

TABLE XII

CASING GAS ANALYSES OF PRODUCING WELL

WELL NUMBER	DATE 1981	SELECTED COMPONENTS: MOLE %			
		CARBON DIOXIDE	NITROGEN	OXYGEN	METHANE
207-21N	4/28	98.45	ND	ND	0.19

TABLE XIII

CASING GAS ANALYSES OF PRODUCING WELL

WELL NUMBER	DATE 1981	SELECTED COMPONENTS: MOLE % CARBON DIOXIDE	NITROGEN	OXYGEN	METHANE
208-21N	4/28	99.10	ND	ND	0.90

TABLE XIV

STEAM QUALITY AT WELLHEAD 590-21N

	TDS ppm	Steam quality
10/20/80	375	42
11/12/80	480	55
11/13/80	500	57
11/14/80	480	55
11/15/80	600	64
11/18/80	500	57
11/19/80	490	56
11/20/80	55-	61
11/24/80	400	46
11/25/80	550	61
11/26/80	370	42
12/1/80	355	39
12/2/80	390	45
12/3/80	440	51
12/4/80	450	52
12/8/80	485	55
12/18/80	600	64
12/29/80	460	53
12/30/80	450	52
12/31/80	350	35
1/2/81	340	36
1/5/81	450	52
1/6/81	315	31
1/7/81	300	28
1/8/81	330	34
1/9/81	380	43
1/12/81	750	71
1/14/81	600	64
1/16/81	370	42
1/19/81	330	35

TABLE XV

CONOCO - CALIFORNIA LEASE - CAT CANYON

Table FOAM CHEMICAL AND NITROGEN INJECTION DATA

	THERMOPHOAM BW-D			NITROGEN INJECTION			
Date 1980	Conc. % v/v	Volume Gel	Injection Rate gpm	Slug Volume SCF	Rate SCFM	Continuous Volume SCFM	Rate SCFM
5/1	10	560	18	6,500	176	14,720	64
5/2	10	560	47	6,140	154	16,600	94
5/3	10	560	33	6,140	192	17,160	64
5/4	10	100	25	-	-	10,370	86
5/5	-	-	-	-	-	-	-
5/6	10	560	46	13,230	152	20,220	76
5/7	10	560	28	11,250	134	19,680	82
5/8	10	560	31	10,760	134	23,910	83
5/9	10	560	28	11,620	145	24,840	92
5/10	10	560	43	10,400	139	19,200	68
5/11	10	560	28	6,330	141	26,570	101
5/12	10	560	43	6,620	154	31,790	112
5/13	10	560	47	6,690	129	27,370	90
5/14	36	280	29	-	-	19,400	63
5/15	36	190	27	-	-	20,470	71
5/16	17	264	27	-	-	15,230	46
5/17	17	410	17	-	-	12,050	43
5/18	-	-	-	-	-	-	-
5/19	17	280	20	-	-	4,520	93
5/20	20	280	20	-	-	11,350	33

FIGURE 1

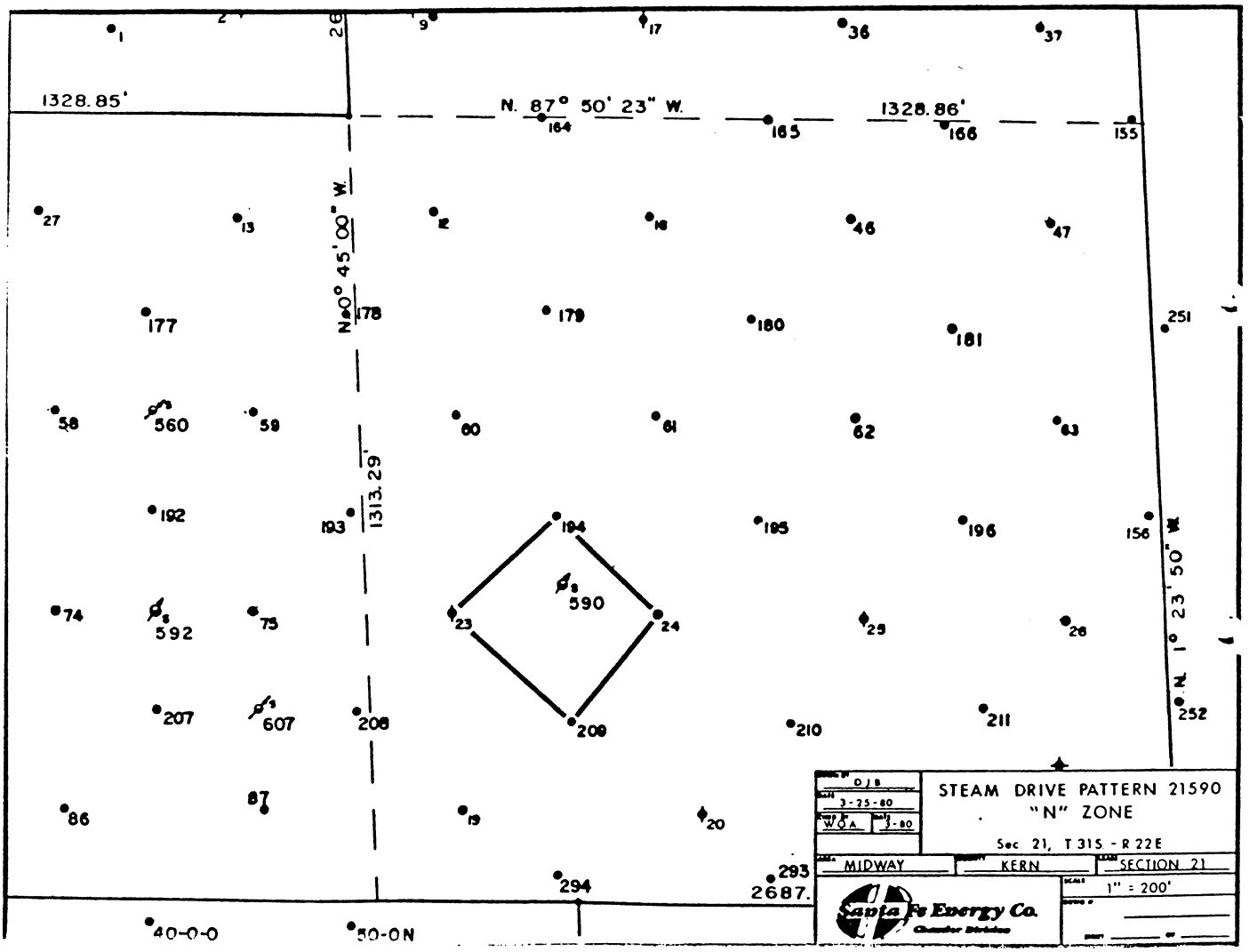

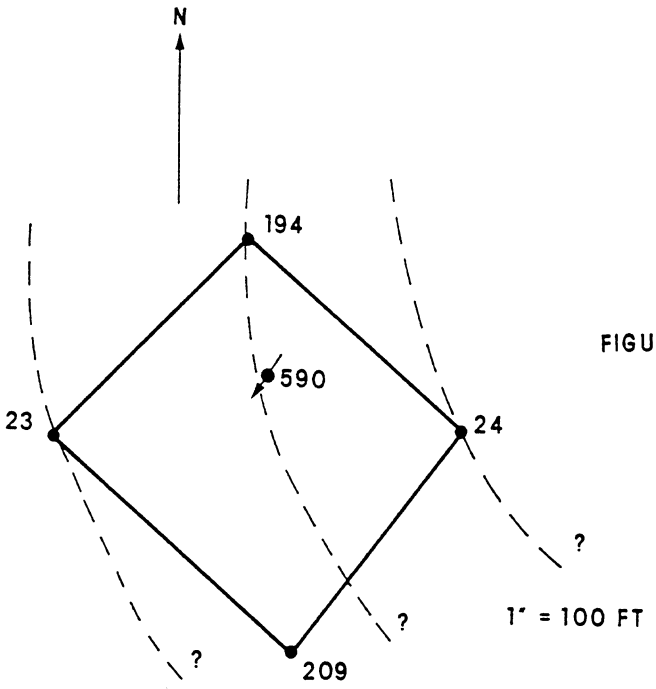

FIGURE 2. PATTERN WELL LOCATIONS FROM LOG LOCATIONS

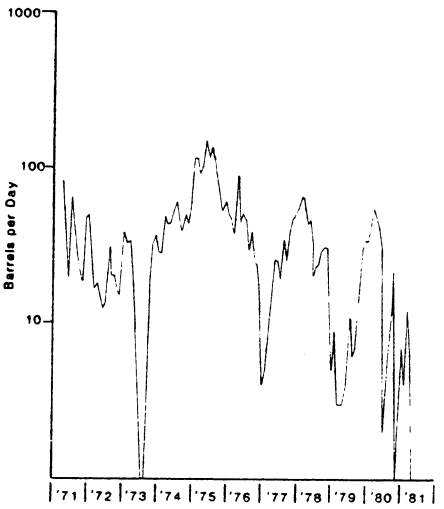

Figure 3

PRODUCTION HISTORY WELL 23-21

WELL NO.: 23-21N

CASING @ 624

LINER: 607-1100

PERFS: 613-1100

PUMP SHOE DEPTH: 1049 KB

BBLS. INJECTED: 5721

GENERATOR NO.: 41

ZERO POINT: K.B.=10

CYCLE NO.: 6

10-19-79 DAYS AFTER INJECTION

REMARKS: ELECT

LEGEND

10-19-79 ——————

9-30-80 — — — — — —

3-19-81 — · — · — · —

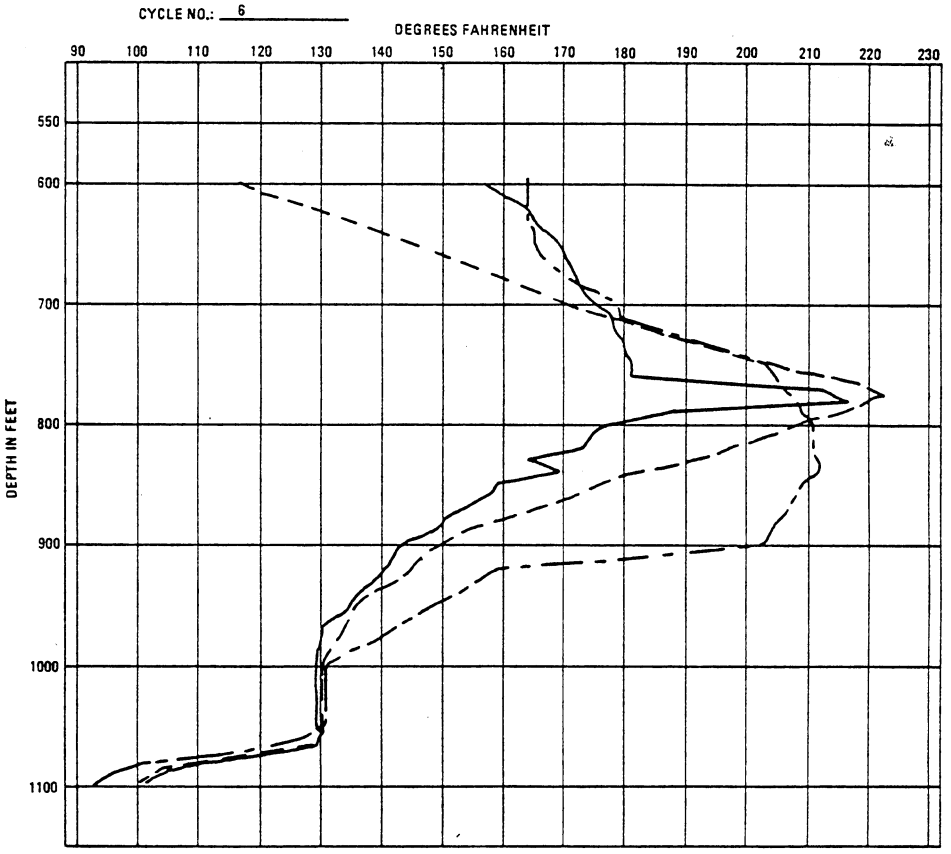

FIGURE 4

WELL NO: 194-21

CASING @ 676

LINER: 660-1100

PERFS: 666-1100

PUMP SHOE DEPTH: 1009 KB

BBLS. INJECTED: 6641

GENERATOR NO.: 41

ZERO POINT: K.B. = 10

CYCLE NO.: 7

12-8-79 DAYS AFTER INJECTION

REMARKS:

LEGEND

9-4-80 ———

9-30-80 — — — — — — —

3-19-81 — · — · — · —

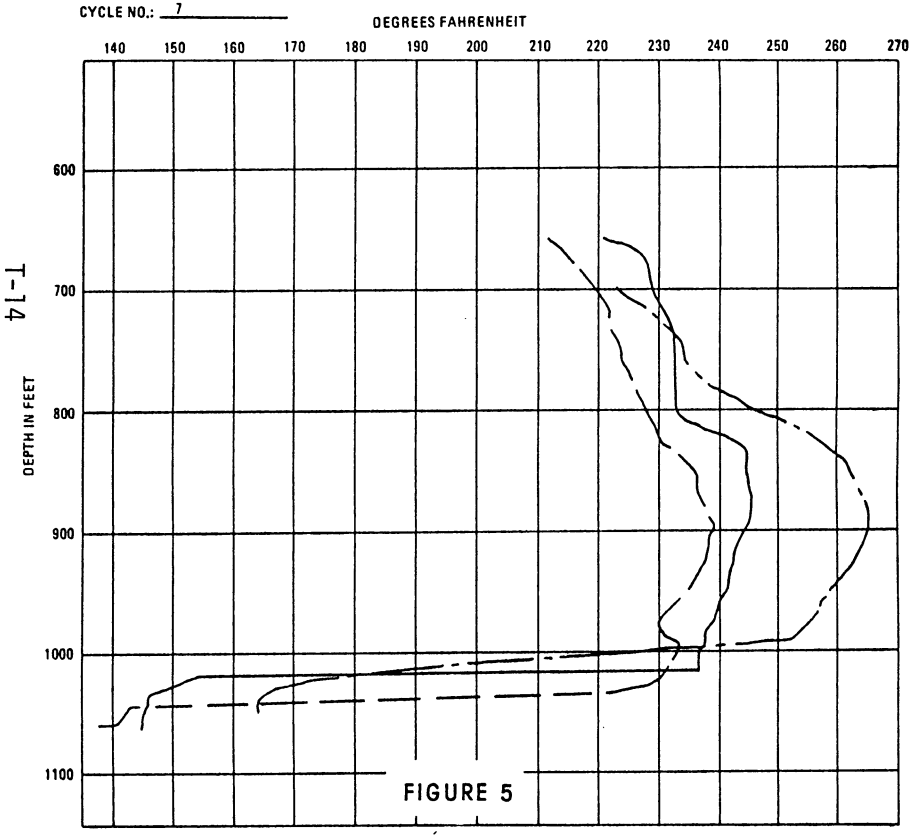

FIGURE 5

WELL NO.: 24-21n

CASING @ 660

LINER: 648-1135

PERFS: 654-1135

PUMP SHOE DEPTH: 1085 M

BBLS. INJECTED: 8205

GENERATOR NO.: 41

11-26-79 DAYS AFTER INJECTION

ZERO POINT: K.B. = 10

CYCLE NO.: 13

REMARKS: ELECT

LEGEND

9-3-80 ———

9-30-80 — — — — — — —

3-19-81 — · — · — · —

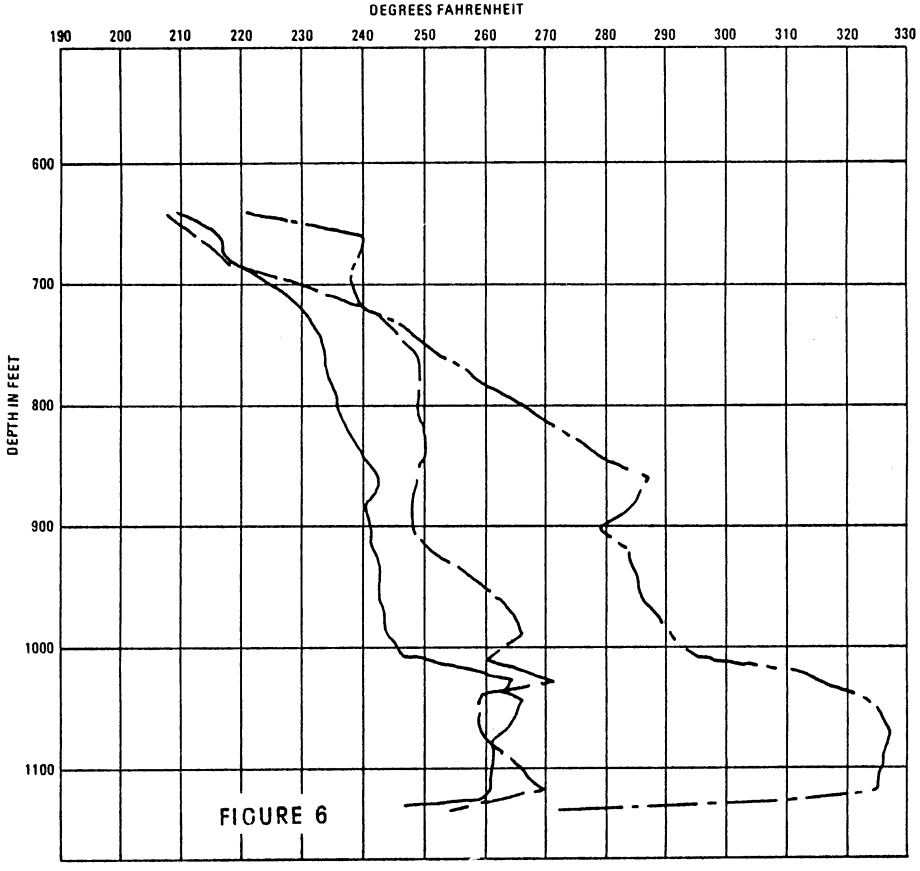

FIGURE 6

WELL NO.: 209-21

CASING @ 655

LINER: 642-1115

PERFS: 648-1115

PUMP SHOE DEPTH: 1051 KB

BBLS. INJECTED: 8255

GENERATOR NO.: 41

ZERO POINT: K.B. = 10

CYCLE NO.: 14

3-27-80 DAYS AFTER INJECTION

REMARKS: ELECT

LEGEND

9-6-80 ——————————

10-1-80 — — — — — — —

3-19-81 — · — · — · — · —

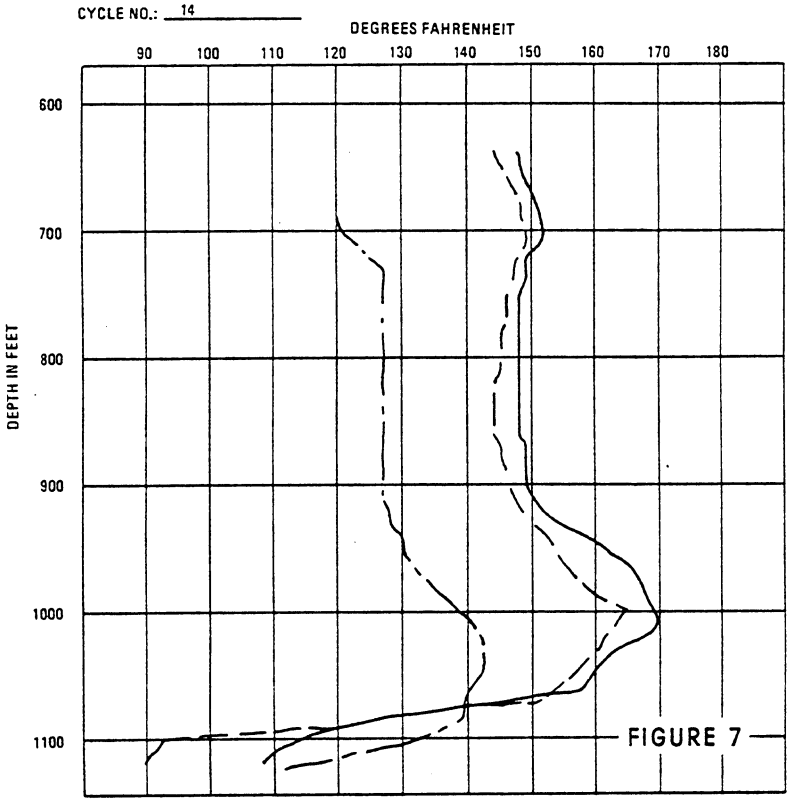

FIGURE 7

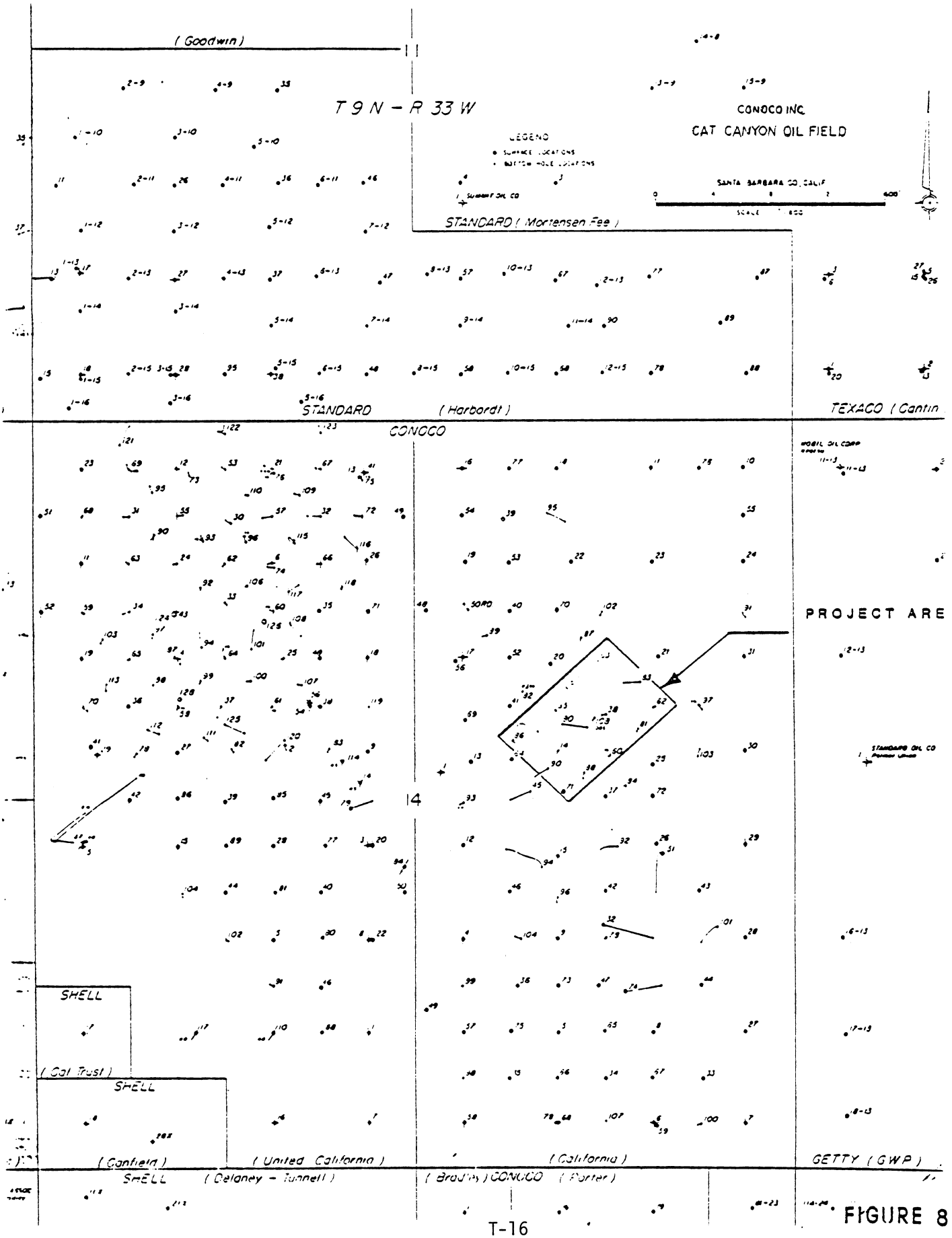
(Goodwin)
T 9 N – R 33 W
CONOCO INC.
CAT CANYON OIL FIELD
LEGEND
SURFACE LOCATIONS
BOTTOM HOLE LOCATIONS
SANTA BARBARA CO., CALIF.
SCALE
STANDARD (Mortensen Fee)
STANDARD (Harbordt)
TEXACO (Cantin
CONOCO
PROJECT ARE
SHELL
(Col Trust)
SHELL
(Canfield)
(United California)
(California)
GETTY (GWP)
SHELL (Delaney – Tunnell)
(Brodie) CONOCO (Porter)
14

FIGURE 8

Sec. 14, T 9 N – R 33 W

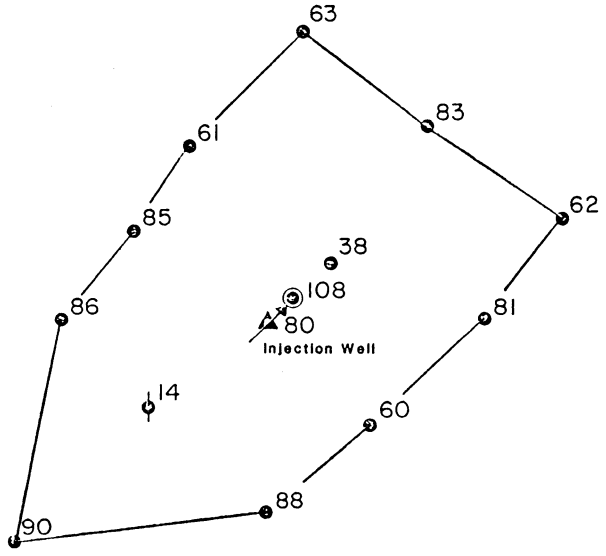

LEGEND

Injection Well

Primary Well to be Influenced by Project

Area to be Influenced by Project

FIGURE 9

CALIFORNIA 38/80 TEST AREA

0 2 4 600'

FEET

FIGURE 10

COMPOSITE LOG

LOWER SISQUOC FORMATION

CONOCO CAT CANYON FIELD

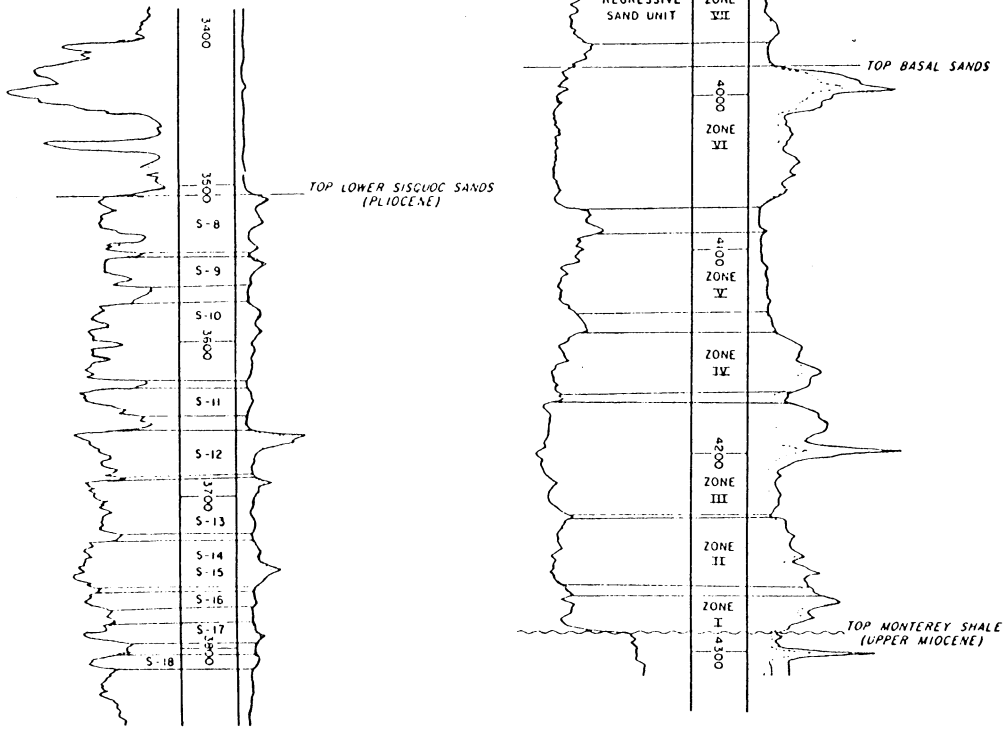

CALIFORNA 38/80 PROFILE SHOWING HOT ZONE

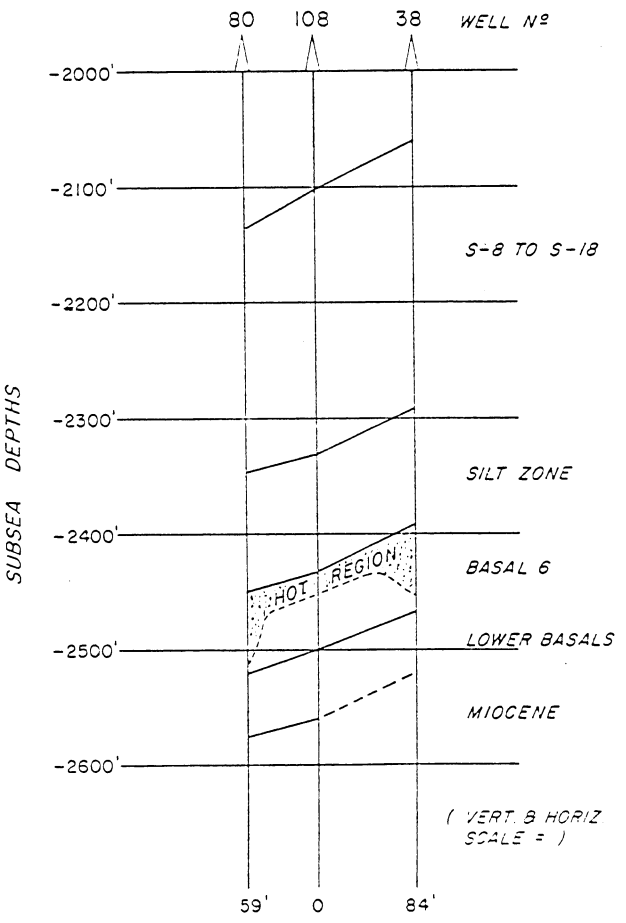

FIGURE 11

IMPROVEMENT OF STEAM INJECTION THROUGH THE USE OF FOAMING ADDITIVES

by

A. Al-Khafaji, S. Mahmood, O. S. Owete, F. Wang,
L. M. Castanier, and W. E. Brigham

Stanford University Petroleum Research Institute
(SUPRI), Stanford, CA

ABSTRACT

One of the main problems in steam injection is mobility control. The efficiency of this process is often reduced because of the tendency of steam to channel and "override." Foam has been found to be an effective mobility control agent. This study has focused on the following areas:

1) The pore-level behavior of foam flow in porous media was studied. To accomplish this, a method for observation of the flow mechanisms was developed.

2) A two-dimensional experimental simulation of the reservoir was designed. Significant improvement of the breakthrough time, gas-oil ratio and oil recovery was observed in the presence of foaming agents. This improvement was attributed to better sweep efficiency due to mobility control.

3) The foaming chemicals were studied at steam-drive field conditions. Thermal longevity, adsorption and partitioning of the surfactants between the water and the oil phase were investigated. Some commercial surfactants showed very promising results.

4) Steam/foam displacement and dynamic adsorption at elevated temperatures will be studied using crude oil and reservoir matrix.

HISTORY OF THE PROJECT

Foam has been widely used by the oil industry for drilling, workover or completion operations. SUPRI began an extensive study of the relevant literature in 1976. It was then decided to apply the foaming technique as a mobility control in steam injection. In 1976-77, measurements of directional permeabilities of cores were made. Testing for temperature stability at 100°C started in 1977. The same year, the tube furnace apparatus was designed and operated up to 205°C. In

Prepared for DOE under Contract No. DE-AC03-76ET12506

1979, the first two-dimensional model was built in plexiglass. Problems of chemical degradation of the plexiglass led to its replacement by glass in 1980. Simultaneously, the temperature stability studies were expanded with a new apparatus working up to 250°C. This paper summarizes the work done during the period July 1, 1980 to June 30, 1981.

INTRODUCTION

One of the most widely used techniques of enhanced oil recovery for heavy oils is steam injection. In this method, steam is injected into a reservoir to reduce the viscosity of the oil by raising its temperature, thus making it more mobile.

Because of the density difference between steam and oil, the steam, being lighter, tends to flow to the top of the layer and "ride" over the oil. This preferential movement of steam through the upper part of the reservoir, termed "gravity override," reduces the amount of reservoir rock contacted by steam. Steam also channels through the more permeable zones of the reservoir. As a consequence of channeling and gravity override, there is a non-uniform distribution of heat through the reservoir leading to early steam breakthrough in production wells and reduced oil recovery.

To improve steam injection recovery, foam is proposed as a mobility control agent. Different authors have studied the rheologic properties of foams (1-30), some experimentally, others theoretically. Even field experiments using foam were conducted. However, past work has been mainly qualitative and further quantitative work in this area is needed.

The Stanford University Petroleum Research Institute project is a comprehensive laboratory study of the use of foaming chemicals as mobility control agents in steam flooding. Brief descriptions follow:

-- A visual investigation using micromodels is being conducted to observe the mechanisms of foam formation and propagation in porous media. Influence of pore structure, flow rates and surfactant concentrations are being studied.

-- Various displacement experiments such as gas drives in two-dimensional models simulate gravity override and channeling in a reservoir. Effects of surfactant concentration, slug size and flow rates are being investigated. Quantitative measurements include material balances, pressure gradients, average residual saturations and frontal behavior.

-- Decomposition of surfactant due to long-term temperature effects, its adsorption by the porous matrix and its phase partitioning in crude oil and water are being studied. The preliminary results indicate that at least two surfactants can be used successfully in steam drive conditions. Further work will be conducted in this area.

-- A steam tube experiment is now being completed to investigate dynamic adsorption and the effect of steam injection on foaming. Calibration experiments correlate well with the temperature profiles

and with analytical calculations. This work will also be pursued in the future.

MICROMODELS EXPERIMENTS

To identify the mechanisms governing the flow behavior of foam in porous media, a visual study of foam flow was made using micromodels. Foam is generated in-situ in the simulated porous media by injecting air into micromodels saturated with a foamer solution. This study will concentrate on pore structure, foamer concentration, and air flow rate.

Literature Review

For the complete literature on the rheology of foams, refer to Refs. 1 through 30. This paper will present a brief summary of the different hypotheses on foam flow, the effect of pore structure, surfactant, surfactant concentration and flow rates.

Effect of Pore Structure. The reduction in the mobility of gas in a porous medium has been shown to be greater for sand with higher absolute permeability (10). Other studies (17) indicated that pore structure affected the blocking action of foam. Raza (4) showed that higher quality foams (larger bubbles) were produced in the high-permeability sands which contained uniformly distributed large pores.

Mast (12) observed that a system of large pores adjoined by smaller ones offered sites of foam regeneration in a porous medium. In uniform-sized porous medium, he noted that "flow could be described as the movement of liquid and gas through a partially-blocked medium." In other words, the characteristic breaking and forming of foam was absent.

Effect of Foamer Concentration. The amount of foamer concentration indirectly affects the reduction of gas mobility by foam. Foamer concentration affects the quality, the size and the nature of foam bubbles that are produced. The average foam bubble diameter is proportional to foam quality, which increases with concentration (3-6).

However, beyond a certain concentration, further increases do not alter the foam quality (4). This is because the surface properties of a surfactant solution do not change considerably with concentration beyond the critical micelle concentration (CMC).

Mast (12) observed that high concentrations of foaming agent produced more stable foam with bubbles which could be displaced from large pores into smaller ones without breaking.

Effect of Gas Flow Rate. The effect of the gas flow rate on gas mobility reduction by foam is not well-documented in the literature, but the effect of injection pressure and pressure differential is known. Fried (11) observed that higher pressure differentials were required to force large bubbles into a core. The large bubbles blocked access to smaller bubbles, creating an even higher pressure differential. Several observations (4,6,12) seem to indicate that the effect of pressure

differential on the flow behavior of foam depends largely on the pressure level at which foam is injected into the porous medium. If foamer concentration and surface properties are not limiting, the pressure gradient is a function of pore structure, the gas or foam flow rate, and to some extent, the distance from the inlet face.

Micromodels have been previously used in the form of either capillary networks (2,3,26,30) or two-dimensional models designed to simulate pore structure (12,24,26,28,29). The technique used in this study is a two-dimensional model which will be described in a technical report to DOE.

Experimental Apparatus

The experimental apparatus for this study was designed and built to meet three main objectives: to create in-situ formation and foam flow in a porous medium; to observe and study the flow of foam; and to measure the pressure drop across the porous medium. Therefore, the apparatus, shown in Fig. 1, consists of a fluid flow system and a pressure measurement system. These will be discussed separately.

Fluid Flow System. The fluid flow system, shown in Fig. 1, consists of a Sage syringe pump, a micromodel, a liquid collector, and a bubble film flowmeter.

A low-rate syringe pump, Sage series 237-2 was used for this experiment. Synchronous motors power a set of drive and idler gears. The drive gear advances a carriage that moves a syringe piston at a constant rate. The syringe contains fluid, water, surfactant solution or air to be injected into the micromodel. Different fluid flow rates are available through one or a combination of three processes: a change of syringe size, interchange of the drive and idler gears, and use of a ten-turn dial. The dial varies the flow rates over a wide range for each size syringe.

Injected fluids pass through a filter with a 5-micron element before contacting the micromodel. The output flow rate of air and foam is measured with a bubble flowmeter. This flowmeter consists of a 1.0 cc pipette graduated in subdivisions of 0.01 cc. The time required for the movement of an air-liquid film through the pipette is used to obtain the flow rate of air, the input flow rate of the injected air, and the varying injection pressure.

At the outlet of the flowmeter, fluids come in contact with a 0.16 cm diameter J-thermocouple. The temperature sensed by this thermocouple is read from a digital thermometer.

Observation System. The purpose of observing the micromodel experiments is for documentation. The upper half of Fig. 1 shows the major components: cycloptic microscope, a light source, a beam splitter, a photographic assembly, a video monitor and a recorder.

The microscope has a binocular telescope system which yields a stereoscopic image of the field of view. The working distance ranges from 3.8 to 11.2 cm depending on the eyepiece and objective magnifications.

Pressure Measurements. Two KP 15 differential pressure transducers are connected in parallel to measure the pressure drop across the micromodel. The lower half of Fig. 1 is a schematic of the setup. A demodulator converts the pressure drop into an electrical signal which can be read off a voltmeter (0 to 10 volts). The voltmeter's output is connected to a chart recorder so that a continuous record of the pressure drop can be kept. Diaphragms of different scales are used in the two transducers. The parallel connection of these transducers enables either of the diaphragms to be used, depending on the range of pressure. This minimizes the errors in the measured pressure drop.

The transducers are calibrated in-situ with either a water or mercury manometer.

Status of the Project

The calibration runs are being performed and results will be available soon. This experiment will be continued next year.

DISPLACEMENT EXPERIMENTS

Two types of two-dimensional models are used to simulate displacement of oil by gas with gravity override and channeling conditions. The main difference between the two models is the permeability of the packs. One model is composed of three layers of different grain sizes, and the other model consists of a homogeneous layer.

Experimental Apparatus

A schematic diagram of the apparatus for both models is presented in Fig. 2. The maximum operating pressure of the system is 20 psig. The model itself is a 4' x 1' x 1.4" sandpack enclosed between a glass plate and a steel plate. Each experiment requires the following steps:

-- Cleaning the model

-- Saturating with 180 cp viscosity oil at irreducible water saturation

-- Injecting a slug of surfactant or water in control runs

-- Injecting nitrogen

-- Measuring pressure change, breakthrough time, flow rates, and material balances

-- Taking pictures of the front and calculating residual liquid saturation

This year, the work has focused on multiple slugs and flow rate optimization.

Results and Discussion

Previous results are published in Refs. 21 through 32. The work done at SUPRI confirms some of these results. Figure 3 presents the results of a run made with two slugs of 0.1 pore volume of SUNTECH IV compared with a control run and a run made with one slug of 0.2 pore volume of SUNTECH IV of the same concentration (1%). The results of this run indicate that recovery is not improved by using multiple slugs instead of one, large slug. A possible explanation for this is that injection of the second slug occurred long after the gas breakthrough and hence was not efficient. Segregation by gravity in the injection well may also have been a factor.

Some general conclusions can be drawn:

-- Oil recovery improved by as much as 20% through the use of foam additives

-- The gas-oil ratio decreased in all surfactant runs

-- The frontal behavior of the process greatly improved in the presence of surfactants

-- Recovery was flowrate dependent

-- The mobility of the gas was significantly reduced by the foam yielding longer breakthrough time and better sweep efficiency

Future work on these models includes trying to inject gas from selected perforations, to optimize slug size and flowrate, and to increase the permeability of the model.

HIGH-TEMPERATURE EXPERIMENTS

To apply this process to steam injection, the chemical used as a foaming agent must withstand high temperatures. In addition, studies on adsorption and phase partitioning are necessary before a successful field application.

Experimental Apparatus

Equipment for measuring the effect of high temperatures (steam temperature--400°F) on the stability, adsorption and phase partitioning of aqueous surfactant has been designed. A schematic diagram is shown in Fig. 4. The equipment consists of a pressure control system, a temperature control system, and 21 stainless steeel cyliners of varying volumes.

The pressure control system applies and controls the confining pressure (500 psi). It consists primarily of nitrogen cylinders, a regulator and a safety valve. The safety valve is adjusted at 550 psi. The pressure gauges of the regulator are calibrated.

The temperature control system includes an air bath and sampling system. Heat is maintained by the air bath at 400°F. The sampling valves are located outside of the air bath and the lines are cooled by ice to avoid flashing.

As an example, Run 4 tests 1% concentration solutions of SUNTECH IV, and CORCO 180A. The results presented in Table 1 and Fig. 5 show that SUNTECH IV is stable at high temperatures, confirming previous results. However, CORCO 180A exhibits degradation.

Therefore, another run (Run 5) focused on SUNTECH IV only. A SUNTECH IV batch was used in these tests, 25% active at 1%, 2% and 5% weight concentrations (0.25, 0.5, and 1.25% active).

Three 500 cc capacity stainless steel cylinders were used for the thermal degradation measurements.

Three 1,000 cc capacity stainless steel cylinders were used for studying surfactant adsorption. Ottawa silica sand, mesh 100, and Keolinite powder, 1% by weight of sand, was the matrix used in these cylinders.

Fifteen 150 cc capacity stainless steel cylinders were fixed on a rotating rod inside the air bath. They chould be rotated from outside the air bath to mix the surfactant solution with the oil. The oil used was from the Kern front field, with an API gravity of 12°. Water from the same reservoir was used to prepare the aqueous surfactant solutions. Measurements of the surfactant concentrations were made by hyamine die titration. pH values of the surfactant were also measured.

The results of this run, presented in Table 2 and Fig. 6, show that the pH value for 1% and 2% concentration solutions remains always above 7. The unusual behavior of the 5% active concentration solution in the porous medium may be due to contamination by clay. As shown in Fig. 6, the concentration of all samples remains stable at high temperatures. Adsorption has some effect, but the results have not been fully assessed. Partitioning in the oil phase increases the first day to values of as much as 30% of the initial concentration. After the first day, the amount of partitioning remains at a constant level. This effect is greater for low surfactant concentrations. This run is still in progress and further results will be presented at the DOE meeting in July.

ONE-DIMENSIONAL STEAM INJECTION APPARATUS

Apparatus Description

The apparatus for injecting dynamic steam with additives is shown in Fig. 7. A 6-foot long, 2-inch diameter stainless steel tube with 19 thermocouples on one side and six pressure taps on the other side was packed with 100 mesh Ottawa sand. The tube was wrapped with insulating material and laid horizontally in an 8-inch diameter aluminum shell. Heating tapes were used to heat the sandpack to reservoir temperature. Steam was generated by a tubular furnace. Two Lapp pumps pumped brine, oil, surfactant solution, and distilled water. Samples were gathered by a fraction collector.

Results to Date

The porosity and absolute permeability of sand can indicate packing problems. The porosity of the experimental sand pack was 0.365 and the absolute permeability was 15 darcys, which agrees with literature data for 100 mesh sandpack (31). However, a higher permeability (5%) was observed in the top left-hand section of the tube.

Figure 8 shows the temperature profile of a saturated steam injection. The sandpack was initially saturated with water at room temperature. Then, steam at 365°F was injected at a mass rate of 170 gm/hour. The downstream pressure was kept constant at 150 psi. Due to high permeability (or the small pressure drop along the sandpack), the variation of saturated temperature along the tube due to pressure drop could not be detected. The sharp front is due to the relatively high injection rate. These results agree with the work of previous researchers (33) and with analytical heat transfer calculations.

CONCLUSIONS

This study has shown that foam can improve oil recovery in steam injection. SUNTECH IV is stable at high temperatures and seems to be effective in the presence of crude oil and porous media.

However, more work is needed in order to understand and quantify the mechanisms of the foaming process. More micromodel studies are necessary to investigate the properties of the flow of foams in porous media under various experimental conditions. SUPRI will continue work in the following areas:

-- Displacement experiments will be continued to study the effect of flow rates, slug size, and concentration of the surfactant. The position of the injection perforations will be varied to study the effect of completions' partial penetration.

-- High temperature experiments will study other surfactants for longevity, adsorption, and phase partitioning. Tests will be conducted at different temperatures from 70°F (23°C) to 400°F (205°C). Different types and amounts of clays will be used and the effect of divalent ions will be investigated.

-- The steam stube experiments will continue to give pressure and temperature profiles under one-dimensional displacement at field conditions. This experiment will also yield dynamic adsorption data.

This project also includes laboratory support for the field experiment conducted in the McManus leases of the Kern River front. This is expected to continue in the future.

ACKNOWLEDGEMENT

This study was realized under DOE contract DE AC03 76 ET 12506. This financial support is gratefully acknowledged. Special thanks to Mr. H. Lechtenberg, project officer, for his constant support of the project.

REFERENCES

1. Marsden, S. S., Class notes for Pet. E. 284, Stanford University, 1979.

2. Marsden, S. S., and Khan, S. A., "The flow of foam through short porous media and apparent viscosity measurements," Soc. Pet. Eng. J. (March, 1966), 17.

3. David, A., and Marsden, S. S., "The rheology of foam," presented at the 44th Annual Fall Meeting of SPE of AIME, Denver, Colo., Sept. 28-Oct. 1, 1969, Paper SPE 2544.

4. Raza, S. H., "Foam in porous media: Characteristics and potential applications," Soc. Pet. Eng. J. (Dec. 1970), 328.

5. Kanda, M., and Schechter, R. S., "The in-situ production of foam in a porous medium," submitted for publication to the Soc. of Pet. Eng. of AIME (Departments of Chemical and Petroleum Engineering, the University of Texas at Austin).

6. Holm, L. W., "The mechanism of gas and liquid flow through porous media in the presence of foam," Soc. Pet. Eng. J. (Dec. 1968), 359.

7. Raza, S. H., and Marsden, S. S., "The streaming potential and rheology of foam," Soc. Pet. Eng. J. (Dec. 1967), 359.

8. Minssieux, L., "Oil displacement by foams in relation to their physical properties in porous media," J. Pet. Tech. (Jan. 1974), 100.

9. Ikoku, C. U., "Transient flow of non-Newtonian power-law fluids in porous media," Ph.D. thesis, Petroleum Engineering Dept., Stanford University, 1978.

10. Bernard, G. G., and Holm, L. W., "Effect of foam on permeability of porous media to gas," Soc. Pet. Eng. J. (Sept. 1964), 267.

11. Fried, A. N., "The foam drive process for increasing the recovery of oil," U.S. Bureau of Mines, R.I. 5866 (1961).

12. Mast, R. F., "Microscopic behavior of foam in porous media," presented at the Annual Fall Meeting of the SPE of AIME, San Antonio, Texas, Oct. 1972, Paper SPE 3997.

13. Bernard, G. G., et al., "Effect of foam on trapped gas saturation and on permeability of porous media to water," Trans. AIME, 234 (1965), 295.

14. Nahid, B. H., "Non-Darcy flow of gas through porous media in the presence of surface active agents," Ph.D. thesis, University of Southern California, Los Angeles, 1971.

15. Kolb, G. E., "Several factors affecting the foam-drive process for the removal of water from consolidated porous media," M.S. degree thesis, Pet. & Nat. Gas Eng., Penn. State Univ. (Dec. 1964).

16. Albrecht, R. A., and Marsden, S. S., "Foams as blocking agents in porous media," Soc. Pet. Eng. J. (March, 1970), 31.

17. Kanda, M., and Schechter, R. S., "On the mechanism of foam formation in porous media," presented at the 51st Annual Fall Meeting of the SPE of AIME, New Orleans, La., Oct. 3-6, 1976, Paper SPE 6200.

18. Deming, J. R., "Fundamental properties of foams and their effect on the efficiency of the foam-drive process," M.S. degree thesis, Pet. & Nat. Gas Eng., Penn. State Univ. (Dec. 1964).

19. Bikerman, J. J., Foams, Springer-Verlag New York Inc., 1973.

20. Handy, L. L., et al., "Thermal stability of surfactants for reservoir application," presented at the SPE of AIME International Symposium on Oilfield and Geothermal Chemistry, Houston, Texas, Jan. 22-24, 1979, Paper SPE 7867.

21. Owete, S. O., et al., "Foam as a mobility control agent in steam injection processes--temperature stability of foaming agents; application to improved steam injection," SPE 8912-B, 50th Annual California Regional Meeting, Pasadena, Calif., April 9-11, 1980.

22. Holm, L. W., "Foam injection test in the Siggins Field, Illinois," J. Pet. Tech. (Dec., 1970), 1499.

23. Elson, D. T., "The effectiveness of foaming agents at elevated temperatures over an extended period of time," M.S. degree report, Pet. Eng., Stanford University, 1979.

24. Sharma, S. K., "A study of the microscopic behavior of the foam drive method," M.S. Report, Stanford University, Dec. 1965.

25. Mattax, C. C., and Kyte, J. R., "Ever see a water flood?", Oil and Gas J. (Oct. 16, 1961), 115.

26. Davis, J. A., and Jones, S. C., "Displacement mechanisms of micellar solutions," J. Pet. Tech. (Dec. 1968), 1415.

27. Jones, S. C., Marathon Oil Co., Notes on etches glass micromodel, contained in a letter to the author, May 1980.

28. Holcomb, D. L., et al., "Foamed hydrocarbon stimulation water sensitive formations," presented at the SPE Rocky Mountain Regional Meeting, Casper, Wyoming, May 14-16, 1980, Paper SPE 9033.

29. Holcomb, D. L., et al., "The chemistry, physical nature and rheology of an aqueous stimulation foam," presented at the Eastern Regional Meeting of SPE of AIME, Morgantown, W.V., Nov. 5-7, 1980, Paper SPE 9530.

30. Holbrook, S. T., et al., "Rheology of mobility control foams," presented at the 1981 SPE/DOE Second Joint Symposium on Enhanced Oil Recovery of the SPE, Tulsa, Oklahoma, April 5-8, 1981, SPE/DOE 9809.

31. Stegemeier, G. L., Laumbach, D. D., and Volek, C. W., "Representing Steam Processes with Vacuum Model," Soc. Pet. Eng. J. (June 1980), 151-174.

32. Chiang, J., Mahmood, S., Sufi, A., L. Castanier, "Foam as a mobility control agent for steam injection," California Regional Meeting, SPE 1980, Paper SPE 8912.

33. Arihara, N., Ramey, H. J., Jr., and Brigham, W. E., "Non-isothermal single and two-phase flow in sandstones," Paper SPE 5380, 1975 California Regional Meeting of SPE.

FRESH SAMPLES

SAMPLE / PROPERTIES	SUNTECH IV + NaCl	SUNTECH IV + NaCl + P.M.	SUNTECH IV + NaCl + Oil + P.M.	SUNTECH IV + $CaCl_2$ + Oil + P.M.	CORCO 180A	CORCO 180A + NaCl + Oil
CONCENTRATION %	1.0	1.0	1.0	1.0	1.0	1.0
pH VALUE	11.40	11.25	11.10	9.20	7.30	7.55

AFTER 3 DAYS

CONCENTRATION %	0.90	0.95	0.99	0.10	0.10	0.15
pH VALUE	10.90	8.45	7.60	6.95	3.00	4.40

AFTER 17 DAYS

CONCENTRATION %	0.90	0.93	0.94	0.08	0.07	0.10
pH VALUE	10.10	6.30	7.10	7.20	3.30	4.70

AFTER 40 DAYS

CONCENTRATION %	0.89	0.93	0.90	0.04	0.07	0.07
pH VALUE	9.65	6.75	6.20	6.50	4.00	4.00

FOURTH RUN

Table 1 : CONCENTRATION AND pH VALUE OF SUNTECH IV AND CORCO 180A.

DAYS	THERMAL TEST		ADSORPTION TEST		PARTITIONING TEST	
	Concentration %	pH Value	Concentration %	pH Value	Concentration %	pH Value
FRESH SAMPLES	1.0	8.6	1.0	8.6	1.0	8.6
	2.0	8.3	2.0	8.3	2.0	8.3
	5.0	8.3	5.0	8.3	5.0	8.3
AFTER ONE DAY	0.98	8.2	0.89	7.3	0.70	7.9
	1.97	7.5	1.73	6.9	1.52	8.2
	4.96	8.0	4.89	6.5	4.41	7.9
AFTER SIX DAYS	0.94	7.8	0.89	7.5	0.70	7.8
	1.92	7.2	1.72	7.0	1.49	6.9
	4.93	8.0	4.85	6.3	4.37	7.9
AFTER TWELVE DAYS	0.93	8.9	0.88	8.2	0.68	7.5
	1.96	7.3	1.78	8.1	1.46	7.9
	4.93	8.1	4.84	6.8	4.43	7.8
AFTER TWENTY DAYS	0.76	9.1	0.84	7.9	0.55	7.7
	1.69	7.2	1.65	7.8	1.08	7.6
	4.89	8.7	4.34	6.9	3.6	7.6

FIFTH RUN

Table 2 : CONCENTRATION AND pH VALUE OF SUNTECH IV – 25% ACTIVE.

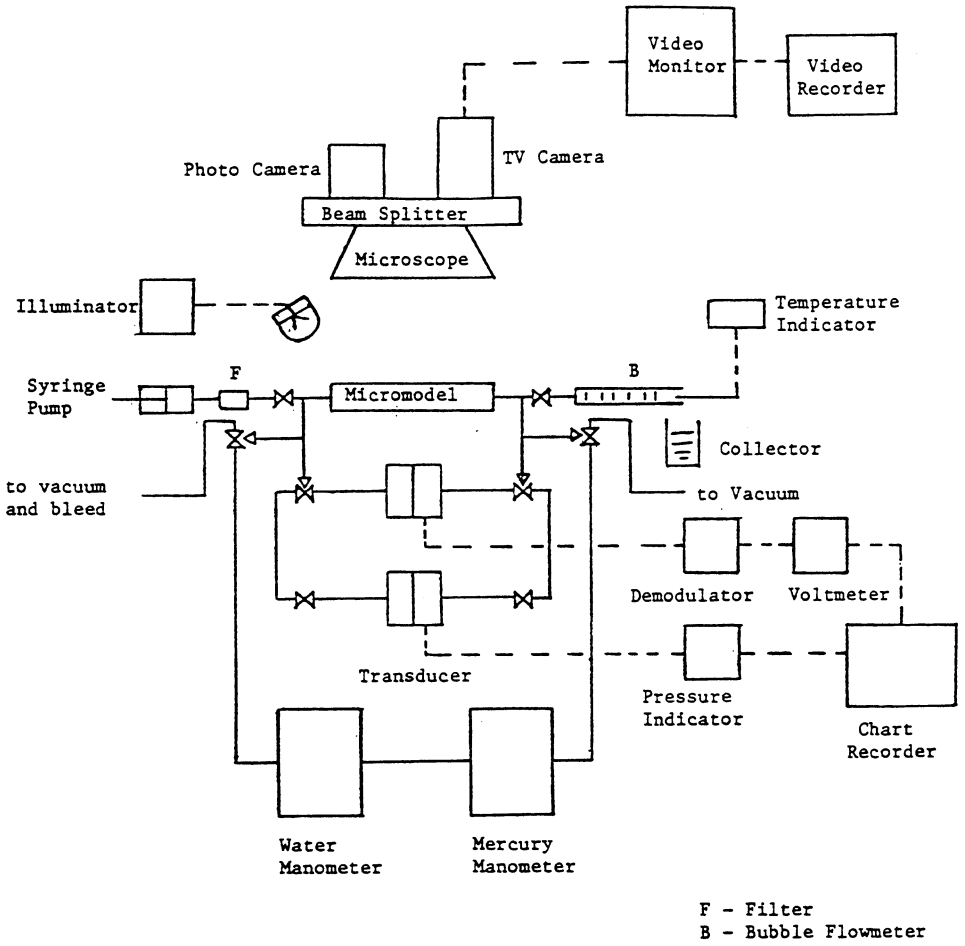

Figure 1: Schematic Diagram of Micromodel Apparatus

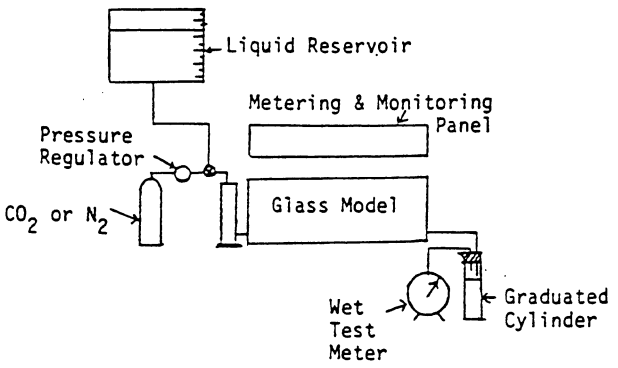

Fig. 2: TWO-DIMENSIONAL APPARATUS

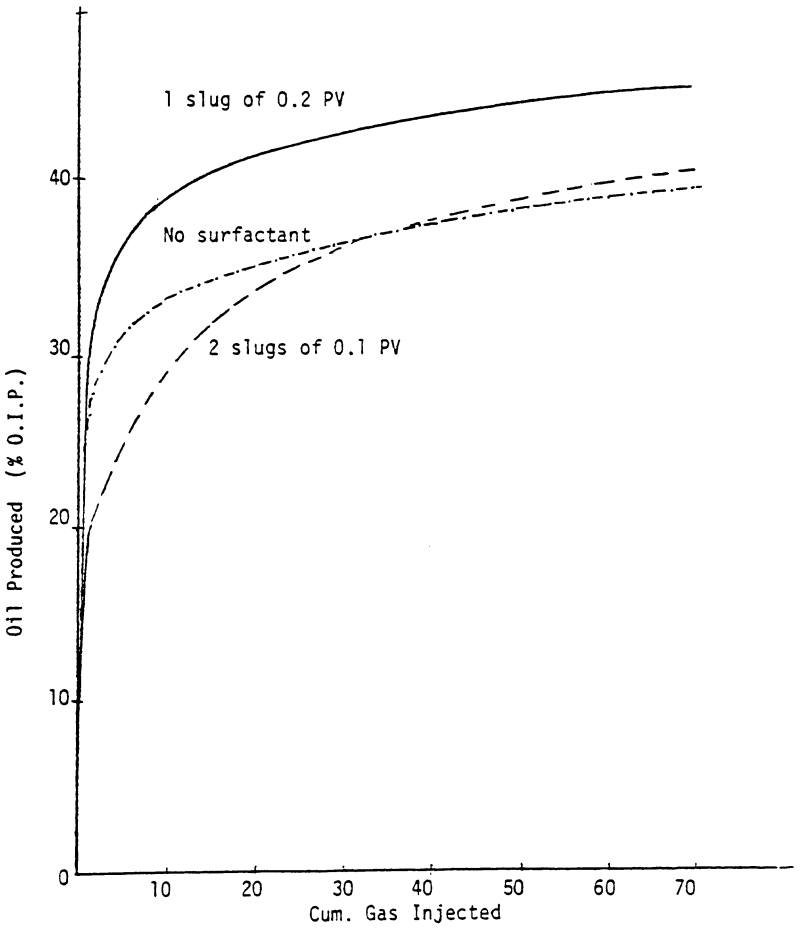

FIGURE 3: GAS THROUGHPUT VS RECOVERY

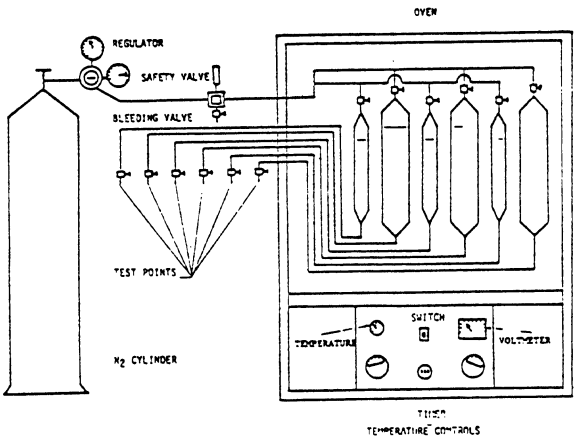

Fig. 4: TEMPERATURE STABILITY APPARATUS

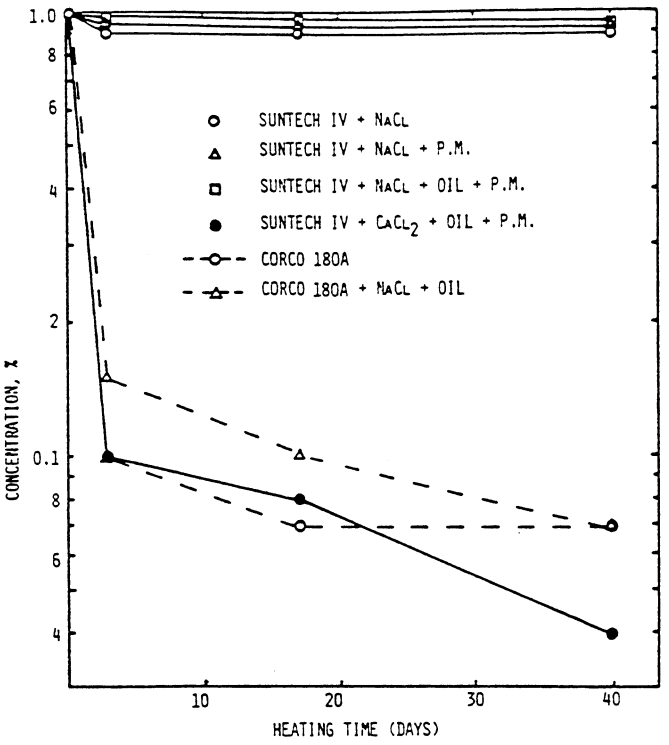

Fig. 5

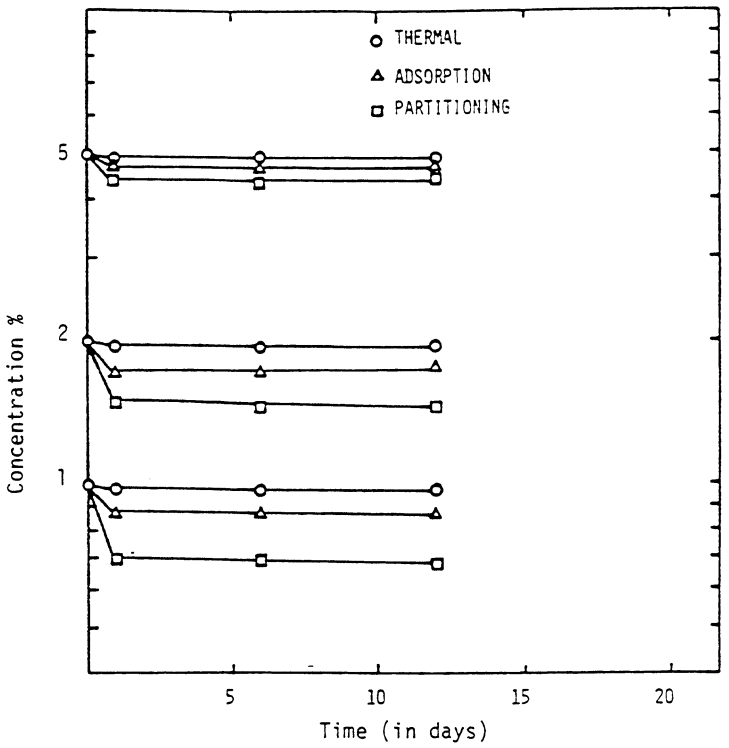

Fig. 6

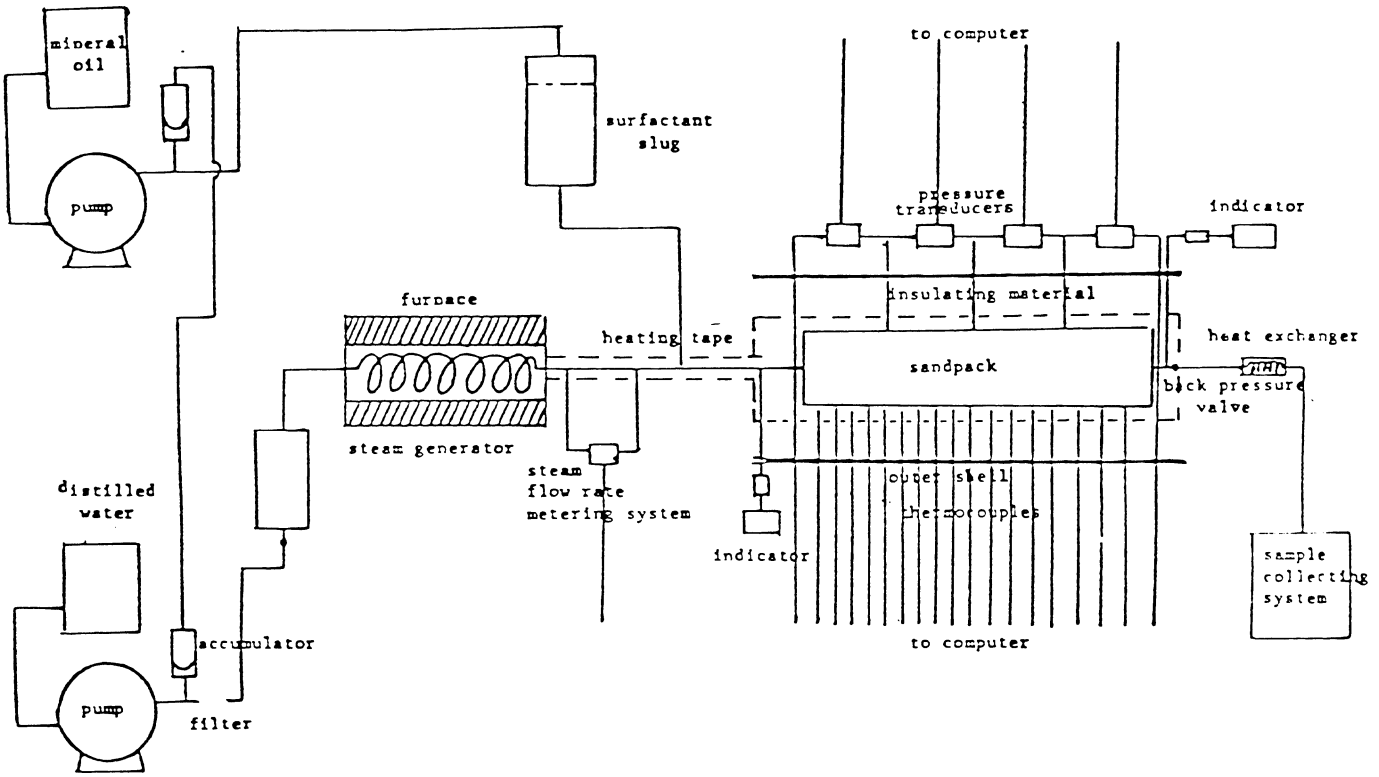

Fig. 7: STEAM FOAM ONE-DIMENSIONAL APPARATUS

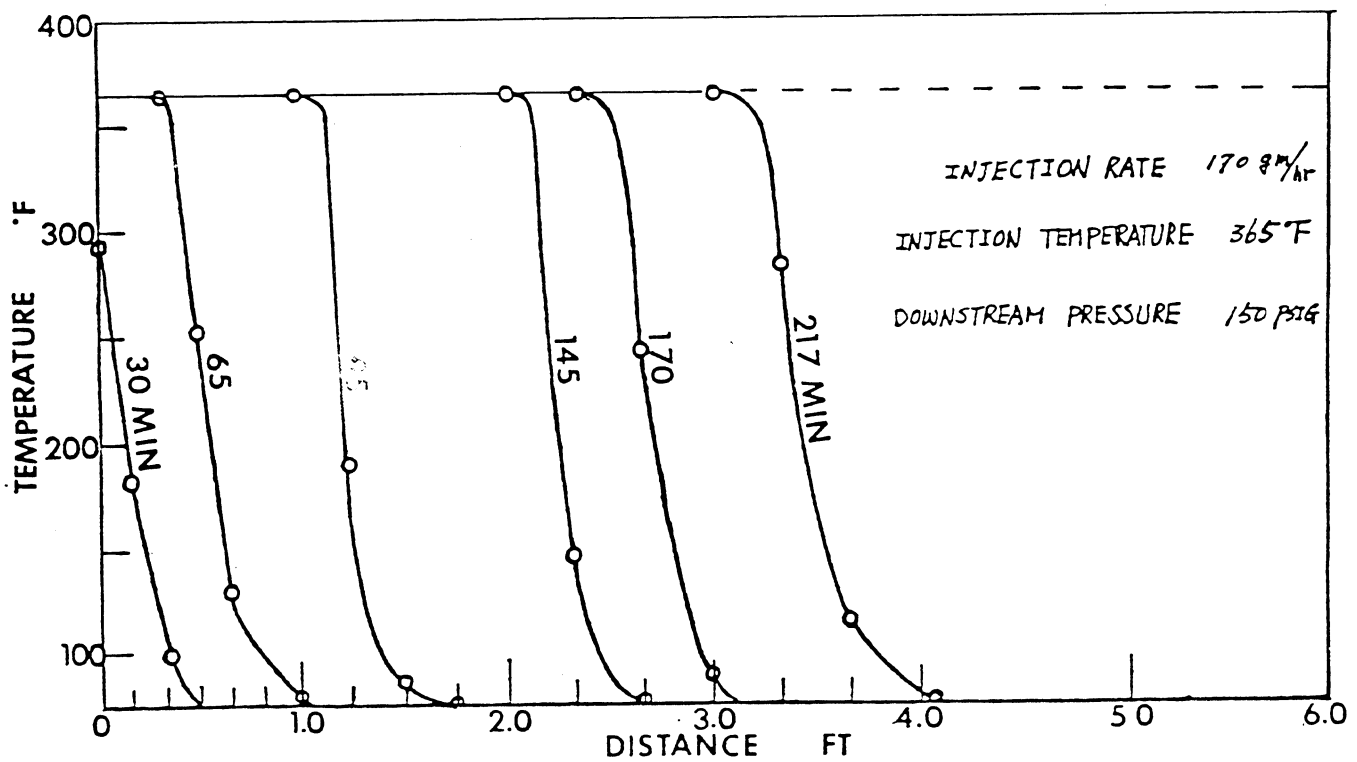

TEMPERATURE VS. DISTANCE FOR STEAM INJECTION

Fig. 8

ABSOLUTE PERMEABILITY AS A FUNCTION OF TEMPERATURE AND PRESSURE

by

Brian D. Gobran, Arshad H. Sufi
and William E. Brigham
Stanford University Petroleum Research Institute

ABSTRACT

While absolute permeability is an important reservoir parameter used in all flow equations, the exact nature of the dependence of porous media on the temperature of the system, confining or overburden pressure and the pore pressure of the flowing fluid is still unknown. When attempting to simulate reservoir conditions with cores in the laboratory, it is necessary to know exactly what variables can be simulated in which ways without changing the characteristics of the core.

This study involves the effects of temperature, confining pressure and pore pressure on the absolute permeability of unconsolidated sand and consolidated sandstone cores. This will be the basis for later work investigating the effects of these variables and others on relative permeability measurements.

HISTORY OF PROJECT

This report contributes to the objectives of Contract DE-AC03-76ET12056 which was initiated in September 1976.

INTRODUCTION

Although absolute permeability was claimed to be ". . . independent of the nature of the fluid and is solely determined by the structure of the porous media" by Muskat (1), many groups of investigators have studied variables which might affect the absolute permeability of a porous medium (2-31).

From all these studies, two conclusions can be drawn. First, increasing the confining or overburden pressure on a core causes a reduction in the absolute permeability. Second, the effect of increasing the temperature of the porous medium and the flowing fluid is not well understood. Because of this incomplete understanding of the effect of temperature on absolute permeability and the applicability of this type of research to thermal oil recovery, a research effort along these lines was initiated at the Stanford University Petroleum Research Institute. Early work at Stanford, on the effect of temperature on absolute permeability, had shown that the combination of water and sandstone was the most sensitive fluid/rock combination. So, the goals of this study were to either confirm and expand on the past Stanford University results or to explain the differences seen by various investigators.

Two early reports of this research project (30,31) were incorrect. In both of them the mistake of including hydrazine in the flowing water

Prepared for DOE under Contract No. DE-AC03-76ET12056

was noted, however, further experimentation led to the discovery of more flaws in the experimental procedure. New results are presented in this study. They have been thoroughly studied, and are considered accurate. In addition, reasons are given for the results seen in the past experiments.

EXPERIMENTAL APPARATUS

Figure 1 is a schematic diagram of the absolute permeability apparatus. The apparatus can operate at a confining pressure of 10,000 psi, pore pressure of 4000 psi, and a temperature of 300°F. Some of the changes in the experimental apparatus during the past year include installation of high pressure differential pressure transducers, removal of the capillary tube viscometer, addition of a pressure intensifier for the confining pressure and a second backpressure regulator (a dome-loaded one).

When the effect of pore pressure on absolute permeability was being investigated, it was discovered that the differential pressure transducers were rated for only 2000 psi. It was also determined that the calibration for the capillary tube viscometer was valid at only one pressure. Experimentation had shown that the viscosity of water remained unchanged after passing through the core and that the flow rates delivered by the pump remained constant over time at all backpressures. Thus, the capillary tube viscometer could be removed, the flow rate could be taken from the measured discharge pump rates, and the tabulated water viscosity could be used directly.

The spring-loaded backpressure regulator developed a bleeding problem when the pump cylinders were switched. The problem was serious enough that the water flashed at the elevated temperatures. A nitrogen dome-loaded backpressure regulator was installed downstream of the spring-loaded one. The dome regulator has far better shut-off abilities when there is no flow and maintains the desired pressure throughout the system at all times.

When operating at high confining pressures, use of the hand pump proved difficult. A pressure intensifier is now used when the confining pressure exceeds 7000 psi. It is easy to increase the pressure to 10,000 psi and small changes in the pressure are made with a simple turn of the handle.

RESULTS

Before any changes in permeability could be attributed to changes in the parameters of interest (temperature, confining pressure, and pore pressure), it was necessary to determine if any other factor could be influencing the calculated value of permeability. Two variables investigated were the effect of flow rate and the effect of throughput volume. Figure 2 shows permeability graphed versus flow rate for an unconsolidated sand at 100°F. Clearly, there is no significant flowrate effect on permeability. Note, also, the error bars indicated on the figure. At low rates, the pressure drop is less and the error is about ± 7% while at high rates,

it is about ± 2%. The effect of throughput on permeability is shown in Fig. 3. Again, this is for an unconsolidated sand at 100°F. A slight reduction in permeability is observed with continued throughput.

The results of an experiment to determine the effect of temperature on the absolute permeability of unconsolidated sand at various confining pressure levels at a constant pore pressure are given in Fig. 4. This figure shows a slight reduction in permeability during the heat-cool cycle at each confining pressure. This is attributed to settling caused by flow and thermal changes in the core. Therefore, it is concluded that there is no reduction in the absolute permeability of unconsolidated sands due to temperature increase. Although only one set of data are shown here, we have a considerable body of additional data which confirms these results.

The effects of confining pressure and pore pressure on the absolute permeability of unconsolidated sand cores are depicted in Figs. 5 and 6, respectively. Increasing the confining pressure on a core seems to reduce the permeability linearly, but the release of pressure does not cause a complete restoration of the permeability. The second application of confining pressure causes permeability to follow the path determined by the initial release (the lower curve). This behavior is likely due to an initial rearrangement of the grains into a tighter structure caused by the confining pressure. Even though the confining pressure is released, there is no force re-opening the pores to their original size. After this tighter packing has taken place, the structure changes elastically with changes in confining pressure.

The effect of changing the pore pressure is significantly different from the effect of changing the confining pressure. Figure 6 shows a linear, repeatable change in absolute permeability with both an increase and then decrease in pore pressure at a fixed confining pressure. When the confining pressure is released, there is no force to re-open the grains; but when the pore pressure is released, the confining pressure acts to close the pores and restore the original permeability. So, from these results for unconsolidated sand, it can be concluded that a repeatable linear change in absolute permeability is observed with a change in pore pressure and a nonlinear repeatable change in permeability with confining pressure changes is observed after the first pressurization of the core.

Similar experiments have been run on Berea sandstone cores and similar results have been obtained. Figure 7 shows permeability as a function of flow rate for a Berea sandstone at 100°F. As with the unconsolidated sand, there is little change in permeability with flow rate changes. One Berea core was fired at 500°C for six hours. Permeability versus throughput for this core is shown in Fig. 8. A similar result was found for an unfired Berea core. This shows that firing does little to settle the clays. While it seems that there continues to be a change in the permeability with throughput, it is important to consider the amount of throughput and that many measurements can be taken between twenty and thirty thousand cubic centimeters with virtually no reduction in permeability cause by throughput.

The effect of temperature on absolute permeability for an unfired Berea core is shown in Fig. 9. The square data points are for the heating cycle with the circles representing the data when cooling. The error bars are shown for a particular measurement. These data show that there is no effect of temperature on the absolute permeability of a throughput-settled Berea sandstone core.

Figure 10 shows the results of confining pressure changes on absolute permeability. With this fired Berea core, a linear decrease with the initial pressurization is observed followed by a repeatable non-linear change when the pressure is released. As described for unconsolidated sand, this is explained as an initial permanent grain rearrangement followed by elastic changes thereafter.

Permeability is graphed versus pore pressure at a fixed confining pressure for a fired Berea sandstone in Fig. 11. A linear increase in permeability with increased pore pressure is found. This corresponds with the increase found with unconsolidated sand. However, unlike unconsolidated sand, this fired consolidated sandstone did not return to its initial permeability when the pore pressure was reduced. In fact, the permeability when measurements were completed was higher than the initial permeability. After these measurements were completed, the confining pressure was reduced to 2000 psi and the core left overnight. During this time the permeability decreased from 170 to 154 millidarcies. These results can be explained as fines migrating through pore throats at the high pore pressures and not plugging again until later, thus giving a temporary increase in permeability when the pore pressure is reduced.

DISCUSSION

The results of this study differ from those of past researchers, especially those presented in references 20 through 24. Some of the past workers in this area found a significant reduction in absolute permeability when water was flowing through sand or sandstone cores. Several explanations can be made for these differences. Figure 8 shows a reduction in permeability due to throughput volume on the order of 30% for a fired Berea sandstone core. Casse in references 20 and 22 found a reduction in absolute permeability of about 30% with temperature increase. Perhaps what he assumed to be temperature dependence was actually throughput dependence. Figure 12 shows our earlier results from reference 30. It was later determined that non-isothermal flow was occurring through the core in these earlier experiments. This, combined with inaccurate temperature determination at ambient conditions, produced the apparent temperature dependence seen in Fig. 12. It is likely that similar problems occurred in previous studies reported by others.

CONCLUSIONS

It can be concluded from this study that the absolute permeability of unconsolidated sand and consolidated sandstone cores behave similarly to changes in temperature, confining pressure and pore pressure. With water as the flowing fluid, temperature had little or no effect on the

absolute permeability of these two porous media. Confining pressure caused a linear decrease in permeability as the pressure was initially applied. When the pressure was released and during subsequent pressurization cycles, the response was repeatable but non-linear. Pore pressure changes affect consolidated and unconsolidated core differently. With unconsolidated sand cores pore pressure cycles caused a linear repeatable changes in absolute permeability. With a fired Berea sandstone, there was a linear increase in permeability with pore pressure increase and then a non-linear decrease when the pore pressure was reduced. This produced a net increase in the absolute permeability. The reasons for this behavior are not known but a reasonable explanation involves migration of fines through pore throats.

ACKNOWLEDGEMENTS

The authors wish to thank the United States Department of Energy (contract number DE-AC03-76ET12056) for support of this work. This support is greatly appreciated.

REFERENCES

1. Muskat, M.: The Flow of Homogeneous Fluids Through Porous Media, McGraw-Hill Book Company, New York, 1937, 71-72.

2. Grunberg, L. and Nissan, A. H.: "The Permeability of Porous Solids to Gases and Liquids," J. Inst. Pet. Tech., 29, No. 236, 193-225.

3. Calhoun, J. C. and Yuster, S. T.: "A Study of the Flow of Homogeneous Fluids Through Ideal Porous Media," Drill. and Prod. Prac., API (1946), 335-355.

4. Fatt, I. and Davis, D. H.: "Reduction in Permeability with Overburden Pressure," Trans., AIME (1952), 195, 329.

5. Fatt, I.: "The Effect of Overburden Pressure on Relative Permeability," Trans., AIME (1953), 198, 325-326.

6. Wyble, D. O.: "Effect of Applied Pressure on the Conductivity, Porosity and Permeability of Sandstones," Trans., AIME (1958), 213, 430-432.

7. McLatchie, A. S., Hemstock, R. A. and Young, J. W.: "The Effective Compressibility of Reservoir Rock and It's Effects on Permeability," Trans., AIME (1958), 213, 386-388.

8. Knutson, C. F. and Bohor, B. F.: "Reservoir Rock Behavior Under Moderate Confining Pressure," Proc.: Fifth Symposium on Rock Mechanics, 1962, 627-659.

9. Dobrynin, V. M.: "Effect of Overburden Pressure on Some Properties of Sandstones," Soc. Pet. Eng. J., (Dec., 1962), 360-366.

10. Gray, D. H., Fatt, I. and Bergamini, G.: "The Effect of Stress on Permeability of Sandstone Cores," Soc. Pet. Eng. J., (June, 1963), 95-100.

11. Somerton, W. H. and Selim, M. A.: "Additional Thermal Data for Porous Rocks," Soc. Pet. Eng. J., (Dec., 1961), 249-253.

12. Somerton, W. H. and Gupta, V. S.: "Role of Fluxing Agents in Thermal Alteration of Sandstones," J. Pet. Tech., (May, 1965), 585-588.

13. Somerton, W. H., Mehta, M. M. and Dean, G. W.: "Thermal Alteration of Sandstones," J. Pet. Tech., (May, 1965), 589-593.

14. Paaswell, R. E.: "Thermal Influence on Flow From a Compressible Porous Medium," Water Resources Research, (1967), 3, No. 1, 271-278.

15. Wilhelmi, B. and Somerton, W. H.: "Simultaneous Measurement of Pore and Elastic Properties of Rocks Under Triaxial Stress Conditions," Soc. Pet. Eng. J., (Sept., 1967), 283-294.

16. Greenberg, D. B., Cresap, R. S. and Malone, T. A.: "Intrinsic Permeability of Hydrological Porous Mediums: Variation with Temperature," Water Resources Research, (Aug., 1968), 791-800.

17. Brace, W. F., Walsh, J. B. and Francos, W. T.: "Permeabilities of Granite Under High Pressure," J. Geoph. Res., (1968), 73, No. 6, 2225-2236.

18. Vairogs, J., Hearn, C. N., Dareing, D. W. and Rhoades, V. W.: "Effect of Rock Stress on Gas Production From Low-Permeability Reservoirs," J. Pet. Tech., (Sept., 1971), 1161-1167.

19. Afinogenov, Y. A.: "How The Liquid Permeability of Rocks Is Affected by Pressure and Temperature," SNIIGIMS (1969), 6, 34-42.

20. Casse, F. J.: "The Effect of Temperature and Confining Pressure on Fluid Flow Properties of Consolidated Rocks," Ph.D. Dissertation, Stanford University, 1974.

21. Weinbrandt, R. M., Ramey, H. J., Jr. and Casse, F. J.: "The Effect of Temperature on Relative and Absolute Permeability of Sandstones," Soc. Pet. Eng. J., (Oct., 1975), 376-384.

22. Casse, F. J. and Ramey, H. J., Jr.: "The Effect of Temperature and Confining Pressure on Single-Phase Flow in Consolidated Rocks," J. Pet. Tech., (Aug., 1979), 1051-1059.

23. Aruna, M.: "The Effects of Temperature and Pressure on Absolute Permeability of Sandstones," Ph.D. Dissertation, Stanford University, 1976.

24. Aruna, M., Arihara, N. and Ramey, H. J., Jr.: "The Effect of Temperature and Stress on the Absolute Permeability of Sandstones and Limestones," Presented at the American Nuclear Society Topical Meeting, April, 1977.

25. Danesh, A., Ehlig-Economides, C, and Ramey, H. J., Jr.: "The Effect of Temperature Level on Absolute Permeability of Unconsolidated Silica and Stainless Steel," Trans., Geothermal Resources Council, (July, 1978), 137-139.

26. Aktan, T. and Farouq Ali, S. M.: "Effect of Cyclic and In-Situ Heating on the Absolute Permeabilities, Elastic Constants, and Electrical Resistivities of Rocks," SPE 5633 presented at the 50th Annual Fall Meeting of the SPE of AIME, Dallas, Texas, Sept.-Oct., 1975.

27. Zoback, M. D. and Byerlee, J. D.: "Permeability and Effective Stress," Am. Assoc. Pet. Geo. Bull., (1975), 59, 1, 154-158.

28. Sanyal, S. K., Marsden, S. S., Jr. and Ramey, H. J., Jr.: "Effect of Temperature on Petrophysical Properties of Reservoir Rocks," SPE 4898 presented at the 49th Annual Fall Meeting of the SPE of AIME, Houston, Texas, Oct., 1974.

29. Sydansk, R. D.: "Discussion of the Effect of Temperature and Confining Pressure on Single-Phase Flow in Consolidated Rocks," J. Pet. Tech., (Aug., 1980), 1329-1330.

30. Gobran, B. D., Sufi, A. H., Sanyal, S. K. and Brigham, W. E.: "Effects of Temperature and Pressure on Permeability," Proceedings, 1980 Annual Heavy Oil/EOR Contractor Presentations, U.S. Department of Energy, July, 1980, 111-123.

31. Gobran, B. D., Brigham, W. E. and Sanyal, S. K.: "The Temperature Dependence of Permeability," Trans., Geothermal Resources Council, (Sept. 1980), 397-400.

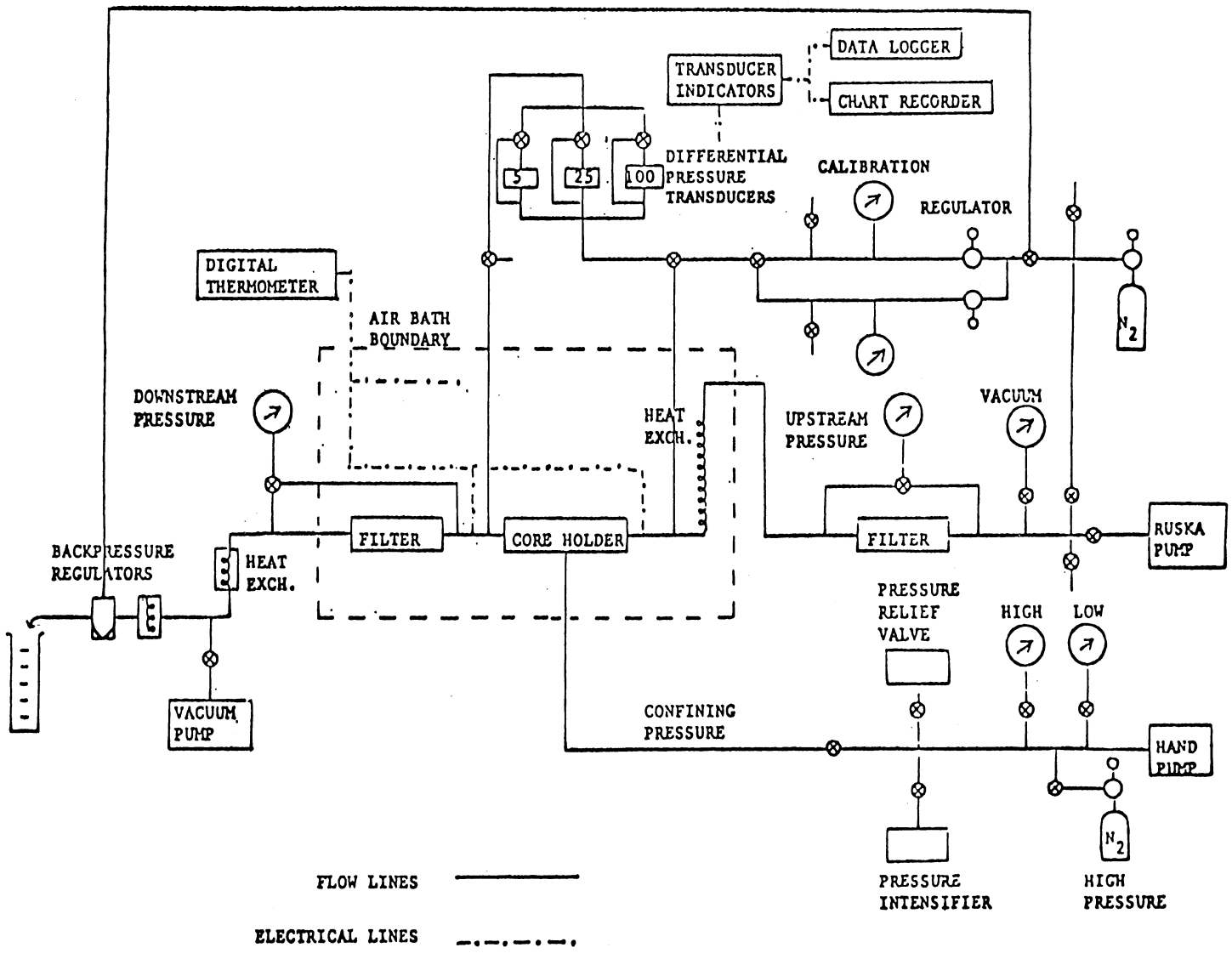

Figure 1. Schematic diagram of the experimental apparatus.

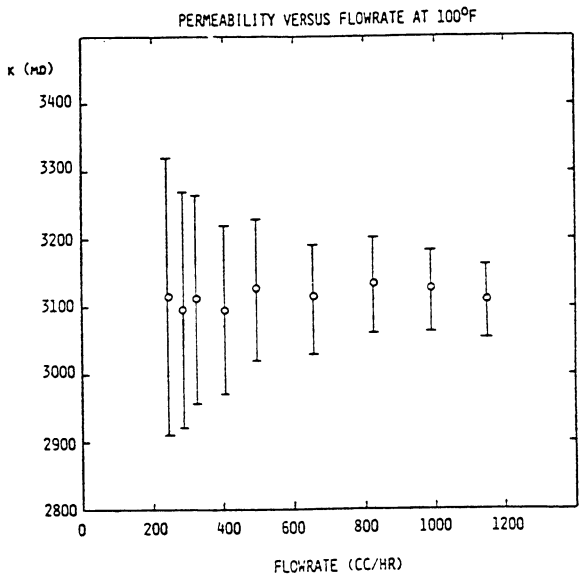

Figure 2. Permeability versus flowrate for sand.

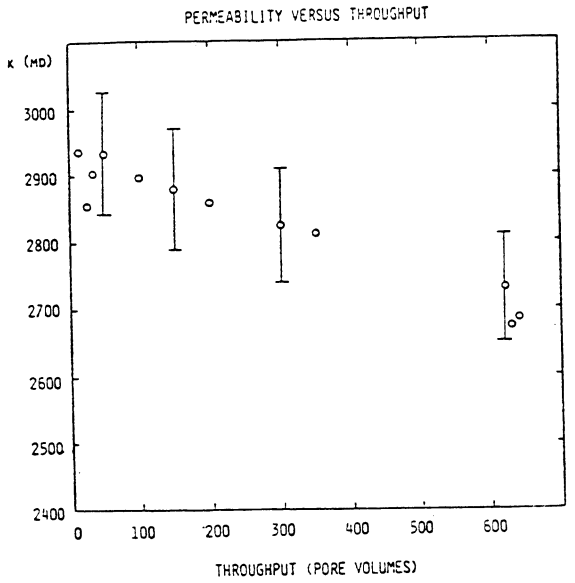

Figure 3. Permeability versus throughput for sand.

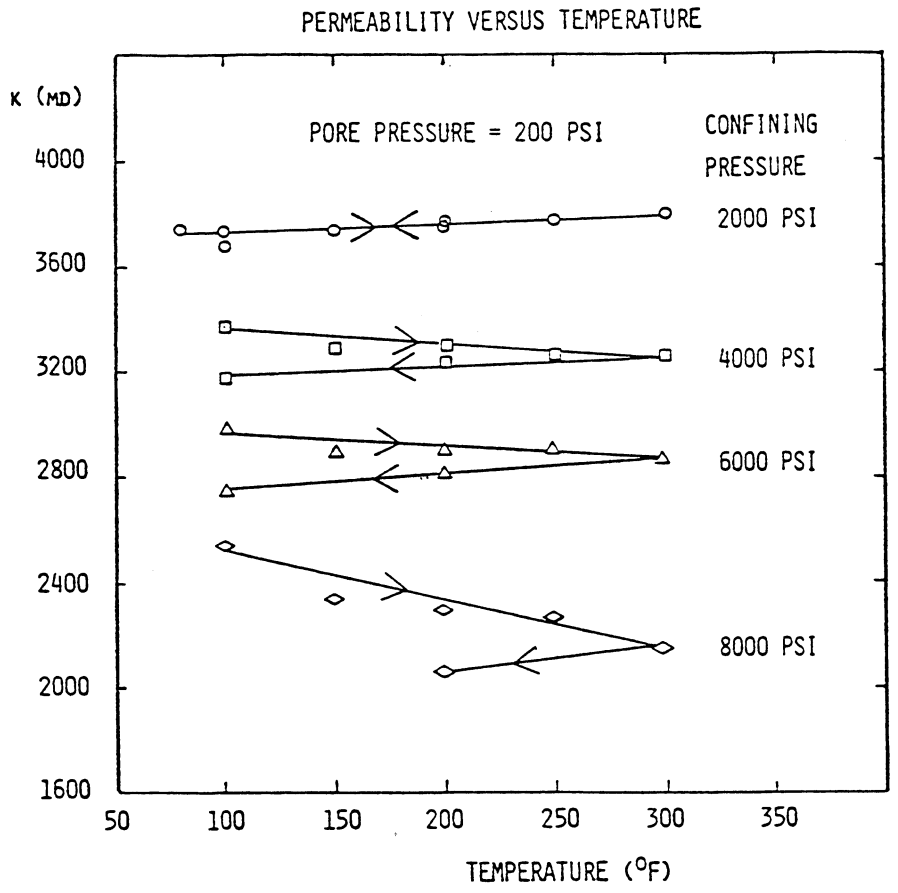

Figure 4. Permeability versus temperature for sand.

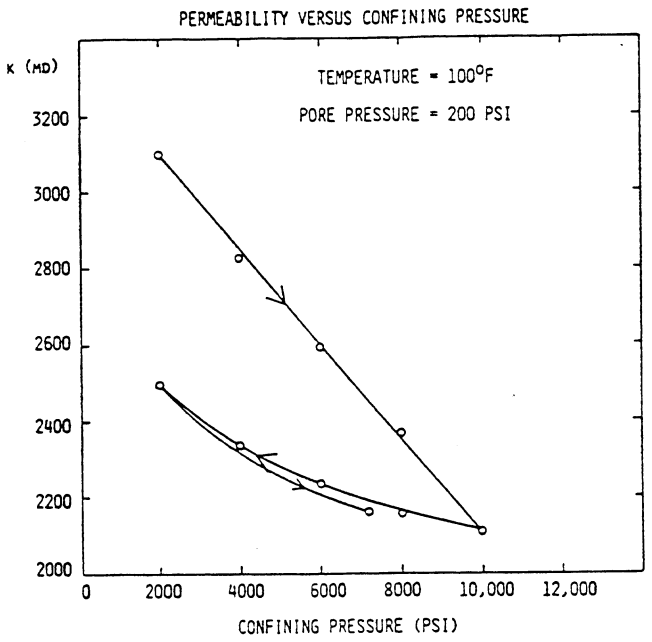

Figure 5. Permeability versus confining pressure for sand.

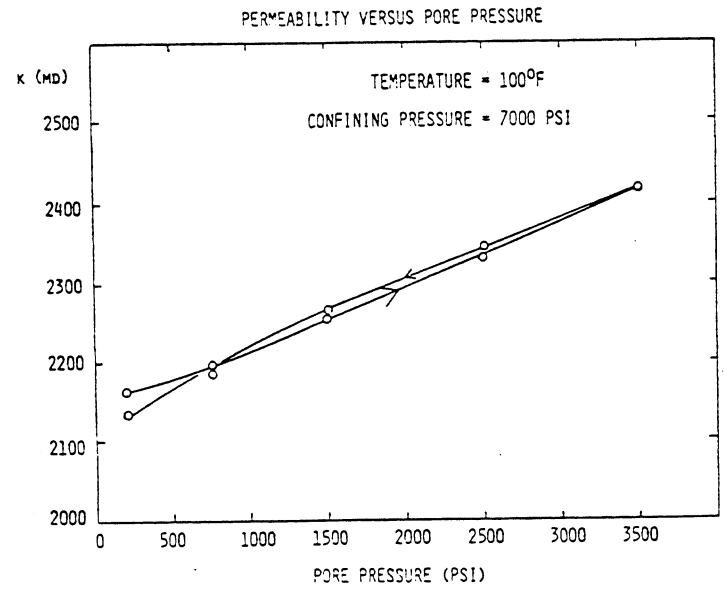

Figure 6. Permeability versus pore pressure for sand.

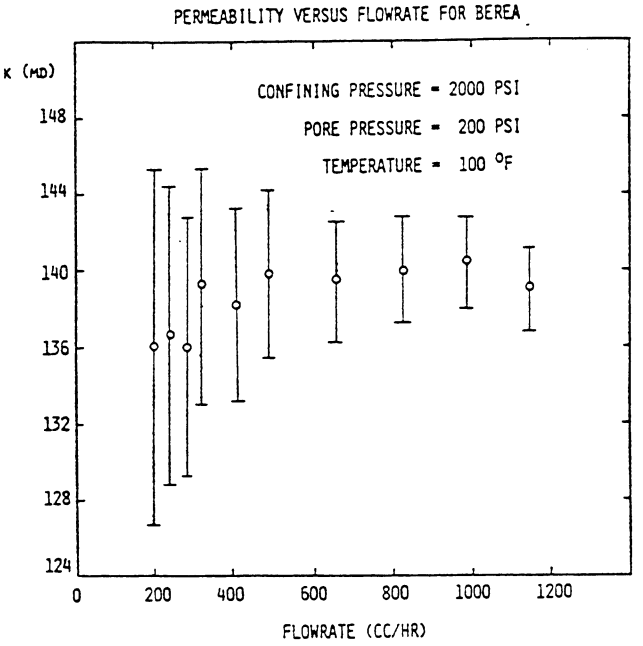

Figure 7. Permeability versus flowrate for Berea.

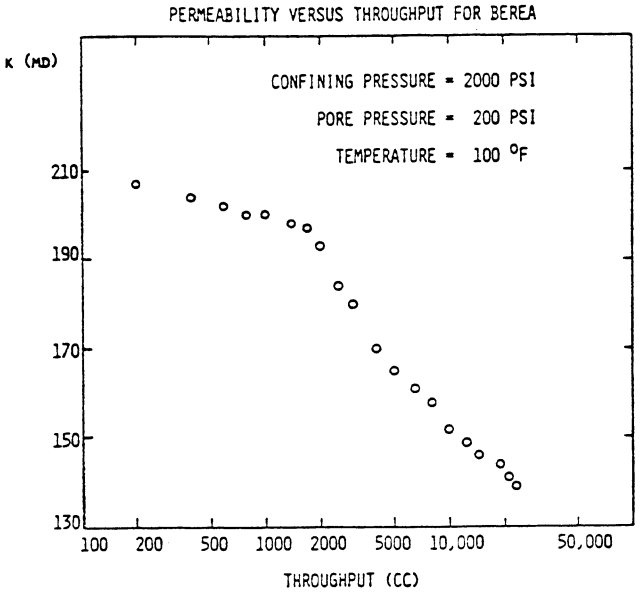

Figure 8. Permeability versus throughput for fired Berea.

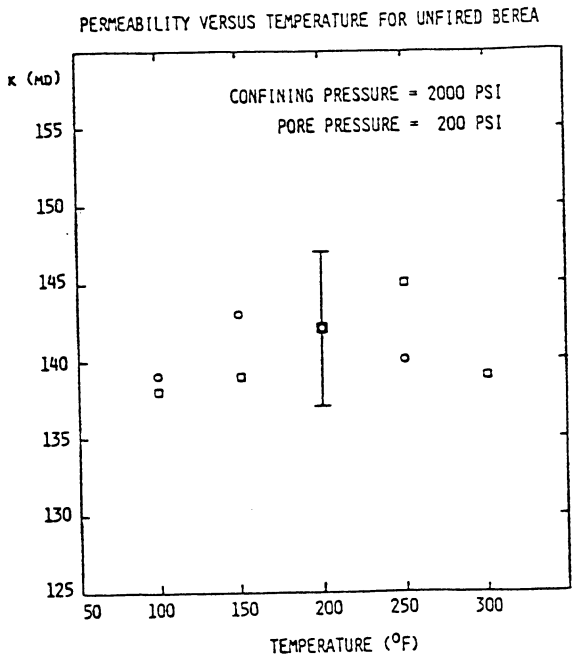

Figure 9. Permeability versus temperature for Berea.

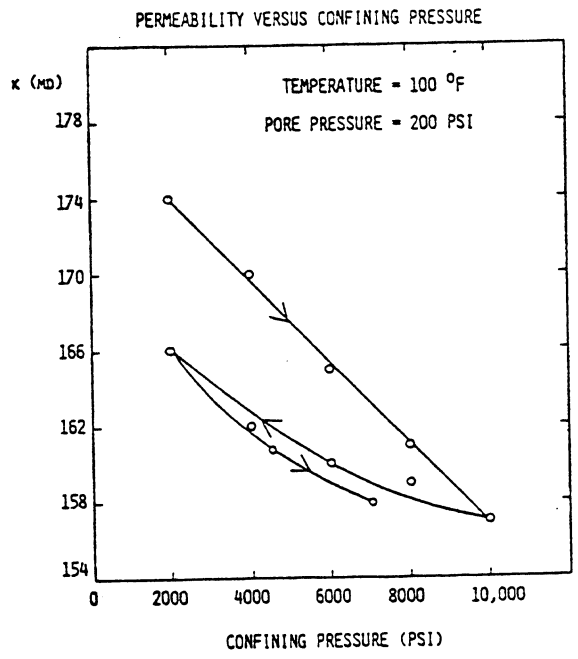

Figure 10. Permeability versus confining pressure for Berea.

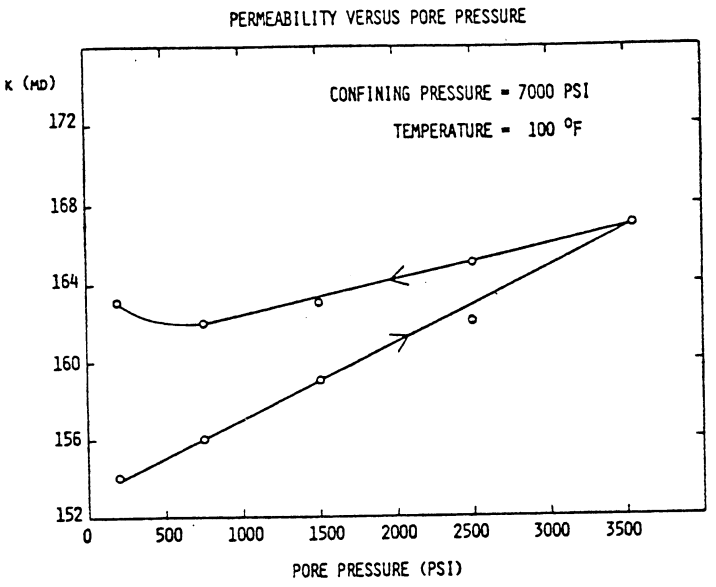

Figure 11. Permeability versus pore pressure for Berea.

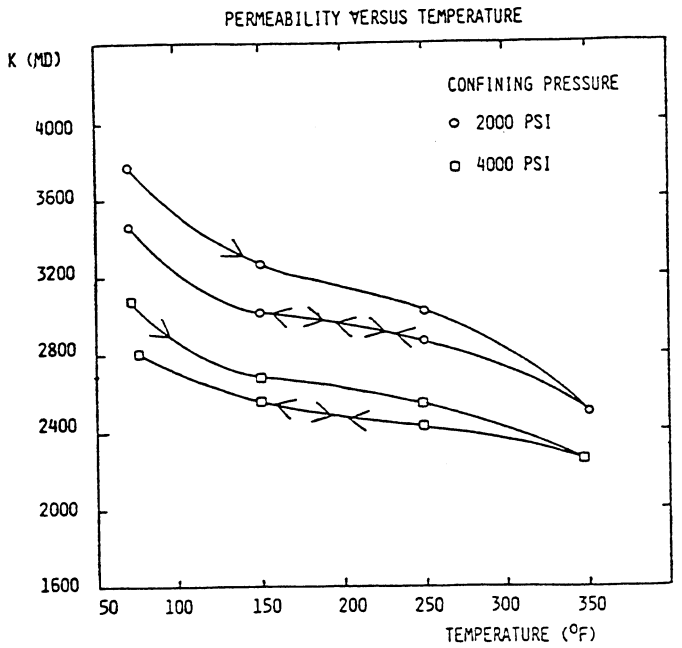

Figure 12. Permeability versus temperature for sand from reference 30.